A Model for the Disruption of *Escherichia coli* by High-Pressure Homogenization

by

Anton Peter Jacob MIDDELBERG

Thesis submitted for the degree of
Doctor of Philosophy

in

The University of Adelaide
Department of Chemical Engineering
Faculty of Engineering

December 1992

Awarded 1993

This work contains no material which has been accepted for the award of any other degree or diploma in any university or any other tertiary institution, and to the best of my knowledge and belief, contains no material previously published or written by another person, except where due reference has been made in the text.

I give consent to this copy of my thesis, when deposited in the University Library, being available for photocopying and loan.

SIGNED : .

DATE : 15th Dec 1992

ACKNOWLEDGMENTS

Several individuals and organizations deserve recognition for their contribution to this thesis. First, I would like to thank my supervisors, Dr. Brian O'Neill and Dr. David Bogle for their guidance and encouragement, and for taking the time to edit this thesis and suggest useful changes. On a personal level, I would like to thank Dr. O'Neill for acting as a mentor during the early stages of my academic career. I am also grateful to Dr. Bogle for encouraging me, as an undergraduate, to pursue a career in Biochemical Engineering.

I am indebted to Associate Professor Pradeep Agarwal and Ashley Hull for the use of their image analysis hardware and the Syzcount™ software they developed. In particular, I would like to acknowledge the assistance which Ashley provided when digitizing and analyzing the numerous photographs of bacteria. The chromatographic analyses described in this thesis were conducted using equipment in the Department of Dentistry. I am grateful to Dr. Tony Rogers and Neville Gully for allowing me to use their chromatographic equipment, and more specifically for helping me to analyze the cell-wall samples. Without their expert assistance and input it is doubtful whether any successful chromatographs would have been obtained. I am also indebted to Professor Joachim-V. Höltje of the Max-Planck-Institut für Entwicklungsbiologie, Tübingen, Germany, for providing chromatographic standards and for his patient responses to my numerous questions. My thanks also go to Dr. Connor Thomas of the Department of Microbiology, who took the electron micrographs included in this thesis. His input in modifying the procedure for preparing sacculi for chromatographic analysis was also essential to the success of this work. I am also grateful to the staff in the Departmental workshop, in particular Bruce Ide and Brian Mulcahy, for machining the pressure transducer into the homogenizer block.

All homogenization and fermentation tests described in this thesis were conducted using the facilities of Bresatec Ltd. I greatly appreciate the after-hours access which they

provided. I am also indebted to APV-Gaulin for donating the new cell-disruption valve used in this study.

Financial support for this work was partly provided by the Pig Research and Development Corporation (Australia). I am grateful for their award of a postgraduate scholarship and for their contributions toward the operating expenses incurred. I would also like to thank the Co-operative Research Centre for Tissue Growth and Repair for financing the latter stages of this work.

I would like to thank my parents for the support and encouragement they have given me throughout my life, and particularly for providing me with the education which has ultimately led to this thesis.

Last, but by no means least, I am indebted to my wife, Rita. Her continual support and encouragement throughout the last three years has been greatly appreciated. More importantly, many of the experimental studies described in this thesis could not have been completed without her dedicated technical assistance during those apparently endless nights of experimental work.

SUMMARY

The optimal design of bioprocesses producing high-volume, low-cost products is conditional upon the availability of flexible unit models accounting for interactions. High-pressure homogenization is a key operation in many bioprocesses. Unfortunately, the principal model describing homogenizer performance is inadequate. While it includes the two key operational parameters (pressure and the number of disruptor passes) explicitly, it relies on two parameters which are both system- and culture-specific (i.e. their value depends on the homogenizer and valve (the system) and the characteristics of the feed culture).

A new model for the disruption of *Escherichia coli* by high-pressure homogenization is developed in this thesis. Disruption is calculated by combining a homogenizer-stress distribution with a cell-strength distribution. The stress distribution includes the key operational parameter, namely homogenizer pressure, and three system-specific parameters. The strength distribution is assumed Gaussian, and is therefore characterized by two parameters (the mean effective strength and the distribution variance).

To allow meaningful comparisons of the model predictions and experimental data, a novel technique for measuring disruption is developed. The technique employs an analytical disc centrifuge which gives a direct measure of disruption. It is extremely accurate at high levels of disruption and does not suffer the disadvantages of traditional direct techniques such as the electronic particle counter (which is subject to fouling) and microscopy (which is tedious).

Model parameters were determined by the non-linear regression of single-pass disruption versus pressure data obtained from twenty-one different *E. coli* B cultures (in excess of 180 data points). Cultures of different strength were obtained using two fermenters and by

varying the time for which a given culture had experienced glucose exhaustion (i.e. the time into the stationary phase). The three system-specific parameters and the distribution variance were constant despite large variations in the culture characteristics. The mean effective strength is a culture-specific parameter and gives a meaningful indication of the relative resistance of a particular culture to disruption. The wall structure of each culture was analyzed by reverse-phase, high-pressure liquid chromatography to determine the fractional peptidoglycan crosslinkage. Cell size was determined by image analysis. Correlations of mean effective strength with peptidoglycan crosslinkage and average cell length were developed.

The model was extended to predict disruption with multiple homogenizer passes without the introduction of additional parameters (apart from the number of homogenizer passes). Multiple-pass predictions are made by repeated application of the homogenizer-stress distribution on the strength distribution. The model successfully predicted the disruption of two different strains of *E. coli* (strains B and JM101) grown on two different carbon sources (glucose and glycerol) with multiple homogenizer passes at three pressures (24, 45 and 66 MPa). Successful predictions with a single pass at a variety of pressures were also made.

The model is the first to allow true *a priori* predictions of disruption for a specified homogenizer system and *E. coli* strain. This is possible as the key parameter (mean effective strength) is correlated with measurable cell properties. The requirement for culture-specific parameters is therefore removed. The model also has the advantage that system and culture variability act on distinct parts of the model (the stress and strength distributions, respectively). With further work it will be possible to determine the effect which other key operational parameters (e.g. temperature and concentration) have on the stress distribution, and hence on disruption. It will also be possible to develop correlations for other strains and to establish the stress distributions for various homogenizer systems.

TABLE OF CONTENTS

LIST OF FIGURES

LIST OF TABLES

CHAPTER 1

INTRODUCTION

The commercialization of a vast array of new products is a feature of the modern biotechnology industry (Thayer, 1991). Products have traditionally been of high-added-value and consequently the engineering challenge is to scale-up existing laboratory procedures rather than to optimize the process. However, this situation is changing as new products with potentially-large markets demanding a low-cost product emerge. Typical proteins in this category are the somatotropins and the insulin-like growth factors. The somatotropins are targeted at a highly-elastic market demanding a high benefit-to-cost ratio (e.g. porcine somatotropin, Petrides *et al.*, (1989)). The insulin-like growth factors must compete with recombinant insulin for market share as a tissue-culture additive. In both instances unit cost will determine flowsheet and possibly company viability.

Engineering considerations in such an environment mirror those in traditional chemical industries, where simulation is widely employed for process design, evaluation and optimization. Its benefits are widely recognized (Biegler, 1989). Simulation packages specifically designed for the biochemical industry are available (Evans, 1988; Petrides *et al.*, 1989; Gritsis and Titchener-Hooker, 1989). These are, however, first-generation packages with restricted capabilities. Their deficiencies result primarily from the lack of sophisticated models for biochemical unit operations. The importance of considering unit interactions in bioprocess design has been identified (Fish and Lilly, 1984). A noticeable deficiency in simulation is the existing models which fail to account for such interactions and which rely on system- and culture-specific parameters. Bioprocess optimization is conditional on the

development of improved models and the formation of appropriate databases of host and protein properties (Gritsis and Titchener-Hooker, 1989).

Escherichia coli has been extensively studied and a sophisticated understanding of its genetics has evolved. Strongly-inducible promoters are readily available and cloning techniques are well established. Unfortunately, *E. coli* suffers from several disadvantages as a host. Most significantly, it does not excrete proteins to the culture medium with the exception of a small class of proteins such as toxins (Hirst *et al.*, 1984) and hemolysins (Goebel and Hedgpeth, 1982). Consequently, many products of commercial interest are located intracellularly. *Bacillus subtilis* has the advantage that proteins are naturally secreted, and consequently it may become a preferred host (Errington and Mountain, 1990). However, its genetics are not as fully understood as those of *E. coli* and it suffers the disadvantage that proteases are often also secreted (Errington and Mountain, 1990). The lack of a procaryotic glycosylation mechanism has resulted in increased use of *Saccharomyces cerevisiae* and mammalian-cell culture (Harris, 1989). *S. cerevisiae* has the disadvantage that only small proteins are secreted and that incorrect glycosylation may result. Mammalian-culture techniques are considerably more complex than for microbial systems and are characterized by low cell densities and consequently low overall productivities. For proteins not requiring glycosylation, *S cerevisiae* and mammalian cells offer little economic advantage over *E. coli* at present. With the development of highly productive fed-batch fermentation protocols for *E. coli* and the lack of a suitable alternative, initial process designs for low-cost high-volume proteins are likely to be based on *E. coli* as the selected host. The problem posed by intracellular product location must therefore be addressed.

Research directed at the excretion of proteins from *E. coli* has met with limited success. Georgiou *et al.* (1985) obtained high levels of the periplasmic protein β-lactamase in the culture medium by judicious host choice under immobilized conditions. Essentially, the host became "leaky" due to protein over-expression. The secretion of cytoplasmic human growth hormone (hGH) to the periplasm has been reported (Hsiung *et al.*, 1986; Chang *et al.*, 1987;

Matteucci and Lipetsky, 1986), but this was not accompanied by excretion to the medium. Hsiung *et al.* (1989) obtained excretion of hGH from the periplasm to the culture medium by the use of bacteriocin release protein (BRP). The use of BRP has also been shown to aid in the release of α-amylase and β-lactamase from the periplasm to the culture medium (Yu and San, 1992). Kato *et al.* (1987) describe an excretion vector for hGH giving mature protein in the culture medium without the use of BRP. Other fusion proteins have also been described which may be excreted by *E. coli* without the use of BRP. Abrahmsen *et al.* (1986) describe a human insulin-like growth factor (IGF-I) fusion protein which is excreted from *E. coli* and can be purified directly by IgG affinity chromatography. Subsequent cleavage of the staphylococcal protein A fragment gives native IGF-I.

Clearly, proteins can be excreted from *E. coli* in some instances. A major requirement for excretion is that the protein is soluble within the cytoplasm. In a soluble form, the product may be subjected to proteolytic degradation. Further, low expression levels are usually required to ensure solubility and prevent the formation of an insoluble protein inclusion body (Schein, 1989). This requirement for low expression levels may adversely impact upon process economics. In some cases, the process simplification resulting from protein excretion may inadequately compensate for the loss of fermenter productivity. Further, a significant research lead time is required to develop excretion vectors for a new product. In some cases, excretion may not be possible. Where excretion is possible, some proteins may be degraded by the highly aerated and sheared extracellular environment in the fermenter (Fish and Lilly, 1984). These considerations suggest that an efficient method of releasing intracellular protein from *E. coli* into the broth will be necessary for large-scale processing, particularly for first-generation processes. These techniques will usually rely on fracturing the cell wall.

An understanding of wall structure is necessary if disruption processes are to be meaningfully discussed. The *E. coli* cell wall is therefore examined in the following section. Methods for large-scale protein release are reviewed in section 1.2. It is shown that

high-pressure homogenization is the most commonly-employed method. As stated, fundamental models accounting for unit interactions are required if biochemical processes are to be optimally designed. The mechanism of disruption during homogenization is therefore discussed in section 1.3, and previous homogenizer modelling work is reviewed in section 1.4. It is shown that existing models are inadequate as they require system- and culture-specific parameters. Consequently, the disruption that will be obtained for a specific microorganism in a specified system (i.e. homogenizer and valve) cannot be predicted unless a culture with precisely the same history has been previously examined. A new model which overcomes the need for culture-specific parameters is required. The culture characteristics influencing homogenizer performance are therefore identified in section 1.5. A new model which removes the requirement for culture-specific parameters is then developed in chapter 2.

1.1 The Cell Wall of *Escherichia coli*

The cell wall of *E. coli* is composed of two primary layers: the outer membrane and the peptidoglycan or murein layer (Figure 1.1). In addition to the wall, a cytoplasmic membrane composed primarily of phospholipids maintains concentration gradients between the cell and its surroundings. This membrane offers no mechanical strength and disrupts due to the osmotic pressure difference between the cell and its environment after removal of the wall. It is therefore neglected in the discussion and modelling of disruption.

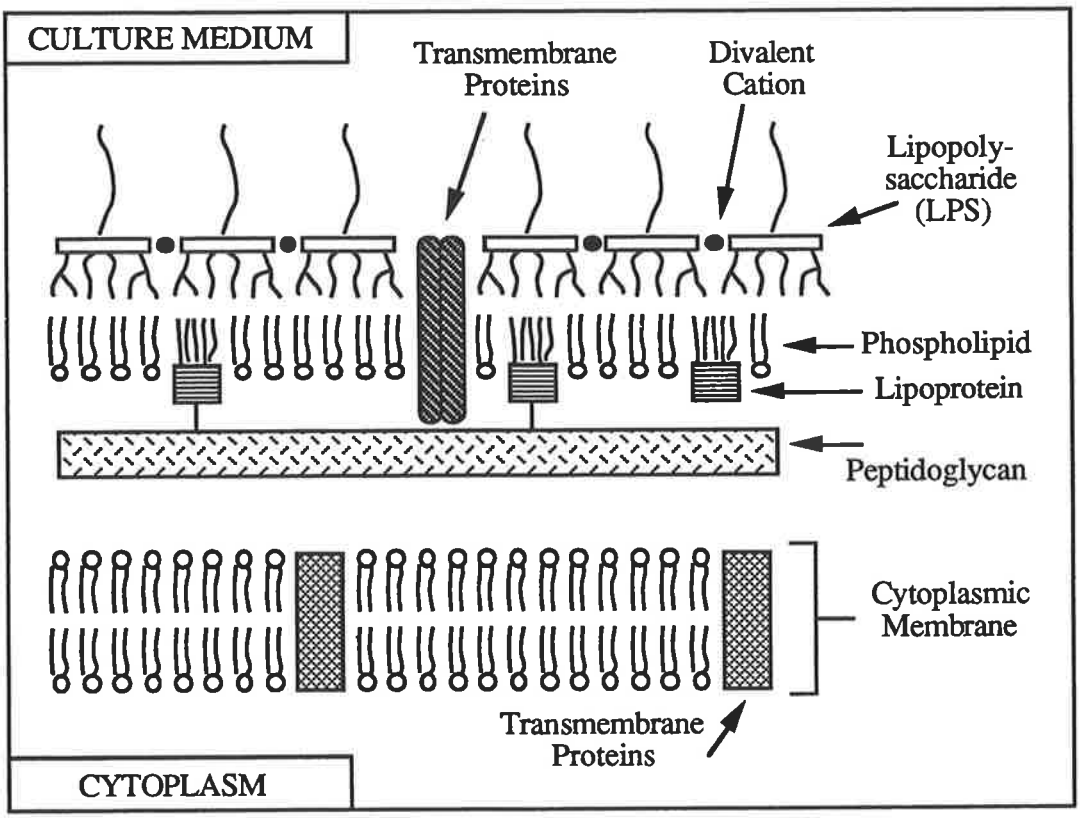

FIGURE 1.1: *Simplified structure of the wall of Escherichia coli showing the relationship with the cytoplasmic membrane (After Rietschel et al., 1986).*

The outer membrane is a complex and incompletely-characterized structure. It consists primarily of a lipid bilayer containing transmembrane proteins, phospholipids and lipopolysaccharide (LPS). Lipopolysaccharide contains a hydrophobic region (Lipid A, also known as endotoxin as it causes a toxic response in mammals) that has fatty acids linked to

diglucosamine phosphate (Hancock, 1984). It is anchored in the outer membrane by binding to outer-membrane proteins and by non-covalent crossbridging of adjacent LPS molecules with divalent cations such as Mg^{2+} and Ca^{2+} (Hancock, 1984). The exact organization of LPS in the outer membrane has not been determined (Zorzopulos *et al.*, 1989). A lipoprotein complex connects the lower portion of the phospholipid bilayer to the peptidoglycan layer. The peptidoglycan or murein layer consists of a series of glycan chains composed of N-acetylglucosamine (NAG) and N-acetylmuramic acid (NAM) linked by β-1,4-glycosidic bonds. Glycan chains have an average length of 30 disaccharide units (Glauner, 1988) with a significant fraction of chains only 10 units long (Höltje and Glauner, 1990). Chains are crosslinked by peptide bonds formed between a meso-diaminopimelic acid (m-A_2pm) residue on one chain and a D-alanine (D-Ala) or a meso-diaminopimelic acid residue on an adjacent chain, as shown in Figure 1.2. Significant structural variation occurs because of the existence of seven different peptidyl moieties (Table 1.1).

TABLE 1.1 : *Peptidyl moieties (***R** *in Figure 1.2) found in the structure of Escherichia coli peptidoglycan (Höltje and Glauner, 1990).*

NAME	AMINO ACID SEQUENCE
Di	– L-Ala – D-Glu
Tri	– L-Ala – D-Glu – m-A_2pm
Tetra	– L-Ala – D-Glu – m-A_2pm – D-Ala
Tetra-Gly4	– L-Ala – D-Glu – m-A_2pm – Gly
Penta	– L-Ala – D-Glu – m-A_2pm – D-Ala – D-Ala
Penta-Gly5	– L-Ala – D-Glu – m-A_2pm – D-Ala – Gly
Tri-Lys-Arg	– L-Ala – D-Glu – L-Lys – L-Arg

The exact architecture of the *E. coli* bacterial cell wall remains a matter of some debate. Early models proposed peptidoglycan as a monolayer, with each disaccharide unit 1.03 nm long and the glycan chains parallel and 1.25 nm apart (Braun *et al.*, 1973). More recent studies using X-ray and electron diffraction have suggested that adjacent chains are only 0.45 nm apart, with peptide side-chains perpendicular to the plane of the polysaccharide chains (Formanek, 1983; Formanek, 1986). Furthermore, the peptidoglycan of *E. coli* is

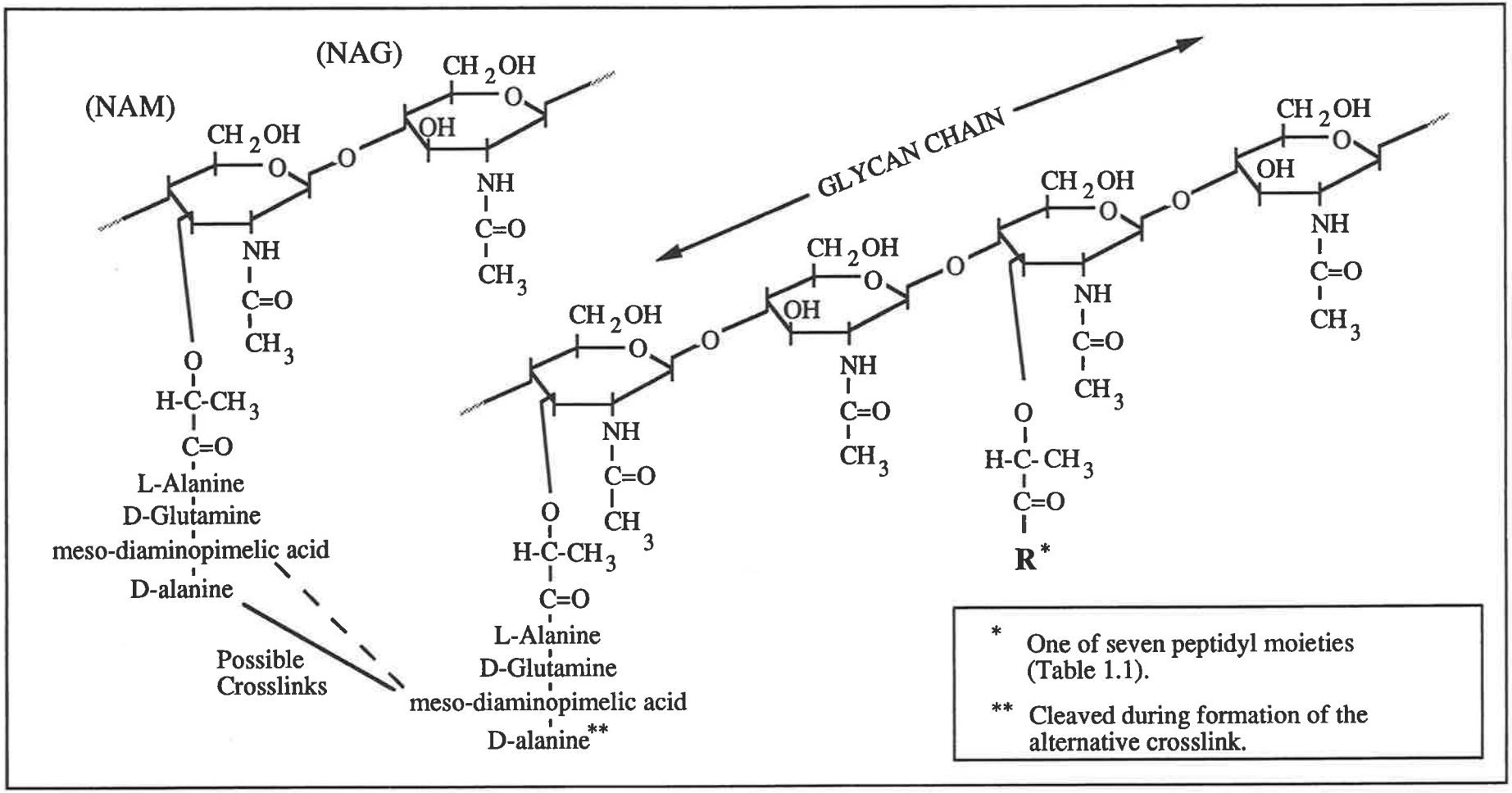

FIGURE 1.2 : *Simplified structure of Escherichia coli peptidoglycan, showing possible crosslinks. (After Höltje and Glauner, 1990)*

no longer proposed to be a monolayer (Glauner *et al.*, 1988). Leduc *et al.* (1989a) demonstrated that peptidoglycan is 6.6±1.5 nm thick for exponentially-growing cells and 8.8±1.8 nm thick for stationary cells. These values correspond to 2-3 and 4-5 layers of polysaccharides, respectively. Labischinski *et al.* (1985) present alternative packing arrangements for peptidoglycan. In these topologies, the peptidoglycan is multi-layered and all polysaccharide chains are parallel.

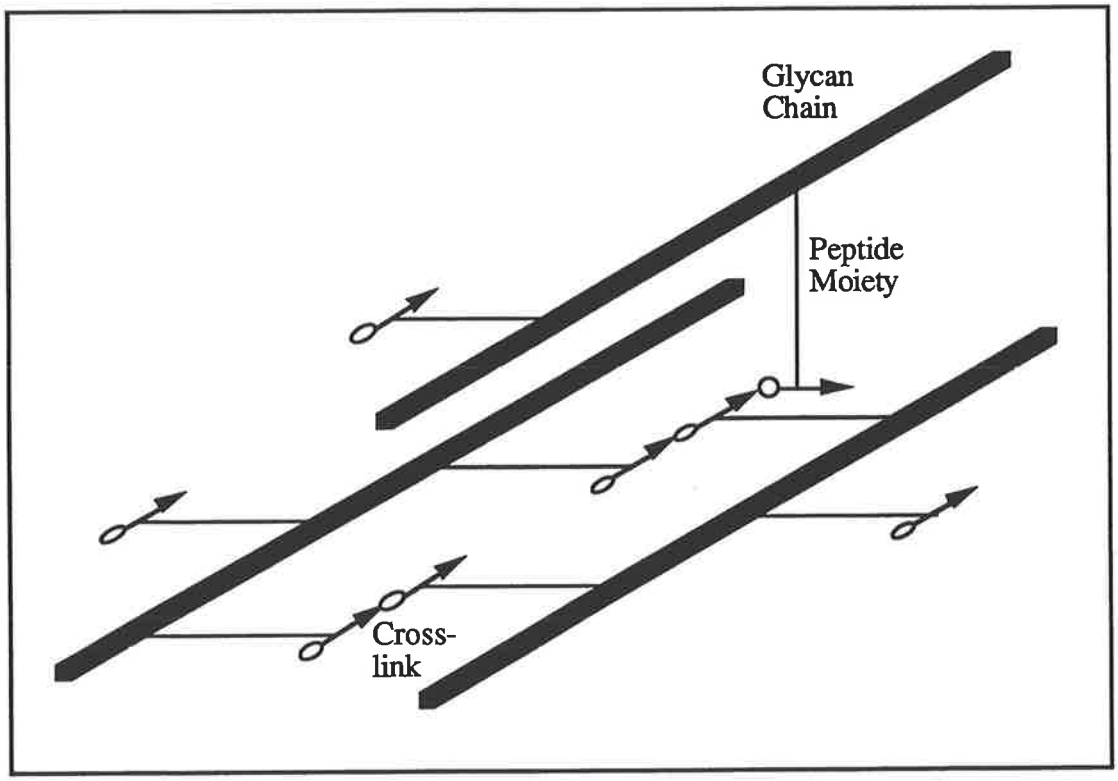

FIGURE 1.3 : *Probable peptidoglycan arrangement showing the relationship between glycan chains and peptide crosslinks (After Höltje and Glauner, 1990).*

These considerations plus evidence that polysaccharide chains are aligned perpendicular to the main (or long) axis of the bacterium (Verwer *et al.*, 1978) support the topologies. A possible relationship between glycan chains and peptide crosslinks is shown in Figure 1.3.

The possible methods for disrupting the cell wall and releasing the intracellular contents will now be reviewed.

1.2 Releasing Intracellular Protein

The release of an intracellular protein to the culture medium necessitates breakage of the cell wall, or permeabilization of the outer membrane for proteins located in the periplasm. Laboratory-scale techniques have previously been reviewed (Hughes *et al.*, 1971). Many methods are available at the laboratory scale, including ultrasonication, the French Press (Hughes *et al.*, 1971) and the Hughes Press (Hughes *et al.*, 1971). Techniques applicable for large-scale disruption are summarized in Figure 1.4. These will now be discussed.

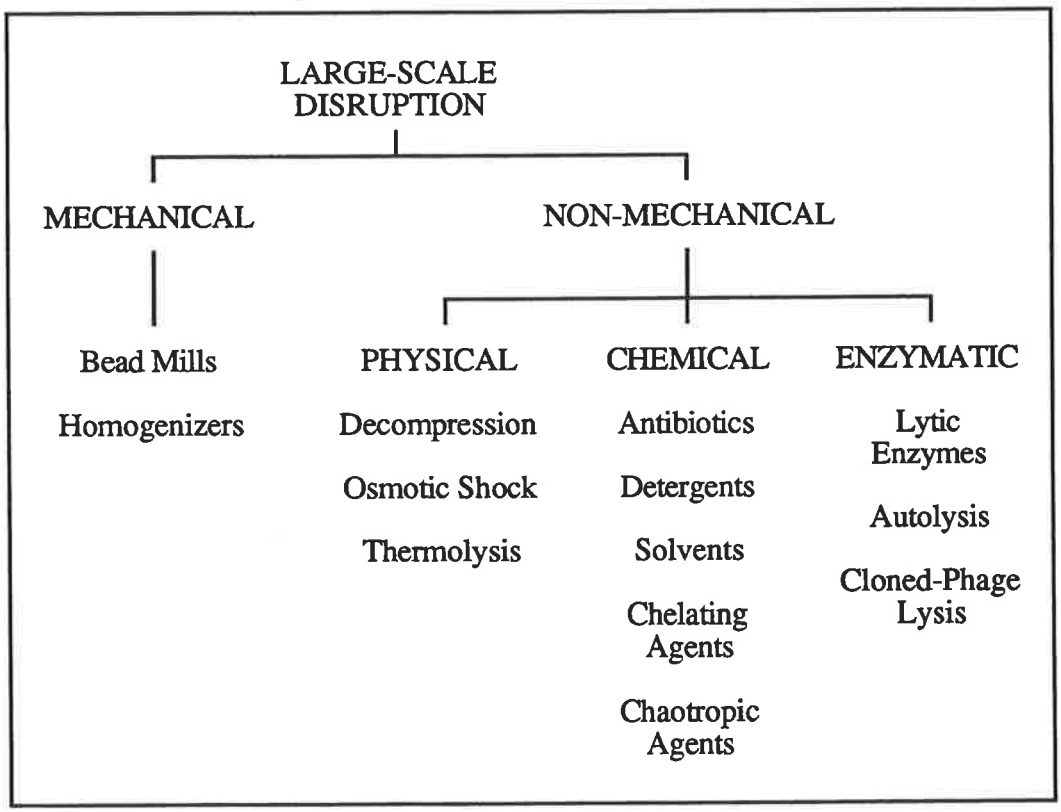

FIGURE 1.4 : *Techniques applicable for the large-scale disruption of microorganisms (After Wimpenny, 1967).*

1.2.1 Non-Mechanical Methods

In explosive decompression, a cell suspension is mixed with pressurized subcritical or supercritical gas for a specified time. Gas enters the cell, and expands on release of the applied pressure causing disruption. The technique has been used with yeast cells and has the advantage that supercritical carbon dioxide is capable of extracting off-flavours (Lin *et al.*, 1991; Lin *et al.*, 1992). *E. coli* have also been disrupted at the laboratory scale using decompression (Fraser, 1951). The technique has the advantage that it is extremely gentle, resulting in large debris and consequent ease of debris removal where the desired product is soluble. This is also a disadvantage, as the technique inherently has a low efficiency. Attempts to disrupt *E. coli* JM101 containing recombinant inclusion bodies were unsuccessful (*author's experience in conjunction with BioEng Inc, Arlington, MA, USA).* The technique proved too gentle to release the inclusion body, although soluble proteins were released.

In osmotic shock, cells are first equilibrated in a medium of high osmotic pressure (e.g. 1M sucrose) which is then suddenly diluted. Water rapidly enters the cell, increasing the internal pressure and causing lysis. The technique is restricted to weakened cells (Hughes *et al.*, 1971). Mild osmotic shock has been used to release proteins from *E. coli* without affecting cell viability (Neu and Heppel, 1965). It is usually considered only for small-scale operation due to the high cost of additives and the increased biological oxygen demand (BOD) of process waste.

Thermolysis on a large scale may become increasingly common. Cells are heated to 50-55°C to disrupt the outer membrane and release periplasmic proteins (Katsui *et al.*, 1982; Tsuchido *et al.*, 1985). At 90°C, Watson *et al.* (1987) report breakage of the cell wall and release of cytoplasmic contents within 10 minutes. Thus, the technique may be optimized for differential protein release. In addition, it can be operated to kill the host, thereby reducing process-validation requirements downstream of the fermenter. An additional

advantage arises if the product is resistant to the temperature used. In such cases, preferential protease deactivation may occur.

Chemical permeabilization of the outer wall membrane is an attractive method for the differential release of proteins (Asenjo and Patrick, 1990). The outer wall of *E. coli* can be permeabilized by a variety of chemical treatments, as reviewed by Naglak *et al.* (1990) and Hancock (1984). Agents such as ethylenediamine tetra-acetic acid (EDTA) disrupt the outer membrane by chelating divalent cations which cross-bridge adjacent LPS molecules. The membrane remains continuous after treatment, exhibiting no obvious fracture (Hancock, 1984). Ryan and Parulekar (1991) obtained enhanced excretion of β-lactamase by immobilized *Escherichia coli* through periodic exposure to EDTA. The treatment had the added advantage that an increase in β-lactamase production occurred due to the stabilization of plasmid-bearing cells. Detergents such as sodium dodecyl sulphate (SDS) and Triton X-100 may also be used to permeabilize the cell wall. They possess a high affinity for hydrophobic species and therefore solubilize the cytoplasmic membrane and outer wall fragments (Schnaitman, 1971). An obvious disadvantage of detergents is their potential to foul downstream microfiltration and ultrafiltration membranes. Non-polar solvents (e.g. toluene) also permeabilize the hydrophobic regions of the outer membrane, thereby allowing soluble protein release. Chaotropic agents such as urea or guanidine have been employed as they solubilize proteins from the membrane. Under harsher conditions than those for permeabilization, cell lysis and release of cytoplasmic contents may occur.

The release of intracellular proteins from *E. coli* at 4°C using a combined treatment of guanidine-HCl and Triton X-100 has been reported (Hettwer and Wang, 1989). Protein release varied in a complex manner with detergent and guanidine-HCl concentration. The process was characterized by low yields and a loss of enzyme activity through denaturation. Observations using electron microscopy suggest that protein release occurred in response to solubilization of the cytoplasmic membrane and molecular alteration of the outer wall. The peptidoglycan layer was not disrupted. Subsequent studies demonstrated that the technique

could also be employed under fermentation conditions (Naglak and Wang, 1992). Protein release in excess of 75% after 1 hour was obtained at 37°C using 0.4M guanidine-HCl plus 0.5% Triton X-100.

The addition of β-lactam antibiotics to a growing culture of *E. coli* causes cell lysis at high concentration. These antibiotics act on a class of proteins known as the penicillin binding proteins. Their action has been reviewed by Spratt (1980). The use of antibiotics on a large scale has not been reported.

Autolysis is an easily scaleable but poorly-understood method of protein release (Hopkins, 1991). The process relies on the production of lytic enzymes by the host which degrade the cell wall thus increasing its porosity and eventually causing lysis. Autolysis occurs in response to solvent shock, pH shock and thermal shock under milder conditions than those employed for lysis (Hopkins, 1991). It is affected by a large number of variables (Hughes *et al.*, 1971). The technique has been employed to prepare autolysed yeast and yeast hydrolysates for several decades (Hopkins, 1991). Leduc and van Heijenoort (1980) report the use of osmotic shock to induce *E. coli* autolysis in the laboratory. The autolysis of growing *E. coli* cultures triggered by low concentrations of moenomycin and cephaloridine has been examined (Leduc *et al.*, 1982; van Heijenoort *et al.*, 1983). Autolysis in harvested exponential-phase *E. coli* occurs in response to low levels of EDTA or osmotic shock (Leduc *et al.*, 1982; van Heijenoort *et al.*, 1983). Tuomanen *et al.* (1988) report that non-growing *E. coli* are resistant to autolysis induced by penicillin and chaotropic agents. At present, the large-scale autolysis of *E. coli* is unreported. This may change as a better understanding of the processes evolves.

The cloned-phage lysis of *E. coli* is likely to receive increased use for large-scale disruption. Sanchez-Ruiz (1989) examined the lysis of *E. coli* 15224 using the cloned phage ϕX174 gene E. Lysis efficiency was monitored by the release of cytoplasmic β-galactosidase. An eighty percent (80%) fractional release of protein was obtained 2.3 h after induction. The

mechanism of lysis is not fully understood. Lubitz *et al.* (1984) propose that the gene product interacts with the regulation of the host autolytic system. One of the disadvantages of phage lysis is that cellular contents may be significantly altered (Engler, 1985).

The addition of foreign lytic enzymes may also be used to cause cell lysis. The disruption of yeast cells by enzymatic lysis has been extensively studied (Andrews and Asenjo, 1987; Hunter and Asenjo, 1988; Hunter and Asenjo, 1990). Lysozyme catalyses the hydrolysis of β-1,4-glycosidic bonds, and may therefore be used to disrupt cell walls containing peptidoglycan (White and Marcus, 1988). In practice, gram-negative bacteria are less susceptible to lysozyme than gram-positive bacteria as the outer lipopolysaccharide (LPS) layer shields the peptidoglycan from the enzyme. For *E. coli*, lysozyme should be employed in conjunction with a chelating agent (e.g. EDTA) which disrupts the outer LPS layer (Salusbury, 1989). In all cases, enzymatic lysis has the advantage that it is specific and mild (Engler, 1985). It also results in large cellular debris which can be easily removed by centrifugation or filtration. Lysozyme derived from egg white is relatively cheap (Hopkins, 1991) although the introduction of protease activity may be a concern if the enzyme is not sufficiently pure. Immobilization of lysozyme may further reduce process operating costs (White and Marcus, 1988). In some cases, the addition of lytic enzyme may complicate downstream processing (Hopkins, 1991).

Huang *et al.* (1991) have developed a novel technique for product release from yeast. A combination of physical, chemical and enzymatic methods was employed to allow differential product release.

The use of non-mechanical methods as a conditioning step before mechanical disruption is likely to receive increasing use. Vogels and Kula (1992) used a short treatment with lytic enzyme or heat before mechanically disrupting *Bacillus cereus*. Greatly-improved disruption and a more favourable debris size distribution resulted when pretreatment was employed.

1.2.2 Mechanical Methods

Mechanical methods such as the bead mill and the high-pressure homogenizer are the preferred choice for the large-scale disruption of microorganisms (Kula and Schütte, 1987). This is partly historical, as non-mechanical methods for large-scale protein release have received scant attention. For many processes, however, mechanical methods will remain the first choice. This is partly due to the cost of chemicals and enzymes necessary for non-mechanical lysis on a large scale, and their relatively low efficiency for *E. coli*. As well, the addition of detergents and chaotropic chemicals may complicate subsequent downstream units (Hopkins, 1991) and inactivate the desired product (White and Marcus, 1988). Further, whenever the desired product is expressed as an insoluble inclusion body, mechanical disruption is the prime alternative. In such cases, the aim is to minimize the debris size to allow collection of the inclusion bodies by centrifugation (Hoare and Dunnill, 1989). Enzymatic or chemical lysis is impractical as large quantities of enzyme and detergent and long residence times will be required to achieve an acceptable debris size. Bead mills and homogenizers also offer the advantages of continuous operation, short residence times to minimize product degradation and contained operation (Keshavarz *et al.*, 1987).

Bead mills were originally designed to wet-grind pigments for the paint industry (Hopkins, 1991; Kula and Schütte, 1987). The mill consists of a horizontal chamber surrounded with a cooling jacket. An agitator shaft rotates within the chamber, and is fitted with impellers (discs, rings or pins) which transfer the kinetic energy of rotation to small glass beads within the chamber (Kula and Schütte, 1987). Cell disruption occurs in the contact zones of the grinding beads (Bunge *et al.*, 1992). Disruption efficiency is affected by many operating variables, including agitator speed, bead size and suspension feed rate (Kula and Schütte, 1987). Two operational regimes have been identified, and are differentiated on the basis of whether or not disruption correlates with specific energy input (Bunge *et al.*, 1992).

High-pressure homogenizers for cell disintegration are modified machines originally developed for the food and pharmaceutical industries (Hopkins, 1991; Kula and Schütte, 1987). The homogenizer is preferred for the large-scale disruption of non-filamentous organisms (Hopkins, 1991). Given this preferred status, it is likely that the homogenizer will receive increased use in first-generation processes. A detailed examination of the unit operation and existing models for the high-pressure homogenizer is therefore appropriate.

1.3 The Mechanism of Disruption During Homogenization

The traditional high-pressure homogenizer consists essentially of a positive-displacement pump which forces a cell suspension through a spring-loaded or hydraulically-controlled valve arrangement (Figure 1.5).

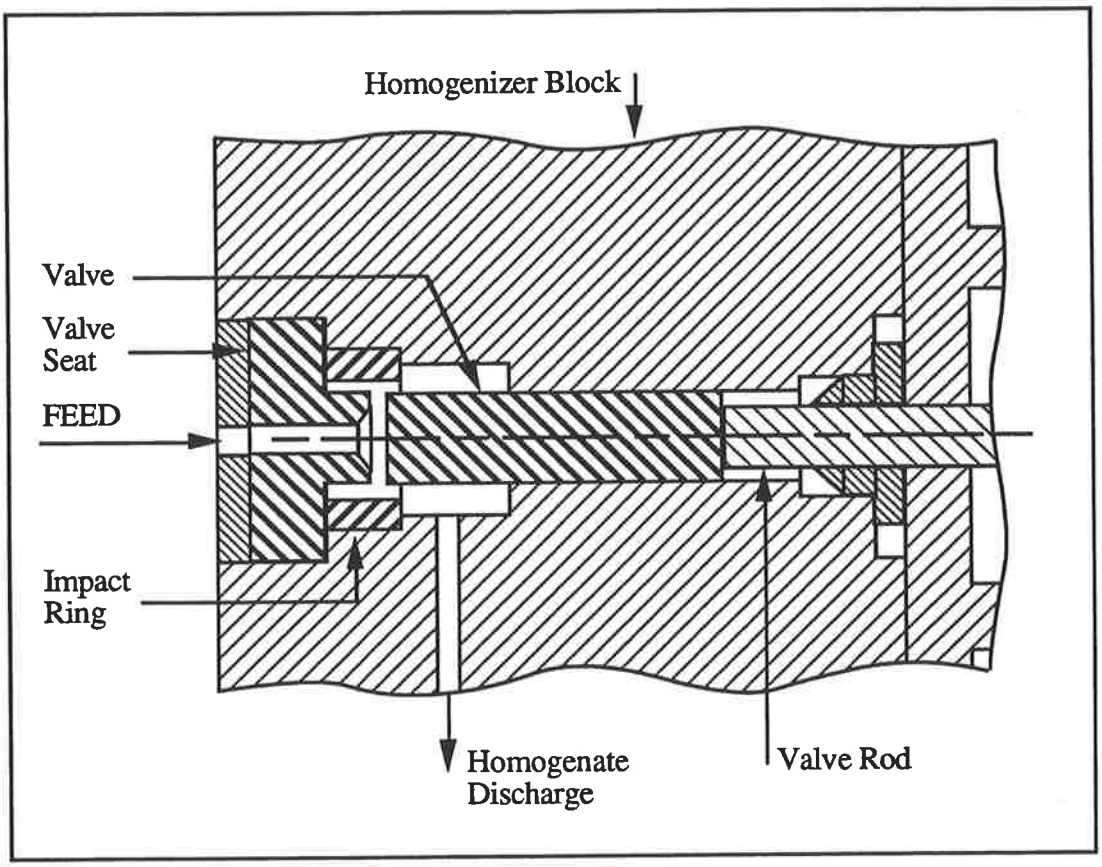

FIGURE 1.5 : *Cross-section of a high-pressure homogenizer showing valve arrangement (APV-Gaulin 15M-8TA).*

As the fluid is compressed, the valve opens and suspension accelerates radially through the slit. The valve lift is low for small homogenizers, typically 10 to 20 μm at high pressure. As a result, high radial velocities (of the order of 200 to 300 m s^{-1}) occur near the valve entrance. Upon leaving the valve, fluid flows radially and strikes an impact ring. The suspension then exits the valve assembly and flows to either a second valve or to discharge.

A common small-scale (55 L h^{-1}) machine is the APV-Gaulin 15M homogenizer which has a single-acting simplex pump capable of operating at 75 MPa. For large-scale processing, homogenizers with multiple pistons providing an almost constant pressure in excess of 100 MPa are available (e.g. APV-Gaulin's 30-CD).

Much of the initial work into the mechanism of homogenization was concerned with the disruption of fat globules. Energy density, depending on the pressure drop and the time scale of the process, is identified as the most significant variable affecting fat globule disruption (Walstra, 1969). Phipps (1971, 1974a) suggests that shattering effects, shearing between valve faces, cavitation and turbulence are not responsible for disruption. Experimental studies suggest that disruption is complete in a zone near the valve entrance (Phipps, 1974b). Viscous shear stresses operating at the inlet to the valve slit are believed important (Phipps, 1975). Pandolfe and Kinney (1983) suggest that turbulence and cavitation are the only important mechanisms. There is general consensus that impingement on the impact ring does not contribute to the disruption of fat globules (McKillop *et al.*, 1955; Pandolfe, 1982; Pandolfe and Kinney, 1983).

Initial attempts to explain the disruption of microorganisms relied on the studies of milk-fat globules. Clearly, the stress field is related to the rate and magnitude of the pressure drop, and these factors have been cited as a major cause of disruption in microorganisms (Brookman, 1974; Brookman, 1975; Kelemen and Sharpe, 1979). However, Brookman's (1975) results may be interpreted in terms of a shear-stress mechanism (Engler, 1979). The application of shear stress has been shown to disrupt human erythrocytes (Williams, 1972). These lack a rigid wall and therefore are particularly shear sensitive. In many homogenizers, flow conditions in the valve may be turbulent (Phipps, 1975) and the buffeting of cells by small-scale eddies has been proposed as an agent for disruption (Doulah *et al.*, 1975). Given the extremely high velocities at the slit entrance, local cavitation in the fluid may occur in certain homogenizers. Cavitation is important in disrupting cells during ultrasound treatment (Doulah, 1977), and may be important in homogenization. Recent studies using a

specially-constructed impingement device identify impact of the fluid leaving the valve slit on the impact ring, and the resultant stresses, as a major cause of disruption (Engler, 1979; Engler and Robinson, 1981). Engler (1979) concludes that rapid release of pressure, by itself, does not cause significant disruption of yeast. Normal stresses are only 20% as efficient as impact (Engler and Robinson, 1981). The importance of impact for the disruption of yeast has been confirmed using a high-pressure homogenizer. Keshavarz Moore *et al.* (1990) show that disruption efficiency is significantly degraded by removing the impact ring or increasing its diameter. This contrasts with the observation that disruption efficiency for fat globules is not reduced by removal of the impact ring.

While impact appears to be the dominant mechanism in yeast disruption, it is likely that a combination of the above stresses is responsible for the disintegration of cells during homogenization.

1.4 Previous Homogenizer Studies and Modelling

A precise and detailed understanding of the homogenization process is not available. This has limited the extent to which the unit operation has been modelled. Existing models are empirical and require system- and culture-specific parameters (i.e. the parameters depend on the particular homogenizer and valve (the system) **and** the characteristics of the feed material (the culture)). As indicated earlier, this is unacceptable if simulation and optimization are to make significant contributions to the design of biochemical processes.

Follows *et al.* (1971) examined the release of enzymes from yeast by homogenization. Enzymes were released at various rates depending on their location within the cell. Soluble enzymes were released at the same rate as total soluble protein. Enzymes located outside the cell membrane were released faster, while enzymes contained within cellular components were released at a slower rate.

The most-widely accepted model for homogenization was developed by Hetherington *et al.* (1971). Yeast disruption in a Manton-Gaulin homogenizer was examined. Soluble protein release was described by a kinetic-rate law as follows,

$$\ln\left(\frac{1}{1-R_p}\right) = k_1 N P^a \qquad -(1.1)$$

where R_p is the fractional release of soluble protein, N is the number of homogenizer passes and P is the homogenizer pressure. The rate constant, k_1, varied with temperature and the exponent, a, equalled 2.9. Gray *et al.* (1972) subsequently determined the exponent as 2.2 for *E. coli* grown on a simple synthetic medium using glycerol as the carbon source. There is some evidence to suggest that the exponent, a, may vary with pressure (Dunnill and Lilly, 1975; Engler and Robinson, 1981).

Augenstein *et al.* (1974) examined the release of a shear-sensitive enzyme from *Bacillus brevis* by high-pressure homogenization. The two competing processes of release and degradation were identified. The rate constant of each process was a function of homogenizer pressure. A plot of enzyme activity in the broth versus an empirical "homogenization factor" revealed a distinct maximum. The homogenization factor, θ_H, is defined by equation (1.2) and is simply a measure of the total cellular disruption by analogy with equation (1.1).

$$\theta_H = N P^{1.8} \qquad -(1.2)$$

Equation (1.1) was modified by Sauer *et al.* (1989) who examined the disruption of recombinant and non-recombinant *E. coli* in a Microfluidizer®. The Microfluidizer operates on a different principle to the high-pressure homogenizer. Essentially, two streams of cell suspension are impacted at high velocity. Sauer *et al.* (1989) determined disruption to be dependent on the type of strain, growth rate and concentration of the cells, disruption pressure, and the number of passes through the disruptor. An additional exponent, b, which varied linearly with cell concentration and dilution rate was introduced, producing a modified equation.

$$\ln\left(\frac{1}{1-R_p}\right) = k_2 N^b P^a \qquad -(1.3)$$

No systematic effects of growth rate and concentration on the exponent a and constant k_2 were determined. Average values for these parameters are presented for specific strains at specific growth rates (i.e. for specific cultures) which allow the disruption to be described to ±20%.

Equation (1.1) was used by Harrison *et al.* (1991) to describe the release of soluble protein from *Alcaligenes eutrophus* by high-pressure homogenization. The release of DNA, R_D,

was seen to be slower than soluble protein release, and was modelled by equation (1.4) for pressures between 30 and 70 MPa.

$$\ln\left(\frac{1}{1-R_D}\right) = k_3 (N-0.75) P^{a'} \qquad -(1.4)$$

The disruption of *Alcaligenes eutrophus* was seen to be a two-stage process. The primary 'rupture' stage involved a point break in the cell envelope. The second 'disintegration' stage involved further breakage of the wall and a reduction of the cell debris size. Disruption was highly dependent upon growth phase, with exponential-phase cells showing an increased dependence on operating pressure. Disruption was not significantly affected by an increase in size of more than 30%. This increase in size was accompanied by a change in cell shape and the accumulation of solid intracellular poly-β-hydroxybutyrate (PHB) granules.

The model proposed by Doulah *et al.* (1975) represents the only attempt to establish a mechanistic model for cell disruption. Cells are assumed to be buffeted by turbulent eddies and consequently oscillate. When the kinetic energy of oscillation exceeds an effective cell-surface energy, disruption occurs. The maximum diameter of a spherical cell surviving homogenization, d_m, was related to pressure by equation (1.5)

$$d_m \propto \frac{\gamma}{P} \qquad -(1.5)$$

where γ represents some effective wall strength, and P is the homogenizer operating pressure. No method for predicting cell-wall strength was presented. Further, the model does not yield a first-order response to multiple passes and does not allow for 100% disruption after repeated passes unless the wall is weakened by repeated passes through the homogenizer (Engler, 1985).

Keshavarz-Moore *et al.* (1990) presented an expression for stagnation pressure at the impact ring (eq. (1.6))

$$P_s \propto \frac{1}{Y^2 h^2} \qquad -(1.6)$$

where h is the slit width and Y is the distance between valve exit and impact ring. The disruption of yeast in an APV-Gaulin 15M homogenizer operating at 46 MPa was examined. The constant k_1 in equation (1.1) was correlated against stagnation pressure for several valve geometries (h varied) and several impact ring diameters (Y varied). As previously indicated, this work stresses the importance of impact as an agent for the disruption of yeast cells.

Engler and Robinson (1981) correlated the disruption of *Candida utilis* against stagnation pressure for an impingement device, where stagnation pressure is given by equation (1.7).

$$P_s = \frac{1}{2} \rho u^2 \qquad -(1.7)$$

The stress created within a fluid upon impingement equals the dynamic pressure of the fluid acting against the plate. A reasonable approximation assumes this stress acts on the impacting cell, thereby justifying the correlation of disruption with this parameter. Note that for a high-pressure homogenizer, velocity, u, is inversely proportional to slit width, h. Hence equations (1.6) and (1.7) are equivalent for constant Y.

1.5 Factors Affecting Homogenizer Performance

The disruption, or the volume fraction of cells destroyed, cannot be predicted for a given system (i.e. homogenizer and valve) with the current models. Both equations (1.1) and (1.3) provide a good description of disruption data, but require culture-specific constants which are difficult to relate to measurable feed characteristics. This point is emphasized by Engler (1985) who writes :

> *"There is not enough information available to predict a priori the relative resistance of various organisms to mechanical disruption."*

The problem is more acute than the above statement implies. The relative resistance of different organisms cannot be predicted, but neither can the relative resistance of different cultures of the same organism. Engler (1979) shows that *Candida utilis* cells grown at a higher specific growth rate were more easily disrupted than those grown at a lower rate. For *E. coli*, Gray *et al.* (1972) report that cells grown on a synthetic medium are more easily disrupted than those grown on a complex medium containing yeast extract. Lilly (1979) states that exponential-phase *E. coli* are easier to disrupt than stationary-phase cultures. Sauer *et al.* (1989) presented values for the exponent a (eq. 1.3) varying between 0.6 and 1.77 depending in an undetermined manner on the strain of *E. coli* and its growth rate. Variation in the constant k_2 was greater, varying over an order of magnitude between 0.27×10^{-3} and 16.0×10^{-3} MPa^{-a}. Unexplained dependencies on strain, growth phase and media in a given system, such as these, must be eliminated and rigorous models developed if simulation is to be employed. The need for a better homogenizer model has been stressed by Gritsis and Titchener-Hooker (1989) :

"The only models existing to describe this key operation are at best semi-empirical by nature and are not based on a firm understanding of the mechanisms which result in disruption."

It has been recognized that the key cell-related parameters affecting disruption are the degree of wall cross-linking and the size and shape of the cell (Kelemen and Sharpe, 1979; Nesaratnam *et al.*, 1982; Engler, 1985). In addition, populations of bacteria such as *E. coli* are heterogenous due to the presence of dividing cells. The degree of heterogeneity may also be an important parameter affecting disruption. Engler and Robinson (1981) suggested that bud scars in yeast may introduce local areas of different strength in the wall. Thacker (1973) has shown that dividing *Saccharomyces cells* are more sensitive to ultrasound than non-dividing cells. Population heterogeneity is also identified as important by Kelemen and Sharpe (1979). A suspension of *Lactobacillus casei* was homogenized at low pressure. No further disruption was obtained when the culture was homogenized a second time at low pressure. This suggested that disruption is a non-random process related to some physical characteristic of the population.

No systematic study of the effects of wall structure, cell size and population heterogeneity has been published. Such a study is certainly possible, particularly for *E. coli* as the wall structure is well understood. We will now briefly review the influence of these parameters on the ease of disruption for *E. coli*.

1.5.1 Wall Structure

The structure of the *E. coli* wall was reviewed in section 1.1. Normally, cell-wall strength is attributed solely to the peptidoglycan layer. Schwarz and Leutgeb (1971) demonstrated that exponential-phase *E. coli* cultures possess a much lower degree of peptidoglycan crosslinkage than stationary-phase cultures using paper chromatography. Subsequent studies employing a more accurate chromatographic technique (Glauner, 1988) confirmed

considerable changes in peptidoglycan structure during the transition from exponential phase to stationary phase (Pisabarro *et al.*, 1985). In particular, the degree of crosslinkage increased significantly. The formation of a novel cross bridge between two adjacent meso-diaminopimelic acid residues in the peptidoglycan (Figure 1.2) is responsible for the major portion of this increase (Glauner and Schwarz, 1983; Glauner *et al.*, 1988). This chromatographic technique also reveals the existence of trimers, thereby confirming the multi-layered architecture of peptidoglycan. Trimers are essentially three disaccharide units joined together by peptide bonds. The frequency of these trimers is higher in slow-growing or stationary-phase bacteria than during exponential growth, implying a denser or thicker peptidoglycan layer (Pisabarro *et al.*, 1985; Tuomanen and Cozens, 1987). This increase in thickness has been measured using electron microscopy (Leduc *et al.*, 1989a).

Stationary-phase bacteria therefore have a thicker and more highly crosslinked peptidoglycan layer. Verwer *et al.* (1980) report that the peptide crosslinks in *E. coli* are broken in preference to the glycan chains during ultrasonication. A thicker wall with a higher degree of crosslinkage will therefore be harder to disrupt mechanically.

The peptidoglycan layer may not be the sole determinant of cell-wall strength. Leduc *et al.* (1989b) found nine different proteins associated with the peptidoglycan layer, including five lipoproteins. The outer membrane of *E. coli* can maintain the cell shape under certain circumstances (Henning, 1975), and it has been proposed that lipopolysaccharides are organized in a network which may serve as the skeleton of the cell wall (Zorzopulos *et al.*, 1989). Studies demonstrate that the amount of lipoprotein covalently bound to the peptidoglycan sacculus is higher in slow-growing or stationary bacteria than during exponential growth (Pisabarro *et al.*, 1985; Tuomanen and Cozens, 1987; Driehuis and Wouters, 1987). The effect of the outer membrane on wall strength may need to be accounted for when modelling any disruption step for *E. coli*.

1.5.2 Cell Size

E. coli are rod-shaped. Individual cell diameters vary by 8% within a population of slowly growing *E. coli* B/r (Trueba and Woldringh, 1980). The variability is lower at higher growth rates. For *E. coli* K12 strain MC4100 *lysA*, diameter variation during the cell cycle is less and possibly negligible (Nanninga *et al.*, 1990). From a modelling perspective, cells within a given population of *E. coli* may be assumed to have the same diameter.

The average cell diameter of an *E. coli* population increases as the culture growth rate is increased (Grover *et al.*, 1977; Pierucci, 1978). Likewise, average cell length increases for faster-growing populations (Grover *et al.*, 1977; Pierucci, 1978). Despite these variations, the general form of the volume distribution is independent of growth rate (Kubitschek, 1969). Nesaratnam *et al.* (1982) studied the disruption of *Klebsiella pneumoniae* by ultrasonication. They suggested that cells were easier to disrupt at high growth rates because of increased cell size. The same dependence of disruption ease on size may be expected for *E. coli*.

1.5.3 Population Heterogeneity

As indicated, septated cells may be easier to disrupt during homogenization than non-dividing cells. This fact is intuitive, as the division site may act as a stress concentration point. The percentage of constricted cells in a population depends on growth rate. Faster-growing populations of *E. coli* B/r possess a higher fraction of constricted cells (Kubitschek, 1969). When a population enters the stationary phase following log growth, the fraction of constricted cells decreases (Wanner and Elgi, 1990). A study by de Jonge *et al.* (1989) shows peptidoglycan crosslinkage, lipoprotein content and average glycan-chain length remain constant throughout the cell cycle. This indicates that dividing cells will have the same wall characteristics as non-dividing cells. The only heterogeneity is therefore due to stress concentration at the septation site.

In summary, faster-growing or exponential-phase populations of *E. coli* possess a lower degree of peptidoglycan crosslinkage, larger individual cells and a higher fraction of constricted cells. They should therefore be easier to disrupt. This correlates with the increased disruption ease of exponential-phase cultures reported by Lilly (1979).

In the next chapter a new model for the disruption of *E. coli* by high-pressure homogenization is developed. In subsequent chapters the model is verified by varying the culture-specific parameters (wall structure, size and septated fraction) and its predictive ability is tested. It will be shown that the model includes the most significant variables affecting the disruption of *E. coli* in a given homogenizer. The model developed in this thesis is the first to allow true *a priori* prediction of disruption for a given system using measurable feed characteristics.

CHAPTER 2

MODEL DEVELOPMENT

Existing models for high-pressure homogenization were reviewed in the preceding chapter. The major deficiency of the principal model of homogenizer performance is that the two parameters (namely a and k_1) vary in an uncorrelated fashion with the properties of the feed cells. A further complication is the variation of these same parameters with the homogenizer valve, or system, used. As indicated, Keshavarz-Moore *et al.* (1990) have made some progress by correlating the first-order rate constant (k_1 in eq. 1.1) with valve design for baker's yeast disrupted at 46 MPa with up to five passes. However, no successful correlation of the key parameters with cell properties for a given homogenizer has been reported. Difficulty in deducing such a correlation is an artefact of the structure of equation (1.1). The model is derived from descriptive rather than prescriptive considerations. The key parameters have no physically-identifiable basis. Therefore, correlation of the key parameters with system and culture variables is exceedingly difficult.

In this chapter a new model for high-pressure homogenization is proposed. The key considerations underpinning this model are :

- Disruption is opposed by the cell wall. This wall possesses "strength", which may be defined as an ability to resist an applied disruptive stress. A given population contains cells with a distribution of strengths. This distribution is a population characteristic, and is independent of the particular applied stress distribution.

- The homogenizer applies a continuous distribution of stresses to a population of cells during homogenization. If the stress applied to a given cell exceeds its strength, disruption results. The form of this distribution is a characteristic of the system (i.e. homogenizer and valve), and is independent of the particular culture used.

This approach separates the system- and culture-specific factors affecting disruption. Therefore, it is possible to maintain the system-specific parameters constant while seeking a correlation of the key culture-related parameters with culture properties, and vice versa. This is preferable to the traditional approach, where system and culture variability influence the same parameters.

The key requirement for the success of this approach is a knowledge of approximate forms for the stress and strength distributions. These will now be proposed. In section 2.3, the distributions are combined to give the final homogenizer model for a single pass through the homogenizer. In section 2.4, the model is extended for multiple passes without the introduction of additional parameters. This extension underlines the advantage of the selected approach. In section 2.5, the underlying assertions of the model are stated. Finally, the experimental aims and the thesis structure are outlined.

2.1 The Cell Strength Distribution

Cells are assumed to possess a distribution of effective strengths, $f_S(S)$, where strength, S, is defined as the ability to resist an applied disruptive stress. In the absence of evidence to the contrary, it is proposed that the distribution of effective strengths, $f_S(S)$, is normal or Gaussian. This postulate is plausible considering the large number of bonds involved in providing strength. The effective-strength distribution is therefore expressed as equation (2.1),

$$f_S(S) = \frac{1}{\sigma\sqrt{2\pi}} \exp\left[\frac{-(S-\bar{S})^2}{2\sigma^2}\right] \qquad \text{-(2.1)}$$

where $\bar{S}$ is the mean effective strength and σ^2 is the distribution variance.

As indicated in section 1.5, a population of *E. coli* is heterogeneous due to the presence of septated cells. Septated cells may be weaker than non-septated cells. The division site will act as a stress concentrator. Therefore, an alternative choice assumes a bimodal distribution of effective strengths. Equation (2.2) presents the form of a bimodal-normal distribution, where x_s is the volume fraction of the population which is septated.

$$f_B(S) = \frac{x_s}{\sigma_s\sqrt{2\pi}} \exp\left[\frac{-(S-\bar{S}_s)^2}{2\sigma_s^2}\right] + \frac{1-x_s}{\sigma_n\sqrt{2\pi}} \exp\left[\frac{-(S-\bar{S}_n)^2}{2\sigma_n^2}\right] \qquad \text{-(2.2)}$$

The distribution of effective strengths is characterized by either two ($\bar{S}$ and σ) or five parameters ($\bar{S}_s$, $\bar{S}_n$, x_s, σ_s and σ_n). These parameters describe the strength characteristics of the culture. They will vary with the cell parameters identified as important in section 1.5, namely cell size and cell wall structure. The parameters will correlate with these properties.

2.2 The Homogenizer Stress Distribution

As outlined in section 1.3, impingement of cells on the impact ring appears to be the dominant mechanism of disruption. The exact processes occurring during impingement have not been characterized. Despite this lack of detailed knowledge, the choice for the stress distribution, $f_D(S)$, should reflect the physics of impact. Vervoorn and Austin (1990) studied the impact of small cylinders (a reasonable approximation to the geometry of *E. coli*) against a plane surface. They reported that the cumulative fraction of impacts with a force greater than F, $f_D(F)$, could be adequately represented by an empirical function of the following form,

$$1 - f_D(F) = \frac{1}{1 + \left(\frac{F}{F_m}\right)^{-5}} \qquad \text{-(2.3)}$$

where F_m is the median maximum force registered at impact (i.e. the force at which 50% of the impacts have a maximum force greater than F_m). Equation (2.3) is proposed as an adequate approximation for a homogenizer. The stress distribution imposed on the cells is therefore given by equation (2.4),

$$f_D(S) = \frac{S_m^d}{S^d + S_m^d} \qquad \text{-(2.4)}$$

where $f_D(S)$ is the fraction of events with a disruptive stress greater than S, d is a general coefficient to be determined and S_m is the median maximum stress experienced. A power-law dependence of S_m on homogenizer pressure (eq. (2.5)) is proposed. This assumption is justifiable, as the median maximum disruptive stress should increase with homogenization pressure regardless of the exact mechanism of disruption.

$$S_m = m P^n \qquad \text{-(2.5)}$$

Combining these considerations produces the final form for $f_D(S)$, equation (2.6).

$$f_D(S) = \frac{(mP^n)^d}{S^d + (mP^n)^d} \qquad -(2.6)$$

Equation (2.6) relates the fraction of events with a disruptive stress greater than S to the disruptive stress and the homogenizer pressure, P. The distribution is characterized by three parameters: m, n and d. The parameters will be independent of the properties of the feed cells provided equation (2.6) is a close approximation to the true homogenizer-stress distribution (i.e. m, n and d will be constant for a given system).

2.3 Disruption : Single Homogenizer Pass

Sections 2.1 and 2.2 give forms for the cell-strength distribution and the homogenizer-stress distribution, respectively. Throughout this thesis, equation (2.1) is assumed to represent the effective-strength distribution due to its simplicity compared with equation (2.2). The effect of neglecting culture heterogeneity is addressed in chapter 7.

Equation (2.6) is an expression for $f_D(S)$, the fraction of events with a disruptive stress greater than S. This may be viewed as the probability that a cell of strength S is disrupted during homogenization. Combination with the cell-strength distribution, equation (2.1), therefore allows disruption to be calculated. This concept is illustrated in Figure 2.1. With reference to the strength distribution, the fraction of cells with an effective strength between S and S+dS is $f_S(S)\,dS$. Multiplying by the probability of disruption, $f_D(S)$, gives the fraction of these cells disrupted during homogenization (eq. (2.7)).

$$dD(S) = f_S(S)\, f_D(S)\, dS \qquad -(2.7)$$

An expression for the total disruption of a bacterial population (i.e. the volume fraction of cells destroyed) is deduced by integration.

$$D = \int_0^\infty f_D(S)\, f_S(S)\, dS \qquad -(2.8)$$

The postulated distributions, equations (2.1) and (2.6), may be used in conjunction with equation (2.8) to determine disruption at a given pressure. Estimates of the five parameters are required. However, the parameters are best considered in two groups :

- Culture-related ($\bar{S}$ and σ);
- System-specific (m, n and d).

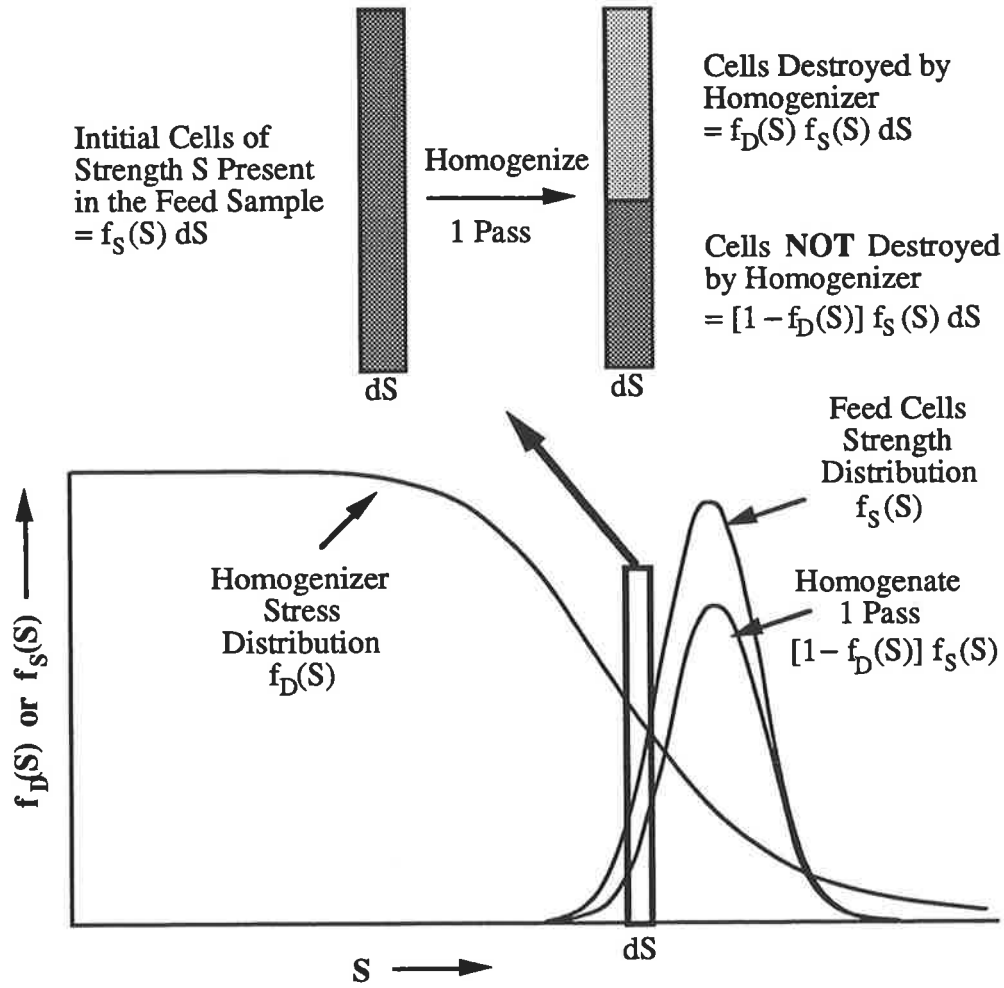

FIGURE 2.1 : *The combination of a homogenizer-stress distribution with a cell strength distribution allows disruption to be calculated.*

2.4 Disruption : Multiple Homogenizer Passes

Repeated application of a stress distribution on the effective-strength distribution allows disruption to be predicted for multiple homogenizer passes. Logically, if $f_D(S)$ is the probability of disruption, then $1-f_D(S)$ is the probability of surviving one homogenizer pass. Equation (2.9) therefore gives the fraction of cells of strength S not disrupted, $d\phi(S)$.

$$d\phi(S) = 1 - dD(S) = [1-f_D(S)]\, f_S(S)\, dS \qquad -(2.9)$$

The probability of surviving N homogenizer passes is $(1-f_D(S))^N$. The fraction of cells of strength S surviving N homogenizer passes is given by equation (2.10).

$$d\phi(S) = [1-f_D(S)]^N\, f_S(S)\, dS \qquad -(2.10)$$

Integration provides the total fraction not disrupted in a given population (1–D). Thus, total disruption for N homogenizer passes is provided by equation (2.11).

$$D = 1 - \int_0^\infty [1-f_D(S)]^N\, f_S(S)\, dS \qquad -(2.11)$$

The concept behind equation (2.11) is illustrated in Figure 2.2. The extension to multiple passes is logical and no additional parameters have been introduced apart from N. Equation (2.11) clearly reduces to equation (2.8) for N=1.

Equation (2.11) emphasizes the utility of separating the system-specific and culture-related parameters. The separate physical effects are readily identifiable. Clearly, equation (2.11) will only predict the correct disruption for multiple homogenizer passes if the selected strength and stress distributions are independent and a close approximation to the true distributions.

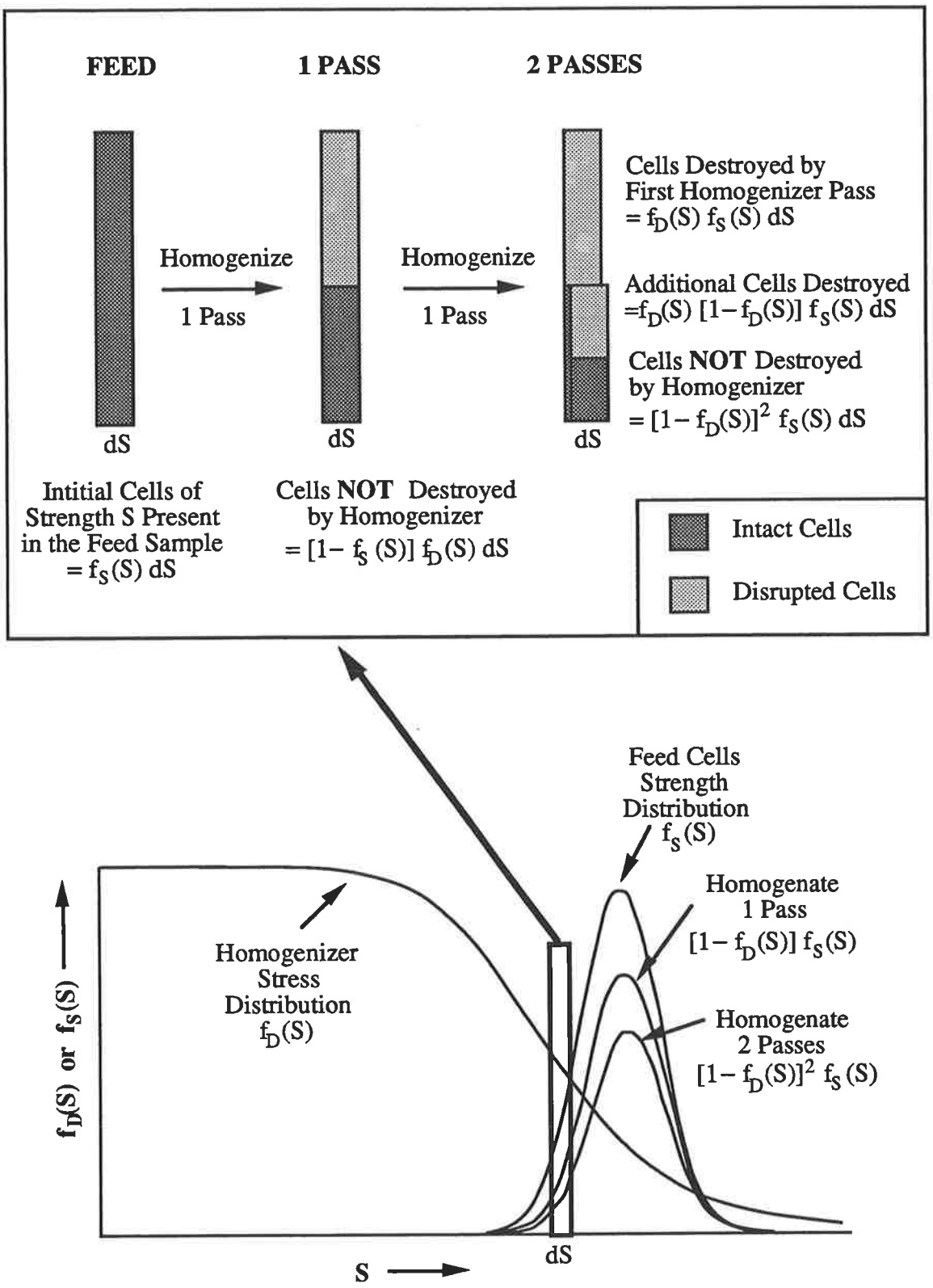

FIGURE 2.2 : *Extension of the homogenizer model to multiple passes by repeated application of the stress distribution.*

2.5 Model Assertions

It is appropriate to state the assertions regarding the proposed model :

i) The homogenizer stress distribution, equation (2.6), is independent of the properties of the feed cells. The parameters m, n and d are **system-specific** and **culture-independent**. Their values are thus uniquely determined by factors affecting the stress distribution (e.g. valve configuration and homogenizer type) regardless of the type of feed material.

ii) Equation (2.1) is a reasonable approximation to the true effective-strength distribution. It is a measure of a **population's** ability to resist disruption, and is therefore **independent** of the particular stress distribution acting.

iii) The effective-strength distribution for *E. coli* will be affected by cell size and wall structure. The mean effective strength of the population, $\bar{S}$, will correlate with these properties.

iv) The effective-strength distribution has a fixed standard deviation for a specified strain of *E. coli* (i.e. σ is constant). No logical reason exists to justify a counter assumption.

The model includes a large number of parameters, reflecting the combinational nature of the problem. Each of the parameters is physically meaningful. Provided the preceding assertions are valid, four of the five parameters become constant in the most important practical application. This corresponds to the case of a fixed homogenizer (m, n and d constant) disrupting a specific strain of *E. coli* (σ constant). Variability in the feed stream is characterized by a single parameter : the mean effective cell strength of the population, $\bar{S}$.

In section 1.5, three key factors were identified as affecting cell strength for *E. coli*, namely wall structure (specifically peptidoglycan crosslinkage and amount of bound lipoprotein), cell size and culture heterogeneity. The effect of culture heterogeneity on strength is neglected by assuming that equation (2.1) is an adequate approximation to the true strength distribution. Mean effective strength, $\bar{S}$, should therefore correlate with wall structure and cell size. Given such a correlation, and the four system- and strain-specific constants, disruption can be predicted with zero degrees of freedom.

In summary, the following are required to allow the prediction of disruption :

a) values of the system-specific parameters (m, n and d);

b) the distribution variance, σ^2, which is assumed to be a strain-specific parameter;

c) a correlation of $\bar{S}$ with measurable cell properties.

2.6 Thesis Structure

Absolute verification of the model would require numerous tests with an infinite variety of homogenizers, valves and bacterial strains. This is obviously not practical given realistic time and equipment constraints. Therefore, the experimental work undertaken in this study aims to verify the previously-stated assertions regarding the model, and to emphasize the model's predictive capabilities. In addition, the effect of including culture heterogeneity explicitly as a model parameter is considered.

To prove the value of the model and the selected approach, a **single system** and a **single bacterial strain** are employed. The influence of culture variability on disruption is characterized and a correlation for mean effective cell strength in terms of physically measurable cell-population characteristics is obtained. The model is then employed to successfully provide true predictions of disruption data for two bacterial strains grown on two different carbon sources, with multiple homogenizer passes at several pressures.

The overall thesis structure is illustrated in Figure 2.3. A prime requirement for successfully modelling homogenization is a sensitive and accurate measure of the dependent variable: **disruption**. Existing techniques are accurate at low levels of disruption. Unfortunately, the absolute error of the measurement increases as complete disruption (D=100%) is approached. Our prime concern as biochemical engineers is to ensure a high level of disruption. However, existing measurement techniques are inadequate for this important practical regime. To overcome this deficiency, a novel method of measuring disruption was developed and compared with traditional techniques. This is explained in the following chapter.

Thereafter, in chapter 4, a series of disruption studies are outlined for a range of *E. coli* cultures. The data are regressed to the proposed model to determine the system- (m, n and d) and strain-specific (σ) parameters. The results support assertions (i) and (iv) by

confirming that the system- and strain-specific variables (m, n, d and σ) are independent of culture variations. Assertion (ii) is supported implicitly, as the stress distribution is continually varying with pressure.

Correlations for mean effective strength ($\bar{S}$) with peptidoglycan crosslinkage and mean cell length are determined in chapter 5. The correlations allow the mean effective strength of a culture to be predicted.

In chapter 6, the results are employed to predict the disruption of *E. coli* with multiple homogenizer passes. The model is shown to accurately predict disruption for two different strains of *E. coli* grown on two different carbon sources. It should be noted that the model parameters are obtained (in chapters 4 and 5) for one strain of *E. coli* grown on glucose. The excellent prediction obtained for multiple passes confirms the fundamental significance of the selected strength and stress distributions.

Equation (2.1) does not account for any effect which culture heterogeneity has on the effective-strength distribution. In chapter 7, the possibility that septated cells are weaker is examined using a culture with an abnormally-high septated fraction. The results suggest that dividing cells are weaker, but also show that the model description is not significantly improved by using a bimodal strength distribution (eq. (2.2)).

Finally, the model is compared with traditional models in chapter 8. Model capabilities and limitations are discussed, and areas requiring further work are identified.

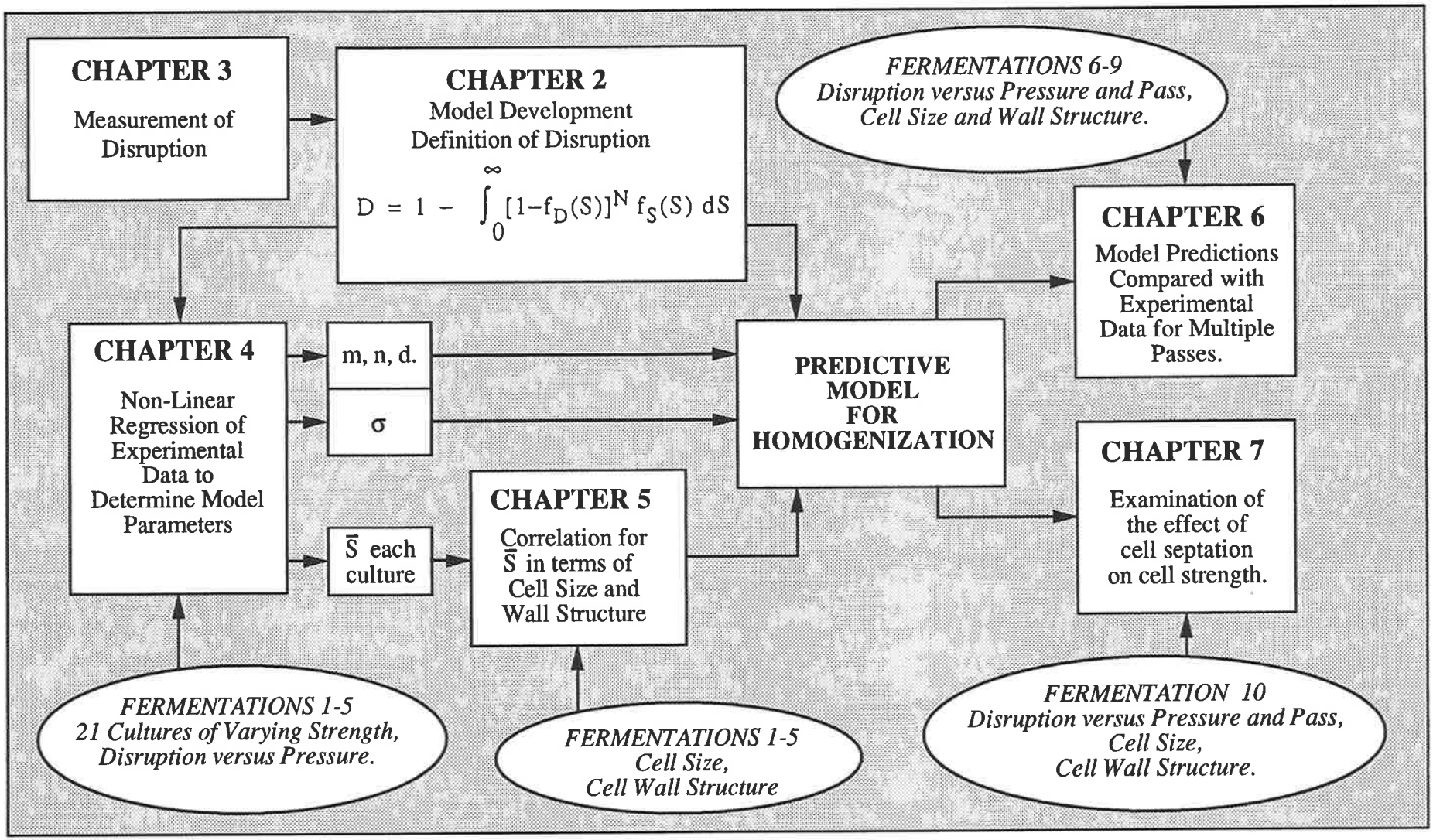

FIGURE 2.3 : *Outline of Overall Thesis Structure. In Addition to the Chapters shown above, Chapter 8 Discusses the Developed Model and compares it with the Kinetic Model.*

CHAPTER 3

ANALYSIS OF DISRUPTION

A sensitive measure of disruption, the dependent variable, is required if homogenization is to be modelled. Further, the uncertainty associated with the measurement must be quantified so that a meaningful comparison of experimental data with the model predictions can be made. In this chapter, existing methods for analyzing disruption are briefly described. A novel method, using an analytical disc centrifuge, is then developed and uncertainties associated with the novel method are quantified. The method is compared with traditional techniques and the final protocol is summarized.

3.0 Traditional Techniques

Engler (1985) provides an excellent summary of techniques for measuring disruption. These may be divided in two classes: direct and indirect. Direct methods count the number of cells surviving homogenization, normally using a microscope or an electronic particle counter. For bacteria, the electronic particle counter lacks sensitivity and is easily fouled by cellular debris if disrupted samples are analyzed. Microscopic observation is tedious if a large number of samples are to be assayed. For these reasons, indirect techniques are generally preferred. Such techniques rely on measuring the increase in cytoplasmic contents in the medium after disruption. Typically, the total release of soluble protein or the activity of an intracellular enzyme in the medium might be measured. For dilute cell suspensions, the fractional release of soluble protein, R_p, is given by equation (3.1),

$$R_p = \frac{C_h - C_o}{C_m - C_o} \qquad -(3.1)$$

where C is the concentration of soluble protein in the aqueous phase of the medium and the subscripts h and o denote disrupted (or homogenate) and undisrupted samples, respectively. C_m is the maximum possible concentration of soluble protein in the aqueous phase and corresponds to complete disruption. Soluble protein concentration may be measured using either the Folin-Lowry (Lowry *et al.*, 1951) or Bradford (1976) assays. Equation (3.1) includes C_o as a correction for protein release prior to homogenization. In most cases the correction will be negligible, as $C_o \approx 0$.

Equation (3.1) is only applicable for dilute suspensions. For concentrated cell suspensions, the aqueous volume fraction increases during disruption as the cytoplasmic contents mix with the suspending medium. Hetherington *et al.* (1971) describe a sample dilution procedure for determining the aqueous volume fraction. A volume of diluent, V_d, is added

to a volume of homogenate, V_h. The aqueous volume fraction, y_h, is then given by equation (3.2)

$$y_h = \frac{V_d}{V_h}\left(\frac{C_d}{C_h - C_d}\right) \qquad \text{-(3.2)}$$

where C_d is the concentration of soluble protein in the aqueous phase of the diluted sample. The aqueous volume fraction is applied as a correction to equation (3.1), giving equation (3.3).

$$R_p = \left(\frac{y_h}{y_m}\right)\left(\frac{C_h - C_o}{C_m - C_o}\right) \qquad \text{-(3.3)}$$

Engler and Robinson (1979) found the dilution procedure was unsatisfactory for samples containing partially denatured material, as protein solubility changed with dilution. They developed a mass balance approach for measuring disruption, using Kjeldahl nitrogen analysis of the homogenate supernatant. The fraction of cells ruptured may be estimated using equation (3.4)

$$R_K = \frac{y_o C_N}{C_{NO} C_c - (1 - y_o) C_N M_c \left(\frac{\rho_c}{\rho_a}\right)} \qquad \text{-(3.4)}$$

where C_N is the total Kjeldahl nitrogen content of the supernatant, C_{NO} is the Kjeldahl nitrogen content of whole cells, ρ_a is the aqueous-phase density, C_c is the suspension concentration, y_o is the aqueous volume fraction of the undisrupted cell sample, ρ_c is the cell density and M_c is the internal moisture content of cells. Engler (1985) concludes that the technique is probably less accurate than the dilution technique because of several assumptions in the derivation. It does, however, offer the advantage that it is relatively insensitive to protein denaturation.

Disruption may also be analyzed using a spectrophotometer. Absorbance measurements of homogenate supernatant at a wavelength of 260 nm will give an estimate of the amount of soluble protein and DNA present. A crude measure of disruption is therefore obtained from equation (3.5),

$$R_{A_{260}} = \frac{A_{260_h} - A_{260_o}}{A_{260_m} - A_{260_o}} \qquad \text{-(3.5)}$$

where A_{260} is the absorbance at 260 nm and $R_{A_{260}}$ is the fractional release of absorbing material.

The techniques described rely on measuring the release of intracellular components. The fractional release, R, is calculated from equations of the form

$$R = \frac{R'_h}{R'_m} \qquad \text{-(3.6)}$$

where R' is the actual concentration of the assayed component in the aqueous phase of the homogenate (h) or fully disrupted (m) samples. The fractional release is then equated to the volume fraction of cells disrupted: the disruption. In some instances this is invalid. This is illustrated, for example, by Harrison *et al.* (1991) who showed that DNA release was a poor measure of disruption compared with direct microscopical determination for *Alcaligenes eutrophus*.

A further limitation of indirect techniques arises from the uncertainty in the calculated fractional release at high levels of disruption. From equation (3.6) the following may be written,

$$\delta R = R\left(\frac{\delta R'_h}{R'_h} + \frac{\delta R'_m}{R'_m} \right) \qquad \text{-(3.7)}$$

where $\delta R'$ is the absolute error in the measured quantity, R'. Equation (3.7) illustrates that at high levels of disruption ($R \rightarrow 1$), the absolute error in R tends toward the sum of the relative errors in the two measured concentrations. Hence, if concentration measurement is accurate to ±2%, complete disruption will be reported as 100±4%. Clearly, the upper limit is not physically meaningful. At low levels of disruption, the error tends toward zero. High levels of disruption will be the desired result in any homogenization process. However, this is the region of greatest uncertainty in the measurement. Consequently, the accuracy of a model at high levels of disruption cannot be proven with great certainty using indirect techniques for measuring disruption. By contrast, direct techniques will be characterized by an equation of the form

$$D = 1 - \frac{\chi_h}{\chi_o} = 1 - \phi \qquad \text{-(3.8)}$$

where χ_h is the volume of intact cells remaining in the homogenate sample, χ_o is the volume of cells in the feed sample and ϕ is the volume fraction of cells surviving the disruption process. The following equation may be written for the uncertainty in the calculated disruption, δD.

$$\delta D = \delta\phi = \phi\left(\frac{\delta\chi_h}{\chi_h} + \frac{\delta\chi_o}{\chi_o}\right) \qquad \text{-(3.9)}$$

At high levels of disruption, the fraction of cells surviving will tend to zero. Consequently, $\delta D \rightarrow 0$ as $D \rightarrow 100\%$. Complete disruption will therefore be reported as 100±0% for direct measurements of disruption.

In the region of interest, namely high levels of disruption, a direct measure of disruption is clearly desirable. This is particularly true if model predictions are to be compared, with any certainty, to experimental measurements of disruption. Unfortunately, the existing direct

measurements (microscopy and electronic particle counting) are unsuitable for measuring disruption (Engler, 1985). A new direct method is required.

Bulk suspension optical density or absorbance at 600 nm is often used as an assay for cell concentration. It is, however, of limited use in analyzing the concentration of cells in a disrupted sample. This limitation occurs due to the presence of cellular debris in the homogenate sample. Debris increases the absorbance of the sample above the level corresponding to the true cell concentration. This increase is not readily characterized, as it depends on the size of the debris and hence the disruption conditions. To obtain a true measurement of cell concentration in a disrupted sample, the debris must therefore be separated from the undisrupted cells. Such a separation is achieved in the analytical disc centrifuge, which will now be described.

3.1 The Disc Centrifuge

The Joyce-Loebl analytical disc centrifuge monitors the settling of a suspension in a centrifugal field (Joyce-Loebl, 1985). Primarily, it is used in particle-size analysis. With reference to Figure 3.1, a rotating disc is loaded with "spin fluid". The sample, containing the particles to be sized, is layered onto the inner radius of this annulus. All particles thus start at nearly the same radius, and experience a net centrifugal force due to the rotation of the disc.

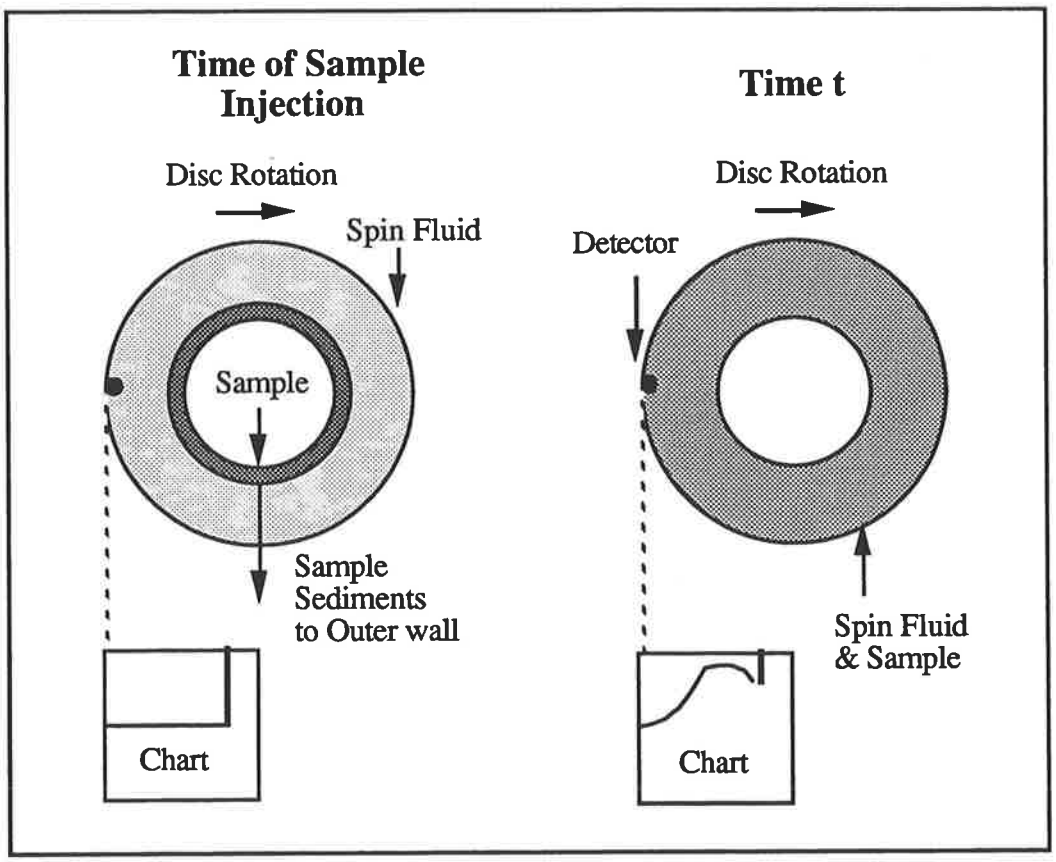

FIGURE 3.1 : *The Joyce-Loebl disc centrifuge.*

The time taken for a particle of Stokes diameter d_s (μm) to reach the detector, τ, neglecting the initial particle acceleration, is given by equation (3.10) (Taylor *et al.*, 1986),

$$\tau = \frac{18\,\eta\,\ln\left(\frac{r_d}{r_o}\right)}{(d_s x 10^{-6})^2\,\Delta\rho\,\omega^2} \qquad \text{-(3.10)}$$

where $\Delta\rho$ is the density difference between the particles and the fluid, ω is the disc angular velocity, η is the fluid viscosity, r_o is the particle start radius (τ=0) and r_d is the detector radius. Large particles reach the detector first. Resolution is excellent, a consequence of the squared dependence of time on diameter. The disc centrifuge measures the absorbance of the spin fluid at r_d, so a plot of absorbance versus time is obtained. This may be presented as a plot of absorbance versus Stokes diameter through equation (3.10).

The high resolution of the instrument is the key to its utility in analyzing disruption. When "sizing" a homogenate sample with the instrument, intact cells reach the detector before the smaller cell debris. A curve of absorbance versus diameter therefore reveals a distinct cell peak. Integration of the portion of the size distribution corresponding to intact cells, and comparison with the feed curve, allows disruption to be calculated.

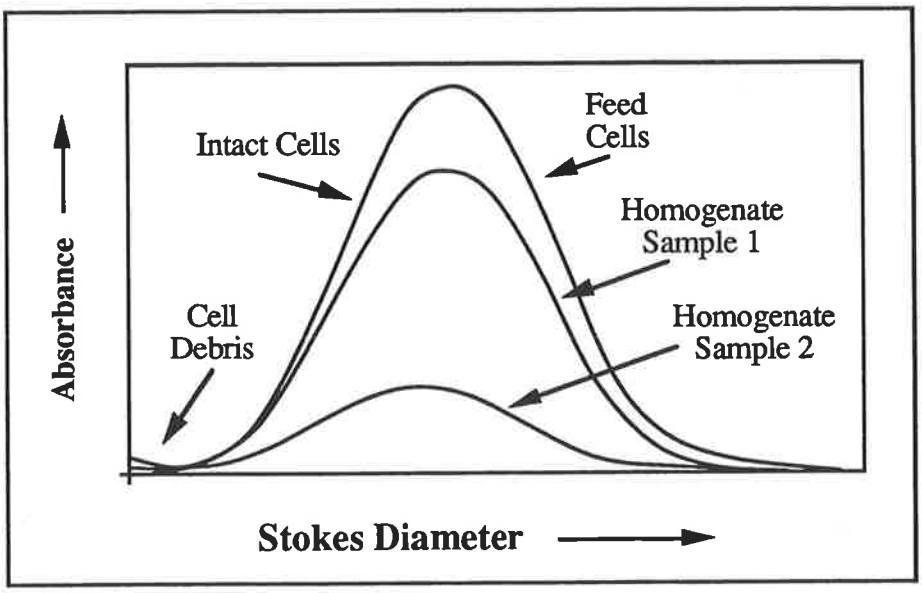

FIGURE 3.2 : *Size distributions determined using the disc centrifuge for undisrupted cells and homogenate samples.*

Figure 3.2 demonstrates the concept of using the disc centrifuge to determine cellular disruption. The area under the curve for homogenate sample 1 is approximately four-fifths of the area under the feed curve. The disruption is therefore approximately 20%. Similarly, the disruption for homogenate sample 2 is approximately 80%.

In the next section, an expression for disruption in terms of the disc centrifuge output is defined. In subsequent sections, a reliable protocol for assaying cell samples is developed, uncertainties in the calculation are quantified and discussed, and the technique is compared with an indirect method for determining disruption.

3.2 Calculating Disruption

Equation (3.8) is the general equation for calculating disruption from direct measurements of total cell volume in a sample. This may be re-written as

$$D = 1 - \frac{\chi_h}{\chi_o} = 1 - \frac{\left.\int_{d_{smin}}^{d_{smax}} f_3(d_s)\, dd_s\right|_h}{\left.\int_{d_{smin}}^{d_{smax}} f_3(d_s)\, dd_s\right|_o} \qquad \text{-(3.11)}$$

where $f_3(d_s)$ is the volume-frequency distribution of cells remaining in either the homogenate (h) or feed (o) sample, and d_{smin} and d_{smax} are the minimum and maximum Stokes diameters of intact cells. In the integration, only the portion of the distribution corresponding to intact cells is considered. For homogenate samples, it is therefore necessary to subtract the debris distribution from the measured size distribution. This may be done using either numerical or graphical deconvolution of the debris and cell distributions (section 3.4).

The analytical disc centrifuge provides a curve of absorbance versus diameter. This must be related to the frequency distribution of the cells if equation (3.11) is to be used to calculate disruption.

Ideally, absorbance is proportional to the cross sectional area of particles in the light beam. For a narrow range of particles absorbance is proportional to the second moment or area-frequency distribution (Oppenheimer, 1983).

$$f_2(d_s)\, \delta d_s \propto A \qquad \text{-(3.12)}$$

This ideal behaviour ceases to hold when the particle size approaches the wavelength of light (Allen, 1968). The breakdown of the laws of geometric optics is accounted for by defining the particle extinction coefficient, K_e, as :

$$K_e = \frac{\text{Light Obscured by the Particle}}{\text{Light which would be obscured Ideally}} \qquad -(3.13)$$

Equation (3.12) therefore becomes (Oppenheimer, 1983)

$$f_2(d_s)\,\delta d_s \propto \frac{A}{K_e} \qquad -(3.14)$$

Oppenheimer (1983) states that a plot of A/K_e versus particle size therefore represents an area distribution for particles with a narrow range of sizes. Husong (1990) notes that the range of particle sizes in the detection zone, δd_s, varies with time. The range of particle sizes is shown to be proportional to the mean particle size in the detection zone, $\bar{d}_s$ (eq. (3.15)).

$$\delta d_s = \frac{dd_s}{dr}\,\delta r \propto \bar{d}_s \qquad -(3.15)$$

It follows that absorbance, corrected for the extinction coefficient, is proportional to the third moment or the volume-frequency distribution (eq. (3.16)).

$$f_3(d_s) \propto \frac{A}{K_e} \qquad -(3.16)$$

An identical conclusion is reached by Allen (1987) and Treasure (1964).

The validity of equation (3.15), and hence equation (3.16), is subject to the following considerations when sizing cells :

i) cells are rod-shaped and may preferentially align themselves during sedimentation. Hence, a fixed Stokes diameter may correspond to a range of physical sizes. A range of particles with differing optical properties may be present in the detection zone at any time;

ii) particles do not start at precisely the same radius;

iii) equation (3.12) assumes a narrow range of particle sizes in the detector at any time, so that higher-order terms can be neglected. The disc centrifuge has a large circular detection region (≈ 1 mm diameter), and therefore integrates a significant fraction (≈ 25%) of the cell distribution at any time.

It is therefore appropriate to write equation (3.17) for a narrow distribution of particles,

$$f_3(d_s) \propto A \frac{d_s^p}{K_e} \qquad \text{-(3.17)}$$

where p is an exponent whose value depends on the validity of equation (3.15) subject to the preceding limitations (p=0 implies that equation (3.15) is correct when the correct extinction coefficient is employed). Equation (3.11) may therefore be written as

$$D = 1 - \frac{J_h \int_{d_{smin}}^{d_{smax}} A \cdot \frac{d_s^p}{K_e} dd_s \Big|_h}{J_o \int_{d_{smin}}^{d_{smax}} A \frac{d_s^p}{K_e} dd_s \Big|_o} \qquad \text{-(3.18)}$$

where J is the dilution factor of the homogenate (h) or feed (o) sample.

The application of equation (3.18) requires the extinction coefficient for cells. Using Mie theory, Allen (1968) derives functional relationships for the extinction coefficient for several

cases including those of a totally reflecting and a non-absorbing sphere. Oppenheimer (1983) provides a relationship for the extinction coefficient for polystyrene in water (K_p), which was used previously to size inclusion bodies (Taylor *et al.*, 1986). No study of the extinction by bacteria has been reported. Equation (3.19) has been fitted to the white-light data for polystyrene reported by Oppenheimer (1983).

$$\left.\begin{aligned} K_p &= 3.25\, d_s^{2.55} \qquad d_s \le 0.5\ \mu m \\ K_p &= 3\, d_s - 0.945 \qquad d_s \ge 0.5\ \mu m \end{aligned}\right\} \qquad \text{-(3.19)}$$

Substituting this into equation (3.18) with p=1 provides the final equation for disruption (eq. (3.20)). The exponent value of p=1 has been selected as it reduces the variation in the polystyrene extinction coefficient over the range of cell sizes ($1.0 < d_s < 1.4\ \mu m$). The ratio K_p/d_s may therefore be viewed as an approximately constant extinction coefficient, K'.

$$D = 1 - \frac{\chi_h}{\chi_o} = 1 - \frac{J_h \int_{d_{smin}}^{d_{smax}} A \frac{d_s}{K_p}\, dd_s \Big|_h}{J_o \int_{d_{smin}}^{d_{smax}} A \frac{d_s}{K_p}\, dd_s \Big|_o} \qquad \text{-(3.20)}$$

Disruption may be calculated in the following manner :

- "Size" the homogenate and undisrupted samples using the disc centrifuge to obtain curves of absorbance versus time;
- Obtain a plot of absorbance versus diameter using equation (3.10) to relate time to Stokes diameter;
- correct the curve with the modified extinction coefficient, $K'=K_p/d_s$;
- deconvolute the debris and undisrupted cell peaks;
- integrate the corrected curve according to equation (3.20) to calculate the disruption.

The calculated disruption will be subject to several sources of error. For an instrument in a temperature-controlled environment, these will be :

a) the use of an incorrect extinction coefficient for cells, $K'=K_p/d_s$;

b) uncertainty in deconvoluting the cell distribution from the debris;

c) random uncertainties in the sizing technique and experimental procedure.

At first glance, the use of an incorrect extinction coefficient appears to invalidate the technique. This would be true if particle size is the parameter of interest. Fortunately, equation (3.20) relies on the ratio of two integrated distributions. The lack of an accurate extinction correlation therefore will have a negligible effect on the final result provided that the homogenate and feed distributions are similar. In such cases, the extinction-coefficient effects will cancel when the ratio is taken. This is illustrated in section 3.5.

The use of equation (3.20) to calculate disruption requires a reproducible method for obtaining plots of A versus d_s from the disc centrifuge. A reliable protocol will be developed in the next section. In section 3.4, the uncertainties in the calculation will be quantified and discussed. In section 3.5, disruption will be assayed using the disc centrifuge and the measurements will be compared with the results of an indirect method. The final protocol for calculating disruption using the disc centrifuge will be summarized in section 3.6.

3.3 'Sizing' *E. coli* with the Disc Centrifuge

The successful application of equation (3.20) to calculate disruption demands a reproducible method of obtaining plots of A versus d_s. The following problems had to be overcome in order to develop a technique for 'sizing' bacteria with the disc centrifuge :

- hydrodynamic instabilities in the disc;
- alterations in the sample resulting from the analysis;
- alterations in the sample resulting from a delay before analysis;
- non-linearity of the plot of absorbance versus diameter with sample concentration.

These problems will be considered sequentially.

3.3.1 Hydrodynamic Instabilities

A rotating fluid annulus, such as in the centrifuge disc, is unstable as the fluid can mix without any change in potential energy (Brugger, 1976). As a result, particles introduced to the top of the rotating spin fluid (Figure 3.1) will rapidly mix throughout the fluid in a random manner. Under such conditions, the plot of absorbance versus time will be meaningless and resolution will be zero.

Brugger (1976) addresses the problem of instability in a disc centrifuge, and suggests that a spin fluid density gradient sufficiently large to overcome all disturbing influences is necessary. It was suggested that stable sedimentation is obtained only in the region of the density gradient, and that under the conditions of a successful run, the density gradient extends throughout the spin fluid.

A density gradient can be established in the disc centrifuge by using a "buffer fluid". The buffer fluid is chosen to have a lower density than the spin fluid. A small volume (typically 1-2 mL) is injected onto the surface of the rotating spin fluid. It is then mixed into the annulus by temporarily accelerating the disc with the machine boost action (Joyce-Loebl, 1985). Ethanol-water mixtures are commonly used as buffer fluids for a water-spin fluid. It is possible to use water as the buffer fluid, if the spin fluid is denser than water (e.g. glycerol-water mixtures). The sample is injected after the density gradient is established, and is usually suspended in the same fluid as the buffer fluid. As bacteria are analyzed in this work, phosphate buffer (20 mM sodium phosphate, 30 mM sodium chloride, pH 7.0) is used in place of water for sample suspensions.

A range of conditions were tested for a water-spin fluid with a 20% ethanol-water buffer fluid, and a 10% glycerol-water spin fluid with a water-buffer fluid. Ink was included in the buffer fluid to test mixing into the spin fluid. The following problems could be associated with unsuccessful runs :

(a) With insufficient boost, the density gradient extends to a certain point within the spin-fluid annulus and then stops. Settling particles behave well until this abrupt density discontinuity is reached and then begin to turbulently mix into the rest of the spin fluid. This resembles the phenomenon of secondary streaming described by the manufacturer (Joyce-Loebl, 1985).

(b) Also with insufficient boost, a condition where the density gradient is not stable can arise. This leads to continued mixing between the buffer layer and the spin fluid during the course of the test. Mixtures containing different quantities of ethanol and water will posses different refractive indices, so that any change in the composition of the spin fluid at the detector will result in a variation in the baseline.

The second phenomenon is clearly illustrated in Figure 3.3, which is a plot of raw machine output (proportional to absorbance) as a function of time. Each plot represents the machine baseline at a disc speed of 8000 r.p.m. using the following scheme :

- Inject 20 mL of water spin fluid and begin data collection;
- Inject 1 mL of 20% v/v ethanol in water 180 seconds later;
- Give three boosts (with the boost button set to 80) 200 seconds after starting data collection. The machine is allowed to re-synchronize between boost actions.

The three peaks at approximately 200 seconds in Figure 3.3 correspond to depression of the boost button. The variation in refractive index is clearly shown. The difference in the two plots is possibly attributable to slight variations in the boost action.

Conditions which give a stable density gradient were determined using ink tracers. The resulting methods are summarized in Table 3.1.

TABLE 3.1 : *Conditions resulting in a hydrodynamically-stable spin fluid with a density gradient extending throughout the annulus.*

	Method I	Method II	Method III
Spin Fluid (SF)	20 mL Water	20 mL 10% w/w Glycerol-Water	15 mL 10% w/w Glycerol-Water
Buffer Fluid (BF)	1.5 mL 20% v/v Ethanol-Water	1.5 mL Water	1.0 mL Water
Sample Volume and Suspension	0.5 mL 20% v/v Ethanol-Phosphate Buffer	0.5 mL Phosphate Buffer	0.5 mL Phosphate Buffer
Disc Speed	8000 r.p.m.	8000 r.p.m.	8000 r.p.m.
Gain	6.0	6.0	6.0
r_o (cm) (eq. (3.10))†	4.01	4.01	4.30
r_d (cm) (eq. (3.10))	4.82	4.82	4.82
η [a] (cP) (eq. (3.10))	1.14	1.36	1.36
$\Delta\rho$ [b] (kg m^{-3}) (eq. (3.10))	106	84	84
Time = 0 s	Inject SF	Inject SF	Inject SF
Time = 60 s	Inject BF	Inject BF	Inject BF
Time = 90 s	Boost 70	Boost 70	Boost 70
Time = 150 s	Boost 70	Boost 50	–
Time = 210 s	Boost 20	Boost 20	–
Time = 300 s	Inject Sample	Inject Sample	Inject Sample

a 90% spin fluid + 10% buffer fluid at 20C using a Brookfield LVT viscometer.
b Difference between cell and fluid (90% spin fluid + 10% buffer fluid) densities. Cell density is assumed to be 1100 kg m^{-3}.
† Calculated using only the spin fluid volume.

The time lags between each successive boost action ensured that stability within the spin fluid had been achieved prior to the next action. The schemes are reproducible, and provide a straight baseline as shown by Figure 3.4. Sample injection would occur at 300 seconds (τ=0). Peaks prior to this time are attributable to the boost action.

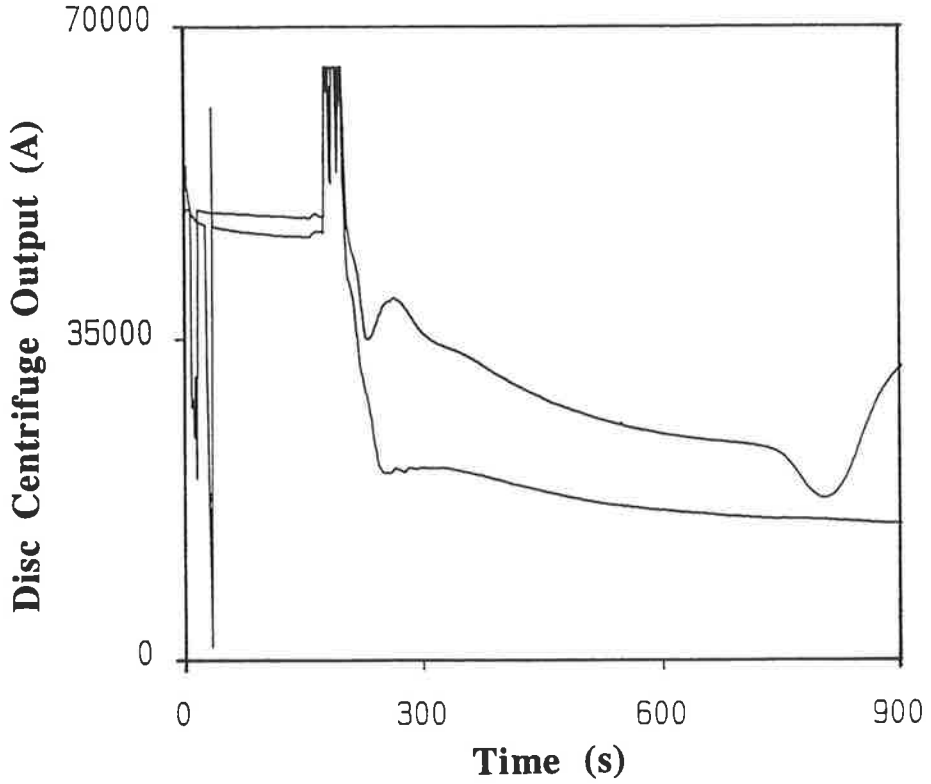

FIGURE 3.3 : *Disc centrifuge output versus time showing baseline variation resulting from unstable boost conditions.*

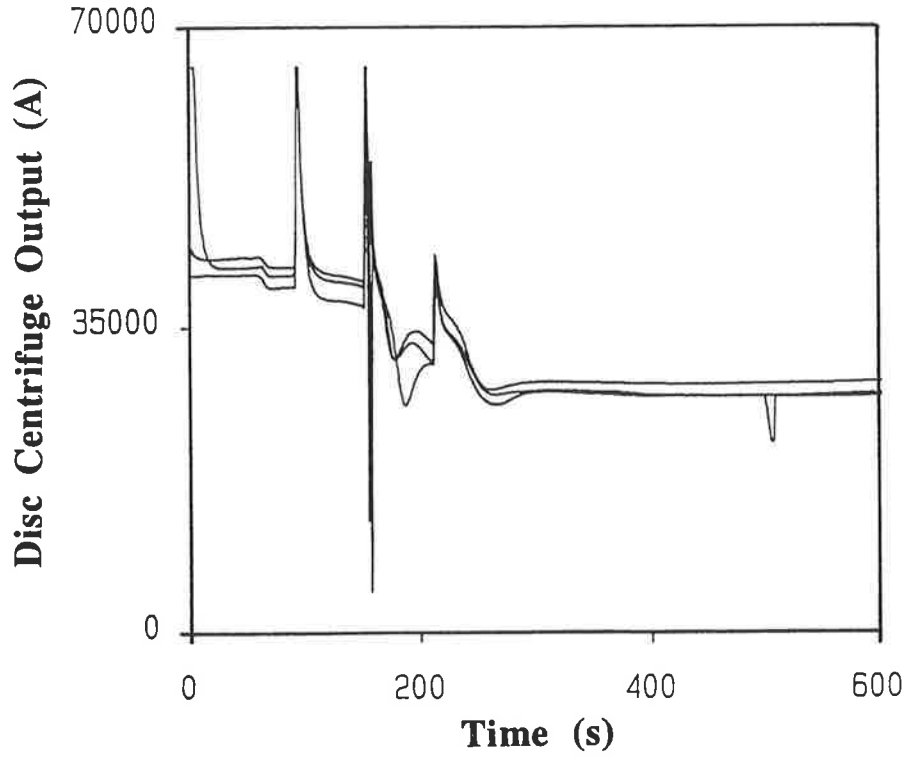

FIGURE 3.4 : *Stable baselines obtained using the standard boost conditions outlined in Table 3.1.*

3.3.2 Sample Variation due to the Methods

Two spin fluid types have been tested, 10%w/w glycerol-water and water, with water and 20%v/v ethanol-water buffer fluids respectively. The sample is suspended in either ethanol-phosphate buffer (Method I) or phosphate buffer (Methods II and III). The use of ethanol is of concern when sizing bacteria, as it is a known dissolver of lipids in high concentration.

To test of the effect of buffer fluid type, *E. coli* cells were suspended in the two types of buffer fluid (20% ethanol-phosphate and phosphate). The samples were 'sized' using the disc centrifuge at various times after suspension using the appropriate standard conditions (Method I or Method II conditions in Table 3.1). The data were processed as described in section 3.2 to generate size distributions. Some of the results are presented as Figures 3.5 and 3.6. Figure 3.7 is a plot of modal Stokes diameter as a function of immersion time for the two tested buffer fluids.

The results clearly illustrate that *E. coli* cells reduce their Stokes diameter in response to exposure to 20%v/v ethanol-phosphate. Immersion in phosphate buffer does not affect the size distribution of the bacteria, so methods II and III are preferred to method I for sizing cells. Method III has the advantage that it is simpler to implement (1 boost only) and is slightly faster due to the lower volume of spin fluid. It is preferred for routine disruption analysis.

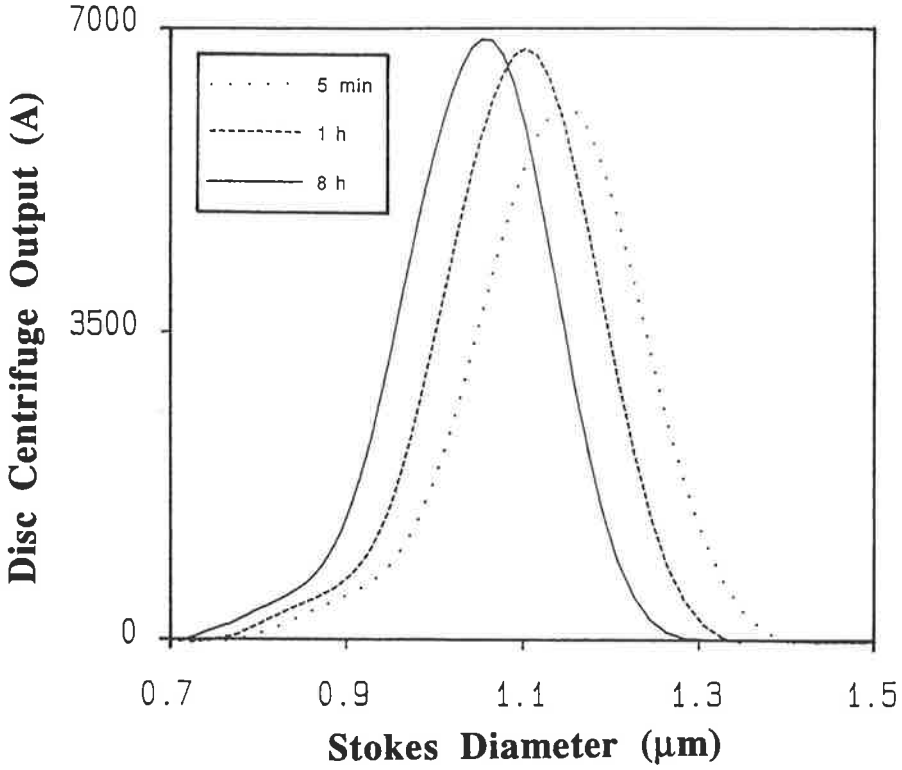

FIGURE 3.5 : *Size distributions for E. coli showing the effect of prolonged exposure to 20% ethanol-phosphate buffer.*

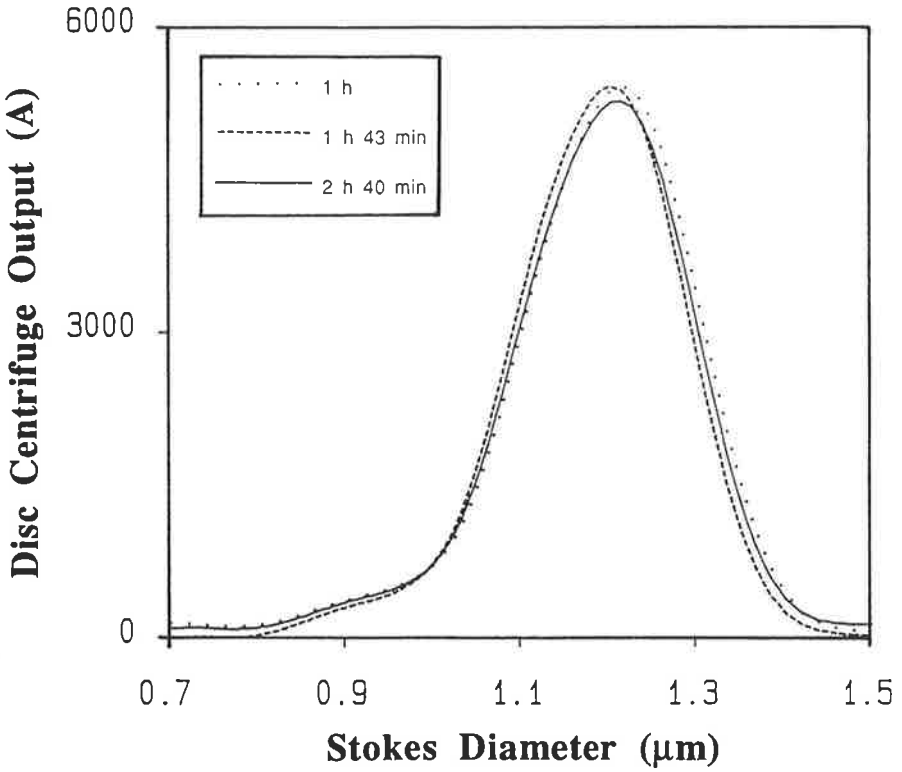

FIGURE 3.6 : *Size distributions for E. coli showing the effect of prolonged exposure to phosphate buffer.*

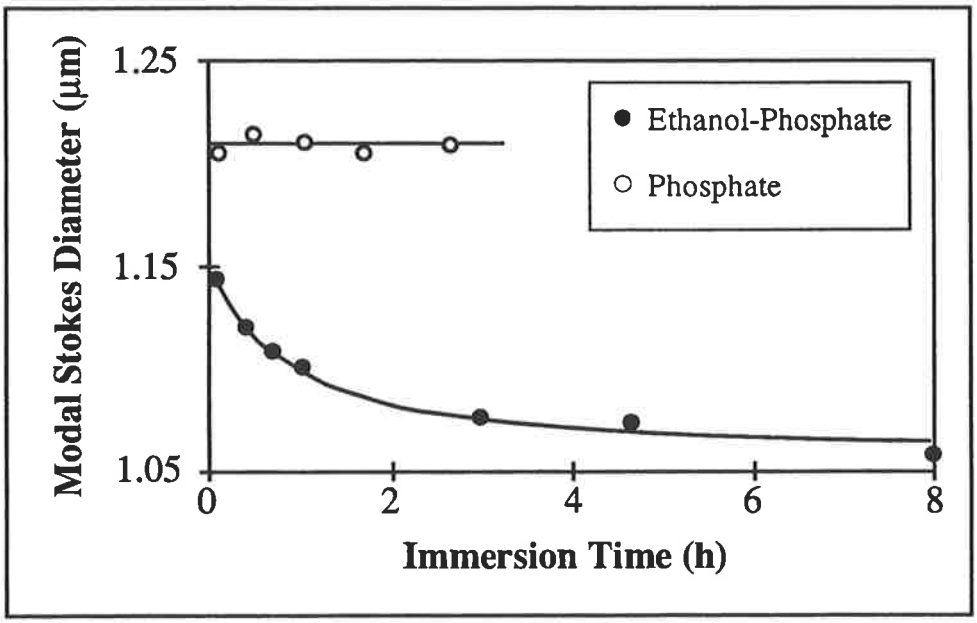

FIGURE 3.7 : *Modal Stokes diameter as a function of immersion time in either 20% ethanol-phosphate or phosphate buffer.*

3.3.3 Sample Variation due to Delayed Analysis

Methods II and III allow a sample of *E. coli* to be analyzed within 10 minutes. Considerable delays may result if a large number of samples are to be assayed. It is likely that samples will change during storage, even at 5°C. This will be particularly true for disrupted samples, where viable cells may metabolize the intracellular components released by disrupted cells. A method of fixation is therefore required to prevent cell growth during storage.

Formaldehyde and glutaraldehyde at low concentration are common agents for fixation. The effect of these fixatives on sample 'size' was investigated to compare the two chemicals. Stationary-phase *E. coli* were centrifuged and the pellet was resuspended in phosphate buffer (20 mM sodium phosphate, 30 mM sodium chloride, pH 7.0, 20°C) to an optical density of approximately 0.5 at 600 nm. Various concentrations of either formaldehyde or glutaraldehyde were added to samples of the suspension, which were then sized using Method II (Table 3.1).

Figure 3.8 shows that the calculated size is independent of the selected formaldehyde concentration. Figure 3.9 shows that size is sensitive to glutaraldehyde concentration. Cell size increases with glutaraldehyde concentration. It is reasonable to conclude that formaldehyde should be used in preference to glutaraldehyde when samples are to be stored prior to analysis. A concentration of 0.02% will therefore be added to samples.

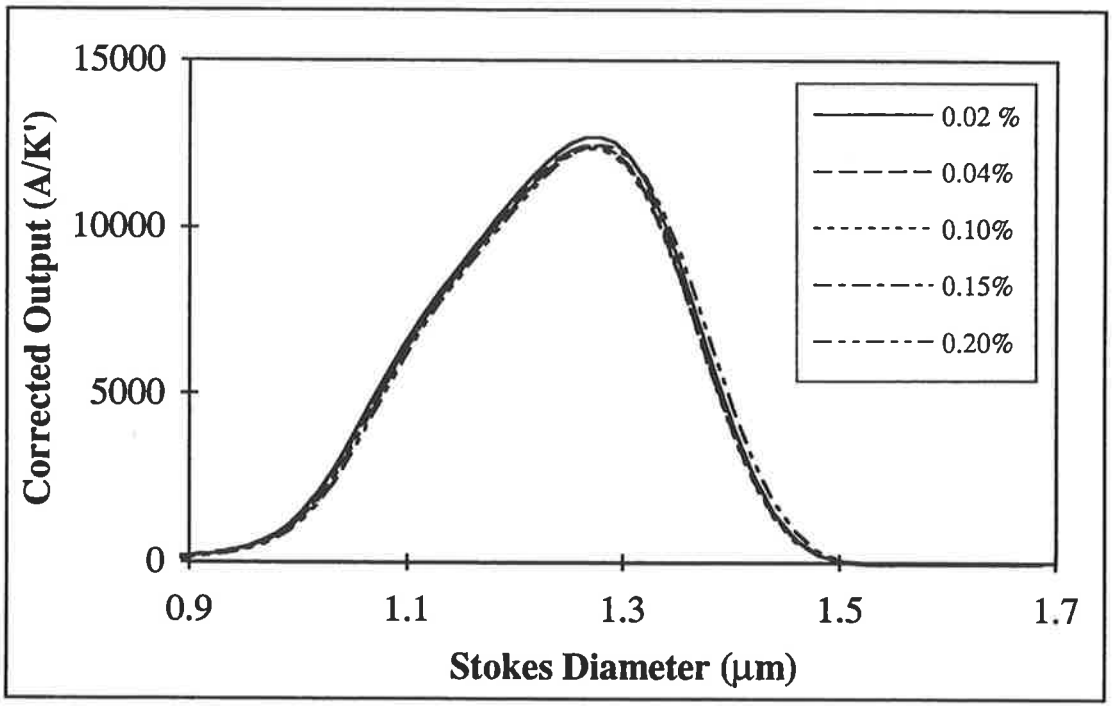

FIGURE 3.8 : *Size distributions for E. coli cells as a function of formaldehyde concentration.*

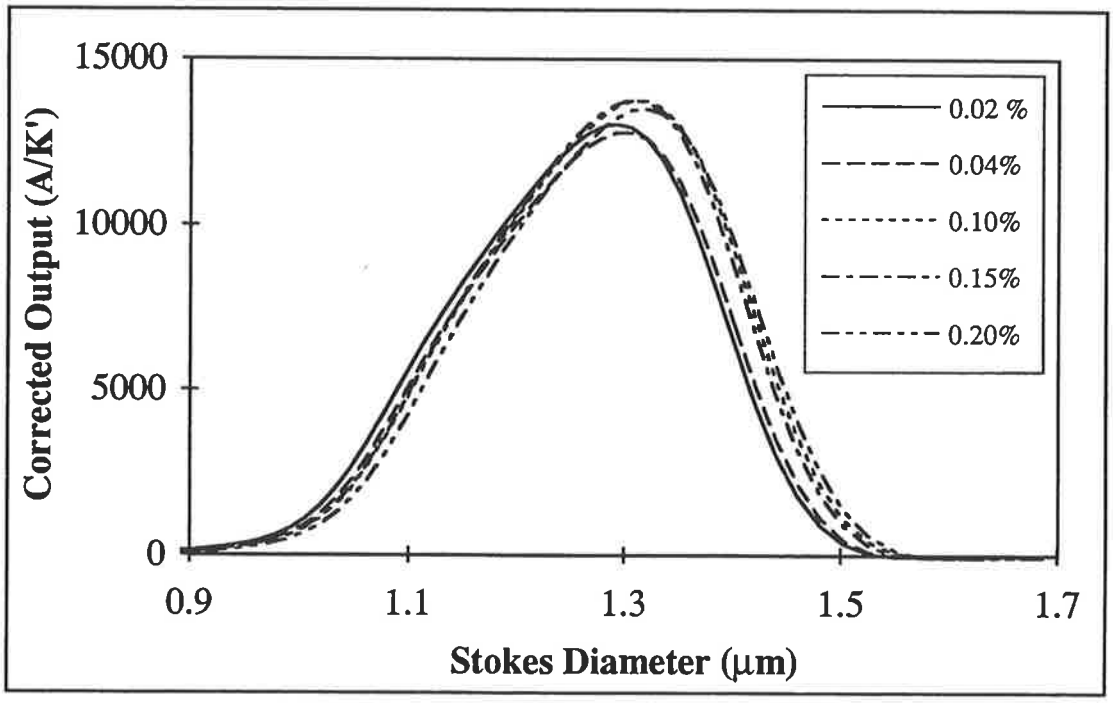

FIGURE 3.9 : *Size distributions for E. coli cells as a function of glutaraldehyde concentration.*

The preceding test merely illustrates that formaldehyde is preferred to glutaraldehyde. It does not prove that samples will not change with storage. In all tests, the following protocol is therefore employed :

- add 0.02 % formaldehyde immediately to feed and homogenate samples which are to be assayed using the disc centrifuge;
- analyze the feed sample and a sample disrupted at a low pressure (e.g. 7 MPa) first;
- store treated samples at 5°C until analysis;
- analyze the remaining samples;
- repeat the analysis of the feed and disrupted sample;
- compare the two feed and disrupted sample size distributions to ensure that the samples have not changed significantly during storage.

In the numerous disruption tests described in subsequent chapters, no evidence of sample variation was discovered with up to two days storage when the preceding method was employed. Considerable change was noted over the same period when formaldehyde was not added.

3.3.4 Concentration Non-Linearity

Sample concentration is a critical parameter in using the disc centrifuge. This is a consequence of the derivation of equation (3.20), where the output from the disc centrifuge was assumed proportional to absorbance. Allen (1987) states that this is true provided that less than 10% of the incident light is cut off by the particles. For narrow distributions such as cells, a significant fraction of particles will be in the detection zone at any time (up to 25%). Sample concentrations must therefore be extremely low to ensure that less than 10% of the incident light is attenuated. Joyce-Loebl (1985) state that *"the concentration should be as low as possible consistent with it being high enough to cause adequate optical attenuation"*. To test the effect of sample concentration, stationary-phase *E. coli* were centrifuged and re-suspended in phosphate buffer to give samples with varying optical densities. These were sized using method III (Table 3.1). The resulting size distributions (normalized to the highest concentration) are shown in Figures 3.10 and 3.11.

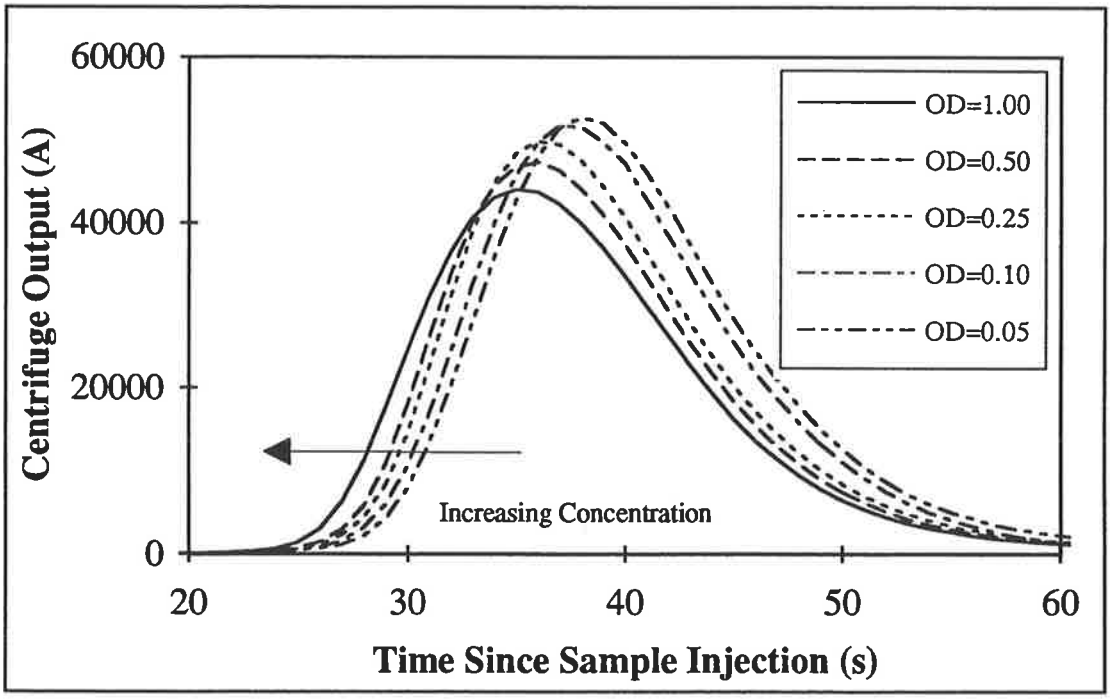

FIGURE 3.10 : *Normalized disc centrifuge output as a function of time for the same sample of E. coli analyzed at different concentrations. (OD is optical density at 600 nm).*

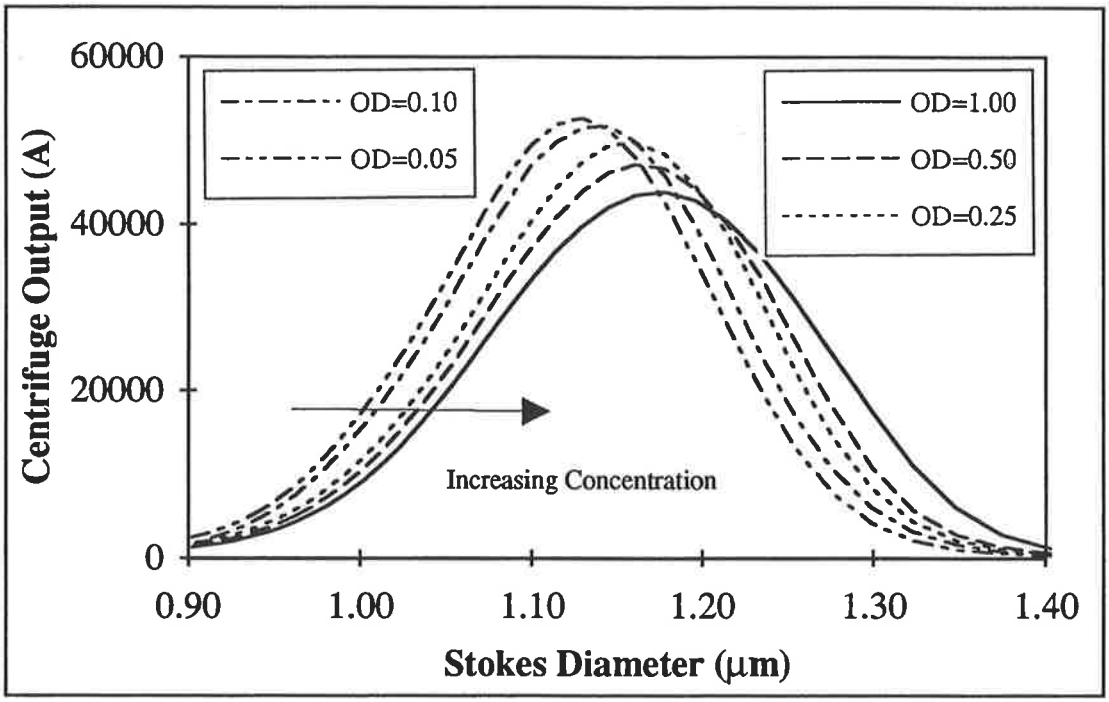

FIGURE 3.11 : *Size distributions for the same sample of E. coli analyzed at different concentrations (Distributions are normalized to the highest concentration; OD is optical density at 600 nm).*

A strong dependence of size distribution on concentration exists. This dependence may be due to either excessive attenuation of the light source or slight streaming. At high levels of attenuation, the output from the disc centrifuge drops below the true optical density (Allen, 1987). As a result, the amount of material will be underpredicted at high concentration. This trend is apparent in Figures 3.10 and 3.11. However, the distribution also appears to shift slightly with concentration. This may be due to slight streaming near the leading edge of the settling particles (Joyce-Loebl, 1985). Such a phenomenon will reduce the time taken for particles to reach the detector, and consequently indicate an increased particle size. Streaming is suppressed by lowering the concentration (Taylor *et al.*, 1986), as the leading edge of the settling particles creates a lower density discontinuity in the fluid. The trends in Figures 3.10 and 3.11 may therefore be due to small-scale streaming. No visible streaming was apparent when sedimentation was viewed using the instrument's inbuilt stroboscope.

Regardless of the precise reason for the concentration dependence, Figures 3.10 and 3.11 demonstrate that the initial sample absorbance (600 nm) must be below 0.1 (this is a practical limit as detection becomes difficult below this). Even at this concentration, slight non-linearity exists. To minimize this, all samples should ideally be analyzed at the same concentration. In analyzing disrupted samples, the debris will increase the bulk sample absorbance above that for whole cells. To ensure that concentration effects are minimized, the following procedure is therefore adopted :

- dilute the undisrupted sample with phosphate buffer to a bulk absorbance of 0.1;
- analyze using the disc centrifuge, noting the maximum output from the instrument, $A_{max,o}$;
- dilute the homogenate sample with phosphate buffer to an absorbance of 0.1;
- analyze using the disc centrifuge, noting the maximum output from the instrument, $A_{max,h}$;
- adjust the concentration of the homogenate sample so that $A_{max,h} = A_{max,o}$;
- analyze the homogenate using the disc centrifuge at the modified concentration.

Although the above procedure is quite tedious, it ensures that the cell concentrations in both the feed and homogenate samples will be approximately the same. Errors due to concentration dependence will therefore be minimized.

3.3.5 Summary of Section 3.3

The following points relate to the analysis of disruption throughout this thesis :

a) Method III (Table 3.1) ensures that a stable density gradient is established for sizing *E. coli*. It is routinely used in this work for analyzing disruption;

b) Significant variation in size distribution occurs when method I (Table 3.1) is used to size *E. coli* because the sample is suspended in 20% ethanol. This method is not used;

c) All samples for analysis are fixed with 0.02% formaldehyde. The protocol outlined in section 3.3.3 is followed to minimize any sample variation with storage;

d) Samples are diluted to a bulk absorbance of less than 0.1 at 600 nm before analysis. To minimize concentration dependence when analyzing disrupted samples, the protocol outlined in section 3.3.4 is followed.

The preceding points ensure that reproducible 'size' distributions (plots of A versus d_s) are obtained using the disc centrifuge. This is a requirement if equation (3.20) is to be used to calculate the disruption. Several sources of error remain in the calculated disruption. These are quantified in the next section.

3.4 Uncertainty in the Calculated Disruption

As indicated in section 3.2, the calculated disruption will be subject to several sources of error. These will be

a) the use of an incorrect extinction coefficient for cells, $K'=K_p/d_s$;

b) uncertainty in deconvoluting the cell distribution from the debris;

c) random uncertainties in the sizing technique and experimental procedure.

In addition, the following sources of error may be identified from section 3.3

d) error in the calculation of the Stokes diameter resulting from inaccurate viscosity and density data. For example, the density of intact cells is assumed to be 1100 kg m^{-3} in Table 3.1;

e) error resulting from concentration non-linearity. This will be minimized by the protocol outlined in section 3.3.4, but is difficult to completely eliminate.

As indicated in section 3.2, the use of an incorrect extinction coefficient will have little impact on the final value of disruption, as the effect will approximately cancel when the ratio is taken in equation (3.20). This is also true for errors in the calculated Stokes diameters (error (d)). Errors (a) and (d) will therefore not be included in the overall estimate of uncertainty for the calculated disruption. The influence of these neglected errors will be demonstrated in the next section.

Disruption is defined by equation (3.20) :

$$D = 1 - \frac{\chi_h}{\chi_o} = 1 - \frac{J_h \int_{d_{smin}}^{d_{smax}} A \frac{d_s}{K_p} dd_s \Big|_h}{J_o \int_{d_{smin}}^{d_{smax}} A \frac{d_s}{K_p} dd_s \Big|_o} \qquad \text{-(3.20)}$$

The output from the disc centrifuge can be presented as a plot of d_sA/K_p (=A/K') versus d_s. χ_h is therefore simply the area under the homogenate curve which corresponds to undisrupted cells, while χ_o is the corresponding area for a feed sample. Figure 3.12 shows the size distribution for a typical homogenate sample, with undisrupted cells and cellular debris clearly distinguishable.

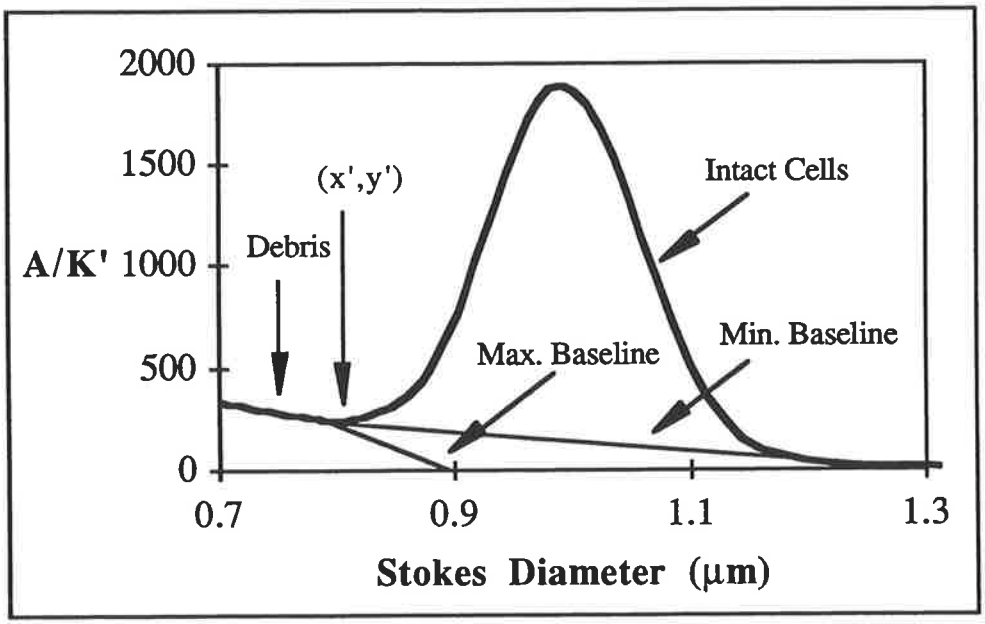

FIGURE 3.12 : *Size distribution for a typical homogenate sample showing the method of baseline construction for deconvoluting debris and cell distributions.*

The following technique is employed to estimate χ_h :

- the minimum separating the debris and cell curves is located at (x',y');

- a lower estimate of the area, χ_{hL}, is obtained by constructing a baseline between (x',y') and (d_{smax},0);
- an upper estimate of the area, χ_{hU}, is obtained by constructing a baseline between (x',y') and (x'+0.1μm,0);
- the area corresponding to undisrupted cells, χ_h, is taken to be the arithmetic average of χ_{hU} and χ_{hL}.

A lower estimate of disruption, D_L, is obtained from equation (3.21),

$$D_L = 1 - \frac{\left(1 + \frac{\delta\chi_h}{\chi_h}\right)\chi_{hU}}{\left(1 - \frac{\delta\chi_o}{\chi_o}\right)\chi_o} \qquad \text{-(3.21)}$$

where $\delta\chi/\chi$ is the fractional uncertainty in the average homogenate (h) and feed (o) distributions resulting from factors other than those already included in χ_{hU} (i.e. technique reproducibility factors). Similarly, an upper estimate of the disruption is obtained from equation (3.22).

$$D_U = 1 - \frac{\left(1 - \frac{\delta\chi_h}{\chi_h}\right)\chi_{hL}}{\left(1 + \frac{\delta\chi_o}{\chi_o}\right)\chi_o} \qquad \text{-(3.22)}$$

Disruption is then taken to be the arithmetic average of D_U and D_L. The uncertainty is simply taken to be half difference between the upper and lower estimates (eq. (3.23)).

$$D = \bar{D} \pm \delta D = \left(\frac{D_U + D_L}{2}\right) \pm \left(\frac{D_U - D_L}{2}\right) \qquad \text{-(3.23)}$$

To estimate the uncertainty in the disruption, δD, estimates of the technique random error, $\delta\chi/\chi$, are required for the feed and homogenate curves (eqs. (3.21) and (3.22)). To estimate this, a sample of undisrupted *E. coli* was 'sized' six times using the disc centrifuge. As the sample consisted entirely of undisrupted cells, deconvolution was unnecessary. The uncertainty in the integrated area of a plot of A/K' versus d_s was ±1.4% (one standard deviation). It is reasonable to set the technique reproducibility to ±1.4% for both the homogenate and feed samples, as deconvolution errors are included in the estimate of χ_{hU} and χ_{hL}. Hence :

$$\frac{\delta\chi_h}{\chi_h} = \frac{\delta\chi_o}{\chi_o} = 1.4\% \qquad \text{-(3.24)}$$

Equation (3.24) does not include errors resulting from sample variability with storage and concentration effects, discussed in section 3.3. While the protocol developed in section 3.3.4 will ensure that the disrupted sample is at approximately the same concentration as the feed sample, it is unlikely that the precise concentration will be achieved. To quantify the error introduced in any given series of assays, the feed distribution is therefore sized at several concentrations about the mean value. A more accurate estimate of the uncertainty in the feed area can therefore be obtained by estimating the error from the multiple distributions. In all tests, equation (3.25) is therefore used

$$\frac{\delta\chi_o}{\chi_o} = \text{Max}\,(\,1.4\%\,,\,\sigma_{exp}\,) \qquad \text{-(3.25)}$$

where σ_{exp} is the experimentally determined standard deviation of the integrated feed areas for a given series of tests.

Equation (3.23) is unlikely to provide minimum and maximum bounds on the calculated disruption, but rather an estimate of the standard deviation of the measure. This follows as

$\delta\chi_h/\chi_h$ and $\delta\chi_o/\chi_o$ correspond to one standard deviation and the deconvolution error is likely to be underpredicted using the preceding method. In comparing the experimental measurements with model predictions, δD is therefore assumed to represent one standard deviation. The number of standard deviations separating model predictions and experimental values is given by equation (3.26).

$$t = \frac{D_{pred} - D_{exp}}{\delta D} \qquad \text{-(3.26)}$$

Equation (3.23) is employed as it is simple to encode and the effect of different factors such as the deconvolution error is clear. It provides an uncertainty which is similar to that calculated by the direct addition of relative and absolute uncertainties. Although errors are likely to be independent, quadrature addition has not been employed. Direct addition compensates for the fact that concentration and storage factors have not been included in the estimate of $\delta\chi_h/\chi_h$.

A method for measuring disruption using the disc centrifuge has now been developed, and the uncertainty associated with the measurement quantified. Techniques for obtaining reproducible plots and minimizing storage and concentration errors have also been developed. To test the developed method, a comparison with a traditional technique is warranted. In the next section, disruption is quantified using the disc centrifuge, and the measurement is compared with the indirect technique of measuring soluble protein release. It is shown that the disc centrifuge is superior when accuracy at high levels of disruption is required. Furthermore, the influence of the extinction coefficient on the calculated disruption is demonstrated to be negligible.

3.5 A Comparison of Techniques

To prove the disc centrifuge as a useful tool for analyzing disruption, it is necessary to compare its performance with a more traditional method.

Disrupted samples were obtained using an APV-Gaulin 15M-8TA high-pressure homogenizer equipped with a ceramic cell disruption (CD) valve. The detailed experimental description is provided in subsequent chapters. The specific samples analyzed in this section are those in chapter 6 (Fermentation 6). The sole point of interest here is the comparison of the disc centrifuge measurements with a more traditional method. Disrupted samples were analyzed using the disc centrifuge with the protocols developed in the preceding sections (Method III, Table 3.1). Disruption was calculated by equation (3.20). Soluble protein measurements on homogenate supernatants (Bio-Rad protein assay, Bio-Rad Laboratories Ltd., Sydney, Australia) were also conducted. The fractional release of soluble protein was calculated by equation (3.1). This was assumed to equal the disruption. The concentration of cells in the feed suspension was quite low (chapter 6) so that correction for the aqueous volume fraction in soluble protein measurements was unnecessary. The results of the analysis are summarized in Figures 3.13 and 3.14. Also shown is the curve obtained by regressing the disruption data obtained using the disc centrifuge to the kinetic model (eq. (1.1)). This curve is shown to emphasize the trend in the data.

Figures 3.13 and 3.14 clearly show that the disc centrifuge provides a reasonable measure of disruption. The comparison with soluble protein measurements is excellent. The data obtained using the disc centrifuge show a smooth trend. This is in contrast to the soluble protein measurements, which exhibit a greater degree of scatter, particularly at high levels of disruption (it should be noted that the regressed line does not represent the true disruption). This stresses the advantage of direct methods for measuring disruption compared with indirect methods (as emphasized by the analysis in section 3.0).

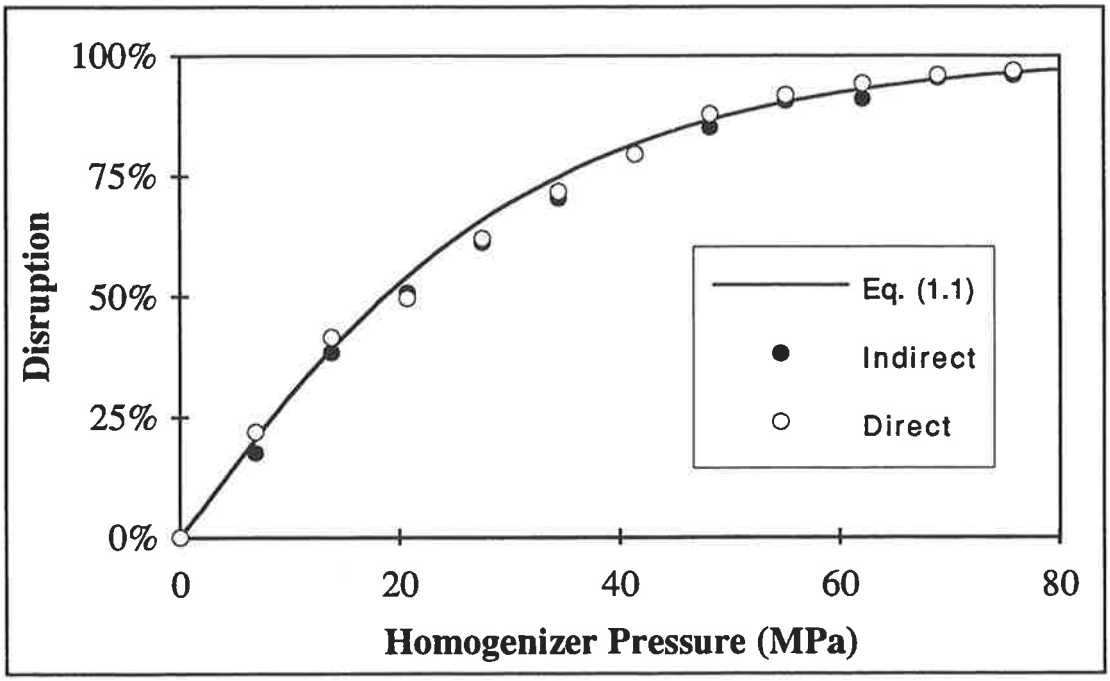

FIGURE 3.13 : *A comparison of disruption versus pressure curves determined by soluble protein measurements (indirect, eq. (3.1)) and by the disc centrifuge (direct, eq. (3.20)).*

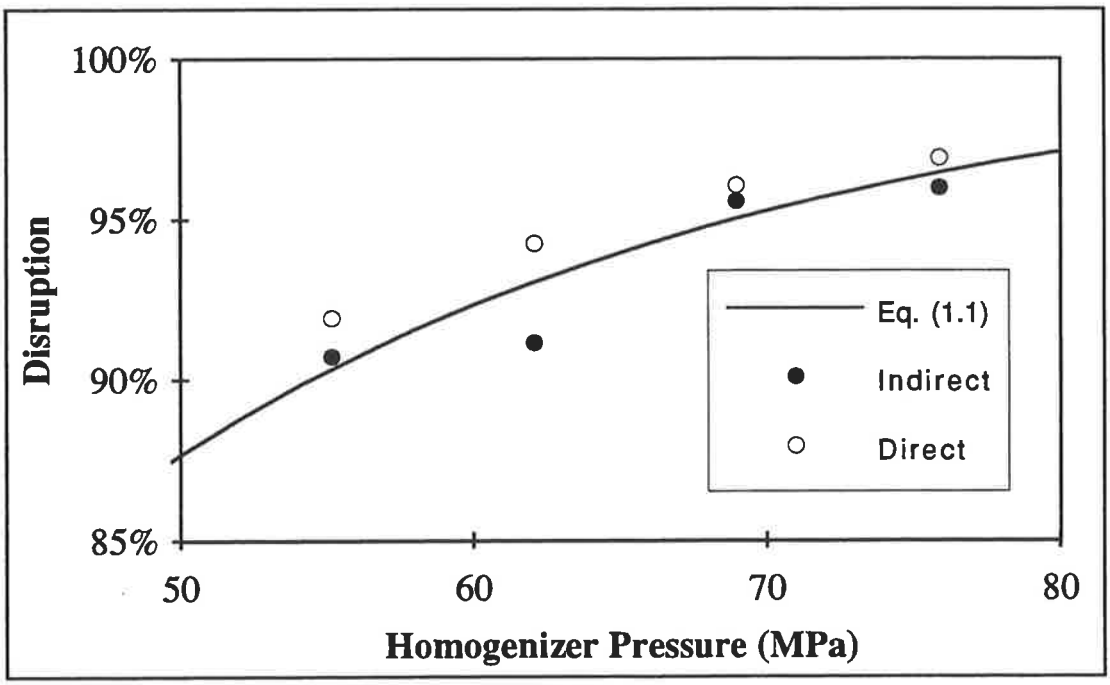

FIGURE 3.14 : *A comparison of disruption versus pressure curves determined by soluble protein measurements (indirect, eq. (3.1)) and by the disc centrifuge (direct, eq. (3.20)). (An enlargement of Figure 3.13 for high pressures.)*

Further, the disc centrifuge does not suffer the limitations of the traditional direct techniques outlined earlier.

In section 3.4, the uncertainty associated with calculating disruption by equation (3.20) was quantified. The final estimate of the true disruption and the uncertainty associated with the measurement is provided by equation (3.23). As stated in section 3.4, this estimate of the uncertainty does not include the errors associated with using an incorrect extinction coefficient, and any error in the calculated Stokes diameter. It was stated that these errors are negligible, as the effects will cancel when the ratio of areas is taken in equation (3.20). To illustrate this assertion, disruption was calculated for samples homogenized at pressures of 6.9 MPa, 41.4 MPa and 75.9 MPa using various extinction coefficients. The extinction coefficients tested were as follows :

i) the actual coefficient used in the definition of disruption, $K_e=K'=K_p/d_s$;

ii) the extinction coefficient for polystyrene, $K_e=K_p$;

iii) a constant extinction coefficient, which is equivalent to stating that $f_3(d_s) \propto A$.

The results of the disruption calculations are shown in Table 3.2. Also shown is the uncertainty for each measure, determined using equation (3.23) with the appropriate extinction coefficient. Disruptions calculated from soluble protein measurements are shown for comparison. The uncertainty is calculated from equation (3.7) with $\delta R'/R'=1.4\%$. This is considered conservative, as six repeat measurements of soluble protein gave a technique standard deviation ($\delta R'/R'$) of 2.0%. The lower value is used to compensate for the direct addition of uncertainties in equation (3.7).

Table 3.2 emphasizes that the use of an incorrect extinction coefficient has a negligible effect on the calculated disruption compared with the calculated uncertainty.

TABLE 3.2 : *The effect of the extinction coefficient on the calculated disruption.*

Pressure (MPa)	DISRUPTION (%)			
	Disc Centrifuge			Soluble Protein
	$K_e = K'$	$K_e = K_p$	K_e = Const	
6.9	21.9±3.3	20.7±3.3	22.4±3.3	17.6±0.5
41.4	79.6±1.5	79.0±1.6	79.9±1.5	79.7±2.2
75.9	96.9±0.3	96.8±0.3	97.0±0.3	96.0±2.7

The trend in errors is also highlighted, with the direct technique showing greatly improved accuracy at high levels of disruption.

3.6 Summary

When modelling disruption, a measure of the volume fraction of cells destroyed (the disruption) is required. The technique should be accurate at high levels of disruption, the regime of most practical importance. Indirect techniques are traditionally employed for measuring disruption, but suffer the following disadvantages :

- Disruption is inferred from measurements of the release of cytoplasmic contents. If the contents are denatured after release, the disruption will be underestimated. While denaturation is of concern, it should be included explicitly in the model and not implicitly through a reduced disruption value.
- Indirect measurements may not equate directly with disruption (e.g. DNA release from *Alcaligenes eutrophus* is a poor measure of disruption, Harrison *et al.*, (1990)).
- The lowest accuracy occurs in the regime of greatest practical interest, namely high levels of disruption.
- Proteins will oxidize. The biuret reactive protein in a given sample, and hence the apparent disruption, will decrease with storage.
- At high cell concentrations, a sample dilution procedure is necessary if soluble protein measurements are employed. The solubility of denatured protein changes with dilution, so incorrect results may be obtained.

The mass balance approach developed by Engler and Robinson (1979) overcomes the problems of variable solubility and protein oxidation, but is probably less accurate than the dilution procedure because of several assumptions in the derivation.

Direct techniques of measuring disruption do not suffer the preceding limitations. In particular, accuracy is greatest at high levels of disruption. However, existing direct techniques, such as microscopy and the electronic particle counter, are unsuitable for

analyzing a great number of samples. A novel method, using the analytical disc centrifuge, has been developed. The following procedure is used to determine disruption with the disc centrifuge :

- treat the feed and disrupted samples with 0.02% formaldehyde;
- analyze the samples using the disc centrifuge (Method III, Table 3.1);
- process the machine output to give a plot of A/K' versus d_s;
- deconvolute the debris and cell peaks (section 3.4);
- integrate the portion of the curves corresponding to undisrupted cells;
- estimate the disruption and the associated uncertainty as outlined in section 3.4.

To ensure that sample variation during storage is minimized, the procedure outlined in section 3.3.3 should be followed. Further, concentration effects during analysis are minimized by following the procedure in section 3.3.4.

The technique provides a direct measure of disruption. It does not suffer the limitations associated with indirect methods. It is extremely accurate at high levels of disruption despite the need to deconvolute the debris and cell peaks. Consequently, meaningful comparisons of the model predictions with experimental data can be made. It has also been shown that the particular choice of extinction coefficient, which is employed to relate the centrifuge output to the volume of cells, has little effect on the calculated disruption. While the technique is a significant advance over existing methods, it suffers the following disadvantages :

- It is less accurate than indirect methods at low levels of disruption;
- The procedure is more time consuming than indirect measurements;
- The disc centrifuge is a relatively expensive instrument.

Fortunately, these disadvantages do not reduce the effectiveness of the method for analyzing disruption. It is therefore employed throughout this thesis.

CHAPTER 4

PARAMETER ESTIMATION

A new model for the disruption of *E. coli* by high-pressure homogenization was developed in chapter 2. Disruption is described by five adjustable parameters, which may be classified as either system-specific or culture-related. Based upon certain premises summarized in section 2.5, four of the five parameters (the system- and strain-specific parameters) are constant for a given system and strain. In this chapter, the disruption of twenty-one cultures of *E. coli* B is examined. Widely-varying resistances to disruption were ensured by varying the time for which each culture experienced glucose starvation. The cultures were homogenized, and disruption versus pressure curves obtained using the analytical disc centrifuge (chapter 3). The data were regressed to the proposed model to determine the four system- and strain-specific parameters and the mean effective strength, $\bar{S}$, for each culture. In the next chapter, mean effective strength is correlated with measurable cell properties.

4.0 Introduction

A new model for homogenization was developed in chapter 2. Disruption for a single homogenizer pass is given by equation (2.8) (or eq. (2.11) with N=1). As stated, the values of five parameters are required. These may be grouped as follows :

- Culture-related, describing the strength distribution ($\bar{S}$ and σ);
- System-specific, describing the stress distribution (m, n and d).

The two culture-related parameters may be further classified as either strain-specific (σ) or culture-specific ($\bar{S}$). In section 2.5, a series of assertions were made relating to the model. Accepting these assertions, the four system- and strain-specific parameters become constant and disruption is described by the single adjustable culture-specific parameter :

- the mean effective cell strength of the non-septated sub-population, $\bar{S}$.

This corresponds to the case of a fixed or known homogenizer disrupting a specified strain of *E. coli*. It was also proposed that $\bar{S}$ should correlate with measurable cell properties.

In this chapter, experimental disruption data are obtained for various cultures of a single *E. coli* strain disrupted with a specific homogenizer. A non-linear regression of the data is presented. The aim is to determine the system- and strain-specific parameters, and to verify that they are indeed constant. The mean effective strength, $\bar{S}$, for each culture is also obtained from the regression. These values of strength are correlated with peptidoglycan crosslinkage and average cell length in the following chapter. In addition to investigating the proposed model, data are regressed to the kinetic model (eq. (1.1)) for comparison.

4.1 Experimental

A series of cultures with widely varying resistances to disruption is required to verify the proposed model. As indicated in chapter 1, such cultures may be obtained by varying the growth media, growth rate or growth phase.

The effects of varying growth media are difficult to predict in advance. Cultures with widely differing strengths cannot be guaranteed. Further, only one type of culture is obtained from each fermentation. Any reasonable experimental design is therefore fermentation intensive. Growth rate is simply controlled with a chemostat. Unfortunately, such equipment was not available for the tests described in this thesis. The present tests therefore relied on different cultures obtained by varying the growth phase. Specifically, fermentations were conducted and samples were withdrawn at various times after exhaustion of the glucose supply. This approach has the advantage that several different cultures may be obtained from a single fermentation. It is also easily implemented with batch fermenters. In addition, a single fermentation was conducted with excess glucose. Consequently, cultures spanning the range of phases from 'approximately exponential' to 'late stationary' were obtained. This is a simple approach, as cells will strengthen themselves during stationary phase as indicated in chapter 1. A range of culture strengths is therefore guaranteed.

4.1.1 Fermentations

A series of five (1-5) fermentations was conducted. The first three fermentations (1-3) employed a 16 L (working volume) Chemap type CF2000 fermenter. Wild type *E. coli* B (P903, Department of Microbiology, The University of Adelaide) were inoculated from a shake flask into 16 L of modified C1 minimal media (Table 4.1) to give an initial absorbance (A_{600}) of approximately 0.002.

TABLE 4.1 : *Composition of the fermentation medium.*

COMPONENT	COMPOSITION ($g\ L^{-1}$)
D-Glucose	3.125
NH_4Cl	2.42
KH_2PO_4	2.38
Na_2HPO_4	3.9
K_2SO_4	1.82
$MgSO_4.7H_2O$	0.625
$FeSO_4.7H_2O$	0.02
$MnSO_4.H_2O$	0.0051
$ZnSO_4.7H_2O$	0.0086
$CuSO_4.5H_2O$	0.00076
Trisodium citrate	0.088
20% antifoam†	0.03

†Chemical Antifoam is Lanquell 217 (Diamond-Shamrock Aust. Pty. Ltd.).

After glucose exhaustion (noted by a sudden increase in dissolved oxygen concentration), 4 L samples of broth were withdrawn from the fermenter at predetermined times (Table 4.2). These were cooled to 20°C in a large beaker using a coil with recirculating ethylene glycol. Cooled samples were homogenized as soon as possible (Table 4.2).

TABLE 4.2 : *Fermentation data.*

Fermentation I.D.	Growth Rate (h^{-1})	Final Density (A_{600})	Sample I.D.	Withdrawal Time (min)†	Delay Before Homogenization (min)††
1	1.20	3.8	1a	5	25
			1b	20	30
			1c	50	35
			1d	70	30
2	1.25	4.0	2a	−5	30
			2b	0^+	45
			2c	10	50
			2d	20	65
3	1.28	4.0	3a	5	40
			3b	15	55
			3c	30	55
			3d	60	40
4	1.44	3.9	4	Excess Glucose	15
5	1.45	3.5	5a	0^+	30
			5b	45	30
			5c	105	35
			5d	180	40
			5e	240	30
			5f	300	30
			5g	390	30
			5h	480	30

† Referenced to glucose exhaustion.
†† Time between sample withdrawal and the commencement of homogenization.

The fourth fermentation was conducted to obtain near exponential-phase cells. The protocol previously described was employed, however the glucose concentration was doubled. When the broth reached an optical density (A_{600}) of 2.9, the temperature set point of the fermenter was altered to 5°C. Additional growth occurring while the broth was cooling yielded a final optical density of 3.9 (Table 4.2).

The fifth fermentation was carried out in a 150 L Bioengineering fermenter. A total of 100 L of media was inoculated from shake flask to give a starting optical density of 0.005. After glucose exhaustion, 10 L samples were withdrawn at varying times (Table 4.2) and cooled to 20°C prior to homogenization.

In all fermentations, the pH was controlled at 6.9 by automatic addition of 4M NaOH. Temperature was controlled at 37°C. Minor foaming occurred. Because of the low cell densities obtained, the fermenter's mechanical foam breaker was sufficient to control this without need for additional chemical antifoam.

4.1.2 Homogenization

Samples were homogenized using an APV-Gaulin 15M-8TA high-pressure homogenizer (Figure 1.5) with a ceramic cell disruption (CD) valve seat (Figure 4.1). The machine is fitted with a second stage which remained set to zero pressure during all tests. All batches were homogenized over a range of pressures to a maximum of 75 MPa. The feed temperature for all fermentations except number 4 was 20°C. Fermentation batch 4 was homogenized at 5°C to minimize growth in the presence of excess glucose.

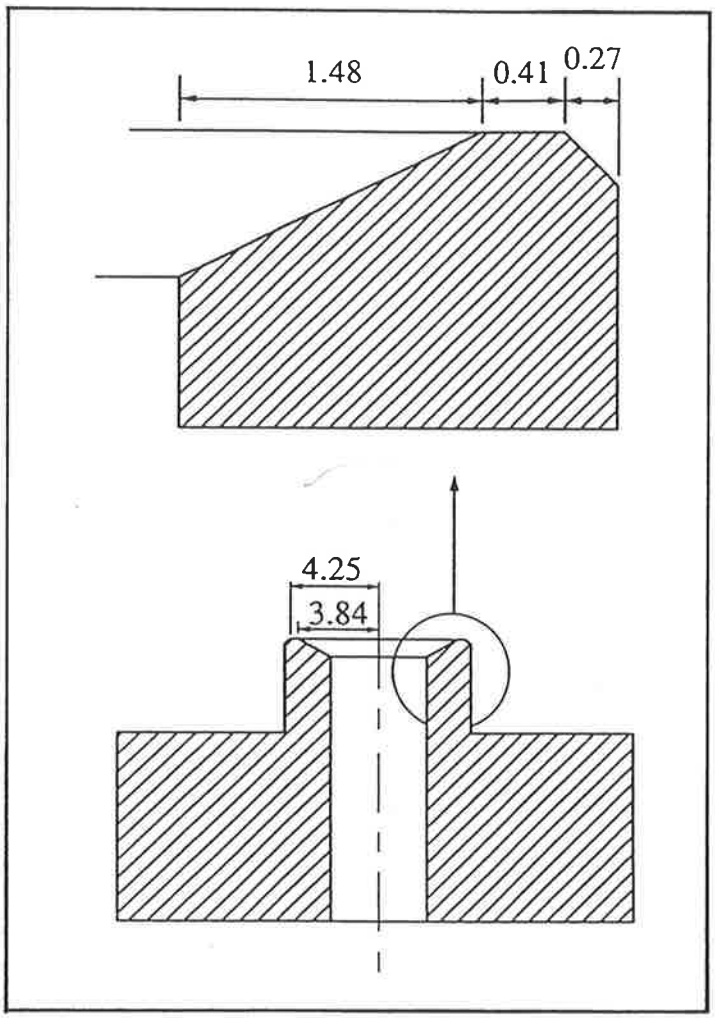

FIGURE 4.1 : *Cell Disruption (CD) homogenizer valve seat. (Drawn to scale: all dimensions are in mm).*

The homogenizer pressure measurement using the fitted pressure gauge is uncertain due to the pulsing nature of the single-acting simplex pump. Pressure transients for all samples were obtained using a Schaevitz P-1041 (Lucas Schaevitz Ltd., Slough, Berkshire, U.K.) pressure transducer fitted to the machine. This transducer was machined into the homogenizer block near the pressure gauge.

Feed and homogenate samples were treated with formaldehyde (0.02% v/v) and stored at 4°C prior to disruption analysis. In addition, 400 mL of feed material was retained for analysis of cell size and cell-wall properties, as detailed in the next chapter.

4.1.3 Analysis

Homogenate and feed samples were analysed using the analytical disc centrifuge, as described in chapter 3. Disruption, and the associated uncertainty, were calculated as outlined in section 3.4. All disruption measurements were completed within two days of the fermentation. Stored samples exhibited no quantifiable change during this period.

4.2 Results

During any typical homogenization, a nominal pressure will be set using the fitted gauge. This will then be the reported "homogenizer pressure". However, this pressure is uncertain due to the pulsing nature of the single-acting simplex pump. In the present tests, a pressure was set using the gauge. An accurate pressure transient was then measured using the attached transducer. For modelling purposes, the homogenizer pressure is reported to be the maximum average pressure recorded during the transient. This is accurately known and is approximately 3.2 MPa higher than the nominal average gauge pressure.

Figure 4.2 presents a series of typical pressure transients for the homogenizer.

Figure 4.3 shows the relationship between the nominal gauge pressure (P_g) and the maximum average pressure (P). The two pressures are related by equation (4.1), which was determined by least-squares regression of the available pressure transients.

$$P = 1.015\,P_g + 3.2 \qquad -(4.1)$$

As expected for the disruption tests, different samples produced widely-varying results. Stationary-phase samples proved the hardest to disrupt, whilst those withdrawn near the point of glucose exhaustion and therefore near exponential phase were more easily disrupted. Disruption data are presented in the next section.

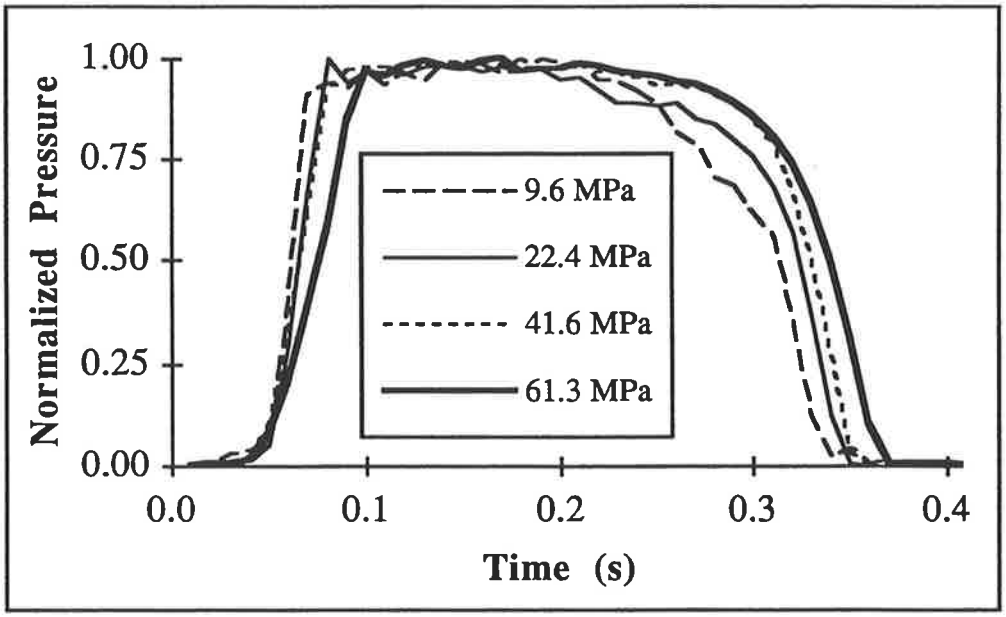

FIGURE 4.2 : *Homogenizer pressure transients*

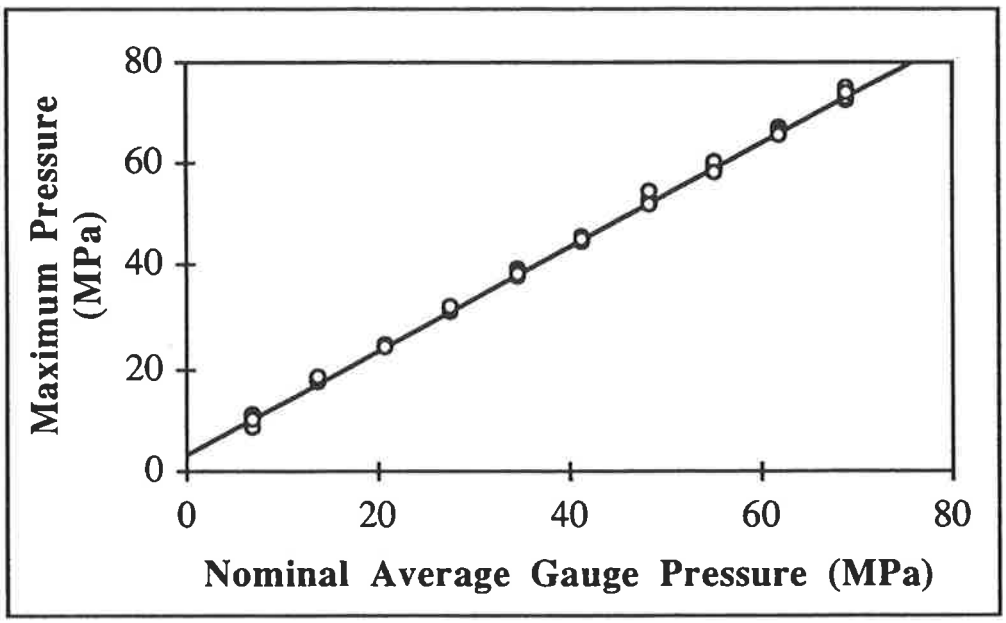

FIGURE 4.3 : *Relationship between the nominal average gauge pressure and the maximum average pressure recorded using the pressure transducer. Scatter about the regressed line results from error in the nominal average gauge pressure.*

4.3 Model Regressions

The disruption data were regressed to the kinetic model and the model developed in chapter 2. In all cases, weighted regression was employed. Weighting factors were determined from the uncertainty calculated for each data point (section 3.4). In all cases, error in the reported homogenizer pressure was assumed negligible.

4.3.1 Kinetic Equation

The most-widely employed model for describing disruption data is the kinetic model, equation (1.1),

$$\ln\left(\frac{1}{1-D}\right) = k_1 N P^a \qquad -(1.1)$$

where a and k_1 are culture-specific parameters. In the above equation, disruption (D) has been substituted for soluble protein release (R_p). Disruption data were regressed to the linearized log-log form of this equation. The parameter values are summarized in Table 4.3. The experimental data and fitted curves are shown in Figures 4.4 to 4.7. Figure 4.8 is a parity plot comparing the regressed and experimental disruption values.

TABLE 4.3 : *Calculated values for a and k_1 in equation (1.1).*

SAMPLE I.D.	CONSTANTS	
	a	k_1 (MPa^{-a})
1a	1.04	0.051
1b	1.18	0.021
1c	1.60	0.0028
1d	1.79	0.0012
2a	1.11	0.033
2b	0.954	0.065
2c	1.14	0.024
2d	1.25	0.012
3a	1.01	0.045
3b	1.17	0.020
3c	1.16	0.020
3d	1.40	0.0068
4	0.635	0.38
5a	0.701	0.24
5b	1.18	0.020
5c	1.38	0.0072
5d	1.47	0.0050
5e	1.64	0.0023
5f	1.73	0.0014
5g	1.71	0.0015
5h	1.65	0.0019

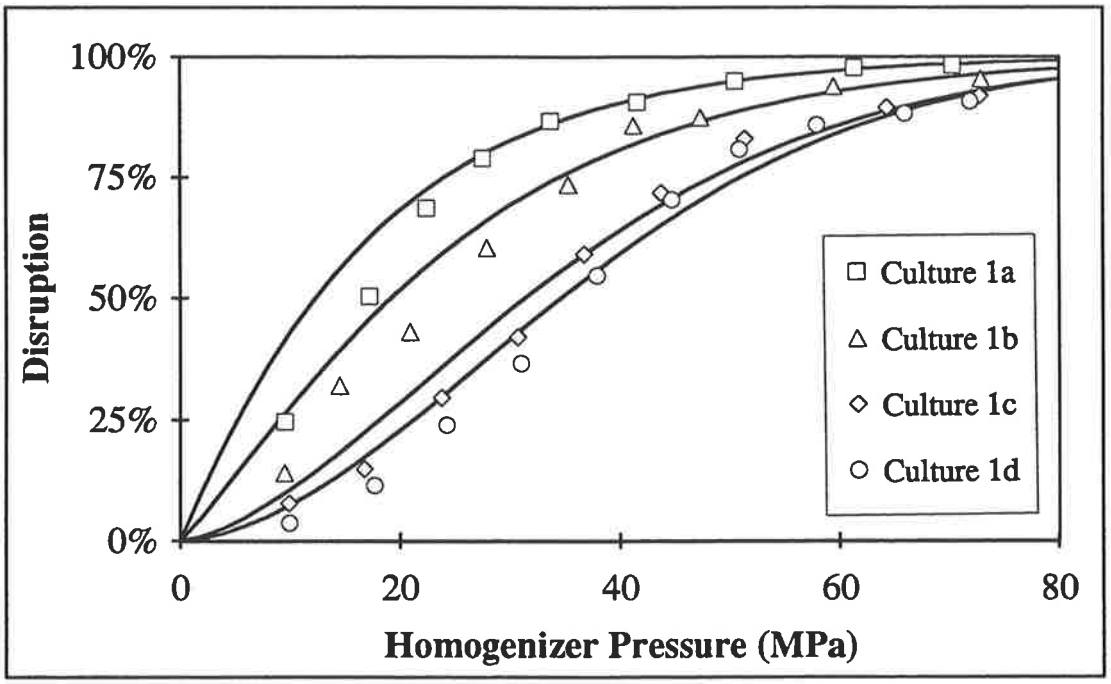

FIGURE 4.4 : *Disruption versus Pressure for fermentation 1.*

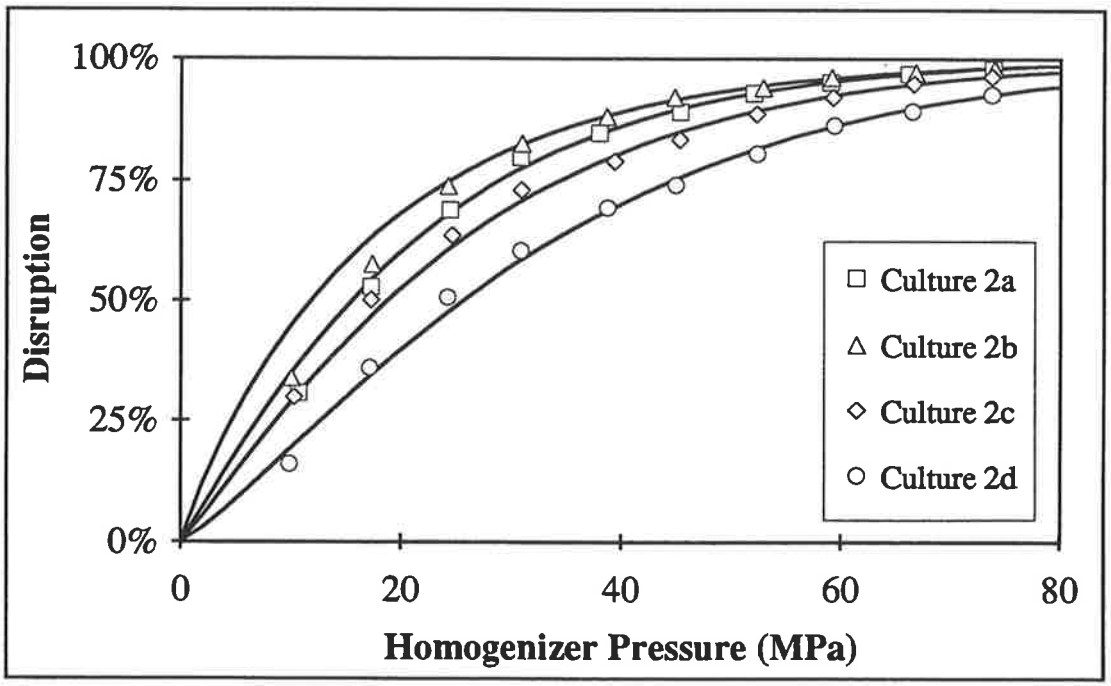

FIGURE 4.5 : *Disruption versus Pressure for fermentation 2.*

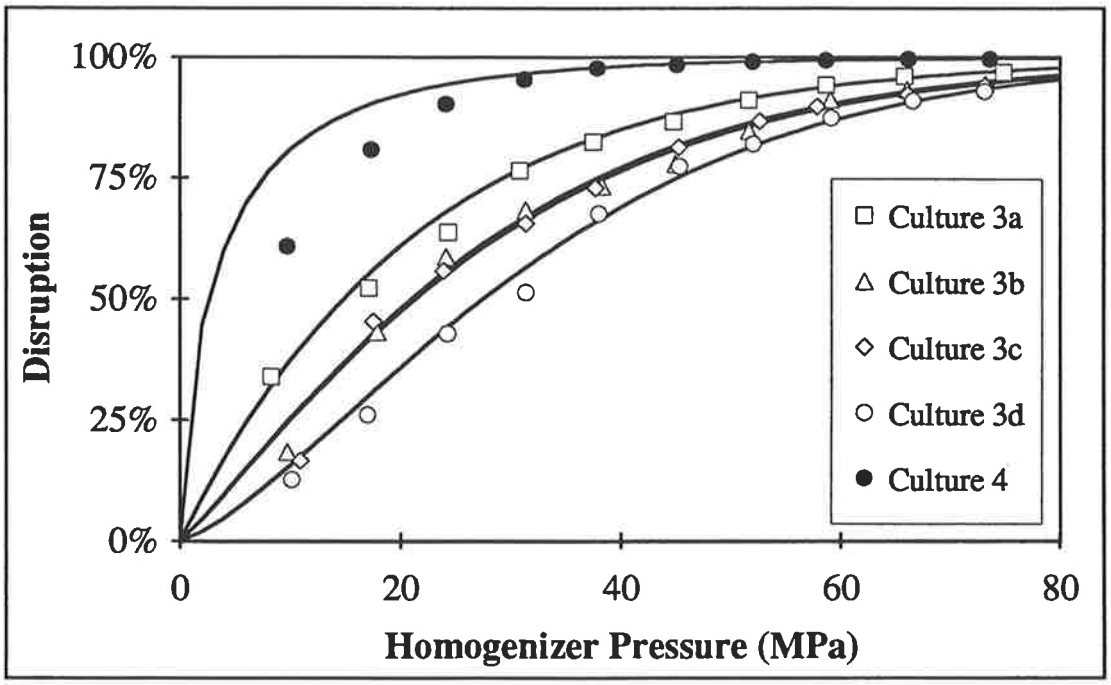

FIGURE 4.6 : *Disruption versus Pressure for fermentations 3 and 4.*

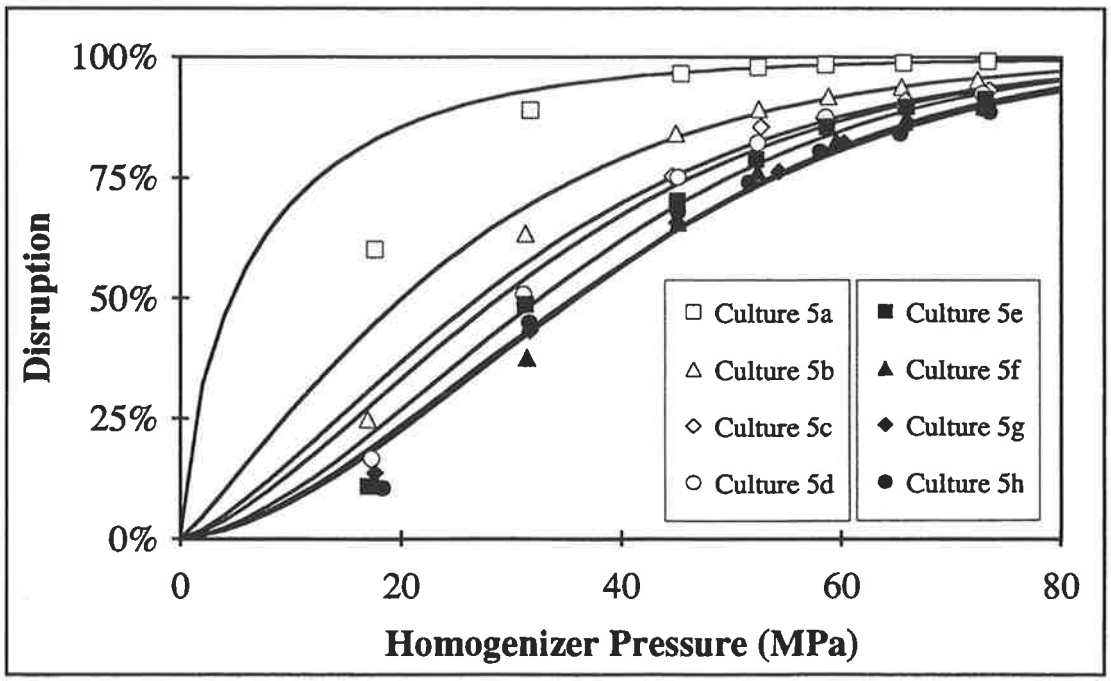

FIGURE 4.7 : *Disruption versus Pressure for fermentation 5.*

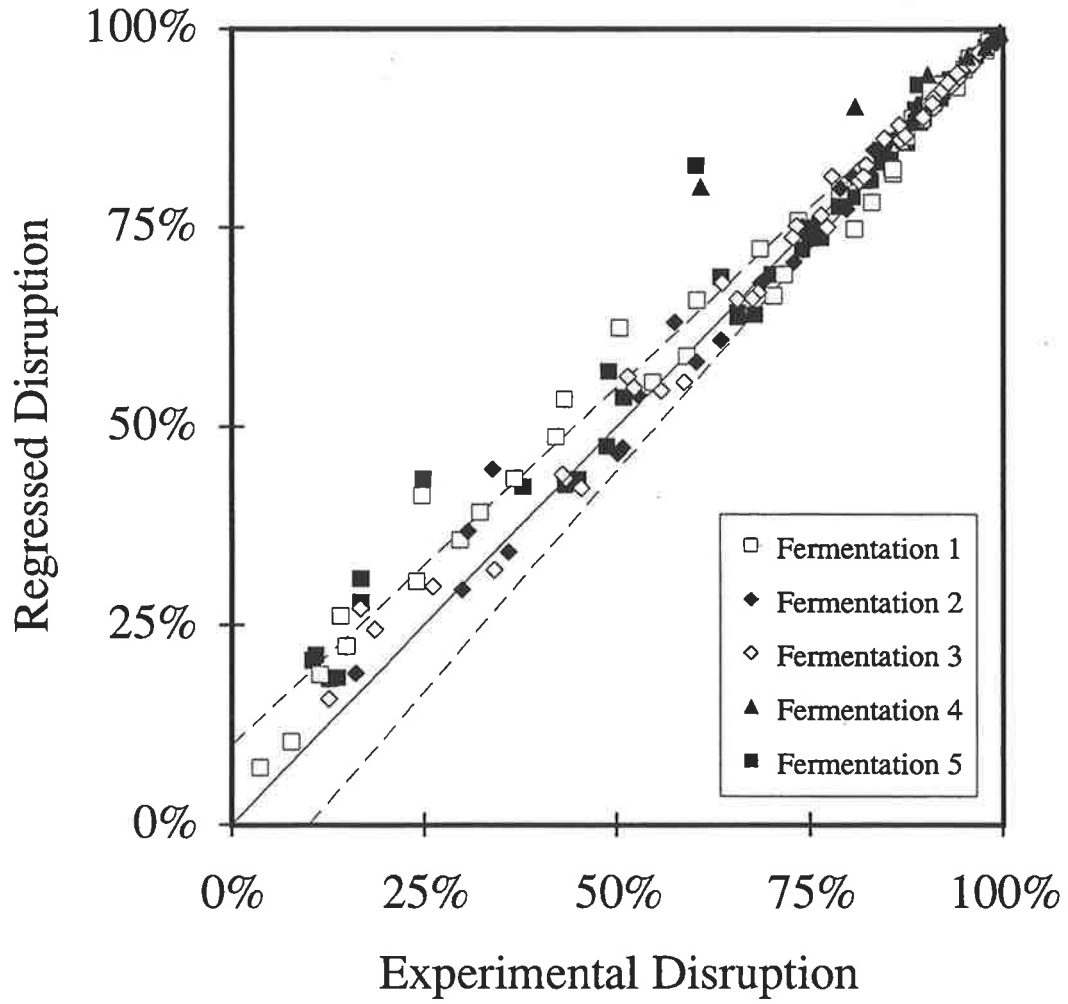

FIGURE 4.8 : *Parity plot comparing experimental data with regressed values from the kinetic model (eq. (1.1)). Dashed lines represent ±10%, reflecting the trend in analytical accuracy.*

4.3.2 Proposed Model : First Regression

The proposed model calculates disruption through equation (2.8),

$$D = \int_0^{\infty} f_D(S)\, f_S(S)\, dS \qquad -(2.8)$$

where the strength and stress distributions are given by equations (2.1) and (2.6), respectively.

$$f_S(S) = \frac{1}{\sigma\sqrt{2\pi}} \exp\left[\frac{-(S-\bar{S})^2}{2\sigma^2}\right] \qquad -(2.1)$$

$$f_D(S) = \frac{(mP^n)^d}{S^d + (mP^n)^d} \qquad -(2.6)$$

A FORTRAN program using the IMSL routine DRNLIN (modified Levenberg-Marquardt method) was coded to perform a non-linear regression of the model to the experimental data. Within the program, the integral was evaluated numerically using Simpson's method, with the limits of integration set to $\bar{S}\pm6\sigma$.

As stated, the values of five parameters are unknown. These may be grouped as follows :

- Culture-specific, describing the strength distribution ($\bar{S}$);
- Strain-specific, describing the strength distribution (σ);
- System-specific, describing the stress distribution (m, n and d).

For the currents series of tests, the assertions presented in section 2.5 state that the four system- and strain-specific parameters are constant (m, n, d, and σ). The most general test of this is to determine the five parameters for each separate culture by non-linear regression.

The four 'constant' parameters can then be compared to see if they remain truly constant as asserted. A slight modification of this strategy was employed. The data from each fermentation run were regressed separately. Each culture was allowed to assume unique values of $\bar{S}$ and σ. The values of the remaining parameters (m, n, d) were constrained to be identical for a given fermentation batch. The results of the non-linear regression are summarized in Table 4.4.

Good agreement between the model and the experimentally-determined disruption data was obtained. Figure 4.9 is a plot of the number of standard deviations separating the experimental and regressed values (t, eq. (3.26)) as a function of homogenizer pressure. Most regressed values lay within three standard deviations of the experimental disruption.

The regression results demonstrate an excellent similarity in the parameters (m, n, d, and σ) between fermentation batches. In particular, the assertion that m and n are constant for a given system and independent of the particular culture is confirmed beyond doubt. The effect of the variation in d is minor given the high value of this exponent. There is no significant correlation of σ with $\bar{S}$ (e.g. σ decreases with increasing $\bar{S}$ for fermentation 1, σ increases with increasing $\bar{S}$ for fermentation 2, σ is approximately constant for fermentations 3, 4 and 5). It is likely that the variation in σ is random and reflects minor differences between the disruption curves. The proposal that σ is constant therefore appears reasonable in the absence of a practical alternative.

TABLE 4.4 : *Calculated coefficients for the proposed model using weighted least-squares non-linear regression (First Regression).*

Ferm. I.D.	m	n	d	Samp. I.D.	Time (min)†	σ (–)	$\bar{S}$ (–)
1	12.6	0.393	8.03	1a	5	4.44	38.72
				1b	20	4.75	43.46
				1c	50	2.61	49.16
				1d	70	1.08	50.24
2	12.7	0.393	6.99	2a	–5	3.78	39.93
				2b	0^+	4.53	38.38
				2c	10	7.24	41.42
				2d	20	8.55	45.84
3	12.9	0.395	6.34	3a	5	3.73	40.98
				3b	15	4.11	44.30
				3c	30	4.14	44.88
				3d	60	3.88	47.29
4	12.7	0.393	7.77	4	XS Gl††	3.85	31.23
5	12.6	0.393	7.92	5a	0^+	3.82	35.91
				5b	45	3.80	45.02
				5c	105	3.58	47.90
				5d	180	3.81	48.46
				5e	240	3.59	49.60
				5f	300	3.29	51.17
				5g	390	3.73	51.29
				5h	480	3.77	51.47

† Time of sample withdrawal after culture glucose exhaustion (Table 4.2).

†† Excess glucose present.

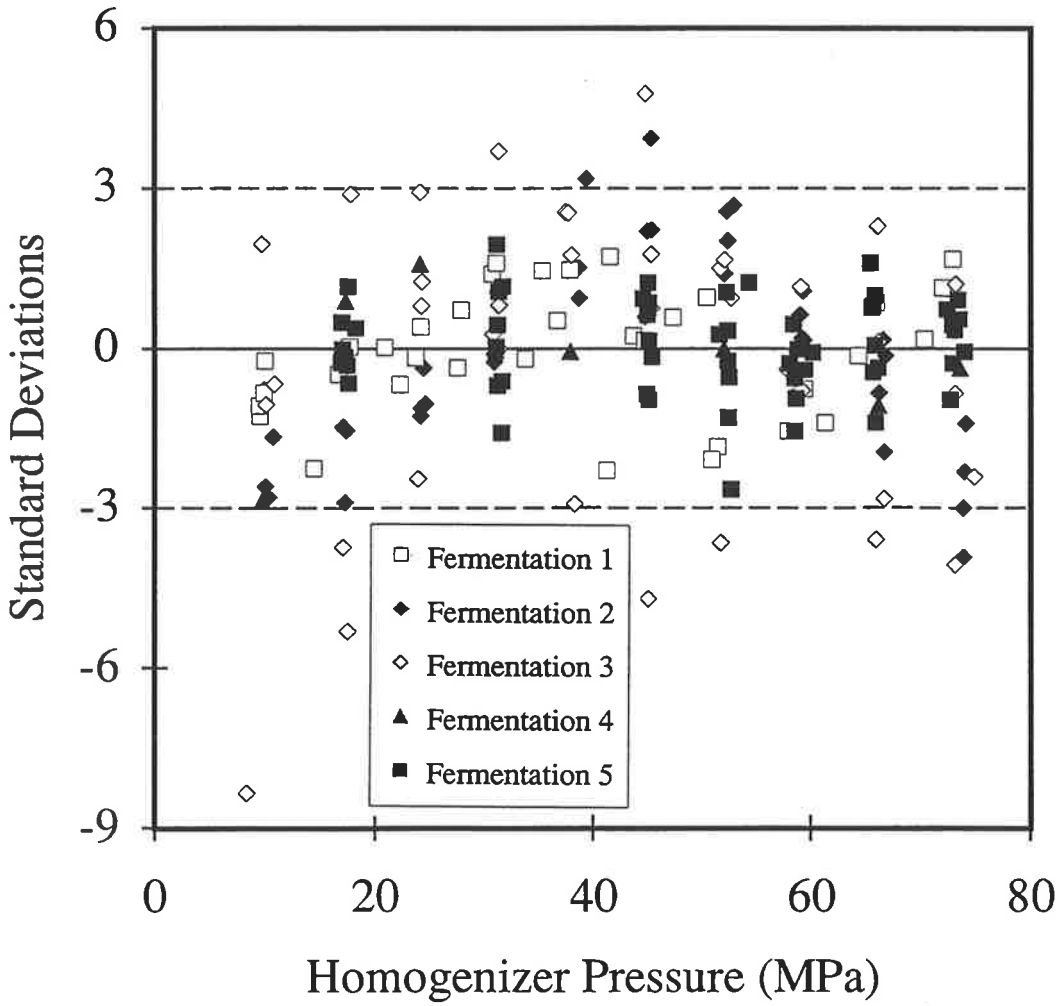

FIGURE 4.9 : *Number of standard deviations separating the experimental and regressed disruption versus homogenizer pressure (Model parameters from Table 4.4)*

4.3.3 Proposed Model : Second Regression

The results of the previous section suggest that four parameters are constant. The non-linear regression was repeated with the additional constraint that the four system- and strain-specific parameters (m, n, d, and σ) are identical for all cultures. The mean effective strength was allowed to vary for each culture. The regression results are summarized in Table 4.5.

Figure 4.10 presents a parity plot for the data. Figure 4.11 plots the number of standard deviations, t, separating the experimental and regressed values, against homogenizer pressure. The expression for t is given by equation (3.26). Figure 4.12 illustrates the model fit to selected experimental data, and shows the regressed kinetic curves (eq. (1.1)) for comparison.

Figure 4.10 confirms that the model describes the experimental data with good accuracy. For the specified homogenizer and strain, disruption is characterized by a single adjustable parameter, $\bar{S}$. A comparison of Figures 4.9 and 4.11 reveals a slight loss of accuracy by constraining the system- and strain-specific parameters to be constant. The greatest loss in accuracy occurs at low homogenization pressures. Practically, this is the region of least interest. A simple explanation of the deviation is available. Error in the pressure measurement is neglected in the estimate of uncertainty. Although such error will be minimized by using the pressure transducer, it is unlikely to be completely eliminated. Any error in the pressure measurement will have the greatest influence at low pressures, where the gradient of the disruption versus pressure curve is greatest.

Figure 4.10 clearly demonstrates that the model has no particular tendency to over- or under-describe disruption. Comparison with Figure 4.8 indicates that the kinetic model (eq. (1.1)) consistently over-describes the experimental data at low levels of disruption.

TABLE 4.5 : *Calculated coefficients for the proposed model using weighted least-squares non-linear regression (Second Regression).*

m	n	d	σ (–)	Samp. I.D.	Time (min)†	$\bar{S}$ (–)
13.3	0.383	7.30	5.09	1a	5	38.09
				1b	20	43.31
				1c	50	48.51
				1d	70	49.39
				2a	–5	40.21
				2b	0^+	39.02
				2c	10	43.26
				2d	20	47.86
				3a	5	41.57
				3b	15	44.89
				3c	30	45.41
				3d	60	47.62
				4	XS Gl††	29.78
				5a	0^+	34.23
				5b	45	44.20
				5c	105	47.28
				5d	180	48.03
				5e	240	49.15
				5f	300	50.68
				5g	390	50.92
				5h	480	51.38

† Time of sample withdrawal after culture glucose exhaustion (Table 4.2).

†† Excess glucose present.

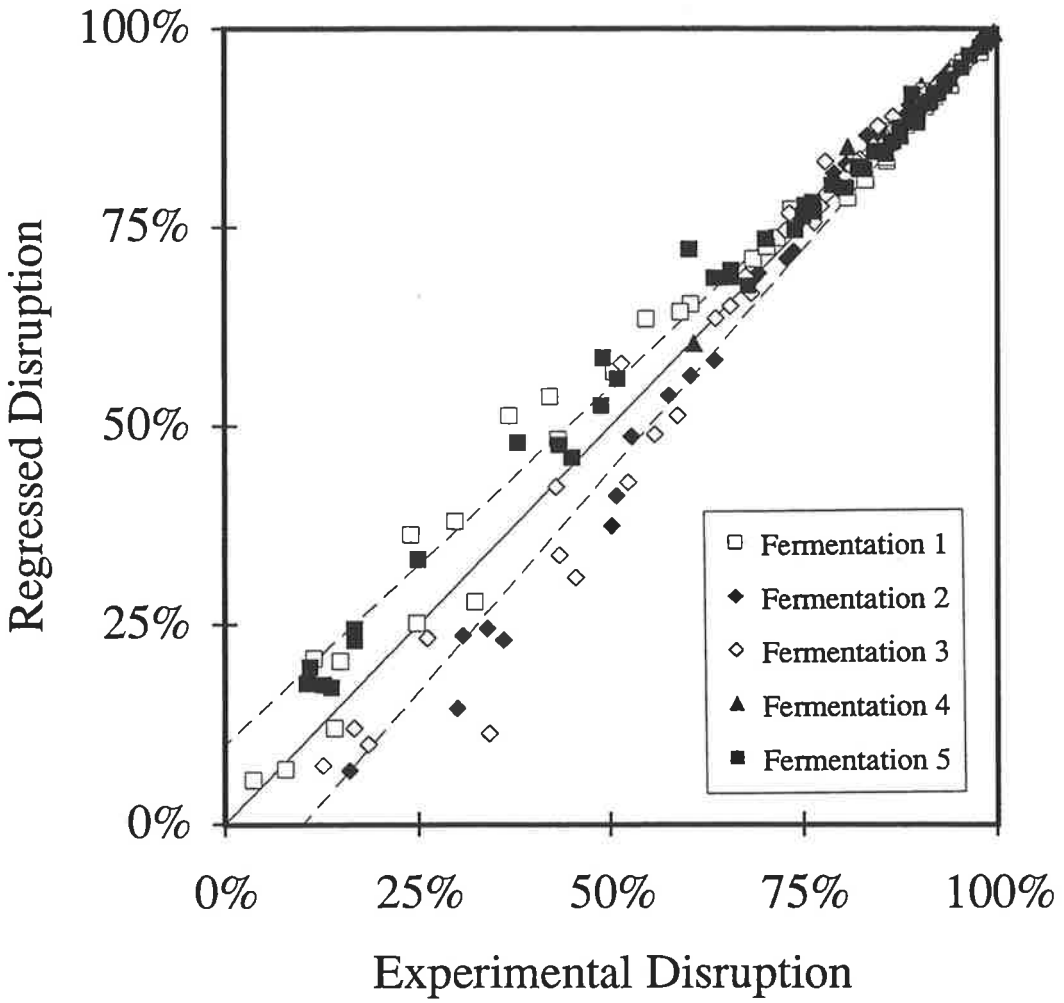

FIGURE 4.10 : *Parity plot comparing experimental data with regressed values from the proposed model (Model parameters from Table 4.5). Dashed lines represent ±10%, reflecting the trend in analytical accuracy.*

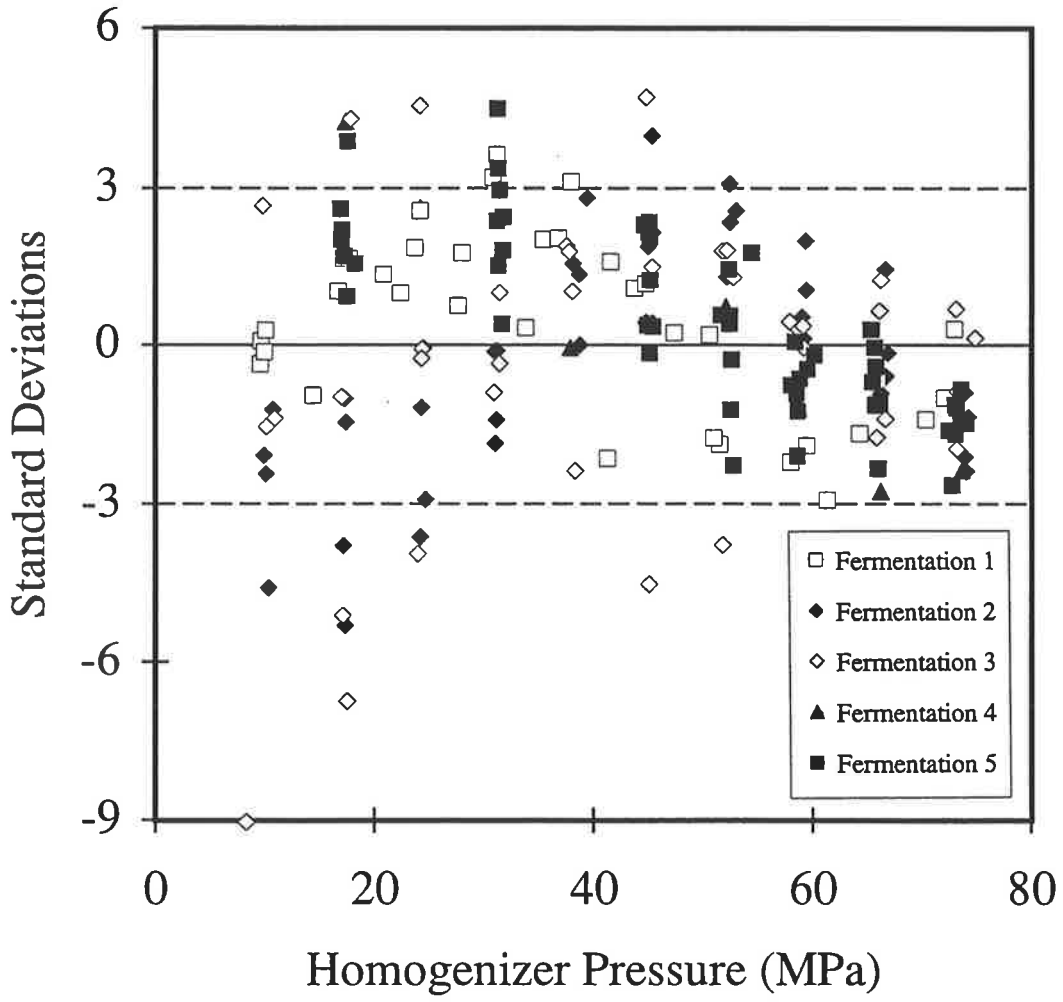

FIGURE 4.11 : *Number of standard deviations separating the experimental and regressed disruption versus homogenizer pressure. (Model parameters from Table 4.5)*

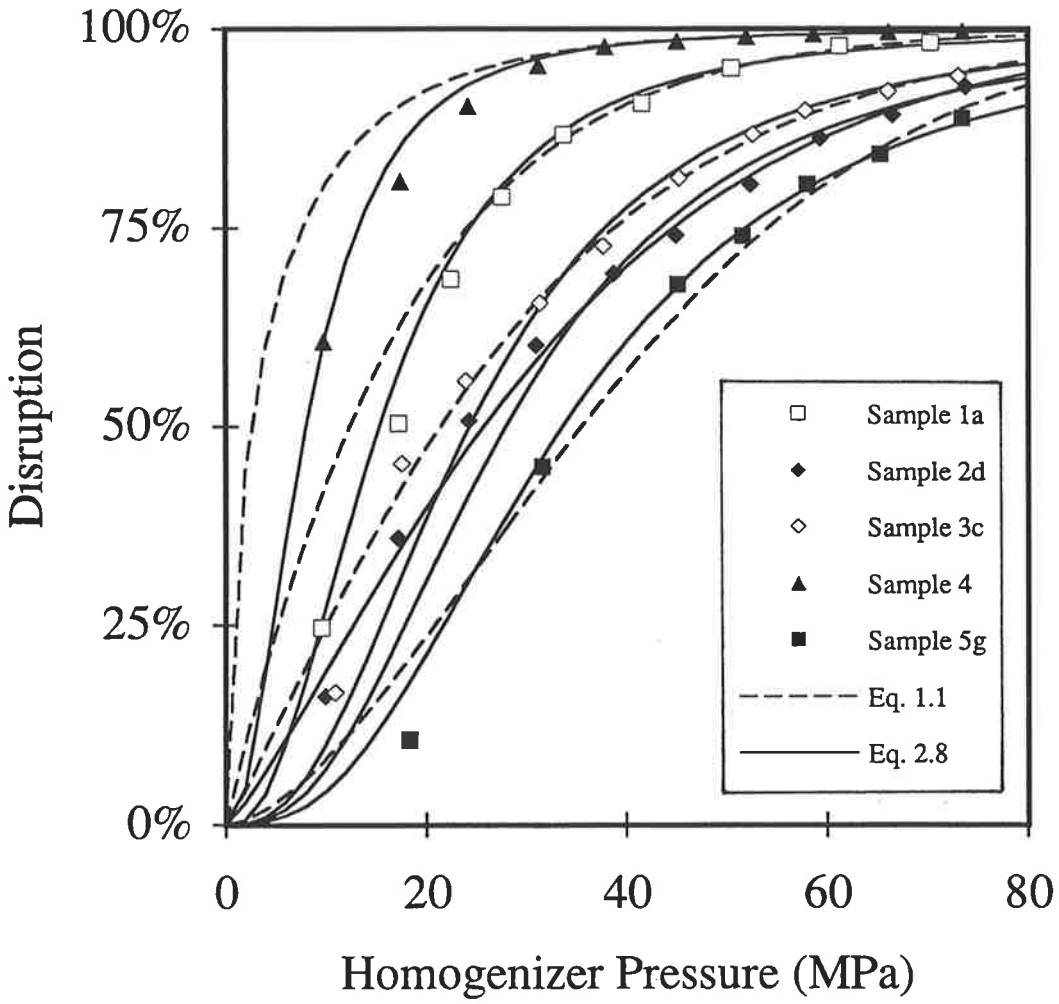

FIGURE 4.12 : *Disruption versus homogenizer pressure. A comparison of selected experimental data with descriptions by the kinetic model (eq. (1.1)) and the proposed model (eq. (2.8)) using the parameters in Tables 4.3 and 4.5, respectively.*

4.3.4 Proposed Model : Stress Discontinuity

Figure 4.11 suggests a bias in the model with homogenizer pressure. Further, it suggests the bias is pronounced for pressures in excess of 35 MPa. This may be due to a change in the form of the stress distribution function at approximately this pressure. Figure 4.2 clearly shows a change in the pressure-transient shape as operating pressure is increased. Such a variation will result in a change in the stress distribution function with pressure.

Another possible cause is a transition in valve hydrodynamics (e.g. from turbulent to laminar) as pressure is increased. The total pressure drop across a homogenizing valve is given by equation (4.2),

$$\frac{P}{\frac{1}{2}\rho u_o^2} = \frac{P_F}{\frac{1}{2}\rho u_o^2} + \left(k + k' \frac{R_{vo}}{R_v}\right) = \frac{P_F}{\frac{1}{2}\rho u_o^2} + k_L \qquad \text{-(4.2)}$$

where k is the inlet loss coefficient, k' is the exit loss coefficient, k_L is the overall loss coefficient and P_F is the pressure loss due to friction across the valve face (Phipps, 1975). The inlet loss coefficient is generally assumed to be 0.5 for sharp inlets and 0.2 if some rounding is introduced. The exit loss coefficient is normally assumed to be unity. The pressure loss due to friction depends on the valve velocity profile. For low-pressure milk homogenizers operating at low Reynolds numbers and small gaps (≤ 100μm) Phipps (1975) determined equation (4.3),

$$\left(\frac{P_F}{\frac{1}{2}\rho u_o^2}\right)_{TP} = \frac{5}{m\ N_{Re}^{0.6}} \left[1 - \left(\frac{R_{vo}}{R_v}\right)^{0.4}\right] \qquad \text{-(4.3)}$$

where the Reynolds number is given by equation (4.4) and m is the dimensionless gap width (eq. (4.5)) (Phipps, 1975).

$$N_{Re} = \frac{\rho Q}{2\pi R_{vo}\eta} \qquad \text{-(4.4)}$$

$$m = \frac{h}{2R_{vo}} \qquad \text{-(4.5)}$$

Equations (4.2) and (4.3) have been previously used to model the 15M homogenizer at high pressure (Keshavarz-Moore *et al.*, 1990). The transition from laminar to turbulent flow is generally assumed to occur at a Reynolds number between 500 and 1000 depending on the gap (Keshavarz-Moore *et al.*, 1990). This is based on a study by Kawaguchi (1971), who demonstrated that the reduced Reynolds number ($m\ N_{Re}$) provides a better criterion for distinguishing between laminar and turbulent flows. The study was conducted with large gaps (minimum 1 mm) and showed laminar flow for reduced Reynolds numbers below approximately 2. The data presented in this chapter was obtained using a homogenizer operating at a reduced Reynolds number of approximately 2.4 at 35 MPa (Table 4.6). This value has not been confirmed experimentally. The only published experimental study on the mechanics of the 15M homogenizer is by Brookman (1974). However, the measurements of valve lift do not satisfy continuity as lift apparently increases with pressure at constant flowrate.

The reduced Reynolds number suggests a transition in flow dynamics is possible at approximately 35 MPa. This result, and the change in pressure-transient shape illustrated in Figure 4.2, provides justification for a discontinuous stress distribution, giving equation (4.6).

$$f_D(S) = \frac{(m'P^{n'})^{d'}}{S^{d'} + (m'P^{n'})^{d'}} \qquad (P < 35\ \text{MPa}) \qquad \text{-(4.6a)}$$

$$f_D(S) = \frac{(mP^{n})^{d}}{S^{d} + (mP^{n})^{d}} \qquad (P \geq 35\ \text{MPa}) \qquad \text{-(4.6b)}$$

TABLE 4.6 : *Calculation of the reduced Reynolds number.*

VARIABLE	VALUE	COMMENTS
R_v	4.25 mm	Valve Outer Radius
R_{vo}	3.84 mm	Valve Inner Radius
η	1.2 mPa.s	Homogenate Viscosity
$Q^{\dagger}$	165 L h^{-1}	Average Valve Flowrate
ρ	1000 kg m^{-3}	Homogenate Density
N_{Re}	1,580	Reynolds number, eq. (4.4)
k_L	1.104	Overall Loss Coefficient
P	35 MPa	Homogenizer Pressure
m	0.0015	Solving eqs. (4.2) and (4.3)
$m\ N_{Re}$	2.4	Reduced Reynolds Number

† Based on valve open for 0.33 sec per sec with an average flowrate of 55 L h^{-1}

4.3.5 Proposed Model : Third Regression

Disruption data were regressed to the model to test the effect of introducing a discontinuous stress distribution as in equation (4.6). The strain-specific parameter (σ), and the six parameters in equation (4.6) were constrained to be the same for all data. The integration limits were set to $\bar{S}\pm 6\sigma$. The mean effective strength, $\bar{S}$, was allowed to vary for each culture. Table 4.7 summarizes the regression results. Figure 4.13 is a plot of the number of standard deviations separating the regressed and experimental values for the modified model. It is analogous to Figure 4.11.

Figure 4.13 shows that the introduction of a stress discontinuity provides a better description of the experimental data. For pressures in excess of 35 MPa the regressed value is within three standard deviations of the experimental value for virtually all data. There is no obvious bias in the model. The description at lower pressures remains less accurate. It is possible that at pressures below 35 MPa the homogenizer stress distribution is not accurately described by equation (4.6). Error at low pressures also results from uncertainty in the pressure measurement as stated in the previous section. Clearly, data obtained at low pressure were adversely affecting the model description at high pressures when a stress discontinuity was not included.

TABLE 4.7 : *Coefficients for the model with a discontinuous stress distribution determined by non-linear least-squares weighted regression. Bracketed parameters (m, n and d) correspond to pressures below 35 MPa.*

m	n	d	σ (–)	Samp. I.D.	Time (min)†	$\bar{S}$ (–)
12.6 (18.8)	0.393 (0.284)	7.85 (7.27)	3.82	1a	5	39.36
				1b	20	43.93
				1c	50	48.90
				1d	70	49.72
				2a	–5	41.42
				2b	0^+	40.27
				2c	10	44.24
				2d	20	48.37
				3a	5	42.59
				3b	15	45.82
				3c	30	46.05
				3d	60	48.15
				4	XS Gl††	31.52
				5a	0^+	35.87
				5b	45	45.06
				5c	105	47.87
				5d	180	48.52
				5e	240	49.56
				5f	300	51.02
				5g	390	51.26
				5h	480	51.56

† Time of sample withdrawal after culture glucose exhaustion (Table 4.2).

†† Excess glucose present.

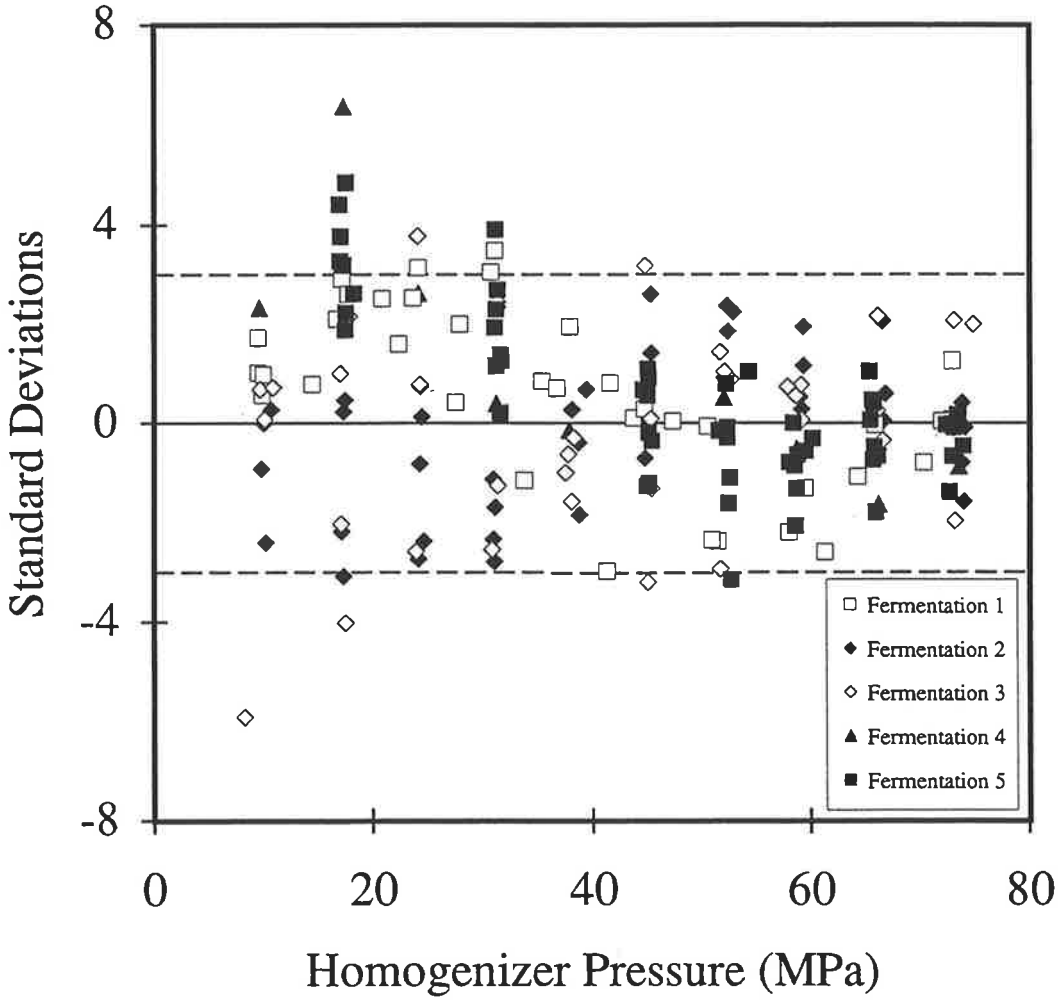

FIGURE 4.13 : *Number of standard deviations separating the experimental and regressed disruption versus homogenizer pressure. (Model parameters from Table 4.7).*

4.4 Summary

Twenty-one (21) cultures of *E. coli* B, with widely varying resistances to disruption, have been homogenized in a 15M-8TA high-pressure homogenizer. The disruption results have been regressed to the model developed in chapter 2, namely :

$$D = \int_0^{\infty} f_D(S)\, f_S(S)\, dS \qquad -(2.8)$$

where $f_S(S)$ and $f_D(S)$ are the strength and stress distributions, respectively, and are given by the following equations.

$$f_S(S) = \frac{1}{\sigma\sqrt{2\pi}} \exp\left[\frac{-(S-\bar{S})^2}{2\sigma^2}\right] \qquad -(2.1)$$

$$f_D(S) = \frac{(mP^n)^d}{S^d + (mP^n)^d} \qquad -(2.6)$$

The model parameters are summarized in Table 4.8 and are constant for the specified system and bacterial strain. The regression results provide strong support for assertion (i) in section 2.5, namely that the homogenizer stress distribution is independent of the properties of the feed culture. Further, assertion (iv), that σ is constant, is supported.

With reference to the parameters in Table 4.8, a stress discontinuity was introduced at 35 MPa. This was considered necessary for the present system, as the pressure transients from the single-acting simplex pump change shape with increasing pressure, particularly at low pressures. The stress discontinuity may also correspond to a change in flow hydrodynamics in the valve.

TABLE 4.8 : *Model parameters determined by non-linear regression.*

PARAMETER	EQN.	VALUE	
σ	2.1	3.82	
m	2.6	18.8	P < 35 MPa
		12.6	P ≥ 35 MPa
n	2.6	0.284	P < 35 MPa
		0.393	P ≥ 35 MPa
d	2.6	7.27	P < 35 MPa
		7.85	P ≥ 35 MPa

With the specified parameters, an excellent description of disruption data is obtained.

In addition to the parameters in Table 4.8, a unique value for $\bar{S}$ was obtained for each culture from the regression (Table 4.7). Disruption is therefore described by the constants in Table 4.8 and a single adjustable parameter, $\bar{S}$. In the next chapter, mean effective strength is correlated with measurable cell properties, thus permitting disruption to be predicted with zero degrees of freedom for the specified homogenizer and bacterial strain.

CHAPTER 5

STRENGTH CORRELATIONS

Cultures with widely-varying strengths were homogenized in the preceding chapter. The disruption data were regressed to the proposed model to determine the four strain- and system-specific constants. In addition, a value of the mean effective strength was determined for each culture. In this chapter, the cultures are analyzed to determine the peptidoglycan composition and average cell size. An empirical correlation of mean effective strength with peptidoglycan crosslinkage and average cell length is determined. An alternative correlation is obtained from statistical thermodynamics. This development offers little numerical improvement over the empirical correlation, but provides the advantage that it is based on a modelling approach and an understanding of wall structure. In conjunction with the constants determined in chapter 4 and the model developed in chapter 2, the correlations may be used to predict disruption for the specified strain and system. This removes the requirement for culture-specific parameters. The predictive capabilities of the model are illustrated in the next chapter.

5.0 Introduction

In the previous chapter, model parameters were obtained for the specified homogenizer system disrupting *E. coli* B. In addition to the four strain- and system-specific constants, a unique value of mean effective strength, $\bar{S}$, was obtained for each culture. These values are summarized in Table 4.7, and demonstrate that effective strength increases during stationary phase. Cells are also characterized by an increasing resistance to disruption during this phase. The regression results therefore suggest that mean effective strength is a good indicator of the ability to resist disruption.

In section 1.5, the following cell characteristics were identified as affecting a population's resistance to disruption :

- wall structure, or murein crosslinkage and amount of bound lipoprotein;
- cell size;
- population heterogeneity.

The effect of heterogeneity on strength is neglected by assuming that the Gaussian distribution (eq. (2.1)) provides a reasonable approximation to the true strength distribution. Hence, mean effective strength should correlate with changes in wall structure and cell size.

The wall structure of *E. coli* was reviewed in section 1.1. Considerable changes in murein structure occur as cells enter stationary phase (section 1.5.1). These changes have been characterized by various microbiological researchers using reverse-phase, high-performance liquid chromatography. In sections 5.1 and 5.2, the technique is employed to characterize the wall structure of the cultures disrupted in chapter 4. Average cell length and diameter are also determined by image analysis. In section 5.3, an empirical correlation of mean effective strength with the culture properties (wall structure and size) is developed. An alternative correlation is obtained from statistical thermodynamics in section 5.4.

5.1 Experimental

A series of five fermentations was described in the previous chapter. Briefly, wild-type *E. coli* B were grown in modified C1 minimal media in either a 16 L or a 100 L (working volume) fermenter. Samples were withdrawn at various times after glucose exhaustion giving cultures with a range of strengths. A fraction of each homogenizer feed sample (400 mL) was retained for analysis of the cell properties. These retained samples were stored at 4°C until the completion of a given set of homogenization tests (< 90 min). It is unlikely that cell-wall structure altered significantly during storage, as the samples had been allowed to stand at 20°C prior to homogenization (Table 4.2). Any change in wall structure due to autolysis occurred prior to homogenisation. The analyzed cell-wall material was therefore assumed to be equivalent to cell-wall material passing through the homogenizer.

5.1.1 Isolation of Murein Sacculi

Murein samples were obtained following the procedure of Glauner (1988) with some modifications. The 400 mL retained feed samples were sedimented by centrifugation (18000 g, 30 min, 4°C). The pellet was re-suspended in 30 mL of ice cold water, and added dropwise to 30 mL of boiling 8% w/w sodium dodecyl sulphate (S.D.S.). Samples were boiled for a further 45 min. Distilled water was periodically added to maintain sample volume. Boiled samples were allowed to cool to room temperature prior to storage as two separate samples at –20°C. Upon completion of all fermentations, the frozen samples (30 mL) were boiled for 5 min to solubilize the precipitated S.D.S. Murein was recovered by centrifugation (50000 g, 90 min, 25°C) and the pellet resuspended in 10 mL of 4% w/w S.D.S. This was boiled for 15 min, allowed to cool to room temperature and then centrifuged (45000 g, 60 min, 25°C). The additional boiling aided pellet re-suspension. After carefully rinsing the centrifuge tube with distilled water, the pellet was resuspended in 10 mL of distilled water and centrifuged again (45000 g, 60 min, 25°C). This step was repeated a further three times to remove S.D.S. from the sample. The final pellet was

resuspended in 5 mL of 10 mM Tris-HCl, pH 7.0. The resuspended sample was treated sequentially with α-amylase (0.1 mg mL^{-1}, 2 h, 37°C) and pronase E (0.2 mg mL^{-1}, 90 min, 60°C). Pronase E from *Streptomyces griseus* and α-amylase from *Bacillus amyloliquefaciens* were supplied by Boehringer-Mannheim, and were stored as stock solutions (10 mg mL^{-1} in 10mM Tris-HCl / 10 mM NaCl, pH 7.0) at –20°C prior to use. Pronase E was pre-digested at 60°C for 2 h prior to use. Treated samples were added to 5 mL of 8% w/w S.D.S., boiled for 15 min, and allowed to stand overnight at room temperature. Samples were then centrifuged and washed using the described protocol (45000 g, 60 min, 25°C). The final pellets were re-suspended in 500 µL buffer (20 mM phosphate, 0.02% sodium azide, pH 6.8).

The existence of sacculi was confirmed by transmission electron microscopy. Approximately 10 µL of sacculi suspension was air dried onto Formvar-coated grids. Grids were washed by floating filmside down on a droplet of 50 mM glycine-NaOH buffer (pH 9.0). Excess fluid was removed with filter paper. Grids were then floated for 1 min on an aqueous 2% w/w uranyl acetate solution for staining. The stain was removed with filter paper, and the specimen was air dried. Electron micrographs were taken with a Philips EM300 transmission electron microscope. Figure 5.1 shows sacculi at a magnification of 27,000 x.

5.1.2 Analysis of Murein Structure

Murein structure was analyzed using the chromatographic method developed by Glauner (1988). Sacculi preparations were digested with mutanolysin from *Streptomyces globisporus* (Sigma chemicals, 275 U mL^{-1}, 16 h, 37°C; Dougherty, 1985). Digested samples were reduced with sodium borohydride (Glauner, 1988) and applied to a reverse-phase, high-performance liquid chromatography (HPLC) column (Shandon ODS-Hypersil 5-µm-diameter particles, 4.6 by 250 mm, Alltech Australia Pty. Ltd.) with a Waters U6K injector (20–100 µL reduced suspension). Elution was with a linear gradient (50 mM

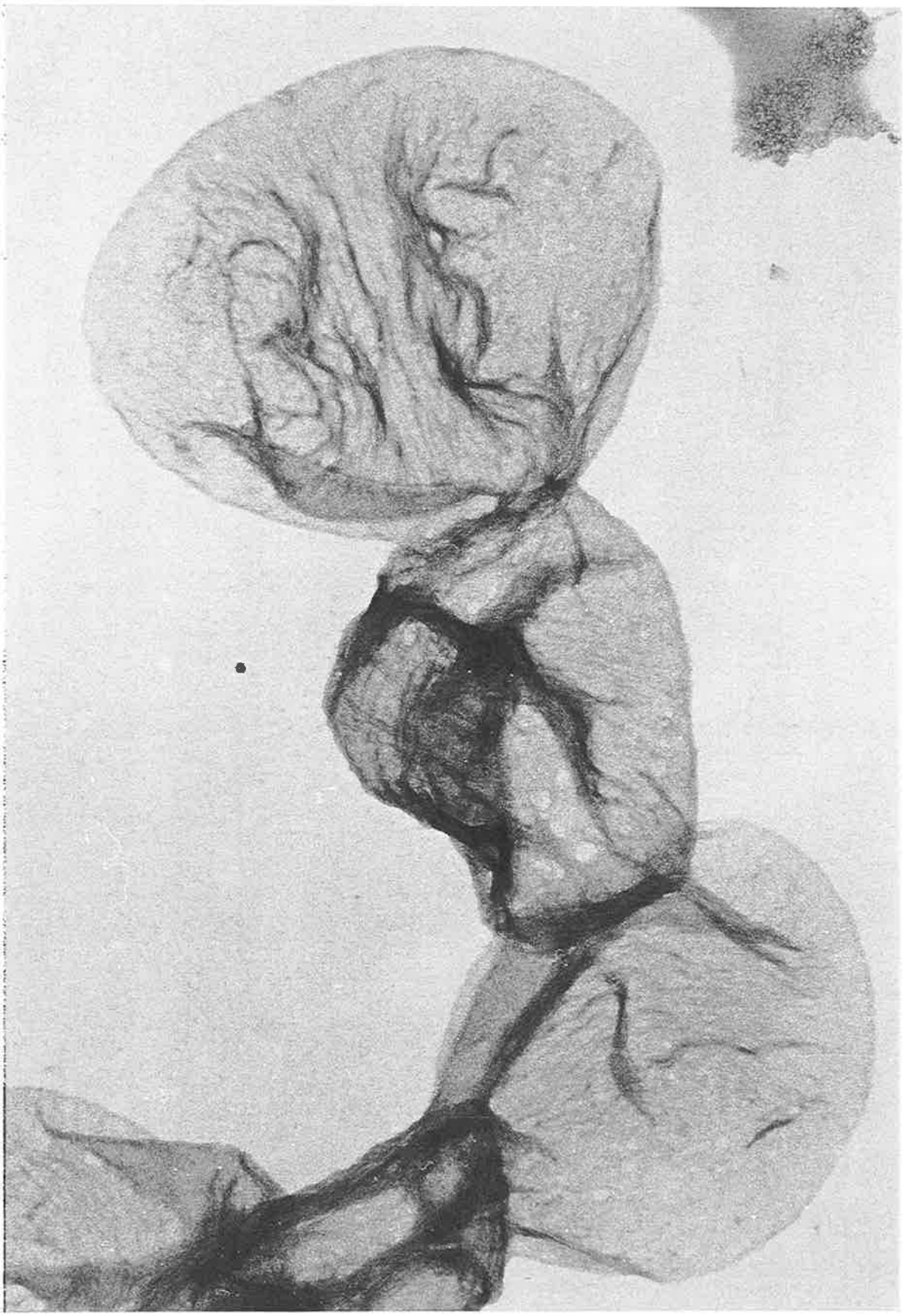

FIGURE 5.1 : *Transmission Electron Micrograph of recovered sacculi (magnification 27,000 times).*

sodium phosphate buffer (pH 4.33) to 50 mM sodium phosphate buffer with 15% methanol (pH 5.10) over 130 min at a flow rate of 0.5 mL min^{-1}) using two Waters 510 pumps controlled by a Waters 680 automated gradient controller. An additional 16 min period of isocratic elution was included prior to the gradient. Muropeptides were detected by measuring the UV absorbance of eluted material at 205 nm. Peak assignments were done using calibration standards generously provided by Prof. J.-V. Höltje of the Max-Planck-Institut für Entwicklungsbiologie.

The area under each identified peak in the chromatogram was determined using Delta chromatography integration software and then corrected for the number of peptide sub-units (Glauner, 1988). The molar percent of any specific moiety was defined as the corrected area for the appropriate peak divided by the total corrected area. The degree of peptidoglycan crosslinkage was calculated using a modification of the procedure of Glauner (1988). The degree of crosslinkage was taken to be the sum of corrected areas for dimers and higher-order crosslinks divided by the total corrected area. This method is preferred in the current application as it gives the total fraction of peptide crosslinks. A crosslinkage of 100% implies that all disaccharide units are crosslinked to at least one other unit. This contrasts with the method of Glauner (1988), where crosslinkage is defined as the percentage of cross bridges of a specified type relative to the total number of disaccharide peptide subunits of this type. With Glauner's (1988) definition, a crosslinkage of 50% implies that all units are crosslinked to at least one other unit.

5.1.3 Analysis of Average Size and Septated Fraction

A sample of each of the retained homogenizer feed cells was photographed using a phase-contrast microscope with a 100x objective lens. A minimum of eighteen random photographs of each sample were taken. The developed negatives were mounted as slides, projected onto a screen and digitized for image analysis. Captured images were analyzed using Syzcount™, an image-analysis software package developed by Mr. A.S. Hull and A/Prof. P.K. Agarwal in the Department of Chemical Engineering at the University of Adelaide. The program calculates the distribution of maximum chord lengths for the detected images. This corresponds to the distribution of cell lengths. It also evaluates the distribution of cell diameters, where diameter is taken as the minimum chord perpendicular to the cell length. The package also determines the distribution of cell cross-sectional areas by direct pixel summation. Cells can be included or excluded from the analysis by specifying bounds on any of the parameters calculated by Syzcount™.

The septated fraction of a population is required if equation (2.2) (a bimodal strength distribution) is to be employed in place of equation (2.1). The effect of representing the true strength distribution with a bimodal function is investigated in chapter 7. The septated fraction of the cultures was therefore determined by image analysis for subsequent use in chapter 7. Rigorous determination of the septated fraction requires that septated cells are individually identified and counted. This is difficult to implement given the large number of cells involved. The following approximate method was therefore employed.

Small cells which were clearly septated were identified and their individual lengths determined using Syzcount™. From these measurements, an average minimum septated length, $\bar{\lambda}_s$, was determined for each culture. If cells are approximated as cylinders with hemispherical ends, equation (5.1) may be written,

$$x_s = \frac{\Sigma \left(\frac{\pi}{6} D_c^3 + \frac{\pi}{4} D_c^2 [L-D_c]\right)_{L \geq \bar{\lambda}_s}}{\Sigma \left(\frac{\pi}{6} D_c^3 + \frac{\pi}{4} D_c^2 [L-D_c]\right)} \qquad -(5.1)$$

where D_c is the cell diameter and L is the cell length from pole to pole. As cell diameter is approximately constant for a given population (section 1.5.2), equation (5.2) may be written.

$$x_s = \frac{\Sigma \left(0.66\, D_c^2 + D_c\, [L-D_c]\right)_{L \geq \bar{\lambda}_s}}{\Sigma \left(0.66\, D_c^2 + D_c\, [L-D_c]\right)} \qquad -(5.2)$$

The projected cross-sectional area of an individual cell is given by equation (5.3),

$$A_i = \frac{\pi}{4} D_c^2 + D_c\, [L-D_c] = 0.79\ D_c^2 + D_c\, [L-D_c] \qquad -(5.3)$$

which is evaluated directly by Syzcount™. The volume fraction of septated cells for a given population, x_s, may therefore be estimated by equation (5.4).

$$x_s \approx \frac{\left(\Sigma\, A_i\right)_{L \geq \bar{\lambda}_s}}{\Sigma\, A_i} \qquad -(5.4)$$

The error introduced by using $0.79D_c^2$ (eq. (5.3)) in place of $0.66D_c^2$ (eq. (5.2)) is negligible, particularly as the term $D_c[L-D_c]$ dominates. Further, the introduced error will be small compared to the error resulting from the initial assumption that cells have perfectly hemispherical ends.

A large uncertainty is associated with each x_s value because of uncertainty in $\bar{\lambda}_s$. This uncertainty is estimated directly by using minimum and maximum likely values for $\bar{\lambda}_s$ in Syzcount™, and determining the resultant septated fraction. An uncertainty also results

from the assumption that all cells greater than $\bar{\lambda}_s$ will be septated, as shown in Figure 5.2. Nevertheless, equation (5.4) is retained as a reasonable approximation.

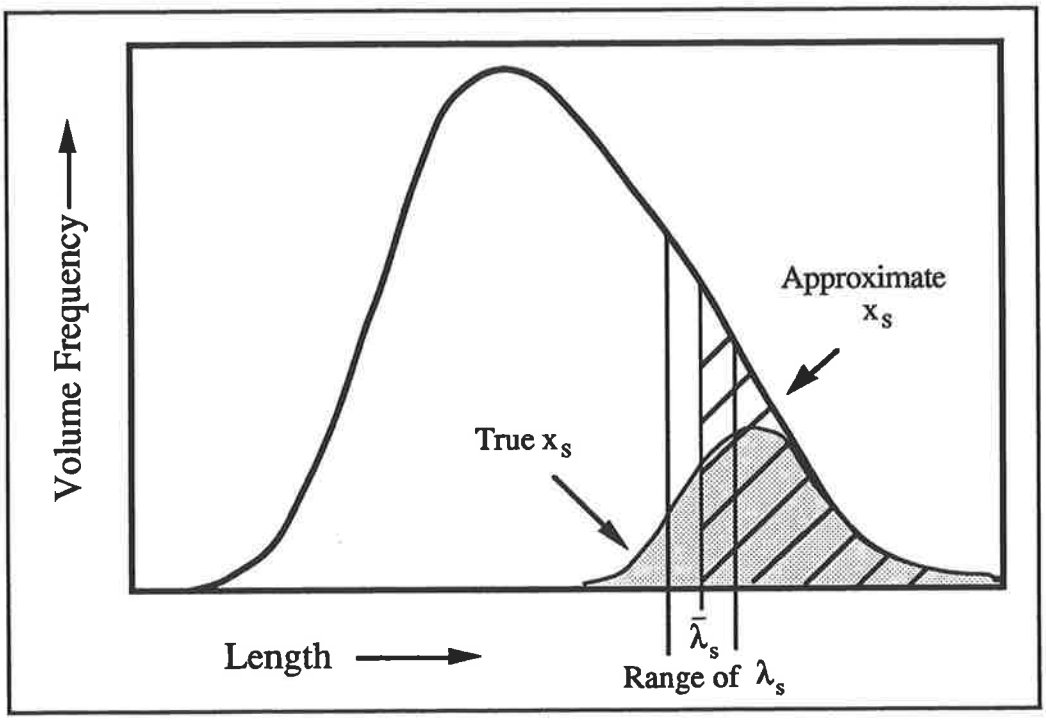

FIGURE 5.2 : *Approximation of the septated volume fraction.*

5.2 Results

Figure 5.3 shows typical chromatograms resulting from the HPLC analysis of murein structure for sample 4 (excess glucose ≈ exponential phase) and sample 5h (late stationary phase). The chromatograms display a marked increase in material with a novel crosslink (Tetra-Tri-A_2Pm) relative to normal crosslinked material (Tetra-Tetra) as cells enter stationary phase. This trend has been routinely found by microbiological researchers, as stated in chapter 1.

Table 5.1 summarizes the characteristics of the cultures disrupted in chapter 4.

Figure 5.4 is a plot of murein crosslinkage and the relative abundance of two crosslinked murein moieties (Tetra-Tri-Lys-Arg and Tetra-Tri-A_2Pm) as a function of time since glucose exhaustion. The significant increase in the amount of bound lipoprotein (as indicated by the relative abundance of Tetra-Tri-Lys-Arg) and crosslinked material during the stationary phase is clearly apparent.

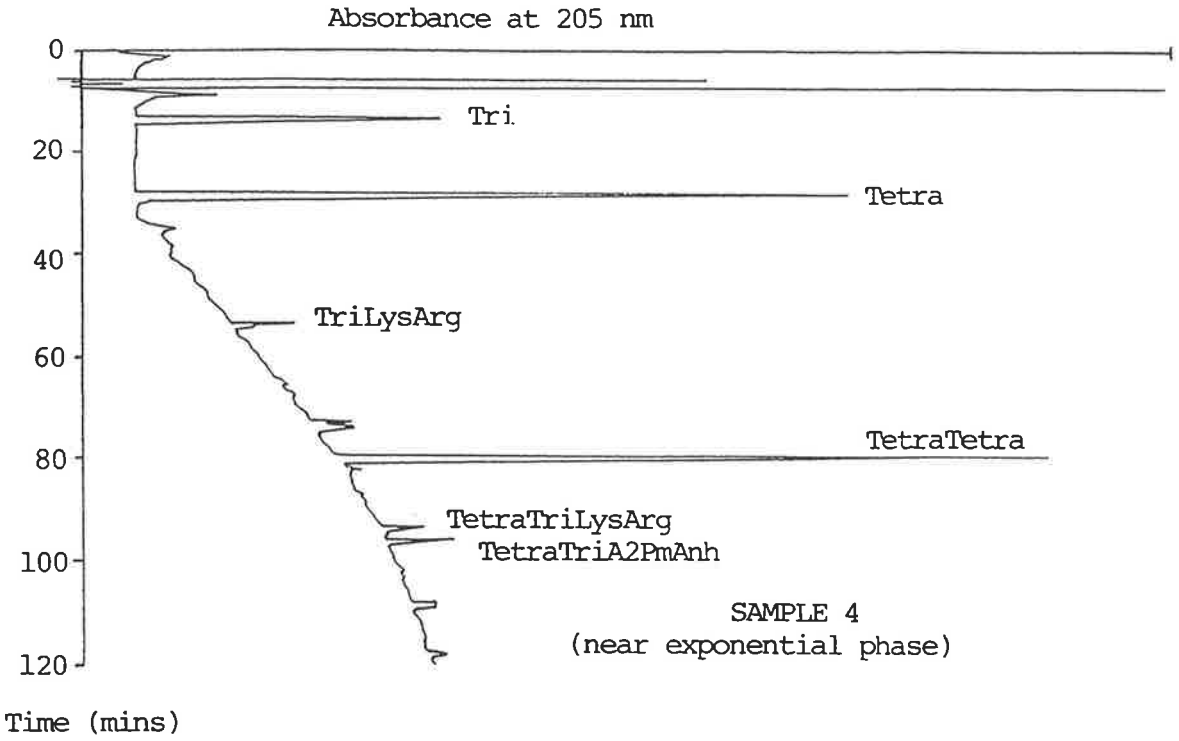

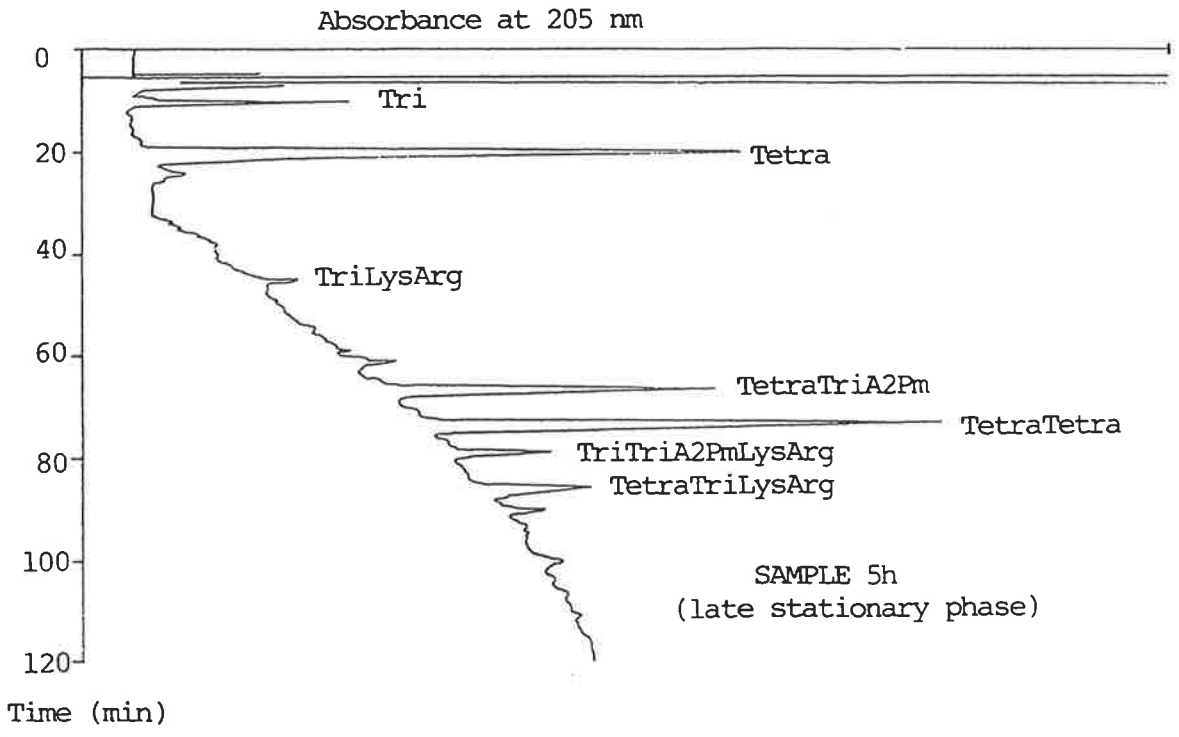

FIGURE 5.3 : *Example chromatograms from the H.P.L.C. analysis of digested and reduced peptidoglycan.*

TABLE 5.1 : *Characteristics of homogenizer feed cultures.*

Samp. I.D.[a]	Time (min)[b]	$\bar{S}$ (-)[c]	$\bar{L}$ (μm)[d]	$\bar{D}$ (μm)[e]	x_s (–)[f]	X (–)[g]	M (mol %)[h]
1a	5	39.36	2.46	1.0	0.10 - 0.16	0.390†	1.1†
1b	20	43.93	2.04	0.96	0.05 - 0.10	0.392	0.6
1c	50	48.90	1.90	1.0	0.06 - 0.12	0.440	0.9
1d	70	49.72	1.85	1.0	0.06 - 0.11	0.466	1.3
2a	–5	41.42	2.54	0.87	0.04 - 0.11	0.401	1.3
2b	0+	40.27	2.70	0.91	0.15 - 0.20	0.403	1.1
2c	10	44.24	2.35	0.93	0.05 - 0.15	0.394	1.1
2d	20	48.37	2.14	0.88	0.04 - 0.10	0.440	1.7
3a	5	42.59	2.30	0.86	0.04 - 0.10	0.379	0.6
3b	15	45.82	2.06	0.87	0.03 - 0.08	0.417	0.8
3c	30	46.05	1.94	0.87	0.04 - 0.09	0.430	1.0
3d	60	48.15	1.95	0.90	0.03 - 0.08	0.441	1.0
4	XS Gl.	31.52	3.69	0.96	0.16 - 0.20	0.390	1.4
5a	0+	35.87	3.23	0.86	0.23 - 0.30	0.390†	1.1†
5b	45	45.06	2.44	0.92	0.16 - 0.23	0.425	1.6
5c	105	47.87	2.30	0.92	0.09 - 0.18	0.488	2.9
5d	180	48.52	2.03	0.82	0.06 - 0.12	0.525	4.6
5e	240	49.56	1.99	0.84	0.05 - 0.12	0.554	5.0
5f	300	51.02	2.01	0.83	0.04 - 0.10	0.561	5.6
5g	390	51.26	2.06	0.85	0.07 - 0.15	0.568	5.7
5h	480	51.56	2.04	0.87	0.05 - 0.15	0.577	5.4

[a] Sample identification (Table 4.2).

[b] Time of sample withdrawal after culture glucose exhaustion (Table 4.2).

[c] Mean effective strength (Table 4.7).

[d] Average length of cells determined by image analysis.

[e] Average diameter of cells determined by image analysis.

[f] Septated volume fraction of the population determined by image analysis.

[g] Peptidoglycan crosslinkage determined by HPLC.

[h] Relative abundance of Tetra-Tri-Lys-Arg (mol%).

† These are average values for samples 2a, 3a and 4, as sacculi were lost during preparation.

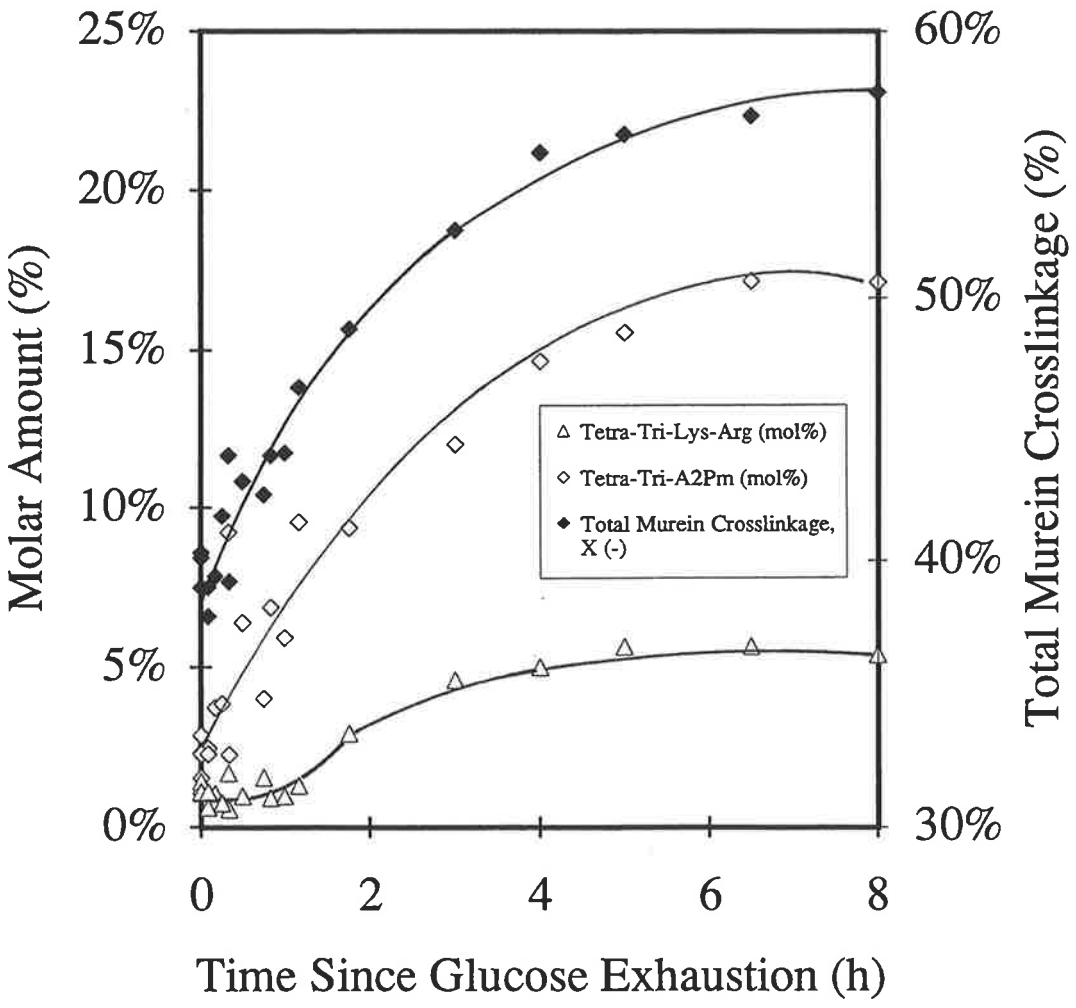

FIGURE 5.4 : *Peptidoglycan characteristics as a function of time.*

5.3 Empirical Correlation

Figure 5.5 presents a plot of average cell length and diameter versus mean effective strength, $\bar{S}$, determined by regression in chapter 4. Also shown is a plot of total murein crosslinkage versus mean effective strength.

Two distinct mechanisms of wall strengthening are apparent. First, for mean effective strengths less than ≈ 43, the degree of crosslinkage is constant and bacteria strengthen by a reduction in length. The increase in strength may be partly due to the change in morphology as cells tend toward a spherical shape. However, it is possible that the thickening of murein observed by Leduc *et al.* (1989a) occurs early in the transition to stationary phase. Length reduction at constant crosslinkage may therefore indicate strengthening through thickening (or increased packing density) of the murein layer. Further, the number of fully developed periseptal annuli (Foley *et al.*, 1989) may decrease as a population enters stationary phase. These annuli may represent points of stress concentration within the wall. Shorter cells with fewer complete annuli will therefore be harder to disrupt by homogenization.

In the second phase ($\bar{S} > 43$), a marked increase in the degree of peptidoglycan crosslinkage is observed with a minor or insignificant change in cell length. An approximately linear relationship between mean cell strength and the degree of crosslinkage exists. This indicates that disruptive stresses are resisted primarily by peptide crosslinks between the glycan chains. Quirk and Woodrow (1984) show that cells are disrupted in a plane perpendicular to their main axis during homogenization. Verwer *et al.* (1978) present evidence suggesting that polysaccharide chains are aligned perpendicular to the main axis. Combined, these studies support the present finding that disruption occurs through breakage of the peptide crosslinks. Furthermore, Verwer *et al.* (1980) report that peptide links are broken in preference to glycan chains during ultrasonication (section 1.5.1).

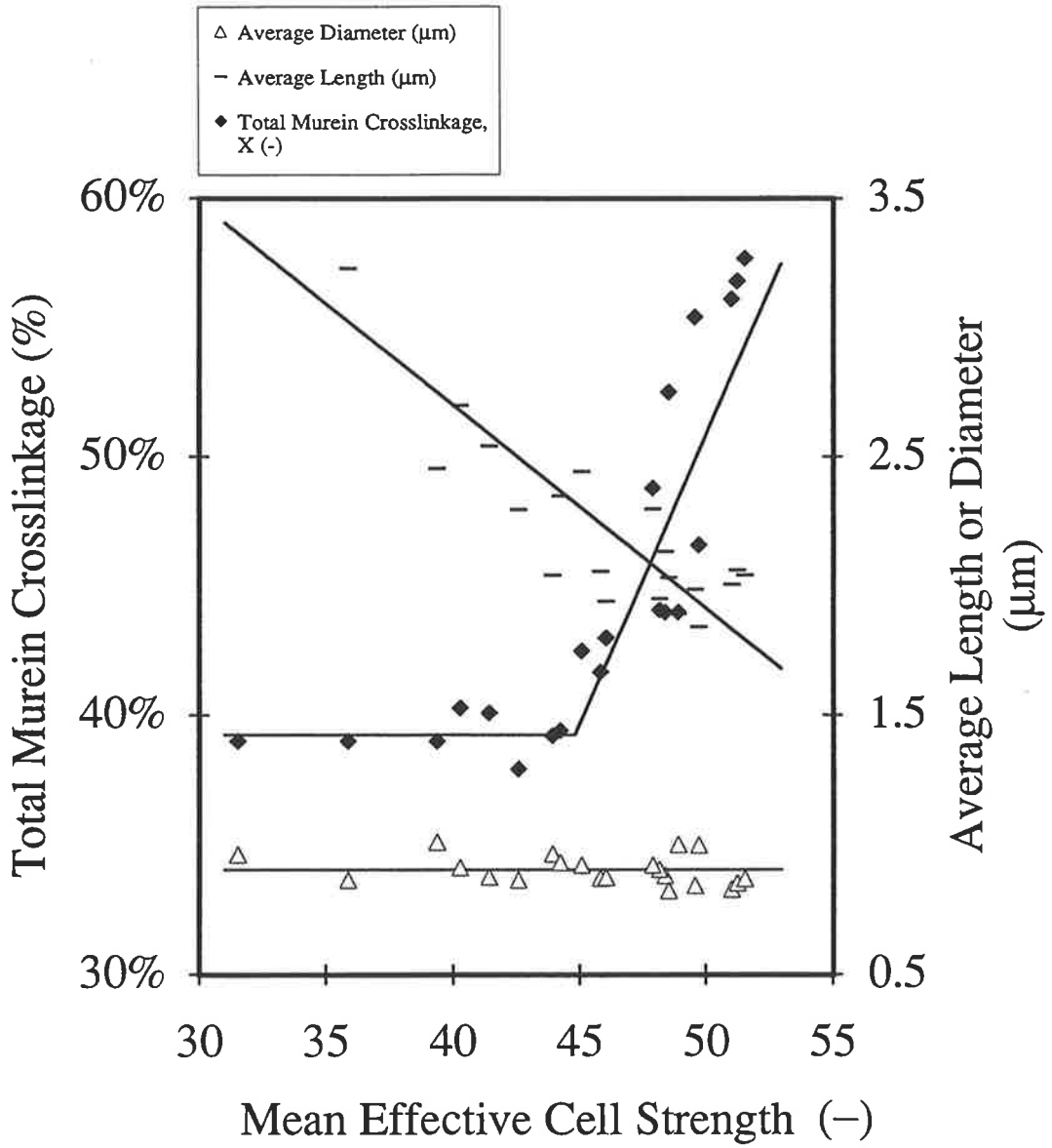

FIGURE 5.5 : *The relationship between murein crosslinkage, average cell length, average cell diameter and mean effective strength (Table 5.1).*

Figure 5.5 suggests a correlation of mean effective cell strength with average cell length and murein crosslinkage. For the cultures examined in chapter 4, no significant variation in the average cell diameter is apparent. Further, variation in the amount of bound lipoprotein approximates variation in the total degree of crosslinkage. It is therefore unlikely that diameter and bound lipoprotein will be significant independent variables.

A multiple-linear correlation of mean effective strength ($\bar{S}$, Table 4.7) with average cell diameter ($\bar{D}$), average cell length ($\bar{L}$), total murein crosslinkage (X) and molar amount of Tetra-Tri-Lys-Arg (M) was determined. Regression results are summarized in Table 5.2. As suggested, average diameter and the relative molar amount of Tetra-Tri-Lys-Arg are not significant independent variables. A strong relationship between M and X was found (correlation coefficient of 0.95), suggesting that any effect of bound lipoprotein on wall strength may be implicitly included in the effect of total crosslinkage.

TABLE 5.2 : *Multiple-linear regression of the full model for mean effective strength (Regression for all data in Table 5.1).*

Variable	Coefficient	Std. Error Estimate	Student's t Statistic†	Prob > t††
Constant	38.330	9.771	3.923	0.001
X	63.454	20.548	3.088	0.006
M	-109.799	71.949	-1.526	0.143
$\bar{L}$	-7.048	0.956	-7.375	0.000
$\bar{D}$	-3.499	6.200	-0.564	0.579

Source	Sum of Squares	Degrees of Freedom	Mean Squares	F-Ratio
Model	533.8	4	133.5	87.4
Error	24.4	16	1.53	(P<0.000)
Total	558.2	20		

† Coefficient divided by the standard error estimate

†† Significance level at which the null hypothesis (H_o : "coefficient is zero") is rejected.

The regression was repeated with only average cell length and murein crosslinkage included as independent variables. The resulting correlation is equation (5.5). The results of the regression are summarized in Table 5.3.

$$\bar{S} = 33.0\,X - 8.06\,\bar{L} + 48.82 \qquad -(5.5)$$

TABLE 5.3 : *Multiple-linear regression of the reduced model for mean effective strength (Regression for all data in Table 5.1).*

Variable	Coefficient	Std. Error Estimate	Student's t Statistic†	Prob > t††
Constant	48.820	3.246	15.039	0.000
X	32.993	4.763	6.926	0.000
$\bar{L}$	-8.055	0.696	-11.581	0.000

Source	Sum of Squares	Degrees of Freedom	Mean Squares	F-Ratio
Model	530.3	2	265.1	170.4
Error	28.0	18	1.56	(P<0.000)
Total	558.3	20		

† Coefficient divided by the standard error estimate

†† Significance level at which the null hypothesis (H_o : "coefficient is zero") is rejected.

Figure 5.6 is a parity plot of mean effective strength determined by regression in chapter 4 versus that predicted by equation (5.5). This simple correlation provides an excellent estimate of mean effective cell strength. Residuals (R) are distributed without bias, and typically represent less than 6% of the regressed value from Table 4.7. This falls within the range of expected error, given the uncertainty in experimental values for X and $\bar{L}$. The coefficient of determination for the regression is 0.95. The probability that $\bar{S}$ is not correlated with each term in equation (5.5) is exceedingly small (t-statistic > 6.9).

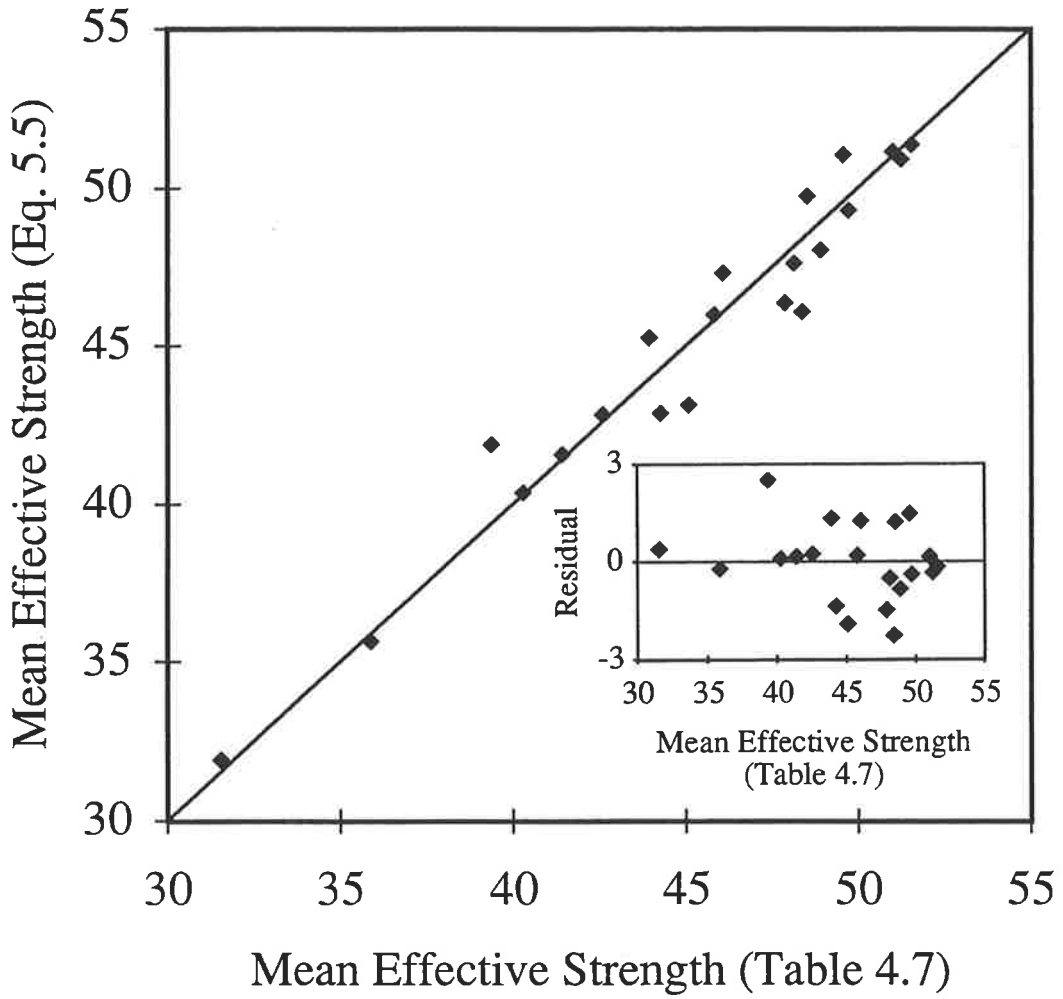

FIGURE 5.6 : *Parity plot of mean effective strength predicted by equation (5.5) versus mean effective strength determined by model regression in the preceding chapter (Table 4.7). The inset is a plot of residuals.*

5.4 Statistical-Thermodynamical Correlation

Equation (5.5) provides a good estimate of mean effective strength. However, it is an empirical correlation and cannot therefore be rationalized in terms of the structure of peptidoglycan. In this section, a correlation for mean effective strength is developed where the variable groupings can be justified from statistical-thermodynamics.

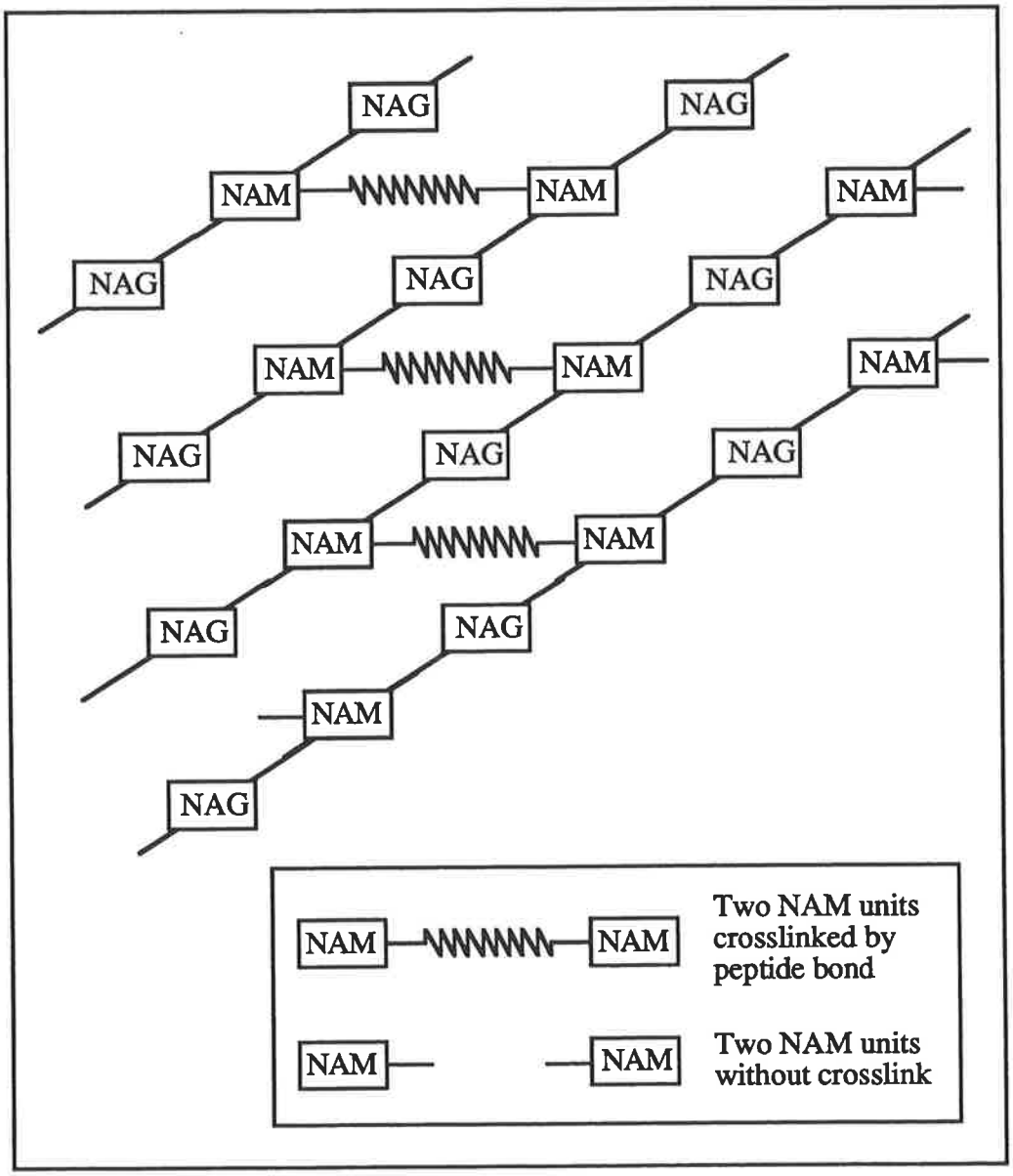

FIGURE 5.7 : *Simplified representation of a single layer of peptidoglycan. Glycan chains composed of N-acetylmuramic acid (NAM) and N-acetylglucosamine (NAG) are crosslinked by peptide bonds (represented by springs).*

Figure 5.7 shows a simplified representation of a single layer of peptidoglycan. A series of parallel glycan chains composed of N-acetylmuramic acid (NAM) and N-acetylglucosamine (NAG) are connected by peptide bonds (harmonic springs) which are subjected to a common stress. The free-energy density of a single peptidoglycan layer at fixed stress, s, is given by equation (5.6) (Blumberg Selinger *et al.*, 1991),

$$g(x,s) = -\frac{s^2}{2Kx} - \mathcal{D}x + T\,[\,x \ln x + (1-x)\ln(1-x)\,] \qquad -(5.6)$$

where x is the fraction of intact bonds, $\mathcal{D}$ is the bond dissociation energy, K is the bond elastic modulus and T is the temperature. The global minimum of the free energy function is the fracture state of all bonds broken (x=0). For low applied stress, s, the function exhibits a local minimum indicating a metastable state. The local and global minima are separated by a specific free energy barrier, which decreases as stress is increased (Blumberg Selinger *et al.*, 1991).

The derivatives of free energy with respect to the fraction of bonds formed are :

$$\frac{\partial g}{\partial x} = \frac{s^2}{2Kx^2} - \mathcal{D} + T\,[\ln x - \ln(1-x)] \qquad -(5.7)$$

$$\frac{\partial^2 g}{\partial x^2} = -\frac{s^2}{Kx^3} + \frac{T}{x(1-x)} \qquad -(5.8)$$

At a certain limiting stress level, s_L, the free-energy barrier will disappear. A plot of g versus x exhibits a stationary inflexion located at some point x_L. This point, and the corresponding stress level, can be found by setting equations (5.7) and (5.8) to zero and solving for x_L and s_L. Specifically, x_L can be determined by solving equation (5.9).

$$\frac{1}{1-x_L} - 2\frac{K\mathcal{D}}{KT} + 2\ln\left(\frac{x_L}{1-x_L}\right) = 0 \qquad -(5.9)$$

Consider a single layer of peptidoglycan with crosslinkage X. If X is greater than X_L, the layer will not fracture until s_L is exceeded. Conversely, for X less than X_L, the layer will disrupt before s_L is reached. When the maximum of the free energy barrier occurs at X, the cell is at its stability limit. A further stress increase will shift the free energy barrier past X. The peptidoglycan layer will disrupt. The critical stress is obtained by setting equation (5.7) equal to zero. The final equations for the critical stress which a layer can support, s_c, are therefore :

$$s_c = X\sqrt{2\,K\mathcal{D} - 2\,KT\,\ln\left(\frac{X}{1-X}\right)} \qquad (X \le X_L) \qquad \text{-(5.10a)}$$

$$s_c = s_L = \sqrt{\frac{KT\,X_L^2}{1-X_L}} \qquad (X > X_L) \qquad \text{-(5.10b)}$$

With the first derivative set to zero, equation (5.8) may be expressed as

$$\left.\frac{\partial^2 g}{\partial x^2}\right|_X = \frac{T}{X}\left(\frac{X-X_L}{(1-X)(1-X_L)} + 2\,\ln\left(\frac{X-X\,X_L}{X_L-X\,X_L}\right)\right) \qquad \text{-(5.11)}$$

For $X \le X_L$, the second derivative is always less than zero and equation (5.10a) guarantees that the maximum of the energy barrier, and not the metastable minimum, is located at X.

Equation (5.10) gives the critical stress which a single layer of peptidoglycan can support. Leduc *et al.* (1989a) observed a thickening of the peptidoglycan layer from 6.6 nm to 8.8 nm during the transition to stationary phase, as stated previously. It is plausible that a reduction in average cell length is a concomitant of this process. If so, it is reasonable to assume that the number of peptidoglycan layers opposing the applied stress, υ, is related to the average cell length by equation (5.12).

$$\upsilon \propto \frac{1}{\bar{L}+L_o} \qquad \text{-(5.12)}$$

The parameter L_o has been included as a direct inverse proportionality between the number of peptidoglycan layers and average cell length is unlikely to exist. The total stress resisted by cells is simply $\upsilon\, s_c$. This total stress is assumed proportional to the mean effective strength of cells, $\bar{S}$. Introducing a proportionality constant gives the final form of the correlation for mean effective cell strength, equation (5.13).

$$\bar{S} = \frac{B\ X}{\bar{L}+L_o}\sqrt{2\ K\mathcal{D} - 2\ KT\ \ln\left(\frac{X}{1-X}\right)} \qquad (X \le X_L) \qquad \text{-(5.13a)}$$

$$\bar{S} = \frac{B}{\bar{L}+L_o}\sqrt{\frac{KT\ X_L^2}{1-X_L}} \qquad (X > X_L) \qquad \text{-(5.13b)}$$

5.4.1 Regression

A FORTRAN program using the IMSL routine DRNLIN (modified Levenberg-Marquardt technique) was written to regress the crosslinkage and length data (Table 5.1) with the mean effective strength values determined in chapter 4 (Table 4.7). The regression gave equation (5.14) as the final correlation. The critical crosslinkage, X_L, was found to be 0.563 with a corresponding critical stress level, s_L, of 2.0.

$$\bar{S} = \frac{128.1\ X}{\bar{L}+2.99}\sqrt{15.23 - 10.91\ \ln\left(\frac{X}{1-X}\right)} \qquad (X \le 0.563) \qquad \text{-(5.14a)}$$

$$\bar{S} = \frac{254.9}{\bar{L}+2.99} \qquad (X > 0.563) \qquad \text{-(5.14b)}$$

A parity plot comparing the regressed strength from Table 4.7 with the predicted value from equation (5.14) is shown in Figure 5.8. Clearly, equation (5.14) gives a good unbiased estimate of mean effective strength. There is little improvement over equation (5.5). However, equation (5.14) is based on a modelling approach to the problem, whereas equation (5.5) is entirely empirical.

Figure 5.9 presents plots of the system free energy (eq. (5.6)) against crosslinkage for various stress levels, s. The features previously described are clearly visible. For stress levels greater than s_L, a cell will be unstable regardless of its degree of crosslinkage. Below s_L, the free-energy maximum shifts to higher crosslinkages as the stress is raised. Cells with a higher peptidoglycan crosslinkage (less than X_L) will therefore be stronger.

Equation (5.14b) predicts that cells obtain no further mechanical benefit in increasing their degree of crosslinkage beyond 56.3% ($\bar{S}$ becomes independent of X). A further increase beyond X_L is unfavourable because of the entropy of mixing term in equation (5.6). The maximum crosslinkage obtained experimentally for this strain is 57.7% (stationary population), which is within experimental error of X_L.

To test the significance of each variable grouping in equation (5.14a), the equation was linearized by taking logarithms. Multiple linear regression (using KT, K$\mathcal{D}$, B and L_o as above) gave equation (5.15).

$$\ln\bar{S} = 1.015 \ln(128.1X) - 1.074 \ln\left(\bar{L}+2.99\right) + \frac{1.044}{2} \ln\left(15.23 - 10.91 \ln\left(\frac{X}{1-X}\right)\right) \qquad \text{-(5.15)}$$

The maximum standard error estimate in each of the three regression coefficients is less than 0.1, yielding a minimum t-statistic exceeding 10. This is a highly significant result.

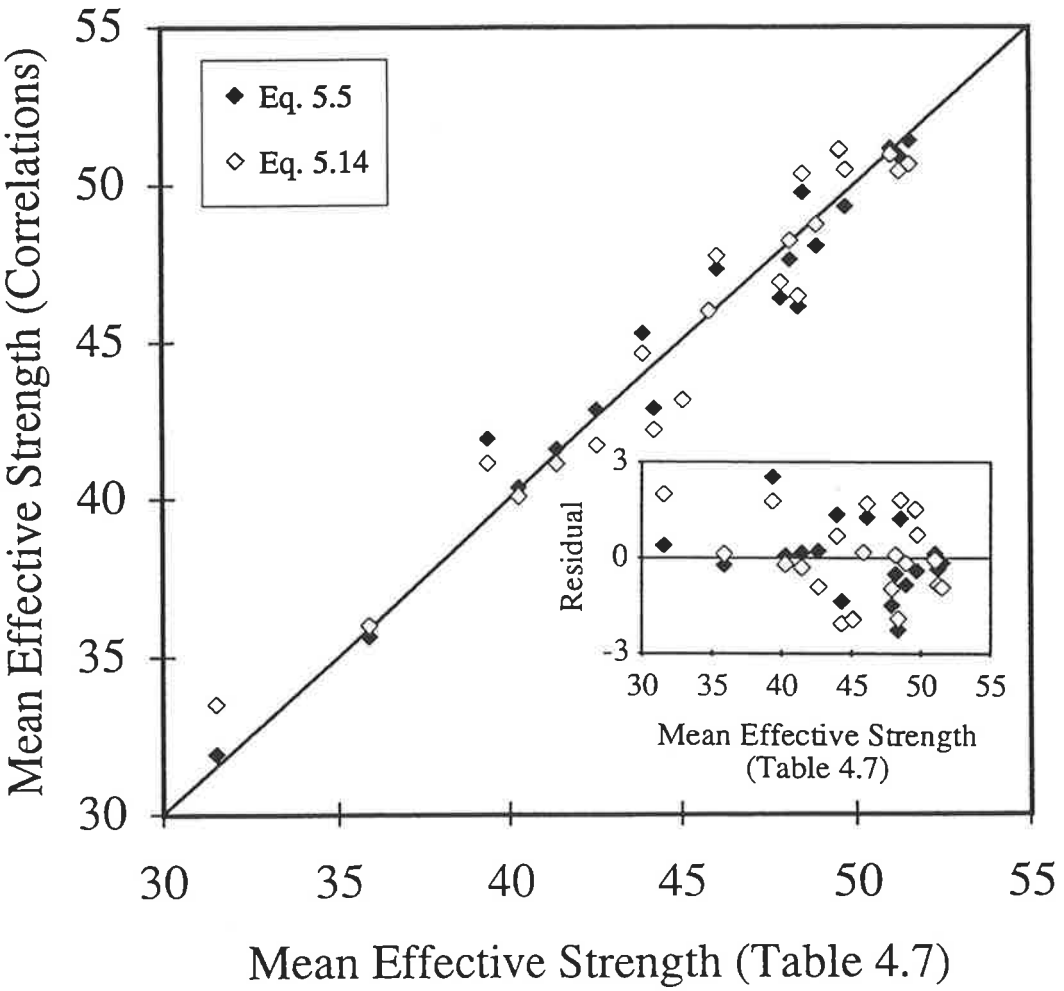

FIGURE 5.8 : *Parity plot of mean effective strength predicted by equations (5.5) and (5.14) versus mean effective strength determined by model regression in the preceding chapter (Table 4.7). The inset is a plot of residuals.*

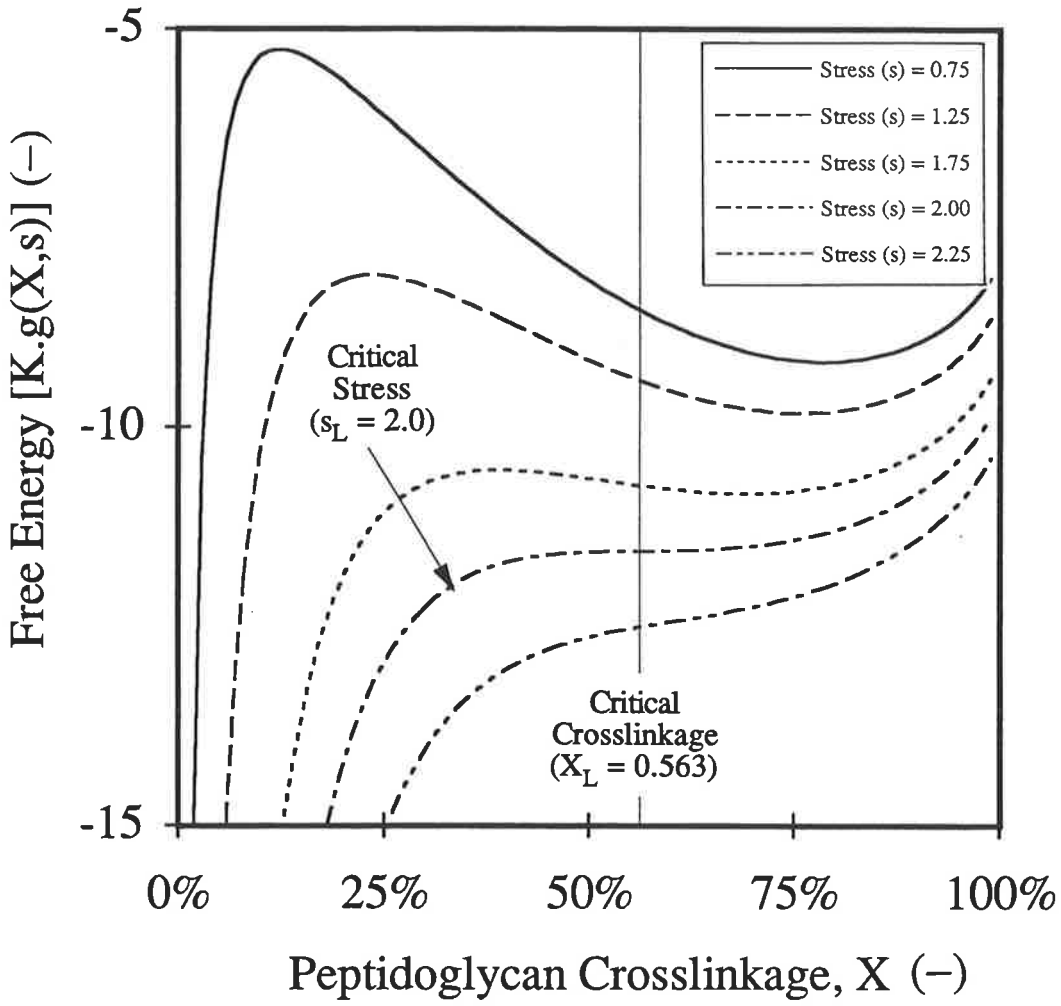

FIGURE 5.9 : *Plot of system free energy (eq. (5.6)) versus peptidoglycan crosslinkage for various stress levels.*

In conclusion, a correlation for mean effective cell strength based on an understanding of cell-wall structure has been developed. This correlation provides a good unbiased estimate of mean effective strength. The final correlation offers no significant numerical advantage over the linear relationship (eq. (5.5)). However, it is based on a physical understanding of the effect which the key measured variables (X and $\bar{L}$) have on mean effective strength.

5.5 Summary

In chapter 4, cultures of widely-varying strength were homogenized, and the disruption versus pressure data were regressed to the model developed in chapter 2. The four system- and strain-specific parameters for the specified homogenizer system and bacterial strain were determined. In addition, the regression provided a value of the mean effective strength, $\bar{S}$, for each culture. In chapter 2, it was stated that this is a property of the culture and should therefore correlate with cell size and the structure of the cell wall.

Retained samples of the cultures described in chapter 4 were boiled in S.D.S. and treated with enzymes to recover purified sacculi. These were digested and analyzed using an established reverse-phase, high-performance liquid chromatographic method. Peptidoglycan composition and degree of crosslinkage were determined for each of the cultures. In addition, the average cell length, average cell diameter and septated volume fraction of each population were determined by image analysis.

Plots of murein crosslinkage and average cell length versus mean effective strength reveal two distinct mechanisms of cell strengthening. In the first phase ($\bar{S}<43$), peptidoglycan crosslinkage remains constant and cell strengthening occurs through a reduction in average cell length. It is possible that this reduction in length is a concomitant of the increase in peptidoglycan thickness as cells enter stationary phase. In the second phase, strengthening occurs through a large increase in peptidoglycan crosslinkage with a small or insignificant change in average cell length.

The following empirical correlation for mean effective strength was determined for all experimental data ($31.5 \leq \bar{S} \leq 51.6$) by multiple linear regression,

$$\bar{S} = 33.0\,X - 8.06\,\bar{L} + 48.82 \qquad \text{-(5.5)}$$

where X is the degree of peptidoglycan crosslinkage and $\bar{L}$ is the average cell length. The amount of bound lipoprotein and the average diameter of non-septated cells were not significant independent variables in the present study.

Equation (5.5) is empirical. The following correlation was obtained from statistical thermodynamics,

$$\bar{S} = \frac{128.1\ X}{\bar{L}+2.99}\sqrt{15.23 - 10.91\ \ln\left(\frac{X}{1-X}\right)} \qquad (X \leq 0.563)\ \text{-(5.14a)}$$

$$\bar{S} = \frac{254.9}{\bar{L}+2.99} \qquad (X > 0.563)\ \text{-(5.14b)}$$

and is also valid over the entire range of mean effective strengths obtained in chapter 4. Equation (5.14) provides little numerical benefit over equation (5.5), but has the advantage that variable groupings can be justified.

The excellent correlation of mean effective strength with measurable cell properties supports the assertion that the strength distribution is a property of the homogenizer feed material (section 2.5).

Equations (5.5) and (5.14) allow the mean effective strength of a culture to be predicted using measurable cell properties (the average cell length and the degree of peptidoglycan crosslinkage). The four strain- and system-specific constants are given in Table 4.8, and will be constant for the specified homogenizer and strain. All model parameters are therefore known or can be calculated. Disruption may thus be predicted with zero degrees of freedom, as illustrated in the next chapter.

CHAPTER 6

MODEL PREDICTIONS

A predictive model for the disruption of *E. coli* B by homogenization has been developed in the preceding chapters. In the present chapter the predictive capabilities of the model are tested using the following cultures :

- Two *E. coli* B cultures grown on glucose;
- One *E. coli* B culture grown on glycerol;
- One *E. coli* JM101 culture grown on glucose.

Culture characteristics are measured and used to predict the mean effective strength with the correlations developed in chapter 5. Disruption versus pressure and disruption versus pass curves are predicted and compared with experimental data.

6.0 Introduction

A model for the disruption of *E. coli* B using a 15M-8TA high-pressure homogenizer has been developed in the preceding chapters. Disruption for a single homogenizer pass may be calculated using equation (2.8),

$$D = \int_0^\infty f_D(S)\, f_S(S)\, dS \qquad -(2.8)$$

where $f_S(S)$ and $f_D(S)$ are the strength and stress distributions, respectively, and are given by the following equations.

$$f_S(S) = \frac{1}{\sigma\sqrt{2\pi}} \exp\left[\frac{-(S-\bar{S})^2}{2\sigma^2}\right] \qquad -(2.1)$$

$$f_D(S) = \frac{(mP^n)^d}{S^d + (mP^n)^d} \qquad -(2.6)$$

The system- and strain-specific constants have been determined in chapter 4, and are given in Table 4.8 (reproduced below).

TABLE 4.8 : *Model parameters determined by non-linear regression.*

PARAMETER	EQN.	VALUE	
σ	2.1	3.82	
m	2.6	18.8	P < 35 MPa
		12.6	P ≥ 35 MPa
n	2.6	0.284	P < 35 MPa
		0.393	P ≥ 35 MPa
d	2.6	7.27	P < 35 MPa
		7.85	P ≥ 35 MPa

In addition to the model parameters in Table 4.8, the mean effective strength, $\bar{S}$, (a culture-specific parameter) is required to predict disruption. This may be calculated using the correlations developed in chapter 5, namely equations (5.5) or (5.14).

$$\bar{S} = 33.0\,X - 8.06\,\bar{L} + 48.82 \qquad \text{-(5.5)}$$

or

$$\bar{S} = \frac{128.1\,X}{\bar{L}+2.99}\sqrt{15.23 - 10.91\,\ln\left(\frac{X}{1-X}\right)} \qquad (X \le 0.563) \quad \text{-(5.14a)}$$

$$\bar{S} = \frac{254.9}{\bar{L}+2.99} \qquad (X > 0.563) \quad \text{-(5.14b)}$$

In the preceding correlations, X is the degree of peptidoglycan crosslinkage and $\bar{L}$ is the average cell length. Peptidoglycan crosslinkage may be measured using high-performance liquid chromatography, while average length may be measured by image analysis (chapter 5). Equation (2.8), in conjunction with the selected distributions, calculated constants and a strength correlation, therefore allows disruption to be predicted for the specified homogenizer system and bacterial strain with zero degrees of freedom.

The preceding parameters and correlations have been deduced using cultures disrupted with a single homogenizer pass. In chapter 2, it was stated that repeated application of the stress distribution on the strength distribution allows disruption to be predicted for multiple homogenizer passes. Specifically, disruption can be calculated by equation (2.11),

$$D = 1 - \int_0^\infty [1-f_D(S)]^N f_S(S)\,dS \qquad \text{-(2.11)}$$

without the need to introduce additional model parameters apart from N, the number of homogenizer passes. It was further stated that equation (2.11) will only predict the correct disruption for multiple homogenizer passes if the selected strength and stress distributions are independent and a close approximation to the true distributions.

To this point, the thesis has focussed on developing the model and deducing the constants and a correlation for mean effective strength. The model has not been employed in a truly predictive role for either single or multiple homogenizer passes. It is essential that its predictive capabilities be tested. Traditional models require culture-specific parameters obtained from the regression of data. As such, they are descriptive rather than predictive.

To test the predictive capabilities of the model, the following are examined :

- Two *E. coli* B cultures grown on glucose;
- One *E. coli* B culture grown on glycerol;
- One *E. coli* JM101 culture grown on glucose.

Cultures are analyzed to determine the average cell length ($\bar{L}$) and the degree of peptidoglycan crosslinkage (X). Mean effective strength ($\bar{S}$) is then calculated using equations (5.5) and (5.14). Disruption versus pressure curves for a single homogenizer pass are predicted and compared with experimental data. To test the extended model for multiple homogenizer passes, disruption versus pass curves are predicted for three separate pressure (24, 45 and 66 MPa) and up to four passes. These curves are compared with experimental data. It should be stressed that the predicted curves **do not rely** on any form of data regression, and therefore represent true *a priori* predictions of disruption.

6.1 Experimental

As indicated in the preceding section, two different strains grown on two different carbon sources are examined. Culture properties are measured to allow a prediction of disruption using the developed model. Predictions are compared with experimentally determined disruption versus pressure and disruption versus pass curves.

6.1.1 Fermentation

Four fermentations (6-9) were conducted using a 16 L (working volume) Chemap CF2000 fermenter. Fermentations 6, 7 and 8 used wild-type *E. coli* B (strain P903, Dept. of Microbiology, University of Adelaide). Fermentation 9 used *E. coli* strain JM101. Modified C1 minimal media (Table 4.1) was used for all fermentations with the following changes: fermentation 9 was supplemented with 0.0375 g L^{-1} thiamine; fermentation 8 used 3.125 g L^{-1} glycerol in place of D-glucose. In all cases, inoculation was from shake flask to give an initial absorbance (A_{600}) of less than 0.0002. Culture pH was automatically controlled at 6.8 with 4M NaOH. Temperature was controlled at 37°C. After exhaustion of the carbon source (noted by a sudden increase in dissolved oxygen concentration) the fermenter's temperature set point was adjusted to 5°C. Cultures were stored at 5°C for various times before homogenization (Table 6.1).

6.1.2 Homogenization

Broths were homogenized using an APV-Gaulin 15M-8TA high-pressure homogenizer with a ceramic cell disruption (CD) valve (Figure 4.1, chapter 4). The machine is fitted with a second stage which remained set to zero pressure during all tests. All batches were homogenized by one pass over a range of pressures to a maximum of 75 MPa. In addition, up to four homogenizer passes at pressures of 24, 45 and 66 MPa were conducted for each culture. Disrupted samples were retained for analysis after each pass. In all cases

homogenizer feed temperature was 5°C. Initial feed pH was 6.8. No pH adjustment was carried out between homogenizer passes. Pressures were set using the fitted gauge. Accurate pressure transients were not measured for the fermentations 6-9. Approximate maximum average pressures (P) were therefore calculated from the nominal gauge pressure (P_g) using equation (4.1).

TABLE 6.1 : *Fermentation data.*

Fermentation	*E. coli* Strain	Growth Media†	Growth Rate (h^{-1})	Final Cell Density (A_{600})	Delay Before Homogenization (h)††
6	Wild B	modC1	1.55	3.0	3.5
7	Wild B	mod C1	1.40	3.4	18
8	Wild B	mod C1 Glycerol	1.04	3.5	3.0
9	JM101	Mod C1 Thiamine	1.06	3.4	3.5

† Growth media is modified C1 minimal media (Table 4.1) supplemented with 0.0375 g L^{-1} thiamine for strain JM101. For fermentation 8, glucose was replaced with glycerol.

†† Time between end of fermentation and the commencement of homogenization.

6.1.3 Disruption Analysis

Disruption was determined using the analytical disc centrifuge (chapter 3). For fermentations 6-8, disruption was also determined by soluble protein measurements on homogenate supernatants (Bio-Rad protein assay, Bio-Rad Laboratories Ltd., Sydney, Australia). Disruption was calculated using equation (3.1). Maximum protein release was determined from the asymptote of the multiple pass data at 66 MPa. No correction for the increase in aqueous volume fraction was necessary, as cell concentrations were less than 5 g L^{-1} (wet weight).

6.1.4 Analysis of Culture Characteristics

The cell-wall structure of each culture was analyzed by high-performance liquid chromatography, as described in chapter 5. Culture samples were also photographed using a phase-contrast microscope at 100x magnification. A minimum of 36 random photographs of each culture were taken. Developed negatives were mounted as slides, projected onto a screen and digitized for image analysis. Captured images were analyzed using Syzcount™. The average cell length ($\bar{L}$), average cell diameter ($\bar{D}$) and the fraction of the population which is septated, x_s, were determined as described in chapter 5.

6.2 Predictions and Results

The characteristics of each of the four cultures are summarized in Table 6.2. The predicted mean effective strength, $\bar{S}$, was calculated using equations (5.5) and (5.14).

TABLE 6.2 : *Culture characteristics and mean effective strength predictions*

Ferm.[a]	$\bar{L}$	$\bar{D}$	x_s	X	$\bar{S}$	$\bar{S}$
	(μm)[b]	(μm)[c]	(–)[d]	(–)[e]	(eq. 5.5)[f]	(eq. 5.14)[f]
6	2.06	0.72	0.109	0.415	45.93	45.83
7	2.32	0.94	0.084	0.457	45.25	45.59
8	2.25	0.75	0.053	0.418	44.53	44.34
9	2.85	0.79	0.066	0.425	39.87	40.11

[a] Fermentation number.

[b] Average cell length determined by image analysis.

[c] Average cell diameter determined by image analysis.

[d] Septated volume fraction determined by image analysis.

[e] Degree of peptidoglycan crosslinkage determined by HPLC.

[f] Predicted mean effective strength using eq. (5.5) or (5.14).

Disruption-pressure curves were predicted using the model and the mean effective strength calculated by equation (5.14). Predicted curves are shown in Figures 6.1 to 6.4 for fermentations 6 to 9, respectively. Experimentally-determined data are superimposed for comparison. Disruption versus pass curves were also predicted using the mean effective strength calculated by equation (5.14). Predicted curves and experimental data are shown in Figures 6.5 to 6.8.

Figure 6.9 shows the number of standard deviations (t, eq. (3.26)) separating the experimental (determined with the disc centrifuge) and predicted values versus homogenizer pressure. Figure 6.10 is the equivalent plot for the multiple pass predictions.

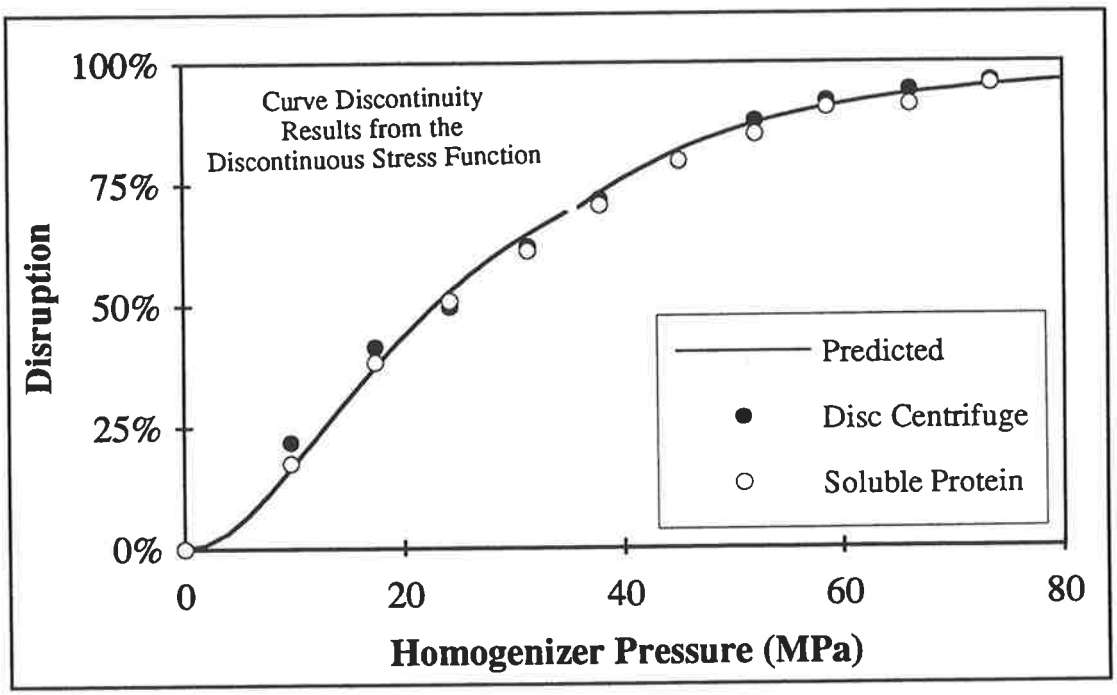

FIGURE 6.1 : *Disruption versus pressure for fermentation 6. Model predictions compared with experimental data.* (*E. coli* B, Glucose)

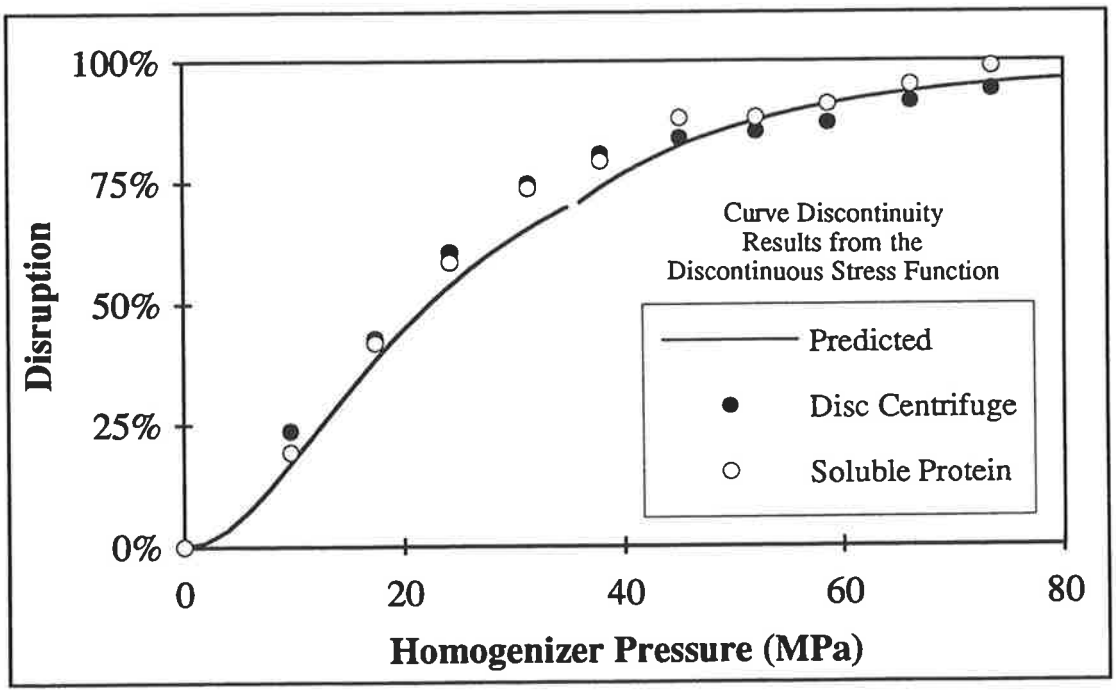

FIGURE 6.2 : *Disruption versus pressure for fermentation 7. Model predictions compared with experimental data.* (*E. coli* B, Glucose)

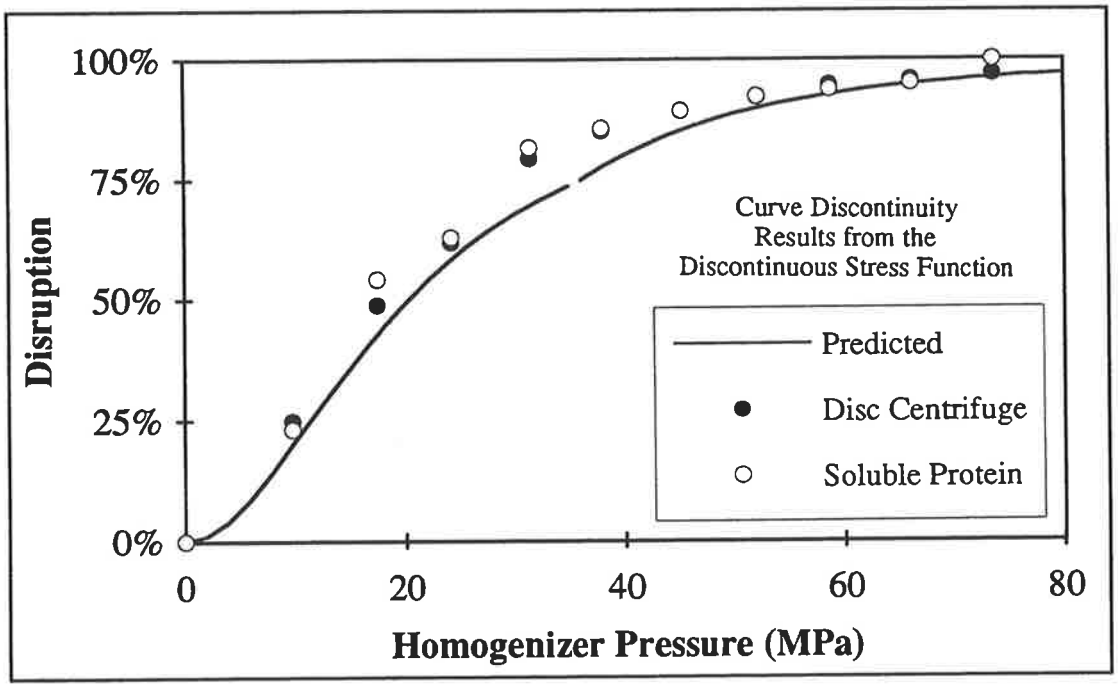

FIGURE 6.3 : *Disruption versus pressure for fermentation 8. Model predictions compared with experimental data.* (*E. coli* B, Glycerol)

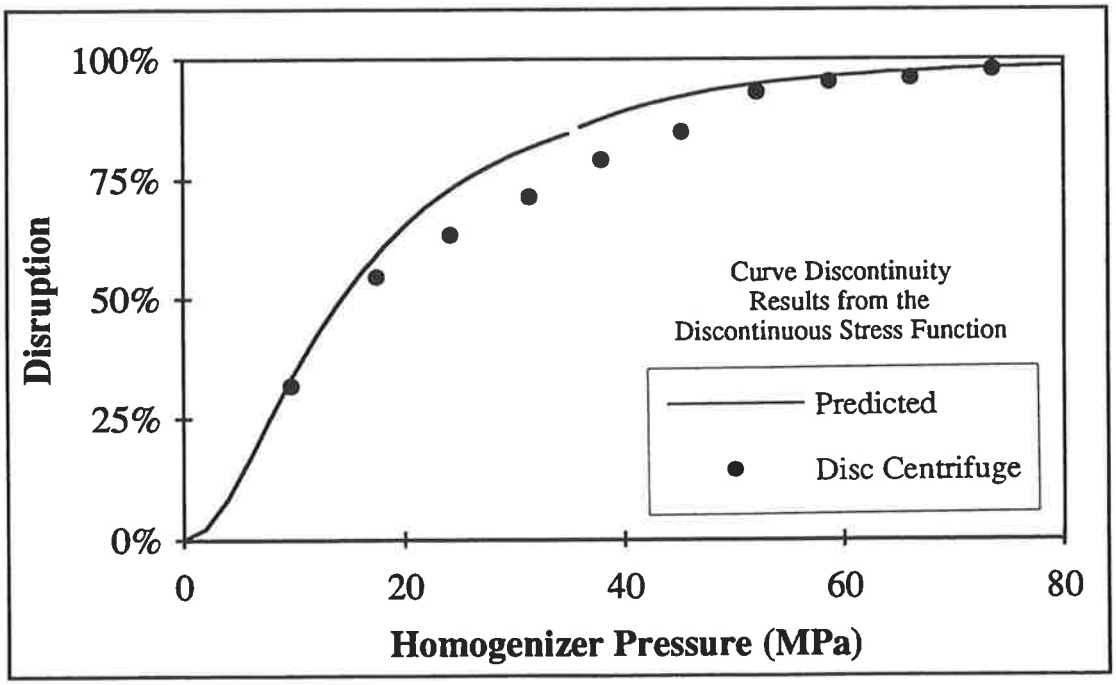

FIGURE 6.4 : *Disruption versus pressure for fermentation 9. Model predictions compared with experimental data.* (*E. coli* JM101, Glucose)

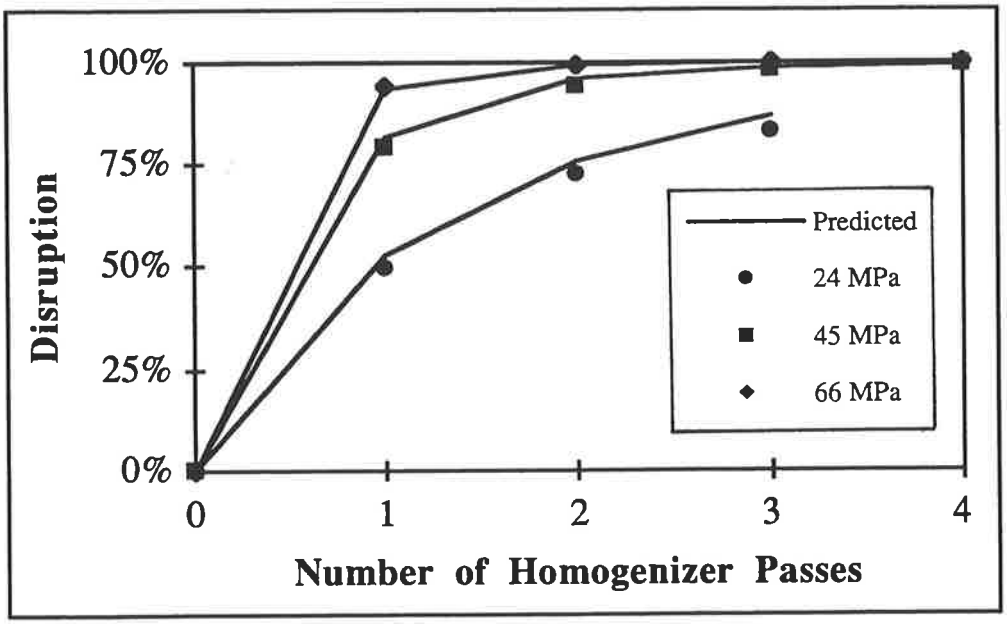

FIGURE 6.5 : *Disruption versus pass for fermentation 6. Model predictions compared with experimental data.* (*E. coli* B, Glucose)

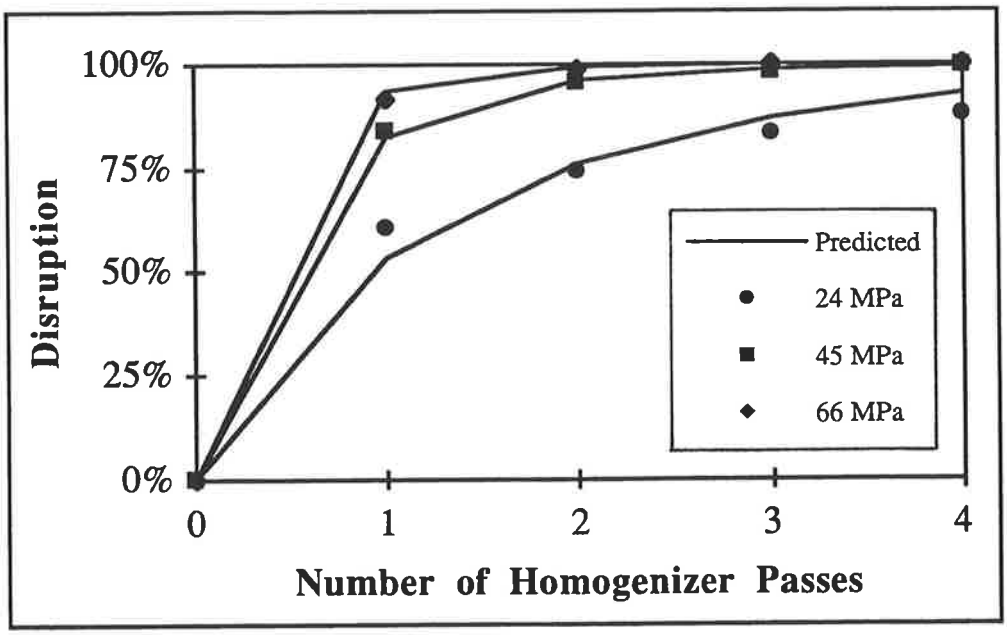

FIGURE 6.6 : *Disruption versus pass for fermentation 7. Model predictions compared with experimental data.* (*E. coli* B, Glucose)

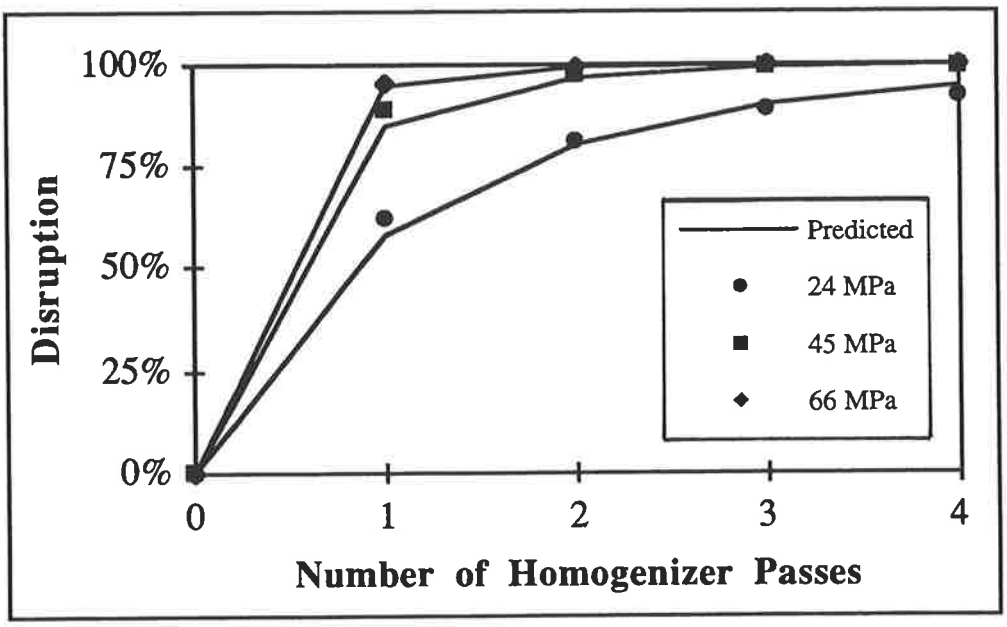

FIGURE 6.7 : *Disruption versus pass for fermentation 8. Model predictions compared with experimental data.* (*E. coli* B, Glycerol)

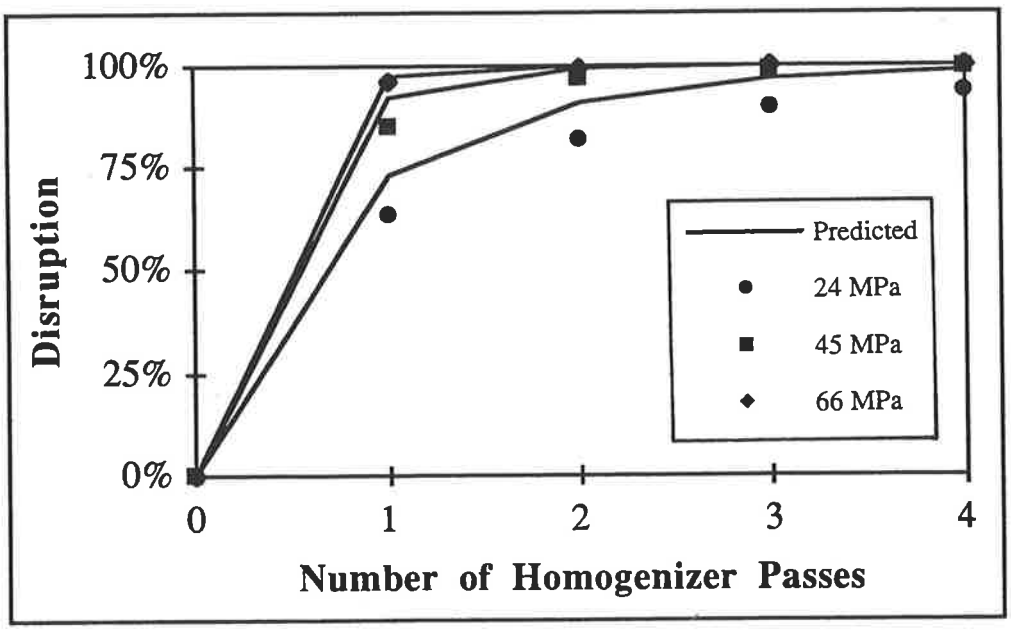

FIGURE 6.8 : *Disruption versus pass for fermentation 9. Model predictions compared with experimental data.* (*E. coli* JM101, Glucose)

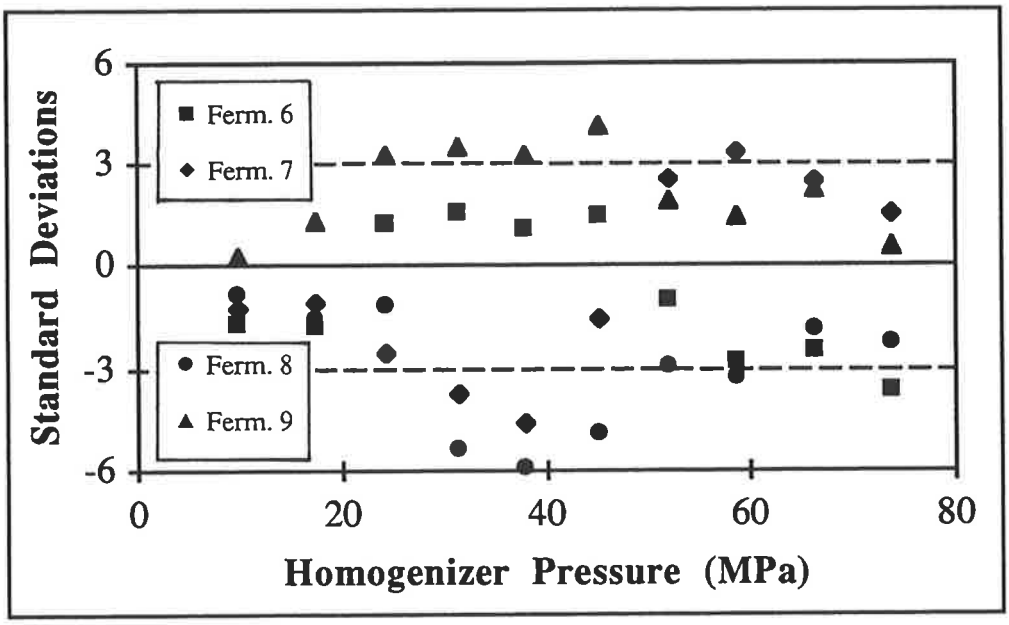

FIGURE 6.9 : *Number of standard deviations (t) separating the predicted and experimentally determined disruption (Disruption vs Pressure data).*

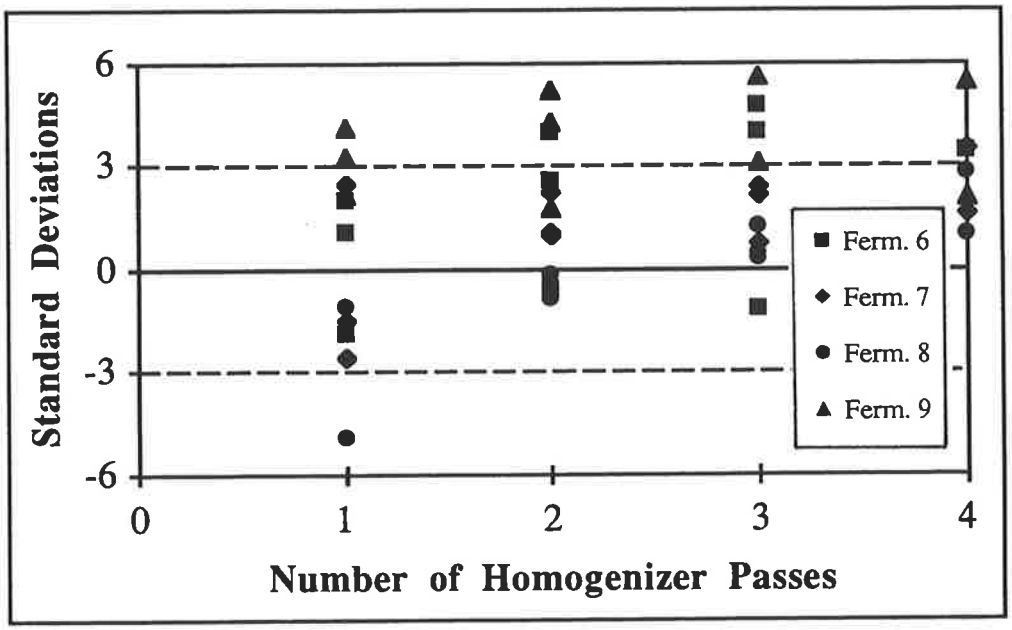

FIGURE 6.10 : *Number of standard deviations (t) separating the predicted and experimentally determined disruption (Disruption vs Pass data).*

6.3 Discussion

The preceding figures show the model predicts the data with good accuracy. The prediction is excellent considering that no knowledge of the experimental disruption data was used to generate the curves. Only measurable population characteristics (Table 6.2) were employed in the model.

Figures 6.1 to 6.4 and Figure 6.9 show that the model has no particular tendency to over- or under-predict disruption for single-pass experiments. Many predictions lie within three standard deviations of the experimental value, particularly at high pressures. Much of the error in the predicted values is due to error in the value for mean effective strength. The correlations used to predict the mean effective strength are accurate to approximately ±6% (chapter 5). The effect of error in $\bar{S}$ on the predicted curves is examined in the next section. The results also confirm that the disc centrifuge gives a meaningful measurement of disruption for *E. coli*. The fraction of cells broken correlates well with soluble protein release. The disc centrifuge has the added advantage that it becomes more accurate at high levels of disruption, as indicated in chapter 3.

Figures 6.5 to 6.8 demonstrate an excellent correspondence between the predicted and experimental disruption values for multiple-pass experiments. This result stresses the predictive power of the model. No prior information on any multiple-pass experiments was required in order to generate the predicted curves. This result confirms the significance of the selected stress and strength distributions. In particular, it emphasizes that :

- $f_S(S)$ is a good approximation to the culture's ability to resist disruptive stresses,
- $f_D(S)$ is a good approximation to the system's stress distribution.

Figure 6.10 displays a tendency for the model to overpredict disruption with multiple passes. This implies that fewer cells are destroyed than the model predicts. This is to be

expected as the selected stress and strength distributions are approximations to reality. In particular, the tendency to slightly overpredict at high levels of disruption may be due to the following :

- *The stress distribution may change after the first pass.*

  The homogenate characteristics will alter with multiple passes. Specifically, DNA will be released and subsequently degraded and this will lead to a variable broth viscosity. Further, debris will be present only after the first pass. Consequently, the stress distribution may not be the same for each pass as assumed in equation (2.11).

- *The stress distribution may be poorly defined in the limit as $S \to \infty$ or $S \to 0$.*

  A small fraction of cells may pass through the valve while it is opening with each pressure stroke. This transient phenomenon leads to a complication in the distribution which is not readily characterized.

- *The feed temperature for the tests is 5 °C, whereas the model parameters were determined for a 20 °C feed temperature.*

  Although the effect of a reduced feed temperature is apparently small for single-pass studies, it may introduce a systematic error which becomes increasingly pronounced with multiple passes.

- *The strength distribution may be more complex than the selected distribution.*

  This point will be addressed further in chapter 7.

Despite the tendency to slightly overpredict with multiple passes, the model provides an excellent *a priori* estimate of disruption. Figure 6.11 is a parity plot comparing the experimental and predicted disruptions. It stresses that in most cases the magnitude of the overprediction is small compared with the actual disruption value. Figure 6.10 shows that in

some cases the experimental and predicted values are separated by up to six standard deviations. Combined with Figure 6.11, this stresses the small experimental tolerances on the measured disruption. Clearly, the existing difference between the experimental and predicted values would not be discernible using traditional indirect techniques for analyzing disruption because of their low accuracy at high levels of disruption (chapter 3). This emphasizes the need for an accurate measure of disruption such as the disc centrifuge.

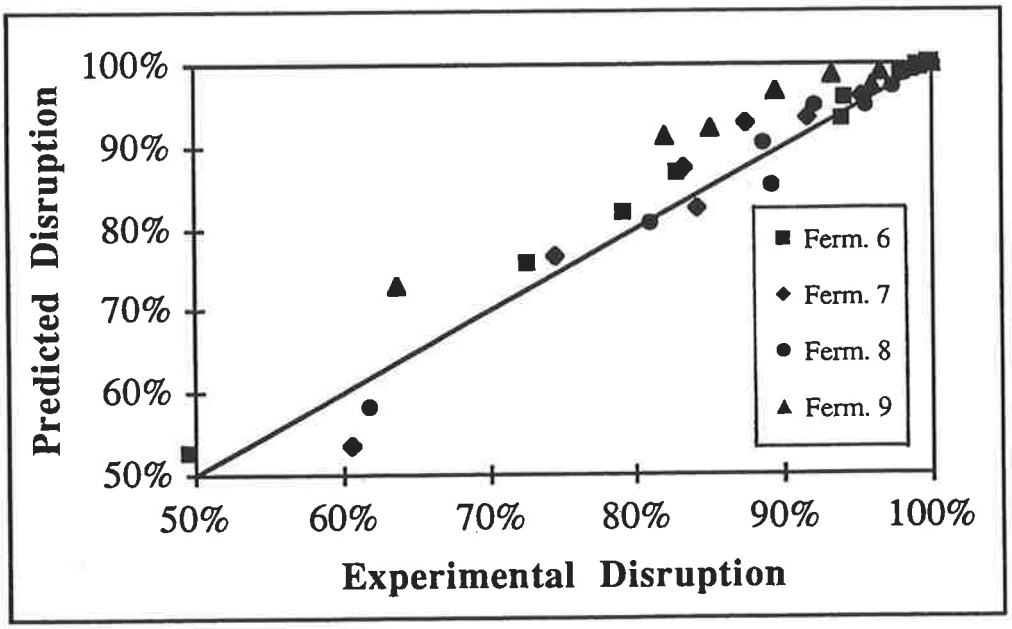

FIGURE 6.11 : *Parity plot comparing the experimental and predicted disruptions for multiple-pass experiments.*

6.4 Regression and Discussion

The difference between the experimental and predicted values is partly explained by the uncertainty in the predicted mean strength, $\bar{S}$. The correlations for mean effective strength are accurate to approximately ±6% (chapter 5). To test the effect of this error, the experimental disruption data determined with the disc centrifuge were regressed using the program described in chapter 4, but with $\bar{S}$ as the only regression parameter. Other model parameters were set to the values in Table 4.8. The regressed strength values thus determined showed a maximum deviation of approximately 6% from the predicted values. This compares favourably with the accuracy of equations (5.5) and (5.14).

TABLE 6.3 : *Comparison of Regressed and Predicted mean effective strengths.*

Ferm.[a]	$\bar{S}$	$\bar{S}$	Deviation	$\bar{S}$	Deviation
	regressed	(eq. 5.5)	(eq. 5.5)	(eq. 5.14)	(eq. 5.14)
6	45.38	45.93	+1.2%	45.83	+1.0%
7	45.18	45.25	0.2%	45.59	+0.9%
8	42.11	44.53	+5.8%	44.34	+5.3%
9	42.34	39.87	−5.8%	40.11	−5.3%

[a] Fermentation number.

Fermentations 8 and 9 show the greatest discrepancy between the predicted and regressed strengths. The regressed disruption versus pressure curves are shown in Figures 6.12 and 6.13. Also shown are the curves obtained using the predicted values for mean effective strength (eq. (5.14)) and the experimental data. The fit to the experimental data is clearly improved by using the regressed value for mean effective strength.

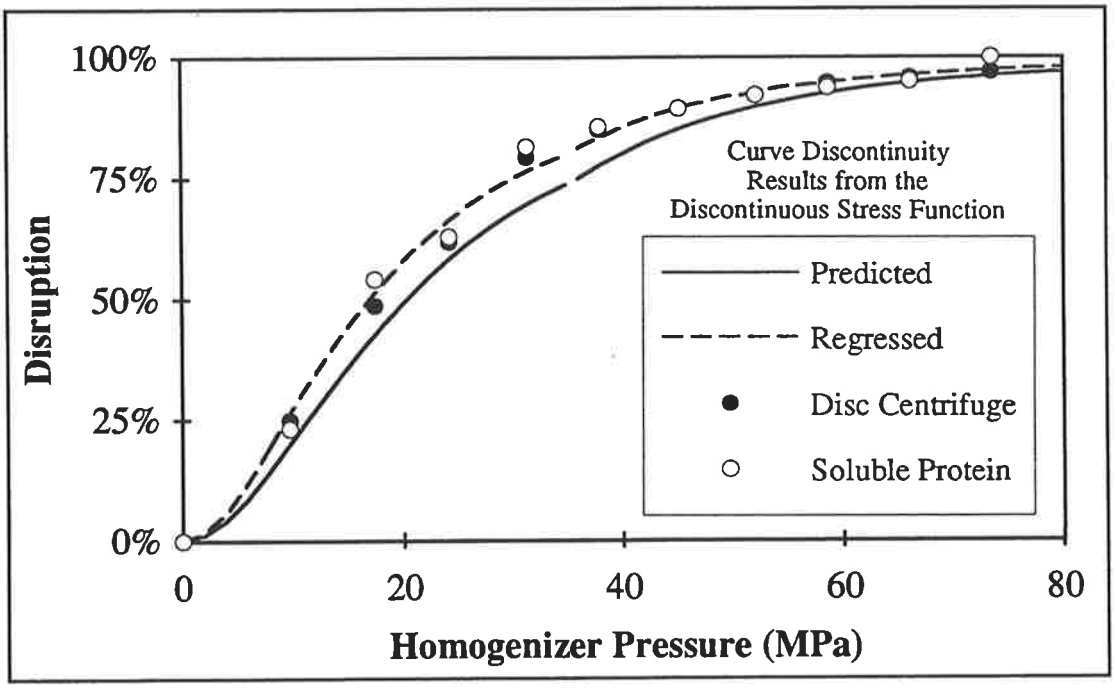

FIGURE 6.12 : *Disruption versus pressure for fermentation 8. Model regressions compared with experimental data.* (*E. coli* B, Glycerol) ($\bar{S}$ is the only regressed parameter. Other parameters from Table 4.8)

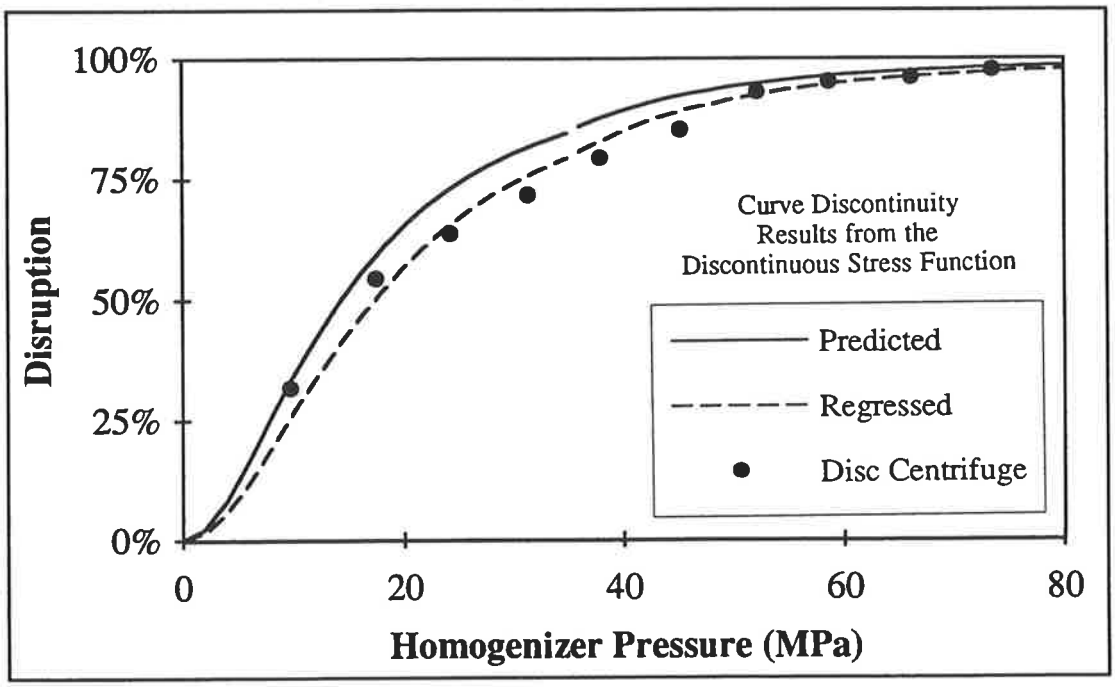

FIGURE 6.13 : *Disruption versus pressure for fermentation 9. Model regressions compared with experimental data.* (*E. coli* JM101, Glucose) ($\bar{S}$ is the only regressed parameter. Other parameters from Table 4.8)

Figure 6.14 is a plot of the number of standard deviations separating the experimental and regressed values and the experimental and predicted values. This graph clearly shows that the model predictions were adversely affected by error in the predicted mean effective strength.

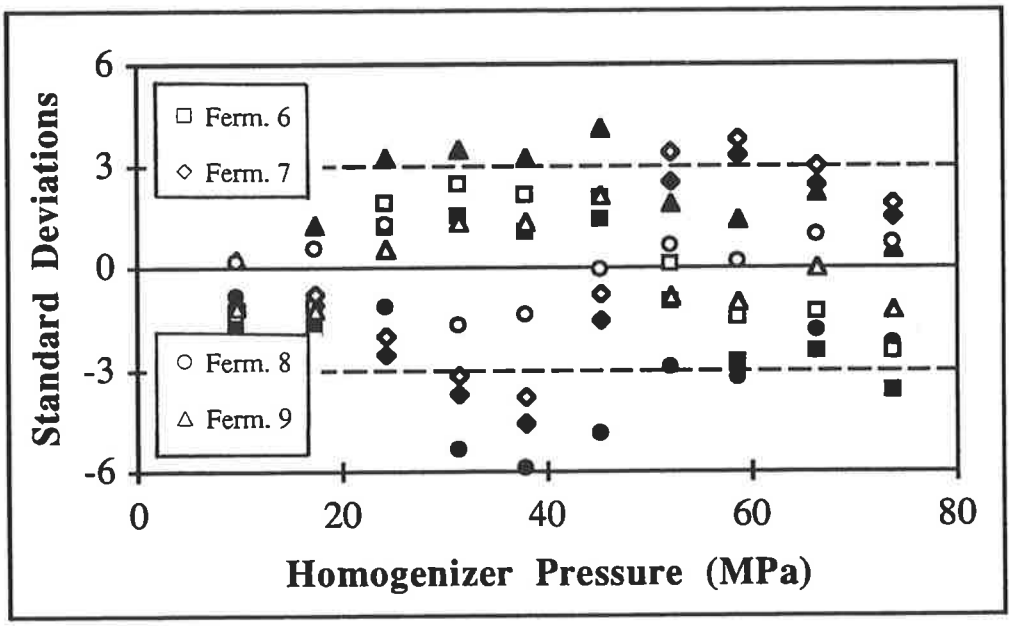

FIGURE 6.14 : *Number of standard deviations (t) separating the predicted and experimental (solid symbols) or regressed and experimental (open symbols) disruption (Disruption vs Pressure data).*

Figure 6.15 is a plot of the number of standard deviations separating the experimental and regressed values and experimental and predicted values for the multiple pass experiments. Error in the predicted mean effective strength has not affected the tendency of the model to slightly overpredict disruption for multiple pass experiments. This is emphasized by Figure 6.16, which is a parity plot comparing the experimental and regressed disruptions for multiple-pass experiments.

These results suggest that for improved prediction accuracy, more precise measurements should be devised for crosslinkage and average length, or multiple measurements should be made. The accuracy of equations (5.5) and (5.14), and hence the model predictions, could

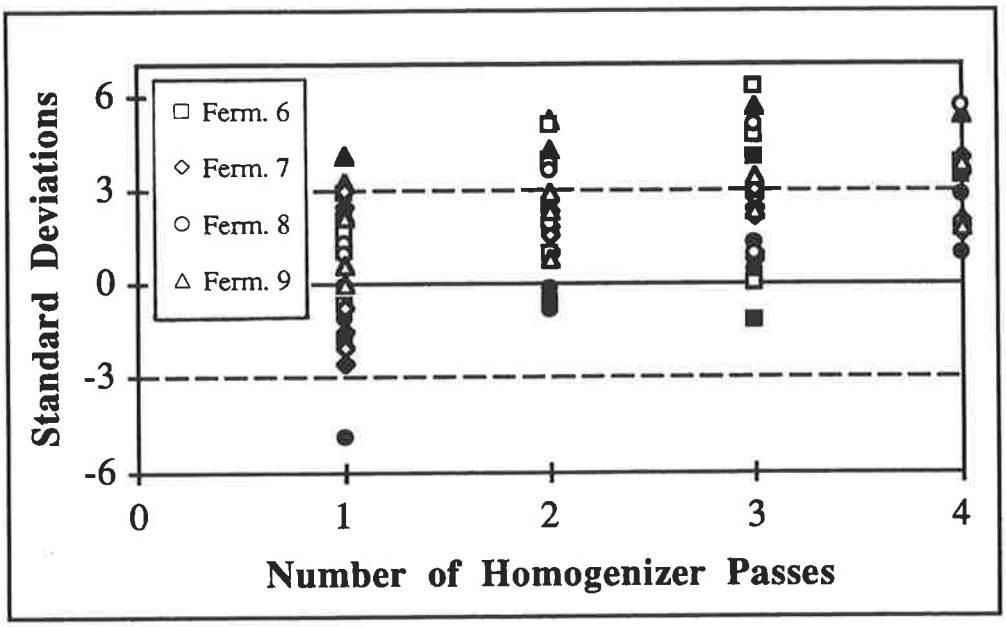

FIGURE 6.15 : *Number of standard deviations (t) separating the predicted and experimental (solid symbols) or regressed and experimental (open symbols) disruption (Disruption vs Pass data).*

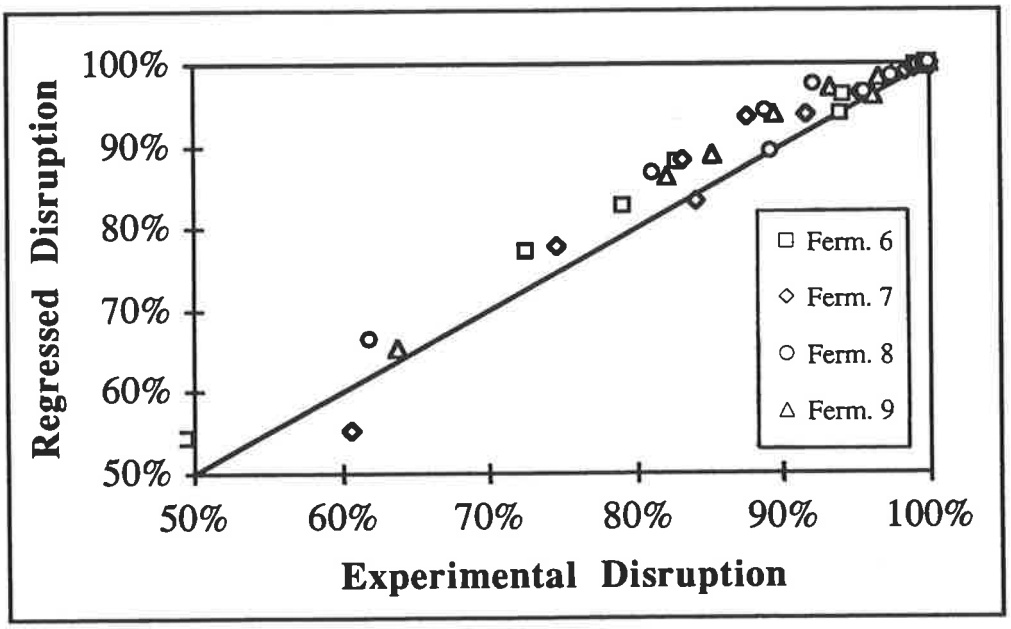

FIGURE 6.16 : *Parity plot comparing the experimental and regressed disruptions for multiple-pass experiments.*

then be improved further. Alternatively, minor variables not included in the correlations such as the degree of bound lipoprotein and diameter may need to be included explicitly. As indicated in chapter 5, these were not important independent variables in the current series of experiments. They may become important if more sensitive measurements can be devised. It should be stressed, however, that the model provides an excellent prediction of disruption in its current form. It is unlikely that greater accuracy would be required from a practical point of view.

Although the correlations for mean effective strength and the model parameters were determined for *E. coli* B grown on glucose, the model has provided good predictions for strain JM101 grown on glucose and strain B grown on glycerol. This work therefore suggests that the model may be used in a predictive capacity for strains of *E. coli* other than wild-type B, and for carbon sources other than glucose. Specifically, it suggests that the distribution variance (σ^2) may be applicable for other strains. It also indicates that the correlations include the most significant variables affecting the strength of *E. coli,* namely peptidoglycan crosslinkage and average cell length. Other factors such as carbon source and strain type influence the disruption primarily through these variables. Further work is required to confirm these assertions beyond refute.

The homogenizer feed temperature was 5°C in all cases. The model was initially developed using a homogenizer feed temperature of 20°C. This does not seem to have adversely affected the model predictions in the current series of tests, except possibly with multiple passes. Temperature would be expected to affect cell strength and possibly the stress distribution through changes in viscosity. Further work into the effect of temperature and concentration needs to be conducted.

6.5 Summary

A model for the disruption of *E. coli* by high-pressure homogenization was developed in chapter 2. The four system- and strain-specific model parameters were obtained in chapter 4 for *E. coli* B disrupted using a 15M-8TA homogenizer with a CD valve. In chapter 5, correlations for mean effective strength (a culture-specific parameter) in terms of measurable culture characteristics were obtained. These allow disruption be predicted with zero degrees of freedom for the specified strain and homogenizer.

To test the predictive capabilities of the model, four cultures were examined. Culture characteristics were measured and used to predict disruption versus pressure and disruption versus pass curves. The model provided an excellent *a priori* prediction of disruption. In particular, the multiple pass experiments confirm that :

- $f_S(S)$ is a good approximation to the culture's ability to resist disruptive stresses,
- $f_D(S)$ is a good approximation to the system's stress distribution.

Regression studies suggested that much of the error in the predicted values was due to error in the predicted values of the mean effective strength. Model predictions can be improved further given more accurate correlations. However, it is unlikely that greater accuracy is required from a practical perspective.

The model was originally developed for *E. coli* B grown on glucose. However, it has been successfully used to predict the multiple-pass disruption of *E. coli* JM101 grown on glucose and *E. coli* B grown on glycerol. This suggests, but does not prove, that the strain-specific parameter (σ) may be applicable for other strains, and that the correlations for mean effective strength include the most significant variables affecting the strength of *E. coli* : namely peptidoglycan crosslinkage and average cell length.

CHAPTER 7

THE EFFECT OF CELL SEPTATION

A predictive model for high-pressure homogenization has been developed, explained and tested in the preceding chapters. Disruption is calculated by coupling a cell-strength distribution with a homogenizer-stress distribution. The effective-strength distribution is approximated by a normal function. This does not allow any difference in strength between septated and non-septated cells. It is possible that septated cells are weaker, as the division site may act as a point of stress concentration. In the present chapter, disruption data from chapter 4 are regressed to the model using a bimodal distribution (eq. (2.2)) in place of the simple normal distribution. The bimodal distribution allows for a difference in strength between septated and non-septated cells. The descriptive and predictive capabilities of the model are compared for each strength distribution. A culture with an artificially-high septated fraction is then obtained using cephalexin, a β-lactam antibiotic which inhibits cell division. Evidence is obtained which suggests, but does not prove, that septated cells are weaker.

7.0 Introduction

A new model for homogenization has been developed and tested in the preceding chapters. Disruption is calculated by combining a cell-strength distribution with a homogenizer-stress distribution, as outlined in chapter 2. A normal distribution for effective cell strength was proposed and employed in chapters 4 to 6. The distribution is given by equation (2.1),

$$f_S(S) = \frac{1}{\sigma\sqrt{2\pi}} \exp\left[\frac{-(S-\bar{S})^2}{2\sigma^2}\right] \qquad -(2.1)$$

where $\bar{S}$ is the mean effective strength and σ^2 is the distribution variance.

A population of *E. coli* is heterogenous as it consists of cells undergoing division (the septated fraction of the population) and cells where cross-wall formation has not commenced (the non-septated fraction). Intuitively, the division site will act as a stress concentrator. Wall stress will therefore be magnified at this site, so it appears reasonable that septated cells should be weaker than those which have not commenced cross-wall formation. As indicated in section 1.5, Engler and Robinson (1981) suggested that bud scars may weaken yeast cells. Furthermore, Thacker (1973) showed that dividing cells of *Saccharomyces cerevisiae* are more sensitive to ultrasound than non-dividing cells. These studies support the suggestion that population heterogeneity may be an important consideration when modelling disruption.

Equation (2.1) assumes a distribution of cell strengths about a single mean effective strength, $\bar{S}$. It neglects any difference in strength between septated and non-septated cells. Equation (2.2) was proposed as an alternative strength distribution which allows such a difference.

$$f_B(S) = \frac{x_s}{\sigma_s\sqrt{2\pi}} \exp\left[\frac{-(S-\bar{S}_s)^2}{2\sigma_s^2}\right] + \frac{1-x_s}{\sigma_n\sqrt{2\pi}} \exp\left[\frac{-(S-\bar{S}_n)^2}{2\sigma_n^2}\right] \qquad -(2.2)$$

Equation (2.2) approximates the effective-strength distribution with a bimodal-normal function. The septated volume fraction, x_s, is included explicitly. Each sub-population is characterized by a mean effective strength, $\bar{S}$, and a distribution variance, σ^2, where the subscripts s and n denote the septated and non-septated fractions, respectively. The use of a bimodal distribution in place of equation (2.1) introduces an additional three parameters to the model (x_s, σ_s, $\bar{S}_s$).

The effect of cell septation on disruption is investigated in this chapter. First, the disruption data from chapter 4 are regressed using equation (2.2) rather than equation (2.1). Model parameters are estimated and correlations (analogous to those in chapter 5) are determined. A comparison with the simpler model used in the previous chapters is provided. The aim is to determine whether a bimodal distribution for effective strength allows a superior description of disruption data. Secondly, an experimental investigation into the effect of cell septation is undertaken. A culture with an abnormally-high septated fraction is obtained using cephalexin. This β-lactam antibiotic binds with penicillin-binding protein III (Spratt, 1980). At low concentrations it inhibits cell division and causes cells to grow as long filaments. The culture is homogenized, and experimental disruption data are compared with model predictions and descriptions. Evidence that septated cells are weaker is sought using optical and electron microscopy.

7.1 Model Regressions

The disruption data obtained in chapter 4 were regressed to the modified model ($f_B(S)$ replacing $f_S(S)$ in eq. (2.8)). A FORTRAN program using the IMSL routine DRNLIN (modified Levenberg-Marquardt method) was coded to perform a non-linear regression of the model to the experimental data. Within the program, equation (2.8) was evaluated using Simpson's method, with the limits of integration set to $\bar{S}_s - 6\sigma_s$ and $\bar{S}_n + 6\sigma_n$. The values of eight parameters are unknown when a bimodal distribution is employed. These may be grouped as follows :

- Culture-related, describing the strength distribution ($\bar{S}_n$, $\bar{S}_s$, σ_n, σ_s and x_s);
- System-specific, describing the stress distribution (m, n and d).

Three regressions (analogous to chapter 4) were conducted.

7.1.1 Modified Model : First Regression

The system-specific parameters and distribution variances (m, n, d, σ_s and σ_n) were constrained to be the same for a given fermentation batch. The remaining parameters ($\bar{S}_s$, $\bar{S}_n$ and x_s) were allowed to vary for each culture. The regression results are summarized in Table 7.1, and suggest that m, n, d, σ_s, and σ_n are constant for all cultures. The results do not confirm that $\bar{S}_s$ is constant, but fail to suggest any correlation with $\bar{S}_n$. It is likely that the variation is random, and results from the strong interaction with x_s. Figure 7.1 plots the number of standard deviations separating the regressed and experimental values versus homogenizer pressure.

7.1.2 Modified Model : Second Regression

The non-linear regression was repeated with the constraint that six parameters (m, n, d, $\overline{S}_s$, σ_s and σ_n) are identical for all cultures. The septated fraction, x_s, was set equal to the average value determined by image analysis (Table 5.1) and $\overline{S}_n$ was allowed to vary for each culture. The regression results are summarized in Table 7.2. Figure 7.2 plots the number of standard deviations, t, separating the experimental and regressed values, against homogenizer pressure.

7.1.3 Modified Model : Third Regression

The final regression was equivalent to that reported in section 4.3.5, but with equation (2.2) replacing equation (2.1). Six parameters (m, n, d, $\overline{S}_s$, σ_s and σ_n) were constrained to be identical for all cultures. However, the three system-specific parameters (m, n and d) were allowed to assume different values for homogenizer pressures above and below 35 MPa (i.e. the stress-function discontinuity described in chapter 4 was introduced). The septated fraction, x_s, was set equal to the average value determined by image analysis (Table 5.1) and $\overline{S}_n$ was allowed to vary for each culture. The regression results are summarized in Table 7.3. Figure 7.3 plots the number of standard deviations, t, separating the experimental and regressed values, against homogenizer pressure.

TABLE 7.1 : *Calculated coefficients for the modified model (first regression).*

Ferm. I.D.†	m	n	d	σ_s (–)	σ_n (–)	Samp. I.D.†	$\bar{S}_s$ (–)	$\bar{S}_n$ (–)	x_s (–)
1	12.4	0.386	8.34	1.76	2.92	1a	16.8	39.36	0.187
						1b	27.1	43.25	0.101
						1c	16.1	47.39	0.010
						1d	23.9	48.14	0.000
2	12.4	0.385	7.30	1.63	3.13	2a	12.0	39.41	0.122
						2b	23.5	39.14	0.239
						2c	23.4	44.27	0.306
						2d	21.0	47.70	0.212
3	12.4	0.386	7.48	1.87	3.40	3a	10.0	42.75	0.306
						3b	27.3	45.78	0.295
						3c	29.1	46.73	0.334
						3d	16.0	46.06	0.074
4	12.4	0.386	8.10	1.70	3.20	4	17.1	32.03	0.231
5	12.4	0.387	8.29	1.68	3.19	5a	18.3	36.51	0.169
						5b	18.1	44.82	0.106
						5c	15.4	46.92	0.033
						5d	32.7	47.72	0.068
						5e	16.2	48.39	0.022
						5f	10.7	49.66	0.003
						5g	12.7	50.36	0.059
						5h	12.5	50.80	0.084

† Fermentation and Sample Identification from chapter 4.

TABLE 7.2 : *Calculated coefficients for the modified model (second regression).*

m	n	d	σ_s (–)	σ_n (–)	$\bar{S}_s$ (–)	Samp. I.D.†	$\bar{S}_n$ (–)	x_s†† (–)
13.0	0.380	7.41	1.71	3.17	17.71	1a	38.80	0.130
						1b	43.31	0.080
						1c	48.37	0.090
						1d	49.18	0.090
						2a	40.39	0.080
						2b	40.05	0.170
						2c	43.49	0.100
						2d	47.61	0.070
						3a	41.63	0.070
						3b	44.62	0.055
						3c	45.10	0.065
						3d	47.27	0.060
						4	31.42	0.180
						5a	36.25	0.263
						5b	45.22	0.190
						5c	47.67	0.134
						5d	47.91	0.089
						5e	48.97	0.084
						5f	50.25	0.068
						5g	50.90	0.110
						5h	51.23	0.100

† Sample identification (chapter 4).

†† Average experimental values (Table 5.1).

TABLE 7.3 : *Calculated coefficients for the modified model (third regression). Bracketed parameters (m, n and d) correspond to pressures below 35 MPa.*

m	n	d	σ_s (–)	σ_n (–)	$\bar{S}_s$ (–)	Samp. I.D.†	$\bar{S}_n$ (–)	x_s†† (–)
12.6 (17.2)	0.39 (0.307)	7.88 (7.53)	1.86	3.02	18.4	1a	40.17	0.130
						1b	44.37	0.080
						1c	49.45	0.090
						1d	50.26	0.090
						2a	41.88	0.080
						2b	41.40	0.170
						2c	44.87	0.100
						2d	48.74	0.070
						3a	42.97	0.070
						3b	46.04	0.055
						3c	46.37	0.065
						3d	48.41	0.060
						4	32.76	0.180
						5a	37.58	0.263
						5b	46.43	0.190
						5c	48.80	0.134
						5d	49.04	0.089
						5e	50.03	0.084
						5f	51.36	0.068
						5g	52.00	0.110
						5h	52.22	0.100

† Sample identification (chapter 4).

†† Average experimental values (Table 5.1).

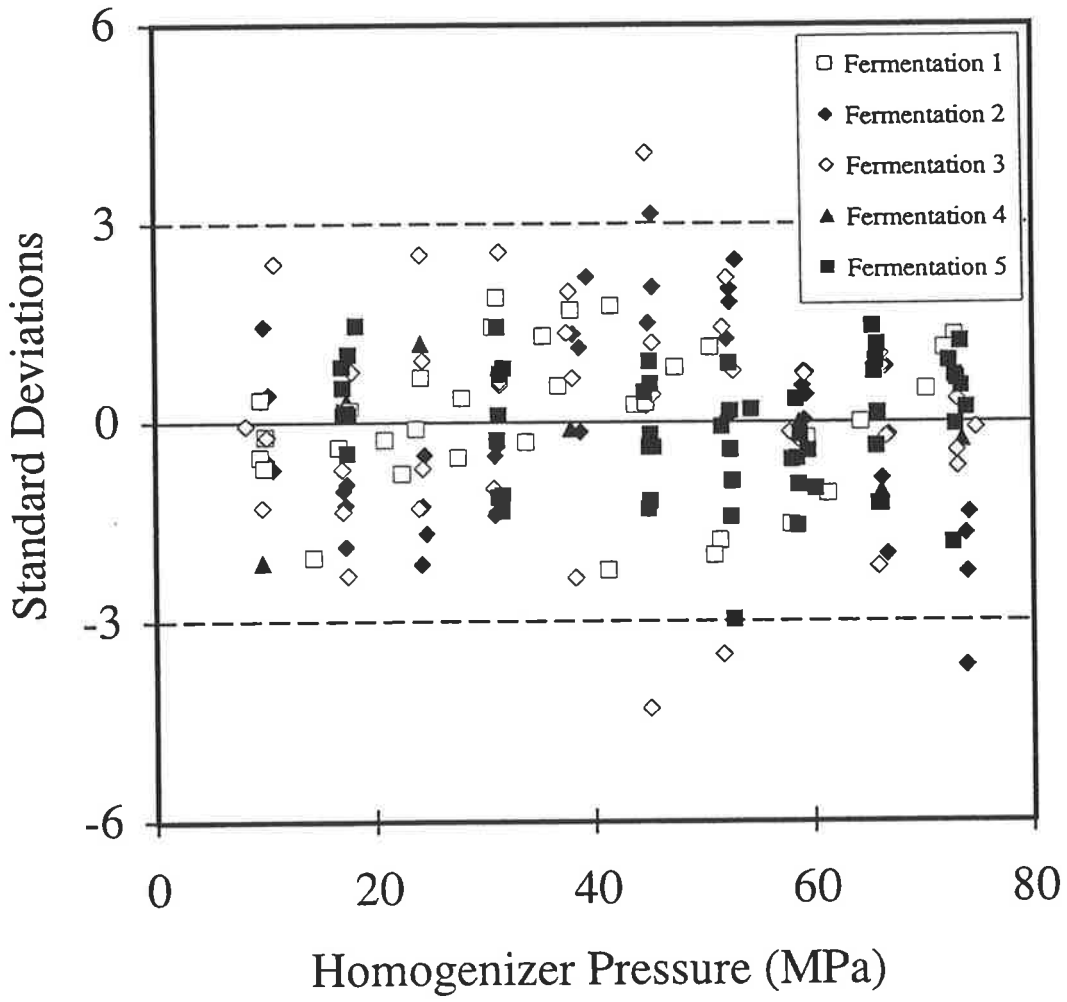

FIGURE 7.1 : *Number of standard deviations separating the experimental and regressed disruption versus homogenizer pressure (First regression).*

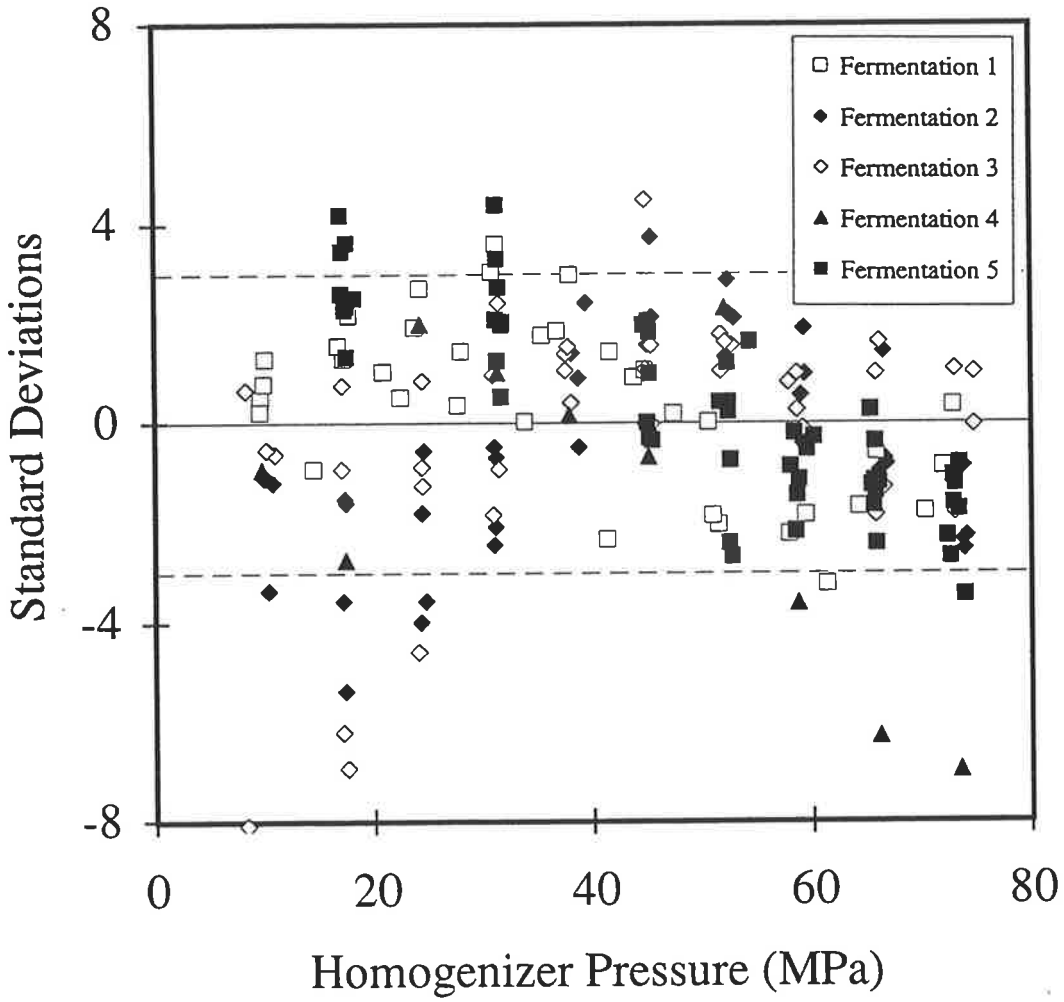

FIGURE 7.2 : *Number of standard deviations separating the experimental and regressed disruption versus homogenizer pressure (Second regression).*

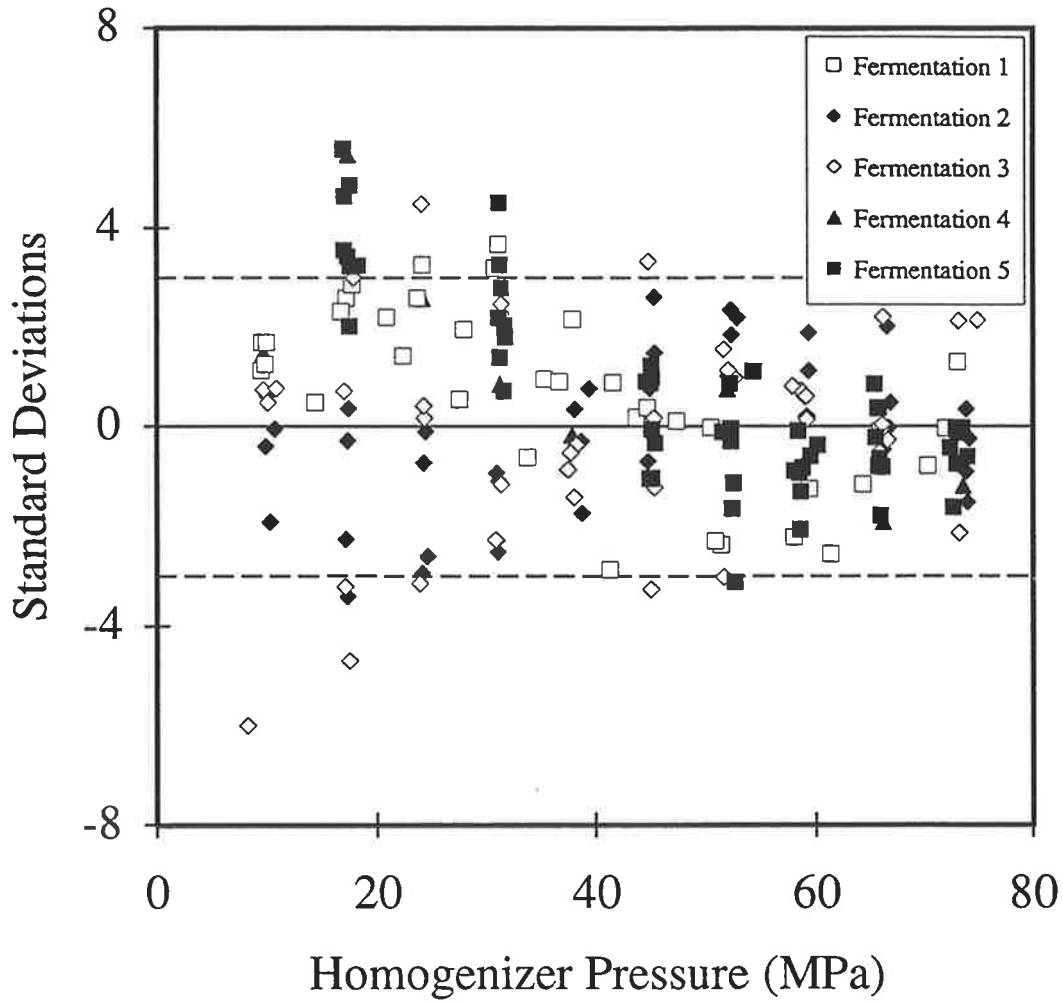

FIGURE 7.3 : *Number of standard deviations separating the experimental and regressed disruption versus homogenizer pressure (Third regression).*

7.1.4 Modified Model : Parameters and Correlations

The results of the third regression give the model parameters summarized in Table 7.4.

TABLE 7.4 : *Model parameters for use with a bimodal strength distribution.*

PARAMETER	EQN.	VALUE	
σ_s	2.2	1.86	
σ_n	2.2	3.02	
$\bar{S}_s$	2.2	18.4	
m	2.6	17.2	P < 35 MPa
		12.6	P ≥ 35 MPa
n	2.6	0.307	P < 35 MPa
		0.39	P ≥ 35 MPa
d	2.6	7.53	P < 35 MPa
		7.88	P ≥ 35 MPa

Two further parameters are required if predictions of disruption are to be made using a bimodal strength distribution. The septated volume fraction of a population may be estimated directly by image analysis (chapter 5). The remaining parameter, $\bar{S}_n$, should correlate with peptidoglycan crosslinkage and average cell length by analogy with the correlations developed in chapter 5 for $\bar{S}$. However, as $\bar{S}_n$ is the mean effective strength of non-septated cells, $\bar{L}$ is replaced by $\bar{L}_n$, the average length of cells in the non-septated sub-population. This can be simply determined using Syzcount™, if cells greater than the minimum average septated length ($\bar{\lambda}_s$, chapter 5) are excluded from the analysis. Table 7.5 summarizes the characteristics of the cultures.

Multiple-linear regression yields equation (7.1), which is analogous to equation (5.5) for use with a normal effective strength distribution.

$$\bar{S}_n = 33.0\,X - 8.50\,\bar{L}_n + 49.72 \qquad -(7.1)$$

This correlation has a coefficient of determination of 0.94.

Non-linear regression gives the following alternative correlation, by analogy with equation (5.14).

$$\bar{S}_n = \frac{127.5\ X}{\bar{L}_n+3.047}\sqrt{15.66 - 11.25\ \ln\left(\frac{X}{1-X}\right)} \quad (X \leq 0.562) \quad \text{-(7.2a)}$$

$$\bar{S}_n = \frac{256.9}{\bar{L}_n+3.047} \quad (X > 0.562) \quad \text{-(7.2b)}$$

Equation (7.1) or equation (7.2) may be used to predict the mean effective strength of non-septated cells. Disruption may therefore be predicted using either of the preceding correlations, plus a measure of the septated volume fraction, x_s, and the parameters in Table 7.4. This is analogous to the model used throughout this thesis. The only difference is that the normal strength distribution (eq. (2.1)) has been replaced with a bimodal distribution (eq. (2.2)).

TABLE 7.5 : *Characteristics of homogenizer feed cultures examined in chapter 4.*

Samp. I.D.[a]	$\bar{S}$ (-)[b]	$\bar{S}_n$ (-)[c]	X (–)[d]	$\bar{L}$ (μm)[e]	$\bar{L}_n$ (μm)[f]	$\bar{D}_n$ (μm)[f]
1a	39.36	40.17	0.390	2.46	2.33	1.0
1b	43.93	44.37	0.392	2.04	1.99	0.96
1c	48.90	49.45	0.440	1.90	1.83	1.0
1d	49.72	50.26	0.466	1.85	1.79	0.99
2a	41.42	41.88	0.401	2.54	2.46	0.87
2b	40.27	41.40	0.403	2.70	2.54	0.91
2c	44.24	44.87	0.394	2.35	2.27	0.93
2d	48.37	48.74	0.440	2.14	2.08	0.88
3a	42.59	42.97	0.379	2.30	2.24	0.86
3b	45.82	46.04	0.417	2.06	2.02	0.87
3c	46.05	46.37	0.430	1.94	1.90	0.87
3d	48.15	48.41	0.441	1.95	1.91	0.90
4	31.52	32.76	0.390	3.69	3.45	0.96
5a	35.87	37.58	0.390	3.23	2.94	0.86
5b	45.06	46.43	0.425	2.44	2.31	0.92
5c	47.87	48.80	0.488	2.30	2.21	0.92
5d	48.52	49.04	0.525	2.03	1.97	0.82
5e	49.56	50.03	0.554	1.99	1.91	0.84
5f	51.02	51.36	0.561	2.01	1.96	0.83
5g	51.26	52.00	0.568	2.06	1.98	0.85
5h	51.56	52.22	0.577	2.04	1.97	0.87

[a] Sample identification (Table 4.2).

[b] Mean effective strength for a normal strength distribution (Table 4.7).

[c] Mean effective strength of non-septated cells for a bimodal strength distribution (Table 7.3).

[d] Peptidoglycan crosslinkage (Table 5.1).

[e] Average cell length determined by image analysis (Table 5.1).

[f] Average length or diameter of cells in the non-septated sub-population.

7.2 A Comparison of Regression Results

A comparison of Figures 7.1 and 4.9 suggests that the introduction of a bimodal distribution has improved the accuracy of the model in describing experimental disruption data. This is, however, hardly surprising as an additional three parameters are introduced in the first regression.

A comparison of Figures 7.2 and 4.11 shows that the introduction of a bimodal distribution provides no numerical benefit when the system-specific parameters and some culture-related parameters are constrained to be identical for all cultures. The same bias of disruption with pressure is apparent, justifying the introduction of a stress discontinuity as in section 4.3.5.

The introduction of a stress discontinuity improves the model's descriptive accuracy, as shown by Figure 7.3. A comparison with Figure 4.13 shows that no benefit is obtained by introducing a bimodal distribution.

The regression results suggest that the complexity introduced by a bimodal distribution (three additional model parameters) is not warranted, as no significant change in the model's accuracy results. Examination of the data in Table 7.5 reveals that the key culture-specific parameter (mean effective strength) is relatively insensitive to the selected form of the strength distribution (value of $\bar{S}$ and $\bar{S}_n$ are almost identical for each culture). Both $\bar{S}$ and $\bar{S}_n$ correlate well with culture properties. The use of a bimodal distribution only introduces a correction to the calculated disruption at low pressures. The model developed in earlier chapters is therefore sufficient for the experimental data examined in this thesis. This point is discussed further in the next section.

7.3 A Comparison of Models

The regression results suggest that no advantage is gained by introducing a bimodal distribution for effective strength. In this section the two possible effective-strength functions, and the corresponding stress distributions, are compared. The disruption versus pressure and disruption versus pass descriptions by each model are also compared, in an attempt to identify situations where a bimodal strength distribution offers advantages over a simple normal representation of mean effective strength.

Correlation of the mean effective strengths in Table 7.4 suggests the following relationship between mean effective strength (eq. (2.1)) and the mean effective strength of non-septated cells (eq. (2.2)) :

$$\bar{S} = 0.986\,\bar{S}_n \qquad (R^2 = 0.993) \qquad -(7.3)$$

Figure 7.4 shows a typical bimodal strength distribution with a ten percent septated fraction and $\bar{S}_n = 40$. A simple normal representation is also shown, where $\bar{S}$ is calculated using equation (7.3). Figure 7.5 shows the stress distribution function for use with either the normal or bimodal strength distributions, at various pressures. No significant differences in the two stress functions are apparent. It is unlikely that the differences would be measurable even if an independent method of determining the stress distribution function were available. This is to be expected, as the stress distribution should be a property of the system and hence independent of the selected strength distribution. Figure 7.6 compares the disruption versus pressure curves predicted using either a normal or a bimodal representation of wall strength, for a culture with an assumed septated volume fraction of ten percent and various values for $\bar{S}_n$. Values for $\bar{S}$ (corresponding to a particular value of $\bar{S}_n$) were calculated by equation (7.3). No significant differences in the curves are apparent at high pressures or for

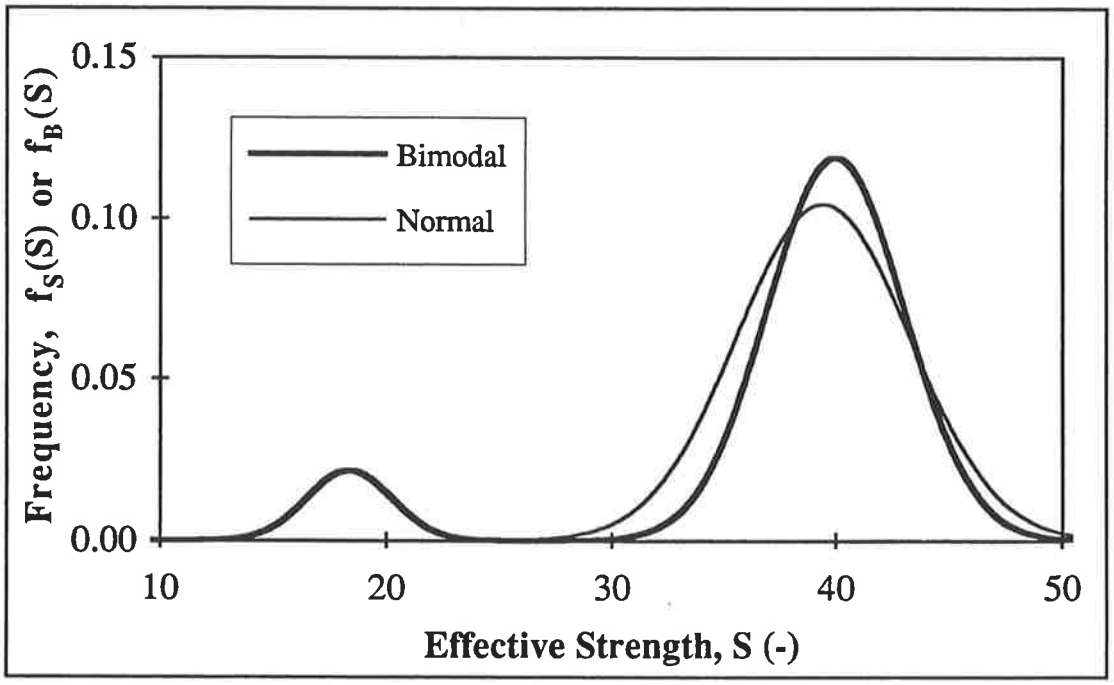

FIGURE 7.4 : *Typical approximations to the effective strength distribution, using either a normal (eq. (2.1)) or bimodal (eq. (2.2)) representation.*

(Bimodal : $\bar{S}_n$=40.0, x_s=10%, other parameters from Table 7.4; Normal : $\bar{S}$ from eq. (7.3), σ from Table 4.8)

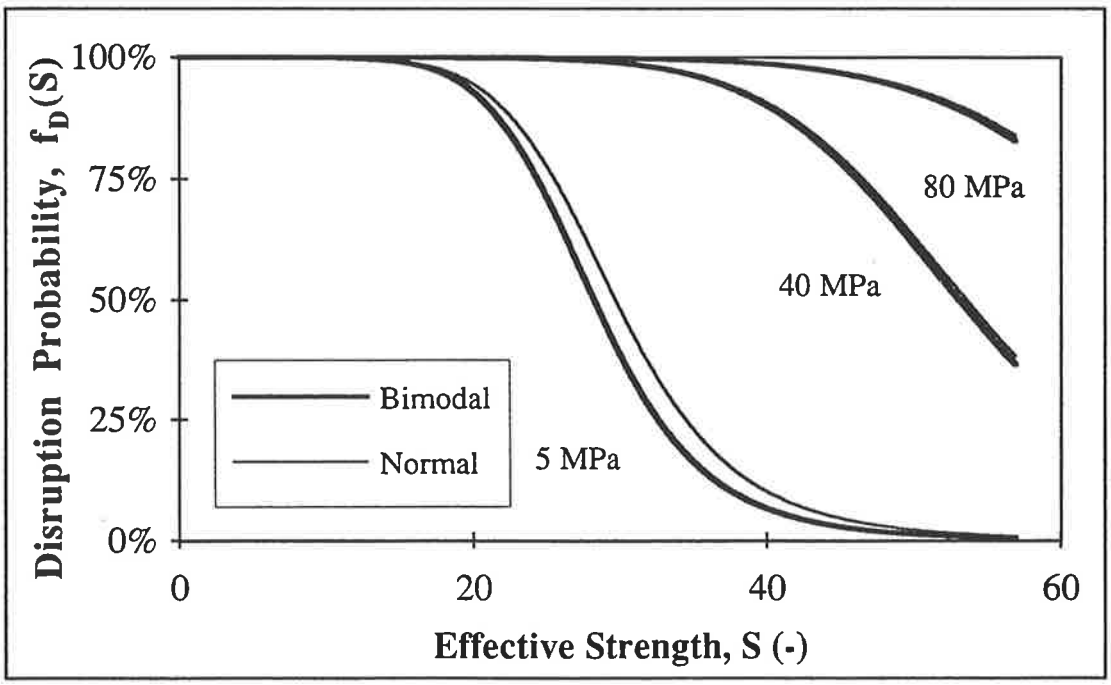

FIGURE 7.5 : *The stress distribution functions for use with either the normal or bimodal strength distributions at various pressures.*

(Model parameters from Table 7.4 (Bimodal) or Table 4.8 (Normal))

'weak' cultures ($\bar{S}_n$ less than approximately 45). The only significant differences in the predicted curves are at very low pressures with 'tough' cells. The differences will be difficult to detect experimentally for the following reasons :

- Pressures below approximately 9 MPa cannot be accurately obtained and maintained using the 15M-8TA homogenizer;
- The analytical technique for measuring disruption is least accurate at low levels of disruption.

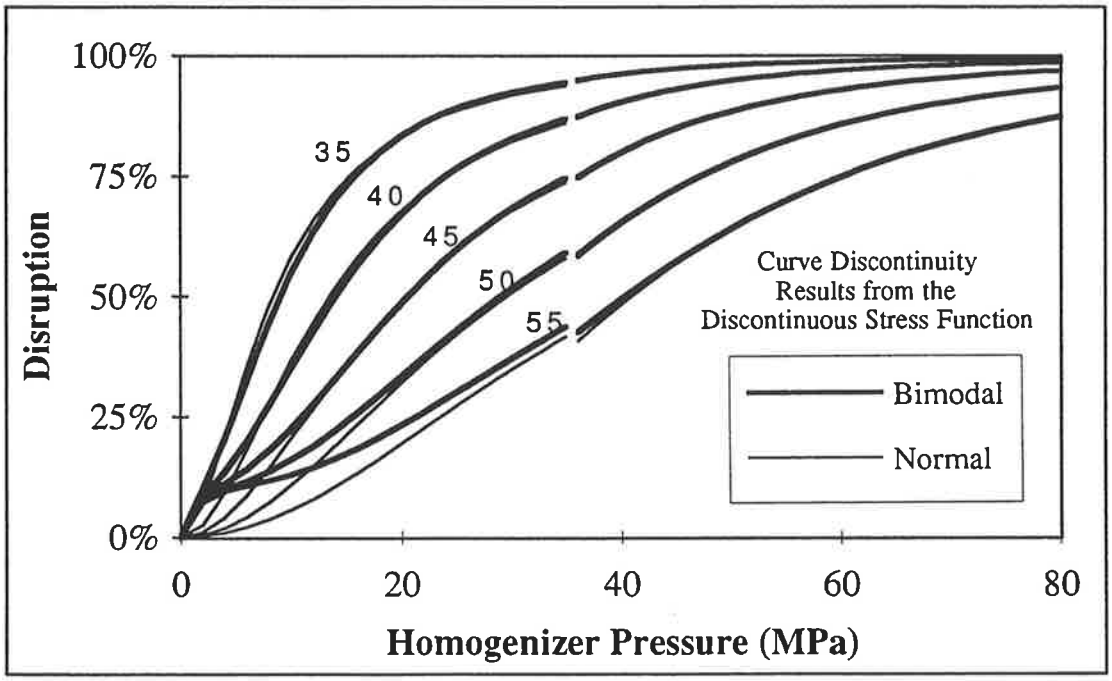

FIGURE 7.6 : *Predicted Disruption versus Pressure curves for a culture with a 10% septated fraction, using either a normal or a bimodal approximation to the true strength distribution* (Numbers are $\bar{S}_n$, $\bar{S}$ from eq. (7.3), Model parameters from Table 7.4 (Bimodal) or Table 4.8 (Normal))

Figure 7.7 is analogous to Figure 7.6, but for a population with an assumed septated volume fraction of thirty percent. Cultures with $\bar{S}_n > 45$ have not been shown, as they will be difficult to obtain with such a high septated fraction. Noticeable differences in the curves are apparent. However, these differences can be reduced by altering the value for $\bar{S}$ slightly.*

* Equation (7.3) was employed to estimate values for $\bar{S}$ (corresponding to a particular value of $\bar{S}_n$) but is likely to be accurate only for low septated fractions similar to those obtained experimentally (i.e. $x_s \approx 10\%$).

Regression studies are therefore unlikely to reveal whether a bimodal distribution is warranted, and hence whether septated cells are weaker.

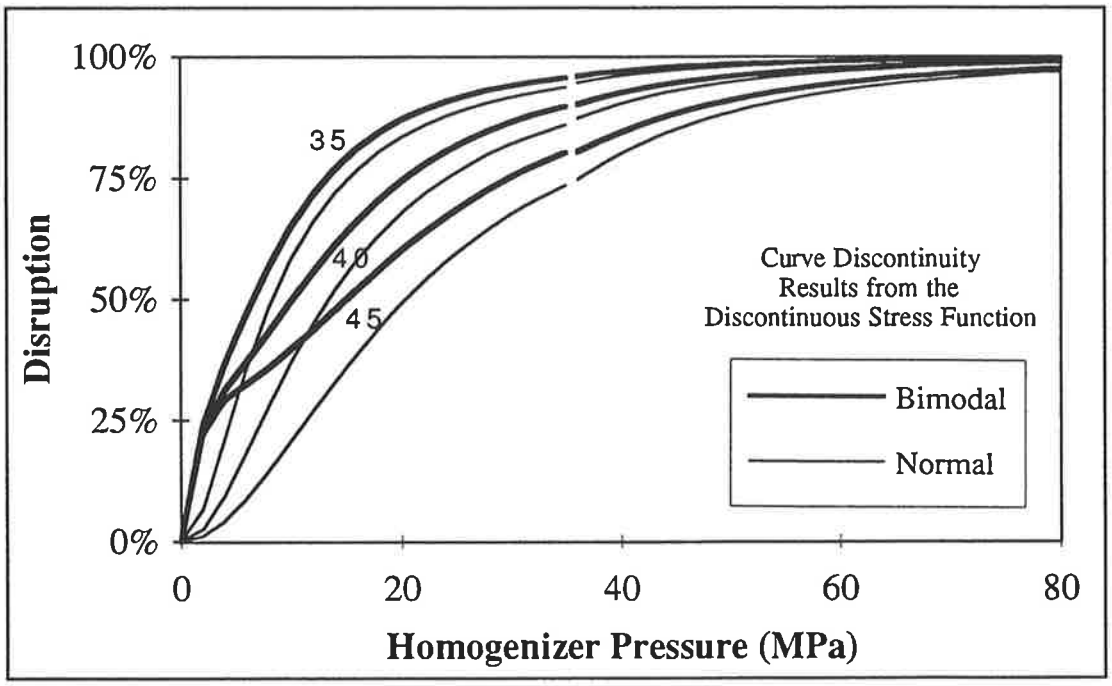

FIGURE 7.7 : *Predicted Disruption versus Pressure curves for a culture with a 30% septated fraction, using either a normal or a bimodal approximation to the true strength distribution* (Numbers are $\bar{S}_n$, $\bar{S}$ from eq. (7.3), Model parameters from Table 7.4 (Bimodal) or Table 4.8 (Normal)).

Figure 7.8 shows disruption versus pass curves predicted for various cultures with a septated fraction of thirty percent at a homogenizer pressure of 24 MPa. The differences between the curves are not significant enough to permit simple experimental differentiation between a bimodal and a normal strength distribution The differences may be further reduced by altering the value for $\bar{S}$ slightly (see preceding footnote).

The preceding considerations strongly suggest that in most situations of practical interest a normal representation of the effective strength distribution will be adequate. Further, it is unlikely that regression studies similar to those conducted throughout this thesis will be able to confirm that septated cells are weaker than non-septated cells. This is, of course, a

specific statement for the homogenizer (i.e. stress distribution) used in this work. Figure 7.4 clearly shows distinct peaks for the septated and non-septated cells in the bimodal representation. For a system with a stress distribution approaching a step-function, the septated volume fraction will be an essential model parameter if septated cells are significantly weaker. For other stress distribution functions, it may therefore be necessary to know whether septated cells are weaker.

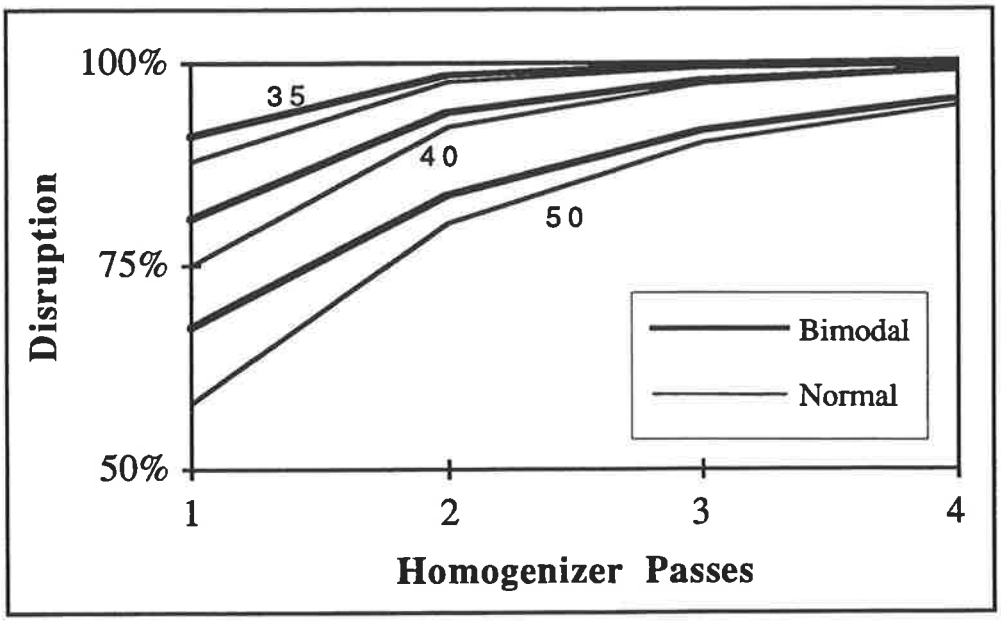

FIGURE 7.8 : *Predicted Disruption versus Pass curves at 24 MPa for various cultures with a 30% septated fraction, using either a normal or a bimodal approximation to the true strength distribution* (Numbers are $\bar{S}_n$, $\bar{S}$ from eq. (7.3), Model parameters from Table 7.4 (Bimodal) or Table 4.8 (Normal)).

A culture with an artificially-high septated fraction is examined in the next section to further investigate the possibility that septated cells are weaker. The culture is homogenized and compared with predictions and descriptions using both a normal and a bimodal distribution. As such studies are unlikely to reveal whether septated cells are weaker, cultures were also examined before and after disruption by optical and electron microscopy.

7.4 Experimental

7.4.1 Fermentation

A single fermentation (fermentation 10) was conducted using a 16 L (working volume) Chemap CF2000 fermenter. Wild type *E. coli* B (P903, Department of Microbiology, The University of Adelaide) were inoculated from a shake flask into 16 L of modified C1 minimal media (Table 4.1) containing 6.25 g L^{-1} of D-glucose to give an initial absorbance (A_{600}) of approximately 0.06. Culture pH was automatically controlled at 6.8 with 4M NaOH. Temperature was controlled at 37°C. Cephalexin (5 μg mL^{-1}, Sigma chemicals) was added when the broth reached an optical density of 0.8. The culture growth rate remained approximately constant at 1.12 h^{-1}. At an absorbance of 3.3, the fermenter's temperature set point was adjusted to 5°C. Additional growth while the broth was cooling gave a final absorbance of 4.4.

7.4.2 Homogenization

The broth was homogenized at various pressures up to 75 MPa using an APV-Gaulin 15M-8TA high-pressure homogenizer with a ceramic cell disruption (CD) valve (Figure 4.1, chapter 4). Homogenizer feed temperature was 5°C. The machine is fitted with a second stage which remained set to zero pressure during all tests. Pressures were set using the fitted gauge. Accurate pressure transients were not measured. Approximate maximum average pressures (P in eq. (2.6)) were therefore calculated from the nominal gauge pressure (P_g) using equation (4.1).

7.4.3 Analysis

Disruption was determined using the analytical disc centrifuge (chapter 3).

The cell-wall structure of the culture was analyzed by high-performance liquid chromatography, as described in chapter 5.

The undisrupted culture was photographed using a phase-contrast microscope at 100x magnification. Developed negatives were mounted as slides, projected onto a screen and digitized for image analysis. Captured images were analyzed using Syzcount. The average cell lengths ($\bar{L}$ and $\bar{L}_n$) and the fraction of the population which is septated, x_s, were determined.

7.4.4 Microscopical Examination

Cultures homogenized at low pressure were examined using a phase-contrast microscope at 100x magnification. Disrupted cultures were also examined by transmission electron microscopy. Formvar-coated grids were floated filmside down on 50 µL drops of diluted suspension. Grids were then washed by floating filmside down on a droplet of 50 mM glycine-NaOH buffer (pH 9.0). Excess fluid was removed with filter paper. Grids were floated for 1 min on an aqueous 2% w/w uranyl acetate solution for staining. The stain was removed with filter paper, and the specimen was air dried. Electron micrographs were taken with a Philips EM300 transmission electron microscope.

7.5 Results and Discussion

The results of the culture analysis, and the mean effective strength predictions, are summarized in Table 7.6. Note that the culture is characterized by a very high septated fraction of fifty-five percent. This is a result of the action of cephalexin (Spratt, 1980).

TABLE 7.6 : *Characteristics of the culture grown in the presence of cephalexin.*

Characteristic	Symbol	Value (normal strength distribution, eq. 2.1)	Value (bimodal strength distribution, eq. 2.2)
Septated Volume Fraction	x_s	not required	0.55
Peptidoglycan Crosslinkage	X	0.452	0.452
Average Cell Length (μm)	$\bar{L}$	5.21	not required
Average Length of non-septated cells (μm)	$\bar{L}_n$	not required	3.65
Predicted Mean Effective Strength	$\bar{S}$	21.8 (eq. 5.5) 29.4 (eq. 5.14)	not applicable
Predicted Mean Effective strength of non-septated cells	$\bar{S}_n$	not applicable	33.6 (eq. 7.1) 36.3 (eq. 7.2)

The predictions of mean effective strength allow disruption versus pressure curves for the culture to be predicted. These are shown in Figure 7.9, with experimental data superimposed for comparison. Figure 7.10 plots the number of standard deviations separating the experimental and predicted values.

Experimental data were regressed to each model using the previously-described non-linear regression packages. In both regressions, mean effective strength ($\bar{S}$ or $\bar{S}_n$) was the only parameter allowed to vary. Other parameters were set to the values in either Table 4.8 (normal distribution) or Table 7.4 (bimodal distribution). For regression with the bimodal distribution the measured septated fraction was employed. The results are presented in Figures 7.11 and 7.12.

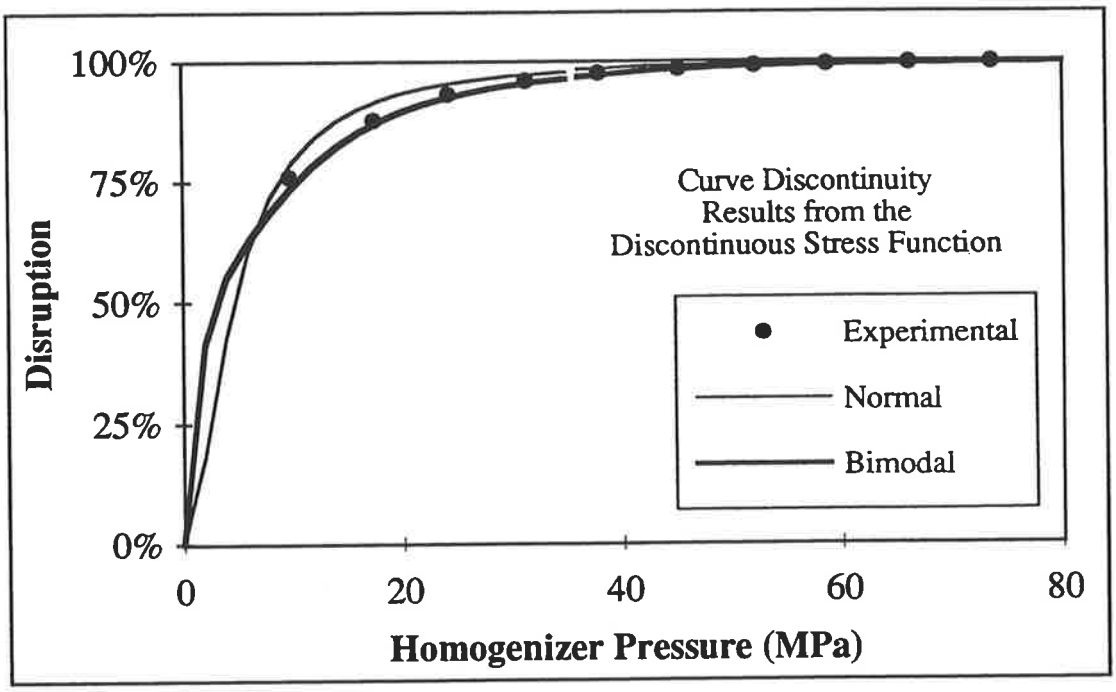

FIGURE 7.9 : *Predicted Disruption versus Pressure curves for a cephalexin-treated culture using both the normal and bimodal approximations to the true strength distribution* (Bimodal : $\bar{S}_n$=36.3 (eq. 7.2), x_s=55% (measured), m, n, d, σ_s, σ_n, $\bar{S}_s$ from Table 7.4; Normal : $\bar{S}$=29.4 (eq. 5.14), m, n, d, σ from Table 4.8)

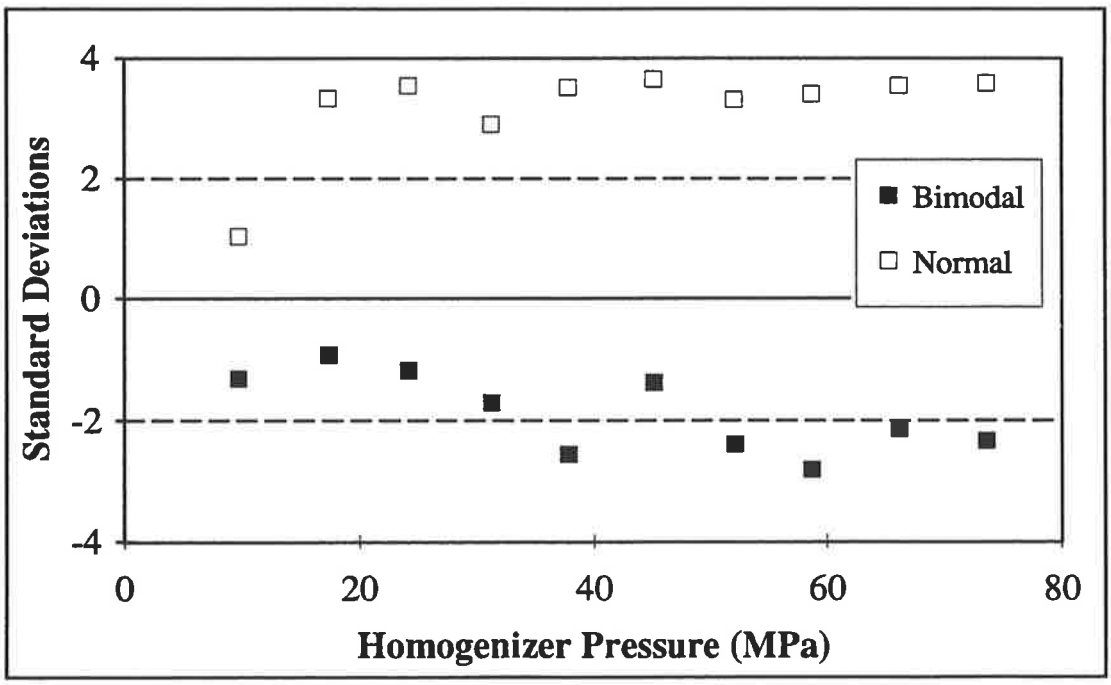

FIGURE 7.10 : *Number of standard deviations separating the experimental and predicted disruption versus homogenizer pressure for a cephalexin-treated culture*

(Bimodal : $\bar{S}_n$=36.3 (eq. 7.2), x_s=55% (measured), m, n, d, σ_s, σ_n, $\bar{S}_s$ from Table 7.4; Normal : $\bar{S}$=29.4 (eq. 5.14), m, n, d, σ from Table 4.8)

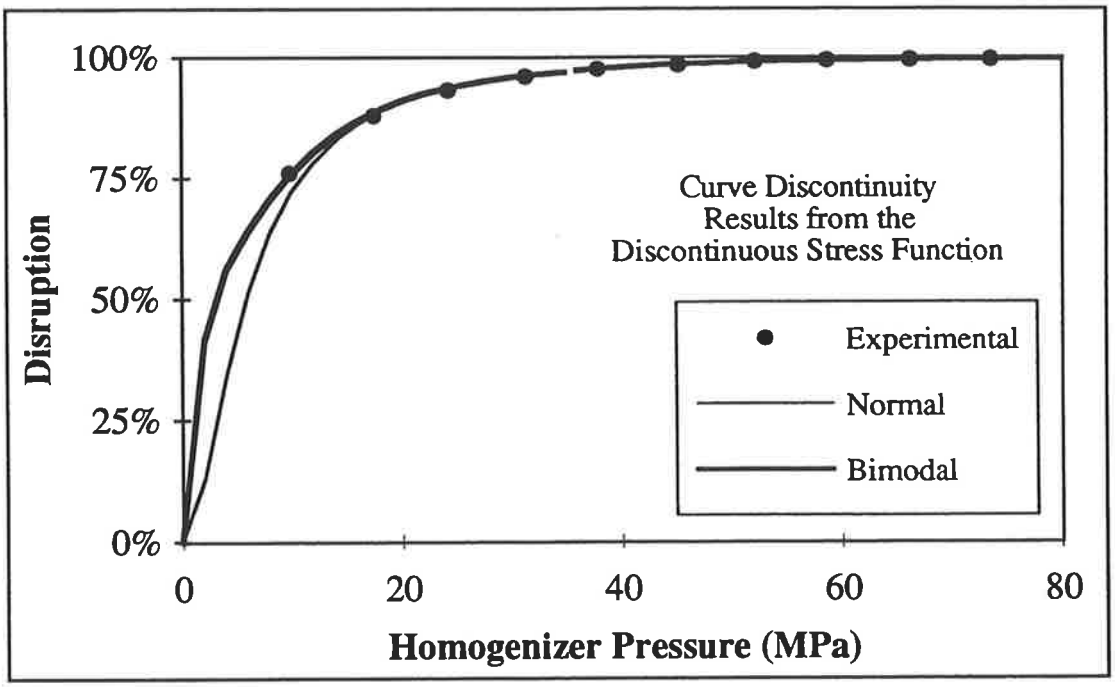

FIGURE 7.11 : *Model regressions to experimental data for the normal and bimodal approximations to the true strength distribution.*

(Bimodal : $\bar{S}_n$=35.4 (Regressed), x_s=55% (measured), m, n, d, σ_s, σ_n, $\bar{S}_s$ from Table 7.4;

Normal : $\bar{S}$=31.2 (Regressed), m, n, d, σ from Table 4.8)

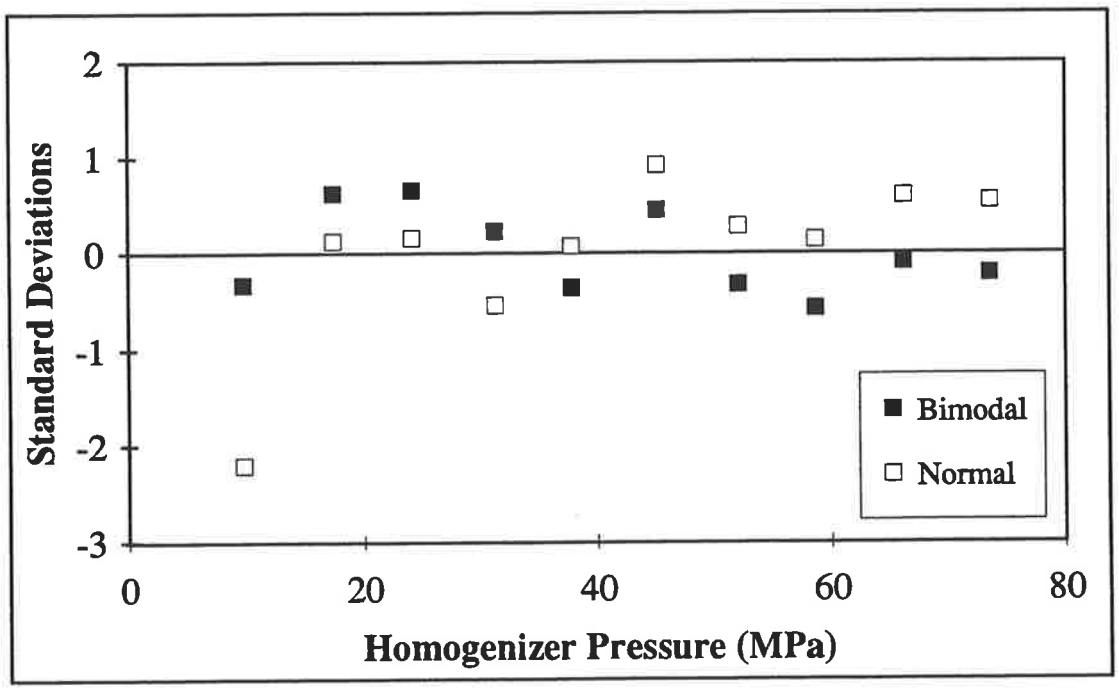

FIGURE 7.12 : *Number of standard deviations separating the experimental and regressed disruption versus homogenizer pressure for a cephalexin-treated culture.*

(Bimodal : $\bar{S}_n$=35.4 (Regressed), x_s=55% (measured), m, n, d, σ_s, σ_n, $\bar{S}_s$ from Table 7.4;

Normal : $\bar{S}$=31.2 (Regressed), m, n, d, σ from Table 4.8)

The preceding regression results suggest that the bimodal distribution provides a marginally improved **description** of the disruption data at low pressures. This suggests, somewhat tentatively, that septated cells may indeed be weaker. For **predictive** purposes, however, the normal and bimodal distributions have virtually equal accuracy due to the error in the prediction of $\bar{S}$ and $\bar{S}_n$. As well, equation (5.5) provides an extremely poor prediction of $\bar{S}$ for the present culture ($\bar{S}$=21.8 predicted by eq. (5.5), $\bar{S}$=31.2 by regression). Equation (5.14) is therefore preferable when using a normal distribution.

Figure 7.13 presents size distributions of the undisrupted culture and a sample homogenized with a single pass at 9.6 MPa. The undisrupted sample exhibits a definite bimodal size distribution, presumably due to the presence of filamentous cells. The disrupted sample exhibits a single mode at a smaller Stokes diameter than the undisrupted culture. Again, the results suggest that septated cells may be weaker.

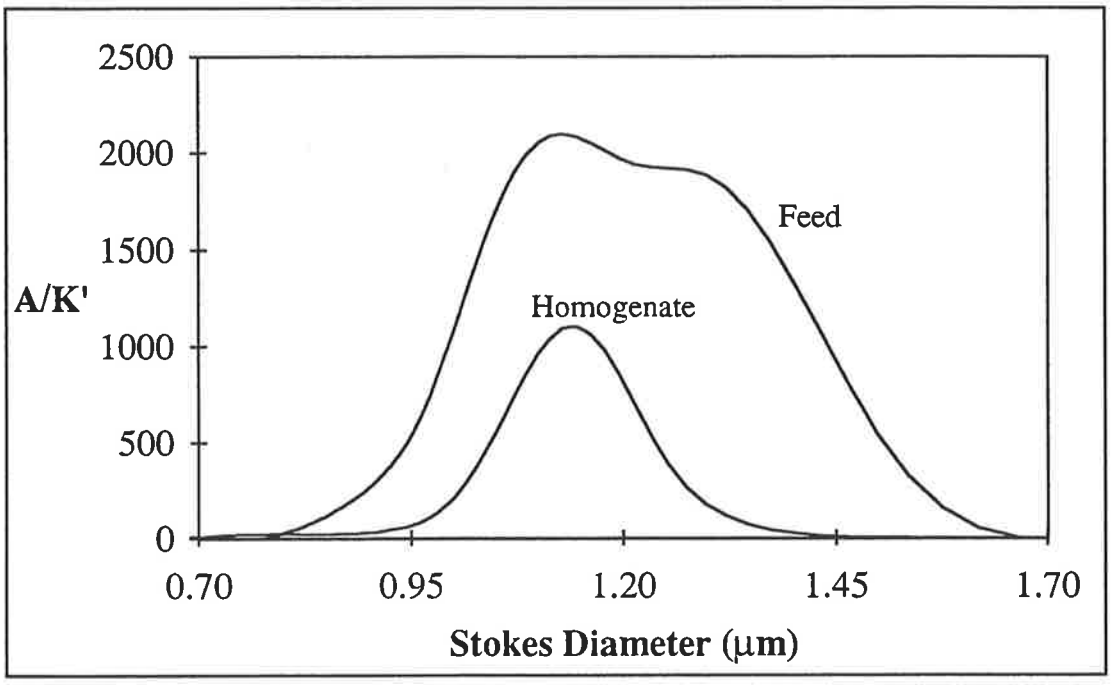

FIGURE 7.13 : *Sample size distributions determined using the analytical disc centrifuge (machine output divided by extinction coefficient; samples are normalized to the same concentration). The homogenate distribution is for 1 pass at 9.6 MPa.*

Figure 7.14 shows a photograph of the undisrupted feed sample and a control sample. Filamentous cells are clearly visible in the cephalexin-treated culture. Figure 7.15 shows a cephalexin-treated sample disrupted once at 9.6 MPa. Some septated cells are still visible, but at a considerably reduced frequency. Filamentous cells were not present. Disrupted cells are also clearly visible, and generally exhibit fractures perpendicular to the main axis of the cell (i.e. cell fragments have the same diameter as intact cells but are considerably shorter). This observation supports the finding in chapter 5 that peptide bonds are the weak point in the cell (provided peptide bonds are aligned perpendicular to the main axis as proposed by Verwer *et al.* (1978)). Figure 7.16 shows a photograph of a cephalexin-treated sample disrupted at 24 MPa. No clearly-septated cells could be found. Figure 7.16 reveals debris of a smaller size than Figure 7.15. This may be simply due to the harsher homogenization conditions or to a different disruption mechanism.

Figures 7.17 to 7.20 are photographs of the culture homogenized at 9.6 MPa taken by transmission electron microscopy (TEM). Figure 7.17 reveals a clear fracture at a division site. This is also shown for a different view field in Figure 7.18. Note that all cells in Figure 7.18 are arguably broken at a division site. Whether fracture at the division site is a general phenomenon cannot, however, be deduced from such limited evidence. Figure 7.19 is a magnification of Figure 7.18, showing a fracture site. Figure 7.20 is a further magnification, showing both ends of a disrupted cell in Figure 7.18. There appears to be some evidence of stress on the polar cap of the cell. This may be due to the sudden pressure release during homogenization or may simply be an artefact of the preparative procedure.

Combined, the evidence **supports** the suggestion that septated cells are weaker. The assertion is **not** proven. For the cultures examined in this thesis, the normal approximation to the true strength distribution provides sufficient predictive accuracy. It is likely that this will be true for most situations of practical interest. However, in cases where a different stress function is used (e.g. a homogenizer having an almost step-function stress distribution), the septated volume fraction may be a critical model parameter, and a more

accurate approximation to the true strength distribution (e.g. a bimodal representation) will be required.

In conclusion, the bimodal representation of the effective strength distribution would appear to be a closer approximation to the true effective strength distribution. However, for modelling purposes, a simple normal approximation is sufficient. The normal distribution also has the following advantages :

i) fewer parameters are required to predict disruption, and

ii) a measure of the septated fraction of the population is not required.

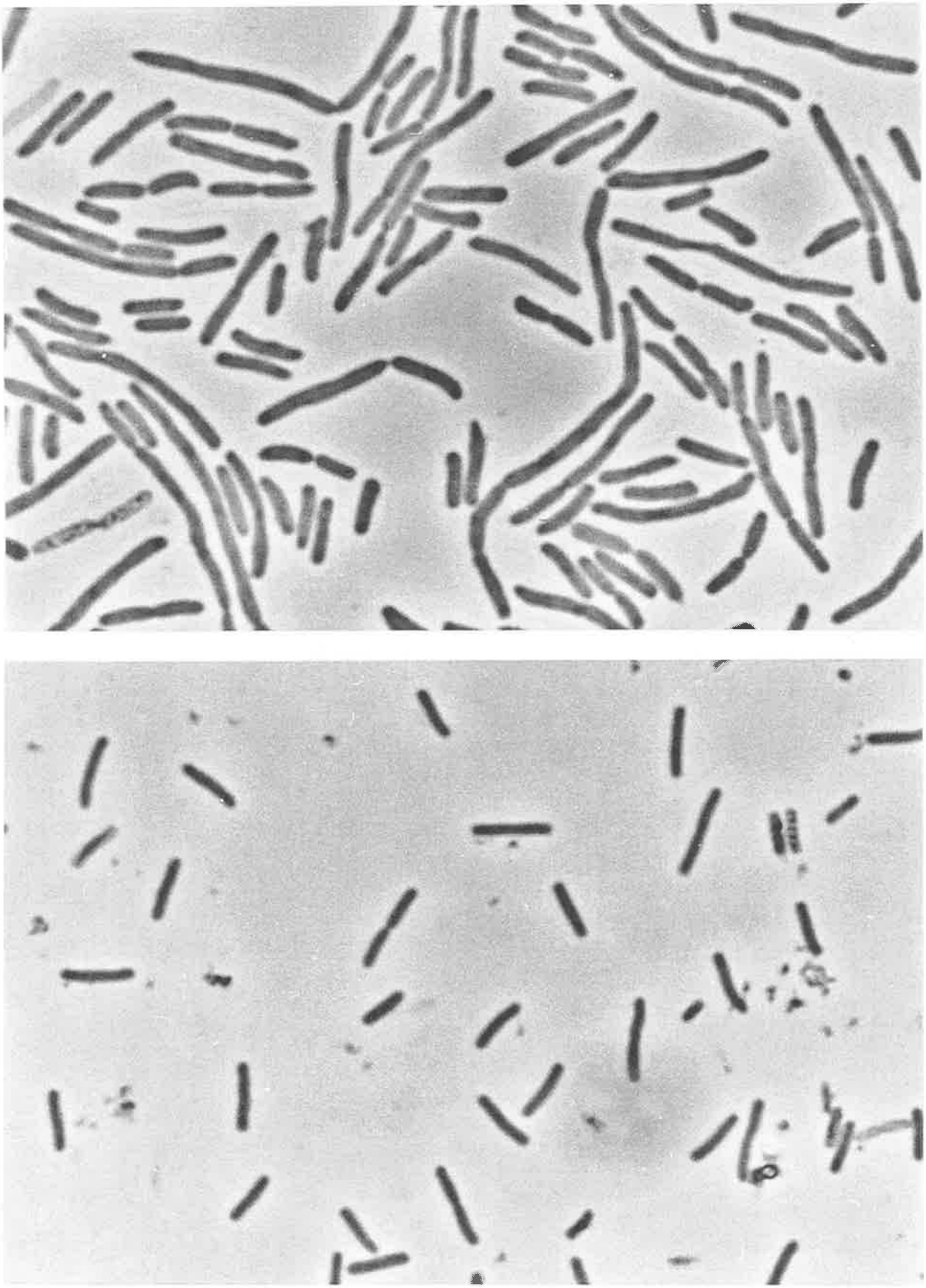

FIGURE 7.14 : *Cephalexin-treated culture before homogenization (top) and a culture grown under similar conditions (Fermentation 4) but without the addition of cephalexin (bottom).*

[Photograph taken with phase-contrast microscope using a 100x objective]

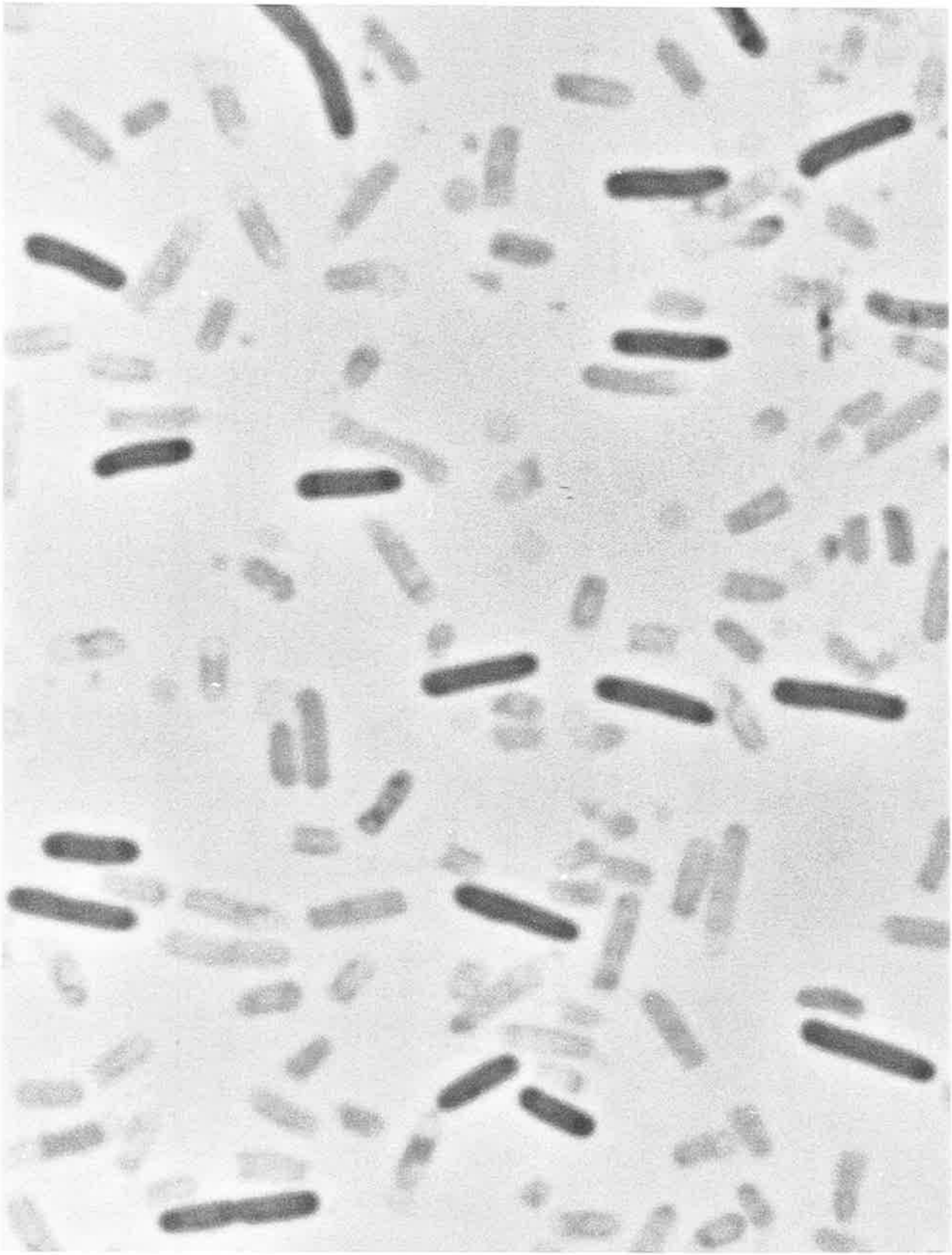

FIGURE 7.15 : *Cephalexin-treated culture homogenized once at 9.6 MPa.*

[Photograph taken with phase-contrast microscope using a 100x objective]

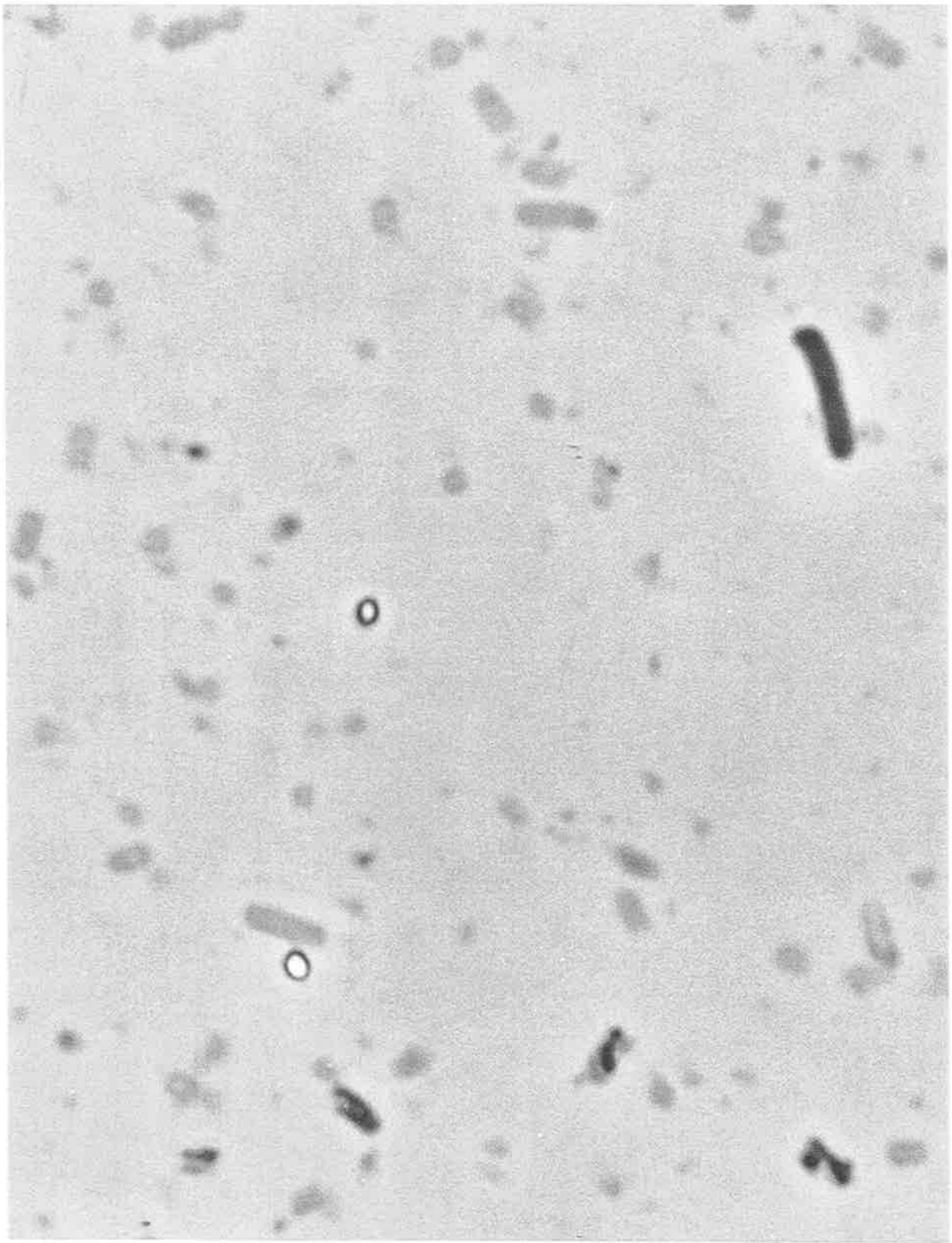

FIGURE 7.16 : *Cephalexin-treated culture homogenized once at 24 MPa.*

[Photograph taken with phase-contrast microscope using a 100x objective]

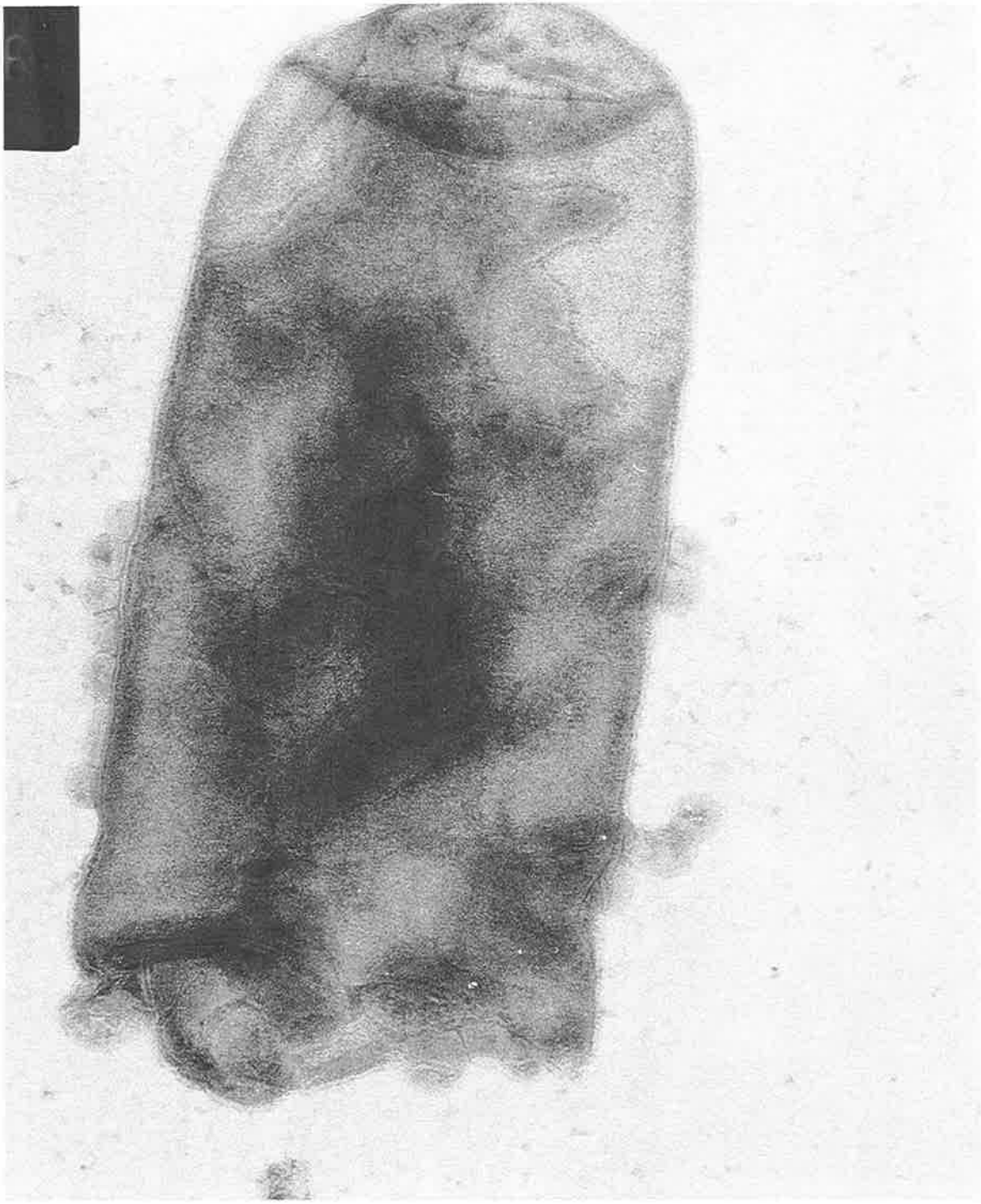

FIGURE 7.17 : *Disrupted cells (1 Pass at 9.6 MPa; Magnification 27,000 x).*

[Taken with a Philips EM300 Transmission Electron Microscope]

FIGURE 7.18 : *Disrupted cells (1 Pass at 9.6 MPa; Magnification 12,500 x).*

[Taken with a Philips EM300 Transmission Electron Microscope]

FIGURE 7.19 : *Disrupted cells (1 Pass at 9.6 MPa; Magnification 27,000 x). (Enlargement of Figure 7.18)*

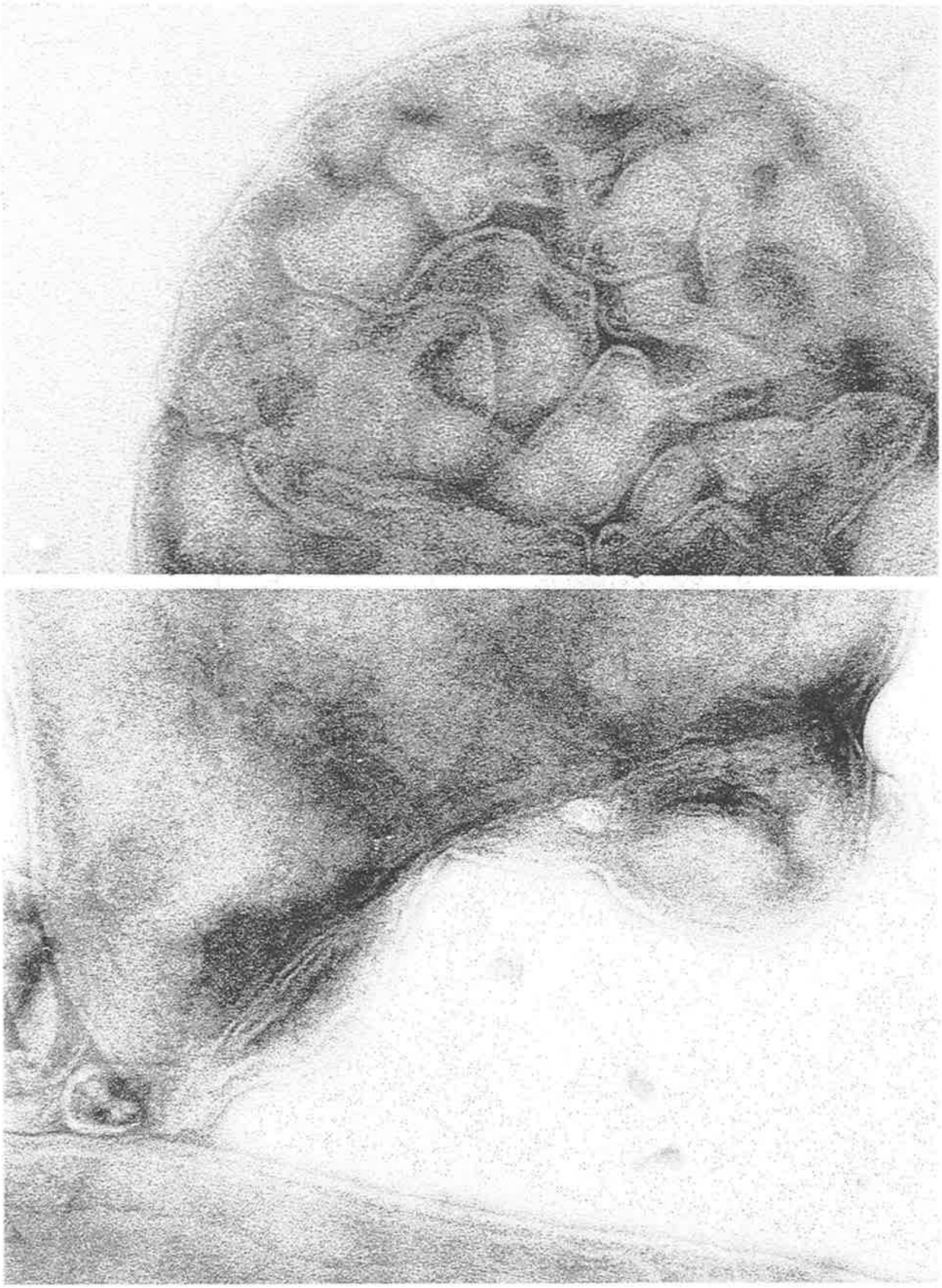

FIGURE 7.20 : *Disrupted cells (1 Pass at 9.6 MPa; Magnification 55,000 x). (Enlargement of Figure 7.18)*

7.6 Summary

A new model for disruption was developed in the preceding chapters. This was based on a normal approximation to the true effective strength distribution. The normal approximation does not allow for a possible difference in strength between septated and non-septated cells. Such a difference is possible as the division site may act as a point of stress concentration. An alternative distribution was therefore presented in chapter 2. This is a bimodal approximation to the true strength distribution. It allows for a difference in strength between the two sub-populations (septated and non-septated).

Experimental disruption data presented in chapter 4 were regressed to the model using the bimodal approximation in place of the normal distribution for effective wall strength. The model parameters summarized in Table 7.4 were determined.

TABLE 7.4 : *Model parameters for use with a bimodal strength distribution.*

PARAMETER	EQN.	VALUE	
σ_s	2.2	1.86	
σ_n	2.2	3.02	
$\bar{S}_s$	2.2	18.4	
m	2.6	17.2	P < 35 MPa
		12.6	P ≥ 35 MPa
n	2.6	0.307	P < 35 MPa
		0.39	P ≥ 35 MPa
d	2.6	7.53	P < 35 MPa
		7.88	P ≥ 35 MPa

In addition, the correlations for the mean effective strength of the non-septated sub-population ($\bar{S}_n$) were determined (eqs. (7.1) and (7.2)). The final model parameter, the septated volume fraction of the population, can be measured directly by image analysis (chapter 5). Consequently, disruption versus pressure and disruption versus pass curves

can be predicted for a given culture using equations (2.8) and (2.11), with a bimodal approximation for effective strength, $f_B(S)$, replacing the normal distribution, $f_S(S)$.

The introduction of a bimodal distribution provided no significant improvement in the model's descriptive accuracy for the data in chapter 4. A detailed comparison of the two models was therefore undertaken in section 7.3. It was shown that a simple normal approximation to the true strength distribution is sufficiently accurate for most situations of practical importance.

A culture with an artificially-high septated fraction was examined in section 7.4. The description obtained with a bimodal approximation is marginally better at low pressures than with a simple normal distribution. However, for predictive purposes the normal and bimodal distributions result in virtually equal accuracy due to the error in predicting $\bar{S}$ and $\bar{S}_n$. Equation (5.5) yielded an extremely poor estimate of $\bar{S}$, suggesting that equation (5.14) should be used for predicting the mean effective strength of the normal distribution.

Microscopical examination of disrupted samples produced qualitative evidence that septated cells may be weaker, and that fracture may preferentially occur at a division site.

In conclusion, the bimodal representation of the effective-strength distribution appears to be a closer approximation to the true effective strength distribution. The possibility that septated cells are weaker is supported but not proven. For modelling purposes, a simple normal approximation is sufficient for the present homogenizer system. The normal distribution also requires fewer parameters. In cases where a different stress function is used (e.g. a homogenizer providing an almost step-function stress distribution), the septated volume fraction may be a critical model parameter. It will then be necessary to approximate the true strength distribution with a more accurate function (e.g. bimodal).

CHAPTER 8

DISCUSSION

The modern biotechnology industry is currently commercializing products targeted at high-volume markets demanding a low-cost product. Bioprocess simulation will play an increasingly important role. Unfortunately, present simulation packages are severely limited by the models currently available to describe biochemical unit operations.

One of the key operations in many processes is disruption. The high-pressure homogenizer is commonly employed for large-scale product release. Equation (1.1) and its derivatives (eqs. (1.3) and (1.4)) are the only models available to describe the homogenization process.

$$\ln\left(\frac{1}{1-D}\right) = k_1 N P^a \qquad -(1.1)$$

In equation (1.1), D is the disruption (i.e. the volume fraction of cells destroyed) and has replaced R_p, the fractional release of soluble protein.

Equation (1.1) includes the two key operational parameters, namely homogenizer pressure, P, and the number of disruptor passes, N. However, the two parameters (a and k_1) are culture- **and** system-specific. They vary with changes in the feed cells (the culture) and the type of homogenizer and valve arrangement (the system). There is also some evidence that the exponent, a, may change with pressure (Dunnill and Lilly, 1975; Engler and Robinson, 1981). Some dependence on operational parameters such as temperature and feed

concentration has also been reported (Hetherington *et al.* (1971), Sauer *et al.* (1989)). Culture specificity is a particular problem, as the parameters vary significantly with the type of microorganism and also the growth conditions of the specified microorganism. It is therefore impractical (if not infeasible) to catalogue values of the two parameters for various microorganisms and systems. At the very least a third parameter, namely the history of the culture (a non-quantitative concept), must be introduced.

As stated in the introduction, Sauer *et al.* (1989) examined the disruption of recombinant and non-recombinant *E. coli* in a Microfluidizer® (a specific system). Disruption was characterized by equation (1.3) which is a derivative of equation (1.1).

$$\ln\left(\frac{1}{1-R_p}\right) = k_2 N^b P^a \qquad -(1.3)$$

The introduced exponent, b, correlated with cell concentration and the dilution rate in continuous studies. However, no systematic effect of growth rate and concentration on the remaining parameters (a and k_2) could be determined. This is despite significant variations in these parameters (the exponent a varied from 0.6 to 1.7; k_2 varied between 0.27×10^{-3} and 16.0×10^{-3} MPa^{-a}). Average parameter values were presented for specific strains at specific growth rates which allowed the disruption data to be described to ±20%. The studies reported in this thesis also show significant variation of the parameters a and k_1 for a specific microorganism with a specific homogenizer (Table 4.3, chapter 4). The exponent, a, varies between 0.64 and 1.79 depending on the time for which the culture had experienced glucose starvation. The constant k_1 varied over two orders of magnitude (between 1.2×10^{-3} and 380×10^{-3} MPa^{-a}). These examples emphasize that equation (1.1) is presently incapable of **predicting** the disruption that will be obtained with a given homogenizer system, unless the history of the culture is known and a culture with exactly the same history has been previously homogenized. Furthermore, the probability of obtaining two cultures with

precisely the same history is very small considering the typical batch to batch variations encountered in bioprocessing, thus highlighting the limited utility of equation (1.1).

Many of the deficiencies in equation (1.1) are a direct consequence of its structure. It was developed from descriptive rather than prescriptive considerations. The model has no physical basis. Culture- and system-variation affect the same two parameters.

A new model has been developed in this thesis. It represents a significant departure from previous homogenizer-modelling approaches. As outlined in chapter 2, a cell-strength distribution, $f_S(S)$, is combined with a homogenizer-stress distribution, $f_D(S)$, to predict disruption using equation (2.8).

$$D = \int_0^\infty f_D(S)\, f_S(S)\, dS \qquad -(2.8)$$

The approach is easily extendable to multiple passes through repeated application of the stress distribution, resulting in equation (2.11).

$$D = 1 - \int_0^\infty [1-f_D(S)]^N f_S(S)\, dS \qquad -(2.11)$$

This approach is based on the actual processes occurring during homogenization. Passage through the homogenizer applies a stress distribution to cells. These resist disruption by virtue of their strength (which is conferred by the cell wall). A complete description of homogenizer performance is predicated on functions describing the strength and stress distributions, coupled with a knowledge of how these functions vary with culture, system and operational parameters.

The philosophy underlying equations (2.8) and (2.11) will be discussed before further consideration of the work undertaken in this thesis. The homogenizer-stress distribution will vary with the system used, and operational parameters such as feed concentration, feed temperature and homogenizer pressure. The strength distribution will vary with the type of microorganism and the characteristics of a specified culture. **Ideally**, the following are required :

- An expression for the **true** homogenizer stress distribution as a function homogenizer and valve design (the system variables), feed temperature, feed concentration and homogenizer pressure (the operational variables).

- An expression for the **true** culture strength distribution as a function of the type of microorganism and the culture parameters identified in section 1.5, namely wall structure, cell size and population heterogeneity.

Realistically, it is unlikely that completely general expressions for the strength and stress distributions will be easily obtainable. Their development will certainly require a massive and expensive effort considering the large number of parameters involved. The following are therefore **realistic** requirements for modelling disruption with equations (2.8) and (2.11) :

- An expression **approximating** the true stress distribution for a **known system** (homogenizer and valve) as a function of the key operational parameters (homogenizer pressure, feed temperature and feed concentration);

- An expression **approximating** the strength distribution for a **specified microorganism** in terms of measurable culture characteristics (wall structure, size and heterogeneity).

Given such expressions, disruption can be predicted when the system and microorganism are specified. Culture specificity is removed as the strength distribution is predicted using measurable culture characteristics. The effect of different systems or microorganisms can be investigated provided the appropriate expressions are known. This approximation provides a more realistic approach than the ideal. Libraries of functions can be easily established for the most commonly-employed systems and microorganisms. A further simplification arises if the expressions have the same general form but are differentiated on the basis of certain system- and microorganism-specific parameters. It is then only necessary to know the appropriate constants for the system and microorganism under consideration.

The value of the selected approach must be emphasized. The function describing the strength distribution is system-independent provided that it is a true property of the microorganism. Likewise, the function describing the stress distribution will not vary despite significant changes in culture properties if it is a valid system characteristic. The separate physical effects are clearly identifiable and will act on **separate** parts of the model. This contrasts with current practice (eq. (1.1)), where culture and system variability affect the same parameters. A correlation of the key parameters (a and k_1) with culture properties may be possible. However, there is no reason why such a correlation should be system-independent. Any correlation of the key parameters with culture properties will therefore be a property of the specified system **and** microorganism.

The model requires approximations for the strength and stress distributions, as stated above. Ideally, these should be **measured** independently. However, such experimental measurements are impractical for the following reasons :

- The stresses which cause disruption are unknown. Hence, it is not clear which experimental measurements are required to determine the stress distribution;

- It is impractical to place "stress" measuring transducers in the closed homogenizer system. Such devices, if they can be defined, will probably alter the actual distribution;

- It is not clear which strength characteristics of the cell provide resistance to disruption, so it is not clear how to measure cell strength;

- The strength of materials often depends on the rate of the applied stress. It is therefore possible that any independent measurement of strength will not be representative of the true resistance to disruption (e.g. strength measurements done at low rates of deformation may not be representative the cell's response to sudden impact or decompression).

- It may not be possible to determine the strength of bacteria considering their size. In some excellent work, Zhang *et al.* (1992) have measured the strength of animal cells using a micromanipulation technique. These are however, considerably larger than bacteria (ca. 10-15 μm diameter). Furthermore, they lack a crosslinked peptidoglycan layer and may therefore be modelled using a simple isotropic surface tension approach.

Clearly, the ideal of independently measured stress and strength distributions appears unachievable at this stage. However, the ideal is not necessary to provide a workable model which is capable of predicting disruption. The problem may be approached by proposing logical choices for the stress and strength distributions, and then showing their independence. This is the approach adopted in this thesis, and will now be discussed further.

A normal or Gaussian distribution was selected to represent the strength distribution (eq. (2.1)).

$$f_S(S) = \frac{1}{\sigma\sqrt{2\pi}} \exp\left[\frac{-(S-\bar{S})^2}{2\sigma^2}\right] \qquad -(2.1)$$

This seems justifiable considering the large number of bonds which must be involved in providing cell strength. Furthermore, Zhang *et al.* (1992) have shown that the membrane surface tension for mammalian cells has a Gaussian probability distribution. The distribution is characterized by two parameters, the mean effective strength, $\bar{S}$, and the distribution variance, σ^2. They are referred to as the culture-related parameters. The choice of stress distribution is less clear. Obviously, cells will not all experience the same stress during homogenization. Some will pass through the valve as it is opening and closing, and even at constant pressure a distribution of stresses is expected because of different cell trajectories through the valve. It is therefore illogical to select a Dirac-delta function for stress. Studies have demonstrated that impact may be a major cause of yeast disruption. A function was therefore selected which describes the experimental distribution of stresses resulting from the impact of small cylinders against a plane surface (eq. (2.4)).

$$f_D(S) = \frac{S_m^d}{S^d + S_m^d} \qquad -(2.4)$$

While impact is unlikely to be the sole cause of disruption, it is likely that equation (2.4) will fit the stress distribution independent of the exact mechanism. This follows as equation (2.4) describes a general function, which will be capable of describing the stress distribution without reference to the underlying mechanism. In equation (2.4), S_m is the median maximum stress experienced. This will be a function of the operational parameters defined above, namely homogenizer pressure, feed temperature and feed concentration. The determination of how S_m (and hence the stress distribution) varies with these parameters is a considerable task by itself. Only the key operational parameter, homogenizer pressure, was therefore considered in this work. The other operational parameters (temperature and

concentration) were maintained constant. A power-law dependence of maximum stress on pressure was proposed, yielding equation (2.6).

$$f_D(S) = \frac{(mP^n)^d}{S^d + (mP^n)^d} \qquad -(2.6)$$

The distribution is characterized by three parameters which will be system-specific. The pressure-related parameters (m and n) determine how the maximum stress varies with the homogenizer pressure. This is the key operational parameter. The exponent, d, determines the distribution width, or how the probability of disruption varies with strength. Equation (2.6) does not include the other operational parameters identified above, namely feed temperature and feed concentration. A more complex function including these parameters should obviously be sought.

Reasonable stress and strength functions have been proposed. The choices are largely empirical. Consequently, there is no reason why the two functions should be independent, and little justification why they should be representative of the true distributions. However, if they are independent and representative the following will be true :

- *The stress distribution will not change with significant changes in the culture.*
  This was **proven** in chapter 4. Twenty-one cultures with widely varying strengths were examined and the constants for the stress distribution were almost invariant despite large changes in the culture characteristics.

- *The strength distribution will not change with the stress distribution.*
  The best way to significantly change the stress distribution is to use an alternative homogenization system. This was not practical in this study, but will be examined subsequently. However, significant variations in the stress distribution were obtained simply by varying the homogenizer pressure (see Figure 7.5). The

strength distribution for a given culture was constant despite these significant changes in stress distribution.

- *The mean effective strength will be a good indicator of how well a given culture resists homogenization. It should correlate with measurable culture characteristics in a logical fashion.*

  Mean effective strength increases as the disruption decreases (i.e. as the cells become stronger). Excellent correlation with cell properties has been demonstrated in chapter 5. Furthermore, the form of the statistical-thermodynamic correlation can be justified in terms of the cell characteristics. Specifically, mean effective strength increases as the peptidoglycan crosslinkage increases. It also increases with a reduction in average cell length, which may be a concomitant of the thickening of the peptidoglycan layer observed by microbiological researchers.

- *The strength variance, σ, is constant despite large changes in the stress distribution and mean strength, $\bar{S}$.*

  There is no logical reason why the distribution variance should not be constant. It was shown to be so in chapter 4.

The preceding points relate directly to the model assertions stated in section 2.5. In addition, the following should be true :

- *The model will predict multiple-pass disruption data without any prior regression studies for multiple pass data.*

  Good predictions were obtained in chapter 6 for multiple-pass studies, although there is a slight tendency for the model to overpredict disruption after the first pass. This may be due to the reduced feed temperature (5°C compared with 20°C) employed in the multiple-pass studies. Another cause is probable inaccuracies in the limiting conditions for the stress distribution (i.e. as $S \rightarrow 0$ and $S \rightarrow \infty$). It is also

possible that the stress distribution is different for each pass due to changes in the nature of the feed material (e.g. broth viscosity changes due to released DNA; cellular debris is present only after the first pass). Regardless, the magnitude of the overprediction is small and of little practical consequence.

Other supporting evidence that the selected stress distribution is a reasonable approximation also appears in chapter 4. It was noted that the shape of the pressure transient varied significantly below 35 MPa. As stated, one of the reasons for employing a distribution in place of a Dirac-delta function was to account for the variation in stress as a result of the pressure transient (i.e. cells experience different stresses as the valve opens or closes). A change in the transient shape should therefore be accompanied by a change in the stress function. This was observed.

The above considerations suggest that the selected distributions are reasonable approximations and may be independent. Certainly, the predictions obtained in chapter 6 are acceptable. It should be noted that chapter 6 studied a different strain and the same strain grown on glycerol instead of glucose. Furthermore, the homogenizer feed temperature was 5°C whereas the model parameters were determined for a feed temperature of 20°C. Reasonably accurate predictions were obtained despite these changes. This results from the fact that the model employs measurable culture characteristics to predict the mean effective strength, and hence the disruption that will be obtained for a specific system.

The correlations developed in chapter 5 provide a prediction of mean effective strength which is within ±6% of the regressed value. It was shown that the accuracy of model predictions could be improved by reducing the error in the mean effective strength estimation (either through improved correlations or better measurements of cell properties). However, it is unlikely that model accuracy needs to be improved in any practical sense. The disruption predictions in chapter 6 were within six standard deviations of the experimental values. At a disruption level of 97%, the predicted value is therefore within

1.8% of the experimental value (Table 3.2 shows the standard deviation of the experimental measurement is approximately 0.3% at this level of disruption). A standard deviation of approximately 2.7% results in the experimental value if disruption is determined by soluble protein measurements (Table 3.2). Currently, most researchers rely on soluble protein measurements. The error in the prediction is therefore less than the typical error in the measurement. Consequently, the predictive accuracy of the model is sufficient for most practical purposes. This example also illustrates the value in using the disc centrifuge to determine disruption (chapter 3). Accurate comparisons of model predictions and experimental data could not be made without the use of the developed method.

The model possesses several advantages compared to the kinetic model (eq. (1.1)). Its primary advantage derives from its structure, as previously explained. Culture and system variability affect distinct parts of the model (i.e. distinct model parameters). Correlation of the strength parameters with culture properties is possible independently of the system parameters. It is possible to predict how a specified culture will respond to changes in the stress distribution using the developed model. Such a prediction is not possible with the kinetic model as the model's parameters are both culture **and** system specific, rather than just system specific (i.e. system-variability confounds the correlation with culture parameters in the kinetic model, while such confounding is not possible in the developed model because of the separation of the culture and system effects). The developed model also has a simplistic advantage over the kinetic model even if philosophical questions regarding model structure are ignored. Specifically, culture-variability affects a single parameter : the mean effective strength, $\bar{S}$. By contrast, both kinetic parameters vary with changes in the culture (Table 4.3). Consequently, the number of parameters which must be correlated with culture characteristics is halved.

A comparison of the kinetic model with the developed model suggests a non-trivial relationship between the parameters. Equation (8.1) may be written by substituting D in equation (1.1) using equation (2.8),

$$\ln \ln \left(\frac{1}{1 - \int_0^{\infty} f_D(S)\, f_S(S)\, dS} \right) = \ln(k_1) + a \ln(P) \qquad -(8.1)$$

where $f_D(S)$ and $f_S(S)$ are the proposed stress and strength distributions (eqs (2.6) and (2.1), respectively). A linear plot of the left hand side versus ln(P) therefore yields the two kinetic parameters, a and k_1. Figure 8.1 presents several such plots for various values of mean effective strength, $\bar{S}$, with all other model parameters set equal to the values determined in chapter 4 (Table 4.8). The plots are non-linear, indicating that the kinetic model is not some limiting case of the proposed model.

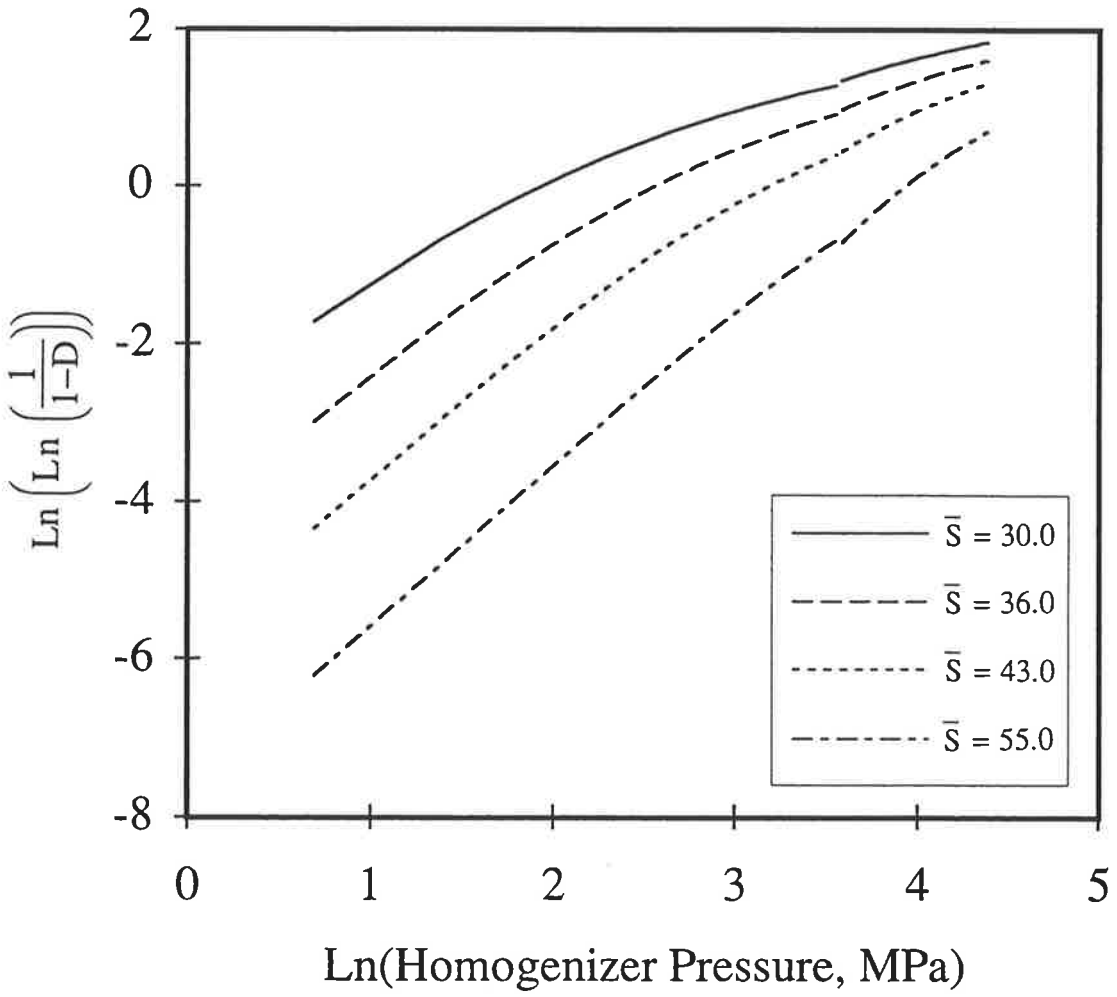

FIGURE 8.1 : *Plots of equation (8.1) using the parameters in Table 4.8.*

[Discontinuity results from the discontinuous stress function]

Figure 8.2 shows the variation of the two kinetic parameters with mean effective strength. Also shown on Figure 8.2 are the relationships which result when the stress distribution parameter (d in eq. (2.6)) is doubled. This emphasizes that the relationship between the kinetic parameters (a and k_1) and the culture properties (X and $\bar{L}$) depends on the particular stress distribution acting. Conversely, the correlation of mean effective strength with the culture characteristics is independent of changes in the stress distribution (assuming the selected strength and stress distributions are truly independent as suggested).

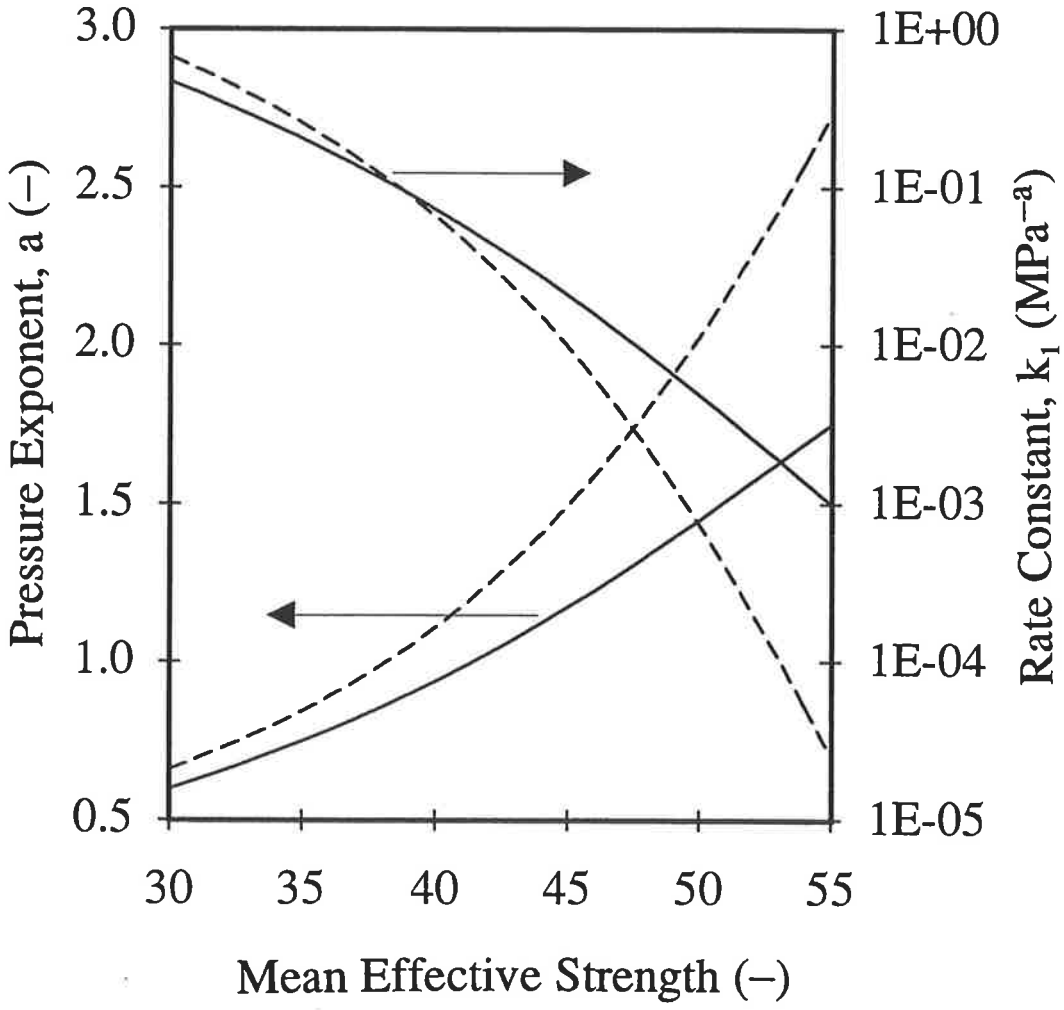

FIGURE 8.2 : *The relationship between the kinetic parameters (a and k_1) and mean effective strength. Dashed lines show the effect of a change in the applied stress distribution (see text for details).*

[Determined using only data for homogenizer pressures in excess of 35 MPa]

Figure 8.2 clearly shows an increase in the pressure exponent, a, as the cells become stronger. Previous work has illustrated an increase in the exponent as cells become harder to disrupt (e.g. Sauer *et al.* (1989) for *E. coli* NM989 at 20 g L^{-1} (dry weight); Present study, chapter 4). Similarly, a large decrease in the rate constant, k_1, is observed with increasing strength. Poorer disruption is usually accompanied by a reduced rate constant (e.g. Sauer *et al.* (1989) for *E. coli* NM989 at 20 g L^{-1} (dry weight); Engler and Robinson (1981) for *Candida utilis* during impingement; Gray *et al.* (1972) for *E. coli* ML308; Present study, chapter 4). The proposed model therefore rationalizes previously reported and incompletely understood trends. Specifically, it confirms previous assertions that the kinetic model's parameters are somehow related to the strength of the organism.

The nature of cell "strength" warrants further detailed discussion. Strength is defined as an ability to resist an applied disruptive stress in chapter 2. If strength had been determined by independent experiments as for the ideal case, it would be dimensional. The mean strength of a population could be expressed in Newtons or Pascals. In the present tests, S is a measure proportional to the true dimensional strength with the constant of proportionality indeterminate. For this reason, S is referred to as **effective** strength and $\bar{S}$ is the mean **effective** strength of the population. In fact, effective strength may be considered to be a dimensionless ratio, as in equation (8.2),

$$S = \frac{S'}{S'_b} \qquad \text{-(8.2)}$$

where S' is the true dimensional strength and S'_b is some unknown base strength (the inverse constant of proportionality). This is shown in Appendix A. The approach is clearly valid as effective strength is proportional to the true dimensional cell strength.

The model has several advantages over existing models, as previously stated. However, measurements of peptidoglycan crosslinkage and average cell length are required to predict mean effective strength and hence disruption. These measurements are tedious and not yet

amenable to on-line measurement. This is, however, a limitation of the available analytical techniques rather than a reflection on the modelling technique. With further work, it may be possible to develop simple on-line assays. It should be noted that ten years ago the analysis of wall structure with the accuracy shown in chapter 5 was not possible. It may become automated in a further ten years. To develop a truly useful model the important variables must be identified and then a method for measuring or inferring them must be established. Traditional modelling efforts have neglected the key culture characteristics, and consequently the model parameters (a and k_1) must be guessed based on previous experience. Naturally, a similar approach could be used with the current model, which has the advantage that only one parameter ($\bar{S}$) must be guessed if the available correlations are ignored!

A further point must be stated regarding model utility. It is likely that the model will be employed in optimization and simulation studies where on-line measurements of the culture characteristics are not required. In such cases it will be necessary to know how the key culture characteristics (X and $\bar{L}$) vary with fermentation conditions. It will then be possible to simulate changes in the fermentation conditions, determine the effect on the culture characteristics and hence establish the effect on the homogenizer. Therefore, the real need is not for rapid on-line assays of crosslinkage and length, but rather for generalized correlations of these characteristics with fermenter design and operating procedures. It might be argued that strength should be correlated with fermenter operating characteristics directly. However, it is likely that any such correlation will be highly fermenter specific. Expressing mean effective strength in terms of culture characteristics has the advantage that the homogenizer and fermenter may be isolated from one another.

To demonstrate the model's utility, let us consider the flowsheet shown in Figure 8.3. A continuous fermentation is conducted to produce a soluble intracellular enzyme. The fermenter effluent is centrifuged to collect the cell mass before disruption. The desired (fictitious) production rate can be achieved with a 10 m^3 fermenter if complete product

release is obtained during homogenization. A simple optimization problem can be stated as follows :

> "What is the optimum number of homogenizer passes to minimize the process capital cost for the partial flowsheet shown in Figure 8.3? The production constraint must be satisfied."

Clearly, some product will be lost if complete disruption is not achieved. To compensate for this loss a larger fermenter must be employed. Consequently, the size of the centrifuge, compressor and sterilizer will also be increased. The trade-off lies between fermenter-associated capital and homogenizer capital.

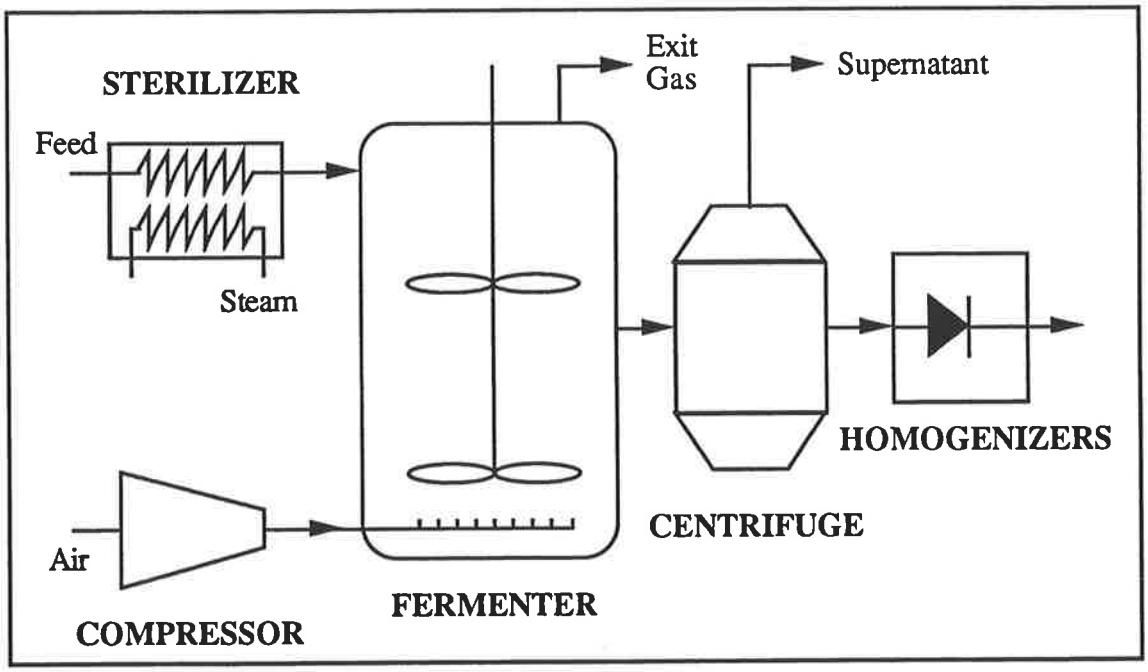

FIGURE 8.3 : *Typical flowsheet for the continuous-flow isolation of a soluble intracellular enzyme from Escherichia coli.*

First, the disruption characteristics of the broth must be ascertained. Continuous studies have not been conducted in this thesis. Regardless, mean effective strength should be correlated with peptidoglycan crosslinkage and average length independent of the exact

fermentation protocol. The only requirements to estimate the ease with which a broth will be disrupted are a measure of its characteristics (X and $\bar{L}$) and an appropriate correlation of mean effective strength with these parameters. Driehuis and Wouters (1987) report the characteristics of *E. coli* W7 grown with glucose limitation at two different growth rates. These characteristics and the predicted mean effective strengths are summarized in Table 8.1.

TABLE 8.1 : *Characteristics of E. coli W7 in continuous culture.*

PARAMETER		SOURCE	μ=0.1 h^{-1}	μ=0.8 h^{-1}
Crosslinkage (–)†	X	Driehaus and Wouters (1987)	0.483	0.461
Average Length (μm)††	$\bar{L}_n$	Driehaus and Wouters (1987)	1.30	2.41
Mean Effective Strength (non-septated)	$\bar{S}_n$	Eq. (7.2)	57.4	45.0
Mean Effective Strength	$\bar{S}$	Eq. (7.3)	56.6	44.3

† Crosslinkage has been calculated as described in chapter 5 using the data published by Driehaus and Wouters (1987).
†† Driehaus and Wouters (1987) measured only non-septated cells. The calculation of mean effective strength is therefore done using equations (7.2) and (7.3) in place of the chapter 5 correlations.

The prediction is that cells grown at a lower dilution rate will be substantially stronger, primarily because of the reported reduction in average cell length. Consequently, disruption will be lower for strains grown at a lower dilution rate. Such a dependence of disruption on dilution rate has been previously reported (but not rationalized) for recombinant *E. coli* NM989 and non-recombinant *E. coli* HB101 in a Microfluidizer® (Sauer *et al.*, 1989). The model developed in this thesis therefore predicts the correct trends for continuous culture although no continuous studies were conducted.

Disruption was predicted for strain W7 at 60 MPa using the data in Table 8.1 for μ=0.1h^{-1} and the model developed in this thesis. The disruption and capital cost versus homogenizer

pass curves are shown in Figure 8.4. The calculations are outlined in Appendix B. Figure 8.4 shows that two homogenizer passes are optimal, corresponding to a disruption of 89%.

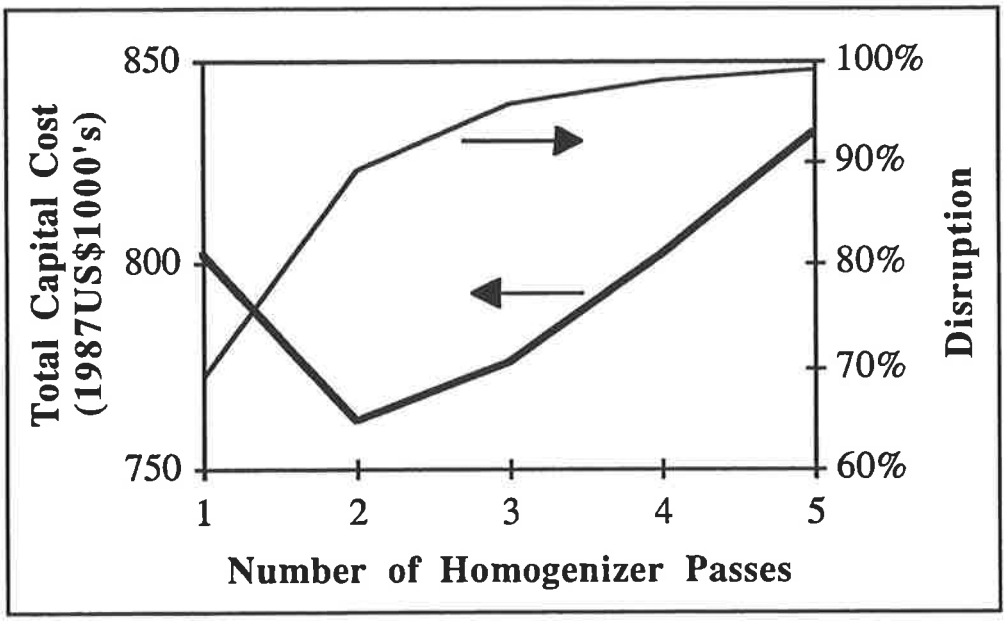

FIGURE 8.4 : *Predicted disruption versus pass and capital cost versus pass curves for E. coli strain W7 grown continuously at* μ=0.1 h^{-1}.

This example is, of course, highly contrived. The following assumptions are made to estimate the disruption, and may be incorrect :

- The correlations for mean effective strength developed in this thesis are applicable for *E. coli* strain W7 cultivated continuously* ;
- The homogenizer used in the process has the same stress characteristic as the homogenizer examined in this thesis.

In addition, simplifying assumptions have been made in the analysis, such as the independence of the downstream unit operations on the homogenization process (Appendix B). However, the example has been presented to emphasize the following point :

* Note that the correlations developed for *E. coli* B grown on glucose have been successfully employed in this thesis to predict the disruption of *E. coli* JM101 and *E. coli* B grown on glycerol. It is therefore possible that the prediction of mean effective strength in Table 8.1 is reasonable.

- The ease of disruption of a strain can be estimated provided its characteristics are known. Driehaus and Wouters (1987) make no statement on the "disruptability" of their strain.

Obviously, if a library of strength correlations and stress functions were available, the exact equations could be selected for the microorganism and system under investigation. Accurate predictions of disruption could then be made.

In concluding, it is clear that the model developed in this thesis is capable of removing the requirement for culture-specific parameters. It provides accurate *a priori* predictions of disruption as a function of pressure and passes for the specified system and strain despite large culture variations. It is therefore capable of accounting for the interaction between the fermenter and homogenizer. However, many different factors influence the disruption obtained during homogenization, and complete characterization of the effect of all parameters is beyond the scope of a single thesis. Regardless, the developed model has the capacity to be readily extended with further work, as its structure is based on a premise of the actual processes occurring during homogenization (a stress is applied and this is resisted by the wall). To maximize the usefulness of the model, the following investigations should be conducted :

- *Tests for many different strains of E. coli.*

  The study on *E. coli* JM101 (chapter 6) suggests that the correlations presented in this thesis may be applicable for strains other than *E. coli* B. This needs to be proven or alternative correlations developed. The ultimate aim must be to establish the generality of the correlations developed in chapter 5 for other *E. coli* strains, or to establish a library of correlations for different strains. It is also possible that the distribution variance, σ^2, is strain-specific. This needs to be tested. Many industrial processes have the product expressed in *E. coli* as an inclusion body.

The influence of protein over-expression on mean effective strength should be examined for this practically important case.

- *Tests for different homogenizer systems.*

  A library of different stress functions (or the appropriate parameters) needs to be established. Further work will confirm whether the proposed strength distribution is truly independent of the homogenizer system, as the initial work in this thesis suggests. In particular, systems characterized by a step-function stress distribution should be examined to determine whether a bimodal strength distribution is required as suggested in chapter 7.

- *Tests with different operational parameters.*

  The effect of feed temperature and feed concentration on the stress distribution needs to be examined. A general correlation of maximum stress with these variables must be determined. It is likely that these variables affect the stress distribution by altering the liquid viscosity.

- *Tests with different microorganisms.*

  These tests may reveal different forms for the strength distribution and strength correlations. Specifically, microorganisms such as yeasts have a completely different wall structure to *E. coli* and should be examined to determine the culture characteristics which confer strength. It is also possible that the stress distribution function will change for different microorganisms, as different microorganisms may be sensitive to different stresses. For example, yeasts may be disrupted by a different mechanism to *E. coli*, and hence a different stress distribution will be required in the model. Regardless, equations (2.8) and (2.11) will be applicable, and it will only be necessary to establish the appropriate functions and correlations, similar to the work conducted in this thesis for *E. coli*.

Initially, libraries of stress and strength functions (and the appropriate correlations) may be established. It will then be a matter of selecting the appropriate functions for the specified microorganism and homogenizer system. Culture and operational specificity will be removed. Ultimately, it may be possible to develop functions for the stress distribution in terms of the specific valve and homogenizer characteristics.

Further work is also required to fully address the question of unit interactions. These are of paramount concern if simulation and optimization studies are to provide useful information in bioprocessing. Specifically, generalized correlations of culture characteristics (X and $\bar{L}$) with fermentation conditions should be sought. It may be necessary to develop a library of such correlations for different fermenter designs. In addition, the present model only addresses the influence which culture variability has on disruption. To date, no models address the question of downstream interactions, although some work has been presented by Siddiqi *et al.* (1991). Homogenizer models which return debris size distributions as a function of operational, system and culture parameters are required to optimize subsequent downstream unit operations such as centrifugation.

APPENDIX A

THE NATURE OF CELL STRENGTH

AIM

To demonstrate that effective strength, S, may be considered to be a dimensionless ratio of true cell strength, S', and some indeterminate base cell strength, S'_b, as in equation (8.2).

$$S = \frac{S'}{S'_b} \qquad \text{-(8.2)}$$

ANALYSIS

Let S' be the true strength of a cell, which can be independently measured in the **ideal** case. For the purpose of this analysis it is defined as having units of force (mN), although stress (Pa) may also be selected. The true strength will be distributed. Hence, define :

S'	True cell strength	mN
$f'_{TS}(S')$	Volume-strength frequency distribution	$\frac{\mu m^3 \text{ cells of strength } S'}{mN}$

Normalizing the strength distribution gives $f'_S(S')$, the strength density function :

$f'_S(S')$ Strength density function $\frac{\mu m^3 \text{ cells of strength } S'}{\mu m^3 \text{ total cells} \times mN}$

Now let $f'_D(S')$ be the volume fraction of cells of strength S' disrupted during homogenization (the probability of disruption). This is termed the homogenizer stress distribution. Hence :

$f'_D(S')$ Probability of disruption $\frac{\mu m^3 \text{ cells of strength } S' \text{ disrupted}}{\mu m^3 \text{ cells of strength } S'}$

The volume fraction of cells of strength S' to S'+dS' is simply $f'_S(S')\, dS'$.

The fraction destroyed during homogenization is obtained by multiplying by $f'_D(S')$. Hence :

dD = volume fraction of cells of strength S' to S'+dS' disrupted

$= f'_D(S')\, f'_S(S')\, dS'$

The total disruption is determined by integration, giving equation (A1).

$$D = \int_0^\infty f'_D(S')\, f'_S(S')\, dS' \qquad \text{-(A1)}$$

The dimensions of D follow from above :

$$[dD] = \frac{\mu m^3 \text{ cells of strength } S' \text{ disrupted}}{\mu m^3 \text{ cells of strength } S'} \times \frac{\mu m^3 \text{ cells of strength } S'}{\mu m^3 \text{ total cells} \times mN} \times mN$$

or $$[dD] = \frac{\mu m^3 \text{ cells of strength } S' \text{ disrupted}}{\mu m^3 \text{ total cells}}$$

Integration over all possible values of S' gives :

$$[D] = \frac{\mu m^3 \text{ cells disrupted}}{\mu m^3 \text{ total cells}}$$

which is consistent with the definition of disruption.

It is proposed that true strength is normally distributed, and that the true stress function is described by equation (A3). This follows from the considerations outlined in chapter 2. Hence :

$$f'_S(S') = \frac{1}{\sigma' \sqrt{2\pi}} \exp\left[\frac{-(S' - \bar{S}')^2}{2(\sigma')^2}\right] \qquad \text{-(A2)}$$

$$f'_D(S') = \frac{(m' P^n)^d}{(S')^d + (m' P^n)^d} \qquad \text{-(A3)}$$

where

$(\sigma')^2$	Variance of true (dimensional) strength distribution	$(mN)^2$
S'	True mean strength	mN
P	Homogenizer pressure	MPa
m'	parameter, equation (A3)	MPa^{-n} mN

Equation (A2) may be rewritten as follows :

$$f'_S(S') = \frac{1}{S'_b \left(\frac{\sigma'}{S'_b}\right)\sqrt{2\pi}} \exp\left[\frac{-\left(\frac{S'}{S'_b} - \frac{\bar{S}'}{S'_b}\right)^2}{2\left(\frac{\sigma'}{S'_b}\right)^2}\right] \qquad \text{-(A4)}$$

Defining :

$$S = \text{effective (cell) strength} = \frac{S'}{S'_b}$$

$$\bar{S} = \text{mean effective (cell) strength} = \frac{\bar{S}'}{S'_b}$$

$$\sigma^2 = \text{distribution variance of effective strengths} = \left(\frac{\sigma'}{S'_b}\right)^2$$

gives :

$$f'_S(S') = \frac{1}{S'_b\,\sigma\sqrt{2\pi}} \exp\left[\frac{-(S-\bar{S})^2}{2\sigma^2}\right] = \frac{f_S(S)}{S'_b} \qquad \text{-(A5)}$$

where $f_S(S)$ is the distribution of effective strengths, as defined in chapter 2.

Equation (A3) may be written as follows :

$$f'_D(S') = \frac{\left(\frac{m'}{S'_b}\,P^n\right)^d}{\left(\frac{S'}{S'_b}\right)^d + \left(\frac{m'}{S'_b}P^n\right)^d} \qquad \text{-(A6)}$$

Defining :

$$\frac{m'}{S'_b} = m = \text{modified parameter with units } MPa^{-n} \qquad \text{-(A7)}$$

and effective strength as before gives :

$$f'_D(S') = \frac{(mP^n)^d}{S^d + (mP^n)^d} = f_D(S) \qquad \text{-(A8)}$$

Hence, the true stress distribution is equivalent to equation (2.6), where the parameters for use with each form (dimensional or dimensionless) are related through equation (A7).

Equation (A1) therefore becomes :

$$D = \int_0^\infty f'_D(S') f'_S(S') dS' = \int_0^\infty f_D(S) \frac{f_S(S)}{S'_b} dS' \qquad \text{-(A9)}$$

From the definition of effective strength :

$$\frac{dS}{dS'} = \frac{1}{S'_b} \qquad \text{-(A10)}$$

So

$$D = \int_0^\infty f'_D(S') f'_S(S') dS' = \int_0^\infty f_D(S) \ f_S(S) dS \qquad \text{-(A11)}$$

Equation (A11) emphasizes that dimensionless distributions may be employed in place of dimensional distributions. The form of the functions will remain the same: the model parameters will assume different values. Model parameters for the dimensional and dimensionless forms are all related by a sole parameter, the base strength S'_b. This will be indeterminate if regression studies are solely employed to determine the model parameters. To determine the true strength, independent measurements must be conducted. As outlined in chapter 8, these may be difficult to implement. More importantly, such measurements are unlikely to improve the utility of the current model. This follows as effective strength is **proportional** to the true strength for all cases. Effective strength therefore has physical meaning and should correlate with cell properties

(as in chapter 5). The fact that the constant of proportionality is unknown does not detract from the model as it is not included explicitly in equation (A11) (i.e. it is an unnecessary parameter).

From the above analysis it is clear that the true strength will be indeterminate using regression studies. Effective strength in this thesis may therefore be viewed as a ratio of the true dimensional strength to some unknown base strength.

APPENDIX B

EXAMPLE

Consider the partial flowsheet shown in Figure 8.3.

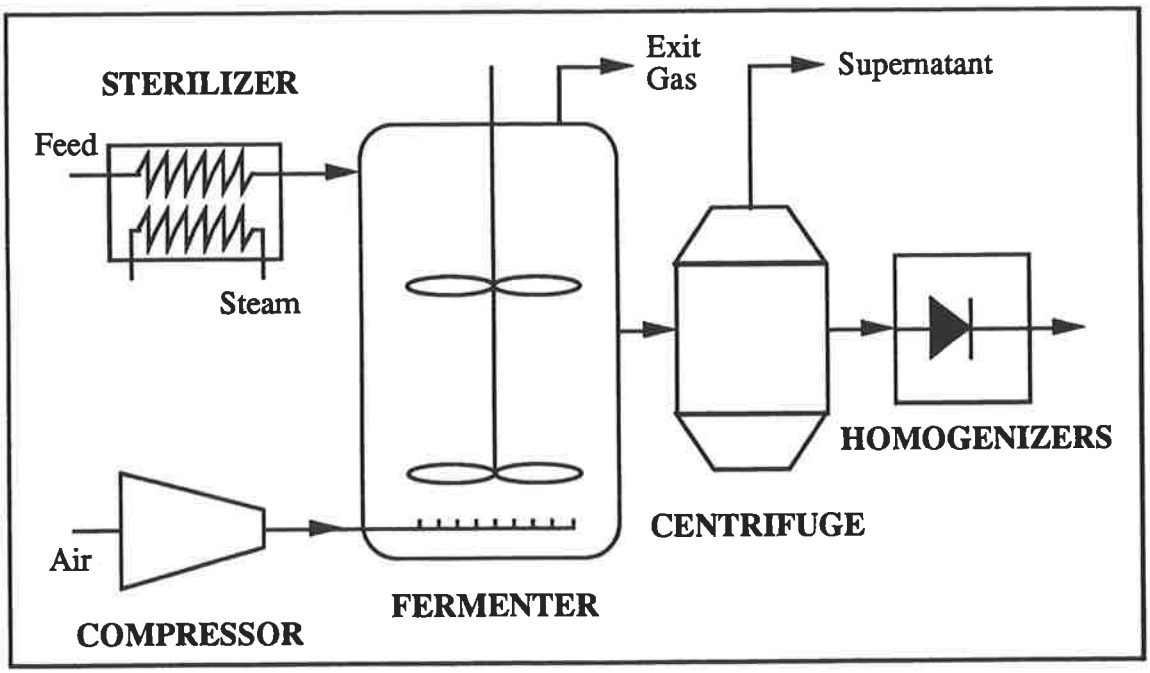

FIGURE 8.3 : *Typical flowsheet for the continuous-flow isolation of a soluble intracellular enzyme from Escherichia coli.*

Cell mass is produced by continuous fermentation at an assumed dilution rate of 0.1 h^{-1}. Fermenter feed is continuously sterilized and air is supplied at 1 v.v.m. (1 fermenter volume per minute). Cell mass is concentrated after leaving the fermenter prior to homogenization. Homogenization is conducted by a series of homogenizers providing one discrete pass per machine (other configurations such as recycle are not considered). The desired product rate can be achieved with a 10 m^3 fermenter **provided** complete

disruption is obtained during homogenization. The optimization question is posed as follows :

> "What is the optimum number of homogenizer passes to minimize the process capital cost for the partial flowsheet shown in Figure 8.3? The production constraint must be satisfied."

At a fixed production rate, fermenter volume must be increased above 10 m^3 if incomplete disruption is obtained. Specifically, the required fermenter volume is given by equation (B1),

$$V_f = \frac{10\,000}{D} \quad L \qquad \text{-(B1)}$$

where D is the disruption obtained during homogenization neglecting any loss of bacteria to the centrifuge supernatant. The compressor capacity at 1 v.v.m. is therefore :

$$q_c = \frac{10\,000}{D} \quad L\ min^{-1} \qquad \text{-(B2)}$$

The required capacity of the continuous sterilizer is simply μV_f or $0.1 V_f$ L h^{-1} for a dilution rate of 0.1 h^{-1}. This is also the feed rate to the disc centrifuge. The centrifuge may be sized using data reported by Petrides *et al.* (1989). *E. coli* JM101 containing recombinant inclusion bodies were collected with 98% efficiency at a feed rate of 1600 L h^{-1} using a centrifuge with an equivalent settling area (Σ) of 120,000 m^2. This corresponds to a volumetric flux (Q/Σ) of 0.0133 L h^{-1} m^{-2}. The required centrifuge size for this normalized flowrate is therefore provided by equation (B3).

$$\Sigma = \frac{\mu V_f}{0.0133} \quad m^2 \qquad \text{-(B3)}$$

The required homogenizer flowrate is assumed constant at 250 L h^{-1}, independent of the fermenter volume. This is equivalent to stating that the centrifuge operates with a minimum concentration factor of 4.0 (i.e. a 10 m^3 fermenter produces 1000 L h^{-1} of broth, and with a concentration factor of 4.0 this gives a homogenizer feed rate of 250 L h^{-1}). Petrides *et al.* (1989) report a concentration factor of 4.0. Higher concentration factors will also be easily obtainable (e.g. Higgins *et al.* (1978) report a concentration factor of 6.7). It is therefore reasonable to assume a constant discharge rate and a variable concentration factor, yielding a constant homogenizer size.

Equipment capital costs may be estimated with the following relations :

Fermenters (By regressing data from Petrides *et al.*, (1989)) :

$$1987US\$ = 10^{4.359}\ V_f^{0.313} \qquad \text{-(B4)}$$

Sterilizers (Assumed relationship based on a single cost by Petrides *et al.*, (1989))

$$1987US\$ = 223500\left(\frac{\mu\ V_f}{6700}\right)^{0.6}$$

Screw Compressors (From manufacturer's data) :

$$1987US\$ = 10^{0.4302}\ q_c^{1.018} \qquad \text{-(B5)}$$

Centrifuges (From manufacturer's data):

$$1987US\$ = 10^{3.588}\ \Sigma^{0.329} \qquad \text{-(B6)}$$

Homogenizers (From manufacturer's data):

$$1987US\$ = 10^{3.495}\ Q^{0.425}$$

$$= 10^{3.495}\ 250^{0.425} = 32{,}668 \text{ per unit} \qquad \text{-(B7)}$$

The characteristics of *E. coli* W7 grown at 0.1 h^{-1} are given in Table 8.1. Disruption may therefore be estimated using the developed model, assuming that the correlations developed for *E. coli* B are applicable and that the homogenizers in the process have the same stress distribution as the system studied in this thesis (see comments in chapter 8). The capital cost may therefore be estimated (Table A1).

TABLE A1 : *Capital Cost Estimation*

Homogenizers	**1**	**2**	**3**	**4**	**5**
Disruption	69%	89%	96%	98%	99%
Fermenter Volume (L)	14,471	11,198	10,427	10,173	10,070
Centrifuge Σ (m^2)	108,500	84,000	78,200	76,300	75,500
Fermenter Cost	458,400	423,000	413,700	410,500	409,200
Compressor Cost	46,300	35,700	33,200	32,300	32,000
Sterilizer Cost	89,100	76,400	73,200	72,100	71,700
Centrifuge Cost	175,700	161,400	157,700	156,400	156,000
Homogenizer Cost	32,700	65,300	98,000	130,700	163,300
TOTAL (1987US$)	802,200	761,900	775,800	802,100	832,200

These results are plotted in Figure 8.4 (chapter 8). Capital costs downstream of the homogenizer are not considered in the present analysis. This provides a reasonable first approximation, as the product flowrate downstream of the fermenters will be invariant with fermenter volume. However, the analysis also neglects any effect which the homogenizer has on the debris size distribution. Harsher homogenization will lead to a smaller average debris size. The effect of this on downstream capital costs (e.g. centrifugation) will not be considered, as no adequate models account for such interactions.

APPENDIX C

PUBLICATIONS LIST

Refereed Journal Publications Related to this Thesis

1) **Middelberg, A.P.J.**; Bogle, I.D.L.; Snoswell, M. 1990. Sizing Biological Samples by Photosedimentation Techniques. *Biotechnol. Prog.*, **6**, 255-261.

2) **Middelberg, A.P.J.**; O'Neill, B.K.; Bogle, I.D.L.; Snoswell, M. 1991. A Novel Technique for the Measurement of Disruption in High-Pressure Homogenization: Studies on *E. coli* Containing Recombinant Inclusion Bodies. *Biotechnol. Bioeng.*, **38**, 363-370.

3) **Middelberg, A.P.J.**; O'Neill, B.K.; Bogle, I.D.L. 1992. A new model for the disruption of *Escherichia coli* by high-pressure homogenisation. I. Model development and verification. *Trans. I.Chem.E.*, **70**, part C, 205-212.

4) **Middelberg, A.P.J.**; O'Neill, B.K.; Bogle, I.D.L.; Gully, N.J.; Rogers, A.H.; Thomas, C.J. 1992. A new model for the disruption of *Escherichia coli* by high-pressure homogenisation. II. A correlation for the effective cell strength. *Trans. I.Chem.E.*, **70**, part C, 213-218.

5) **Middelberg, A.P.J.**; O'Neill, B.K. 1992. A correlation for the effective strength of *Escherichia coli* during homogenization. *Biotechnol. Prog.*, (In Press).

6) **Middelberg, A.P.J.**; O'Neill, B.K.; Thomas, C.J. A simplified model for the disruption of *Escherichia coli* : the effect of cell septation. *Biotechnol. Prog.*, (Submitted, 1992).

7) **Middelberg, A.P.J.** Extension of the wall-strength model for high-pressure homogenization to multiple passes. *Trans. I. Chem. E.*, part C, (Submitted, 1992).

Publications not directly related to this thesis

1) **Middelberg, A.P.J.**; Bogle, I.D.L.; Snoswell, M. 1989. Simulation of a Novel Biochemical Process. Chemeca '89, Australian Chemical Engineering Conference, Broadbeach, Qld. Australia, August 1989; Paper 20a.

2) **Middelberg, A.P.J.**; O'Neill, B.K. 1991. Monitoring the Centrifugal Recovery of Recombinant Protein Inclusion Bodies. *Aust. J. Biotech.*, **5** (2), 87-92.

3) Thomas, J.C.; **Middelberg, A.P.J.**; Hamel, J.-F.; Snoswell, M.A. 1991. High-Resolution Particle Size Analysis in Biotechnology Process Control. *Biotechnol. Prog.*, **7**, 377-379.

4) **Middelberg, A.P.J.**; O'Neill, B.K.; Bogle, I.D.L. 1991. Modelling bioprocess interactions for optimal design and operating strategies. Chemeca '91, Australian Chemical Engineering Conference, Newcastle, NSW. Australia, September 1991; 706-712.

5) Bogle, I.D.L.; Hounslow, M.J.; **Middelberg, A.P.J.** 1991. Modelling of inclusion body formation for optimisation of recovery in biochemical processes. Presented at PSE'91. Fourth International Symposium on Process Systems Engineering. University of Waterloo, Canada.

6) **Middelberg, A.P.J.**; O'Neill, B.K.; Bogle, I.D.L. 1992. Modelling bioprocess interactions for optimal design and operating strategies. *Trans. I.Chem.E.*, **70**, Part C, 8-12.

7) Bogle, I.D.L.; **Middelberg, A.P.J.**; O'Neill, B.K. Modelling of inclusion body formation for optimisation of recovery in biochemical processes. Presented at Bioprocess Simulation in Practice, First Conference on Biotechnology in the "Pentagonal" countries, April 14, 1992, Graz, Austria.

NOMENCLATURE

A	Output from the analytical disc centrifuge ($\propto$ absorbance), (–)
a	Pressure exponent for the kinetic model (eq. 1.1 or eq. 1.3), (–)
a'	Pressure exponent (eq. 1.4), (–)
A_{260}	Absorbance at 260 nm, (–)
A_i	Projected cross-sectional area of an individual cell, (μm^2)
B	Constant (eq. 5.13)
b	Exponent (eq. 1.3), (–)
C	Concentration of soluble protein in the aqueous phase, (kg m^{-3})
C_c	Cell concentration dry basis, (kg m^{-3})
C_N	Total Kjeldahl Nitrogen content of supernatant (kg m^{-3})
C_{NO}	Total Kjeldahl Nitrogen content of whole cells (kg kg^{-1} dry wt)
D	Disruption (volume fraction of cells destroyed during homogenization), (–)
$\bar{D}$	Average cell diameter, (μm)
D_c	Cell diameter, (μm)
d	Coefficient determining the stress distribution width, (–)
d_m	Maximum diameter of a cell surviving homogenization (eq. 1.5), (μm)
d_s	Stokes diameter, (μm)
$\bar{d}_s$	Mean particle size in the disc centrifuge detection zone, (μm)
d_{smax}	Maximum Stokes diameter of intact (i.e. undisrupted) cells, (μm)
d_{smin}	Minimum Stokes diameter of intact (i.e. undisrupted) cells, (μm)
F	Force at impact (eq. 2.3), (N)
$f_2(d_s)$	Area-frequency distribution of undisrupted cells, (μm^{-1})
$f_3(d_s)$	Volume-frequency distribution of undisrupted cells, (μm^{-1})
$f_B(S)$	Effective strength volume-frequency distribution assuming a bimodal-Gaussian function (eq. 2.2), (–)

$f_D(F)$	Cumulative fraction of impacts with force greater than F (eq. 2.3), (–)
$f_D(S)$	Cumulative fraction of events during homogenization with a stress greater than S (i.e. the probability of disruption), (–)
F_m	Force at which 50% of the impacts have a maximum force greater than F_m (eq. 2.3), (N)
$f_S(S)$	Effective strength volume-frequency distribution (or effective strength distribution) assuming a Gaussian function (eq. 2.1), (–)
g	Free energy density of a single peptidoglycan layer (eq. 5.6), (energy per bond)*
h	Valve lift, (m)
J	Dilution factor (i.e. sample volume after dilution divided by sample volume before dilution), (–)
K	Bond elastic modulus, (energy per bond)*
k	Valve inlet loss coefficient, (–)
K'	Modified extinction coefficient (K_p/d_s), (μm^{-1})
k'	Valve exit loss coefficient, (–)
k_1	Rate constant for the kinetic model (eq. 1.1), (MPa^{-a})
k_2	Rate constant for the modified kinetic model (eq. 1.3), (MPa^{-a})
k_3	Rate constant for the release of DNA from *A. eutrophus* (eq. 1.4), (MPa^{-a})
K_e	Particle extinction coefficient (eq. 3.13), (–)
k_L	Overall loss coefficient, (–)
K_p	Extinction coefficient for polystyrene spheres (eq. 3.19), (–)
L	Cell length from pole to pole, (μm)
$\bar{L}$	Average cell length, (μm)
L_o	Parameter (eq. 5.12), (μm)
M	Relative abundance of a Tet-Tri-Lys-Arg, (mol%)
M_c	Internal moisture mass fraction of cells, (–)

* Units are arbitrary (Blumberg-Selinger *et al.*, 1991).

m	Constant (eq. 2.5), (MPa^{-n})
m	Dimensionless gap width (eq. 4.5), (–)
N	Number of discrete homogenizer passes, (–)
N_{Re}	Reynolds number (eq. 4.4), (–)
n	Exponent (eq. 2.5), (–)
P	Homogenizer pressure**, (MPa)
p	exponent (eq. 3.17), (–)
P_F	Pressure loss due to friction across the valve face, (Pa)
P_g	Nominal gauge pressure during homogenization, (MPa)
P_s	Stagnation pressure at the impact ring, (Pa)
Q	Flowrate of suspension through the homogenizer valve, ($m^3\ s^{-1}$)
R	Fractional release of an assayed component, (–)
R'	Actual measured concentration of the assayed component, ($kg\ m^{-3}$)
$R_{A_{260}}$	Fractional release of absorbing material at 260 nm, (–)
R_D	Fractional release of DNA (eq. 1.4), (–)
r_d	Detector radius (eq. 3.10), (m)
R_K	Fraction of cells ruptured as determined by Kjeldahl Nitrogen analysis, (–)
r_o	Particle start radius (eq. 3.10), (m)
R_p	Fractional release of soluble protein, (–)
R_v	Valve radius, (m)
R_{vo}	Valve inner radius, (m)
S	Effective strength, (–)
$\bar{S}$	Mean effective strength, (–)
s	Stress applied to a single peptidoglycan layer, (energy per bond)*
s_c	Critical stress at which a single peptidoglycan layer disrupts, (energy per bond)*

** Defined in this study as the maximum average pressure recorded during the transient (see Section 4.2).

s_L	Limiting stress at which the free-energy barrier disappears, (energy per bond)*
S_m	Median maximum stress experienced during homogenization (i.e. the stress at which 50% of the events have a stress greater than S_m), (–)
T	Temperature (eq. 5.6), (energy per bond)*
t	Number of standard deviations (eq. 3.26), (–)
u	Fluid velocity, (m s^{-1})
u_o	Fluid velocity at the valve inlet (i.e. at R_{vo}), (m s^{-1})
V	Sample volume, (m^3)
X	Degree of peptidoglycan crosslinkage (Section 5.1.2), (–)
x	Fraction of intact bonds (eq. 5.6), (–)
X_L	Limiting peptidoglycan crosslinkage, (–)
x_L	Fraction of intact bonds corresponding to the stationary inflexion at an applied stress level s_L, (–)
x_s	Volume fraction of the bacterial population which is septated, (–)
Y	Distance between the valve exit and the impact ring (eq. 1.6), (m)
y	Aqueous volume fraction, (–)

Greek Symbols

χ	Volume of intact cells, (m^3)
$\mathcal{D}$	Bond dissociation energy, (energy per bond)*
$\Delta\rho$	Density difference between particles and fluid (eq. 3.10), (kg m^{-3})
ϕ	Volume fraction of cells surviving the homogenization process, (–)
γ	A conceptual wall strength (eq. 1.5), (–)
$\bar{\lambda}_s$	Average minimum length of septated cells, (μm)
η	Fluid viscosity, (Pa s)
θ_H	Empirical homogenization factor (eq. 1.2), (–)
ρ	Density, (kg m^{-3})

σ^2	Variance of the effective strength distribution, (–)
τ	Time taken for a particle to reach the detector (eq. 3.10), (s)
υ	Number of peptidoglycan layers opposing the applied stress, (–)
ω	Angular velocity of the disc centrifuge, (s^{-1})
μ	Bacterial growth rate, (h^{-1})

Subscripts

a	Aqueous phase
c	Cells
d	Diluent or diluted sample
h	Homogenate sample (i.e. the sample after disruption)
L	Lower limit
m	Maximum concentration corresponding to 100% disruption
n	Non-septated sub-population of bacteria
o	Feed sample (i.e. the sample before disruption)
s	Septated sub-population of bacteria
U	Upper limit

Abrahmsen, L.; Moks, T.; Nilsson, B.; Uhlen, M. 1986. Secretion of heterologous gene products to the culture medium of *Escherichia coli*. *Nucleic Acids Res.*, **14**, 7487-7500.

Allen, T. 1968. Determination of the size distribution and specific surface of fine powders by photoextinction methods I. Theoretical estimate of variation in extinction coefficient with particle size using a white light source. *Powder Technol.*, **2**, 133-140.

Allen, T. 1987. Photocentrifuges. *Powder Technol.*, **50**, 193-200.

Andrews, B.A.; Asenjo, J.A. 1987. Continuous-Culture Studies of Synthesis and Regulation of Extracellular β(1-3)Glucanase and Protease Enzymes from *Oerskovia Xanthineolytica*. *Biotechnol. Bioeng.*, **30**, 628-637.

Asenjo, J.A.; Patrick, I. 1990. Large-scale protein purification. In *Protein purification applications: a practical approach*. E.L.V. Harris and S. Angal (-eds.), Chap. 1, IRL Press at Oxford University Press, Oxford, 1-27.

Augenstein, D.C.; Thrasher, K.; Sinskey, A.J.; Wang, D.I.C. 1974. Optimization in the Recovery of a Labile Intracellular Enzyme. *Biotechnol. Bioeng.*, **16**, 1433-1447.

Biegler, L.T. 1989. Chemical Process Simulation. *Chem. Eng. Prog.*, **85**, 50-61.

Blumberg Selinger, R.L.; Wang, Z.-G.; Gelbart, W.M.; Ben-Shaul, A. 1991. Statistical-thermodynamic approach to fracture. *Phys. Rev. A.*, **43**, 4396-4400.

Bradford, M.M. 1976. A rapid and sensitive method for the quantitation of microgram quantities of protein utilizing the principle of protein-dye binding. *Anal. Biochem.*, **72**, 248-254.

Braun, V.; Gnirke, H.; Henning, U.; Rehn, K. 1973. Model for the structure of the Shape-Maintaining Layer of the *Escherichia coli* Cell Envelope. *J. Bacteriol.*, **114**, 1264-1270.

Brookman, J.S.G. 1974. Mechanism of Cell Disintegration in a High Pressure Homogenizer. *Biotechnol. Bioeng.*, **16**, 371-383.

Brookman, J.S.G. 1975. Further Studies on the Mechanism of Cell Disruption by Extreme Pressure Extrusion. *Biotechnol. Bioeng.*, **17**, 465-479.

Brugger, K. 1976. The particle size determination of pigments with the disc centrifuge. *Powder Technol.*, **13**, 215-221.

Bunge, F.; Pietzsch, M.; Müller, R.; Syldatk, C. 1992. Mechanical disruption of *Arthrobacter sp. DSM* 3747 in stirred ball mills for the release of hydantoin-cleaving enzymes. *Chem. Eng. Sci.*, **47**, 225-232.

Chang, C.N.; Rey, M.; Bochner, B.; Heyneker, H.; Gray, G. 1987. High-level secretion of human growth hormone by *Escherichia coli. Gene*, **55**, 189-196.

de Jonge, B.L.M.; Wientjes, F.B.; Jurida, I.; Driehuis, F.; Wouters, J.T.M.; Nanninga, N. 1989. Peptidoglycan Synthesis during the Cell Cycle of *Escherichia coli:* Composition and Mode of Insertion. *J. Bacteriol.*, **171**, 5783-5794.

Dougherty, T.J. 1985. Analysis of *Neisseria gonorrhoeae* peptidoglycan by reverse-phase, high-pressure liquid chromatography. *J. Bacteriol.*, **163**, 69-74.

Doulah, M.S. 1977. Mechanism of Disintegration of Biological Cells in Ultrasonic Cavitation. *Biotechnol. Bioeng.*, **19**, 649-660.

Doulah, M.S.; Hammond, T.H.; Brookman, J.S.G. 1975. A Hydrodynamic Mechanism for the Disintegration of *Saccharomyces cerevesiae* in an Industrial Homogenizer. *Biotechnol. Bioeng.*, **17**, 845-858.

Driehuis, F; Wouters, J.T.M. 1987. Effect of Growth Rate and Cell Shape on the Peptidoglycan Composition in *Escherichia coli. J. Bacteriol.*, **169**, 97-101.

Dunnill, P.; Lilly, M.D. 1975. Protein extraction and recovery from microbial cells. In *Single-Cell Protein II*, S.R. Tannenbaum and D.I.C. Wang (-eds.), Chap. 8, MIT Press, Cambridge, MA, 179-207.

Engler, C.R. 1979. Disruption of Microorganisms in High Pressure Flow Devices. Ph.D. Thesis, University of Waterloo, Waterloo, Ontario, Canada.

Engler, C.R. 1985. Disruption of Microbial Cells. In *Comprehensive Biotechnology, Vol. 2*, M. Moo-Young, A.E. Humphrey, C.L. Cooney (-eds.), Chap. 20, Pergamon, Oxford, 305-324.

Engler, C.R.; Robinson, C.W. 1979. New method of measuring cell-wall rupture. *Biotechnol. Bioeng.*, **21**, 1861-1869.

Engler, C.R.; Robinson, C.W. 1981. Disruption of *Candida utilis* Cells in High Pressure Flow Devices. *Biotechnol. Bioeng.*, **23**, 765-780.

Errington, J.; Mountain, A. 1990. Is Bacillus an Alternative Expression System? In *Protein Production by Biotechnology*, T.J.R. Harris (ed.), Chap. 1, Elsevier, London, 1-14.

Evans, L.B. 1988. Bioprocess Simulation: A New Tool for Process Development. *Bio/Technology*, **6**, 200-203.

Fish, N.M.; Lilly, M.D. 1984. The Interactions Between Fermentation and Protein Recovery. *Bio/Technology*, **2**, 623-627.

Foley, M.; Brass, J.M.; Birmingham, J.; Cook, W.R.; Garland, P.B.; Higgins, C.F.; Rothfield, L.I. 1989. Compartmentalization of the periplasm at cell division sites in *Escherichia coli* as shown by fluorescence photobleaching experiments. *Molecular Microbiol.*, **3**(10), 1329-1336.

Follows, M.; Hetherington, P.J.; Dunnill, P.; Lilly, M.D. 1971. Release of Enzymes from Bakers' Yeast by Disruption in an Industrial Homogenizer. *Biotechnol. Bioeng.*, **13**, 549-560.

Formanek, H. 1983. A Three Dimensional Model of the Murein Layer Explaining one Step of its Biosynthesis by Self-assembly, in *The Target of Penicillin*, Walter de Gruyter & Co., Berlin, 55-60.

Formanek, H. 1986. A Three Dimensional Model of Peptidoglycan Corresponding with the Results of X-ray- and Electron Diffraction, High-resolution Electron Microscopy and the Properties of the Peptidoglycan, in *Biological Properties of Peptidoglycan*, Walter de Gruyter & Co., Berlin, 43-48.

Fraser, D. 1951. Bursting Bacteria by Release of Gas Pressure. *Nature*, **167**, 33-34.

Georgiou, G.; Chalmers, J.J.; Shuler, M.L.; Wilson, D.B. 1985. Continuous Immobilized Recombinant Protein Production from *E. coli* Capable of Selective Protein Excretion: A Feasibility Study. *Biotechnol. Prog.*, **1**, 75-79.

Glauner, B. 1988. Separation and Quantification of Muropeptides with High-Performance Liquid Chromatography. *Anal. Biochem.*, **172**, 451-464.

Glauner, B.; Höltje, J.-V.; Schwarz, U. 1988. The Composition of the Murein of *Escherichia coli*. *J. Biol. Chem.*, **263**, 10088-10095.

Glauner, B.; Schwarz, U. 1983. The analysis of murein composition with High-Pressure-Liquid Chromatography, in *The Target of Penicillin*, Walter de Gruyter & Co., Berlin, 29-34.

Goebel, W.; Hedgpeth, J. 1982. Cloning and Functional Characterization of the Plasmid-Encoded Hemolysin Determinant of *Escherichia coli*. *J. Bacteriol.*, **151**, 1290-1298.

Gray, P.P.; Dunnill, P.; Lilly, M.D. 1972. The Continuous-flow Isolation of Enzymes. *Proc. IV IFS: Ferment. Technol. Today*, G. Terui - ed., 347-351.

Gritsis, D.; Titchener-Hooker, N.J. 1989. Biochemical Process Simulation. *IChemE Symposium 114*, Computer Integrated Process Engineering (CIPE 89), IChemE Rugby/Hemisphere Publishing Corp., Philadelphia, USA, 69-78.

Grover, N.B.; Woldringh, C.L.; Zaritsky, A.; Rosenberger, R.F. 1977. Elongation of rod-shaped bacteria. *J. theor. Biol.*, **67**, 181-193.

Hancock, R.E.W. 1984. Alterations in Outer Membrane Permeability. *Ann. Rev. Microbiol.*, **38**, 237-264.

Harris, E.L.V. 1989. Initial Planning: Introduction. In *Protein purification methods: a practical approach*. E.L.V. Harris and S. Angal (-eds.), Chap. 1, IRL Press at Oxford University Press, Oxford, 1-3.

Harrison, S.T.L.; Chase, H.A.; Dennis, J.S. 1991. The disruption of *Alcaligenes eutrophus* by high pressure homogenisation: Key factors involved in the process. *Bioseparation*, **2**, 155-166.

Henning, U. 1975. Determination of cell shape in bacteria. *Ann. Rev. Microbiol.*, **29**, 45-60.

Hetherington, P.J.; Follows, M.; Dunnill, P.; Lilly, M.D. 1971. Release of Protein from Baker's Yeast (*Saccharomyces cerevisiae*) by Disruption in an Industrial Homogeniser. *Trans. Instn. Chem. Engrs.*, **49**, 142-148.

Hettwer, D.; Wang, H. 1989. Protein Release from *Escherichia coli* Cells Permeabilized with Guanidine-HCl and Triton X100. *Biotechnol. Bioeng.*, **33**, 886-895.

Hirst, T.R.; Randall, L.L.; Hardy, S.J.S. 1984. Cellular Location of Heat-Labile Enterotoxin in *Escherichia coli*. *J. Bacteriol.*, **157**, 637-642.

Hoare, M.; Dunnill, P. 1989. Biochemical engineering challenges of purifying useful proteins. *Phil. Trans. R. Soc. Lond. B*, **324**, 497-507.

Hopkins, T.R. 1991. Physical and Chemical Cell Disruption for the Recovery of Intracellular Proteins. In *Purification and Analysis of Recombinant Proteins*. R. Seetharam and S.K. Sharma (-eds.), Chap. 3, Marcel Dekker, New York, 57-83.

Höltje, J.-V.; Glauner, B. 1990. Structure and Metabolism of the Murein Sacculus. *Inst. Pasteur Res. Microbiol.*, **141**, 75-103.

Hsiung, H.M.; Cantrell, A.; Luirink, J.; Oudega, B.; Veros, A.J.; Becker, G.W. 1989. Use of Bacteriocin Release Protein in *E. coli* for Excretion of Human Growth Hormone into the Culture Medium. *Bio/Technology*, **7**, 267-271.

Hsiung, H.M.; Mayne, N.G.; Becker, G.W. 1986. High-level expression, efficient secretion and folding of human growth hormone in *Escherichia coli*. *Bio/Technology*, **4**, 991-995.

Huang, R.-B.; Andrews, B.A.; Asenjo, J.A. 1991. Differential Product Release (DPR) of Proteins from Yeast: A New Technique for Selective Product Recovery from Microbial Cells. *Biotechnol. Bioeng.*, **38**, 977-985.

Hughes, D.E.; Wimpenny, J.W.T.; Lloyd, D. 1971. The disintegration of micro-organisms. In *Methods in Microbiology*. J.R. Norris and D.W. Ribbons (-eds.), **5B**, Chap. 1, Academic, New York, 1-54.

Hunter, J.B.; Asenjo, J.A. 1988. A Structured Mechanistic Model of Kinetics of Enzymatic Lysis and Disruption of Yeast Cells. *Biotechnol. Bioeng.*, **31**, 929-943.

Hunter, J.B.; Asenjo, J.A. 1990. A Population Balance Model of the Enzymatic Lysis of Microbial Cells. *Biotechnol. Bioeng.*, **35**, 31-42.

Husong, T. 1990. A Unified Derivation for Calculating Particle Size Distribution for Line-Start Incremental Sedimentation Methods. *Powder Technol.*, **61**, 231-236.

Joyce-Loebl Ltd. 1985. Instruction manual for the Joyce Loebl disc centrifuge. Joyce-Loebl Ltd.: Gateshead, U.K., 1985.

Kato, C.; Kobayashi, T.; Kudo, T.; Furusato, T.; Murakami, Y.; Tanaka, T.; Baba, H.; Oishi, T.; Ohtsuka, E.; Ikehara, M.; Yanagida, T.; Kato, H.; Moriyama, S.; Horikoshi, K. 1987. Construction of an excretion vector and extracellular production of human growth hormone from *Escherichia coli*. *Gene*, **54**, 197-202.

Katsui, N.; Tsuchido, T.; Hiramatsu, R.; Fujikawa, S.; Takano, M.; Shibasaki, I. 1982. Heat-Induced Blebbing and Vesiculation of the Outer Membrane of *Escherichia coli*. *J. Bacteriol.*, **151**, 1523-1531.

Kawaguchi, T. 1971. Entrance Loss for Turbulent Flow without Swirl between Parallel Discs. *Bulletin of JSME*, **14**, 355-363.

Kelemen, M.V.; Sharpe, J.E.E. 1979. Controlled Cell Disruption: A Comparison of the Forces Required to Disrupt Different Microorganisms. *J. Cell Sci.*, **35**, 431-441.

Keshavarz Moore, E.; Hoare, M.; Dunnill, P. 1990. Disruption of baker's yeast in a high-pressure homogenizer: New evidence on mechanism. *Enzyme. Microb. Technol.*, **12**, 764-770.

Keshavarz, E.; Hoare, M.; Dunnill, P. 1987. Biochemical engineering aspects of cell disruption. In *Separations for Biotechnology*. M.S. Verrall and M.J. Hudson (-eds.), Chap. 3, Ellis Horwood, Chichester, 62-79.

Kubitschek, H.E. 1969. Growth during the Bacterial Cell Cycle: Analysis of Cell Distribution. *Biophys. J.*, **9**, 792-809.

Kula, M.-R.; Schütte, H. 1987. Purification of Proteins and the Disruption of Microbial Cells. *Biotechnol. Prog.*, **3**, 31-42.

Labischinski, H.; Barnickel, G.; Naumann, D.; Keller, P. 1985. Conformational and Topological Aspects of the Three-Dimensional Architecture of Bacterial Peptidoglycan. *Ann. Inst. Pasteur/Microbiol.*, **136 A**, 45-50.

Leduc, M.; Frehel, C.; Siegel, E.; van Heijenoort, J. 1989a. Multilayered Distribution of Peptidoglycan in the Periplasmic Space of *Escherichia coli*. *J. Gen. Microbiol.*, **135**, 1243-1254.

Leduc, M.; Joseleau-Petit, D.; Rothfield, L.I. 1989b. Interactions of membrane lipoproteins with the murein sacculus of *Escherichia coli* as shown by chemical crosslinking studies of intact cells. *FEMS Microbiol. Lett.*, **60**, 11-14.

Leduc, M.; Kasra, R.; van Heijenoort, J. 1982. Induction and Control of the Autolytic System of *Escherichia coli*. *J. Bacteriol.*, **152**, 26-34.

Leduc, M.; van Heijenoort, J. 1980. Autolysis of *Escherichia coli*. *J. Bacteriol.*, **142**, 52-59.

Lilly, M.D. 1979. Production of intracellular microbial enzymes. *Appl. Biochemistry and Bioengineering*, **2**, 1-26.

Lin, H.-M.; Chan, E.-C.; Chen, C.; Chen, L.-F. 1991. Disintegration of Yeast Cells by Pressurized Carbon Dioxide. *Biotechnol. Prog.*, **7**, 201-204.

Lin, H.-M.; Yang, Z.; Chen, L.-F. 1992. An Improved Method for Disruption of Microbial Cells with Pressurized Carbon Dioxide. *Biotechnol. Prog.*, **8**, 165-166.

Lowry, O.H.; Rosenbrough, N.J.; Farr, A.L.; Randall, R.J. 1951. Protein measurement with the Folin phenol reagent. *J. Biol. Chem.*, **193**, 265-275.

Lubitz, W.; Halfman, G.; Plapp, R. 1984. Lysis of *Escherichia coli* after infection with ϕX174 depends on the regulation of the cellular autolytic system. *J. Gen. Microbiol.*, **130**, 1079-1087.

Matteucci, M.; Lipetsky, H. 1986. Alkaline Phosphatase Fusions: A Tag to Identify Mutations that Result in Increased Expression of Secreted Human Growth Hormone from *E. coli*. *Bio/Technology*, **4**, 51-55.

McKillop, A.A.; Dunkley, W.L.; Brockmeyer, R.L.; Perry, R.L. 1955. The cavitation theory of homogenization. *J. Dairy Sci.*, **38**, 273-283.

Naglak, T.J.; Hettwer, D.J.; Wang, H.Y. 1990. Chemical Permeabilization of Cells for Intracellular Product Release. In *Separation Processes in Biotechnology*. J.A. Asenjo (-ed.), Marcel Dekker, New York, 177-205.

Naglak, T.J.; Wang, H.Y. 1992. Rapid Protein Release from *Escherichia coli* by Chemical Permeabilization Under Fermentation Conditions. *Biotechnol. Bioeng.*, **39**, 732-740.

Nanninga, N.; Wientjes, F.B.; de Jonge, B.L.M.; Woldringh, C.L. 1990. Polar Cap Formation During Cell Division in *Escherichia coli*. *Inst. Pasteur Res. Microbiol.*, **141**, 103-118.

Nesaratnam, S.T.; Wase, D.A.J.; Blakebrough, N. 1982. The susceptibility to ultrasonic disintegration of *Klebsiella pneumoniae* NCTC 418. *Eur. J. Appl. Microbiol. Biotechnol.*, **15**, 56-58.

Neu, H.C.; Heppel, L.A. 1965. The release of enzymes from *Escherichia coli* by osmotic shock and during the formation of spheroplasts. *J. Biol. Chem.*, **240**, 3685-3692.

Oppenheimer, L.E. 1983. Interpretation of disc centrifuge data. *J. Colloid Interface Sci.*, **92**, 350-357.

Pandolfe, W.D. 1982. Development of the New Gaulin Micro-Gap™ Homogenizing Valve. *J. Dairy Sci.*, **65**, 2035-2044.

Pandolfe, W.D.; Kinney, R.R. 1983. Recent Developments in the Understanding of Homogenization Parameters. Presented at 1983 Summer National Meeting, AIChE, Denver, CO.

Petrides, D.; Cooney, C.L.; Evans, L.B.; Field, R.P.; Snoswell, M. 1989. Bioprocess Simulation: An Integrated Approach to Process Development. *Computers chem. Engng.*, **13**, 553-561.

Phipps, L.W. 1971. Mechanism of Oil Droplet Fragmentation in High Pressure Homogenizers. *Nature*, **233**, 617-619.

Phipps, L.W. 1974a. Cavitation and separated flow in a simple homogenizing valve and their influence on the break-up of fat globules in milk. *J. Dairy Res.*, **41**, 1-8.

Phipps, L.W. 1974b. Some operating characteristics of a simple homogenizing poppet valve; pressure profiles and separation: zone of fat globule dispersion. *J. Dairy Res.*, **41**, 339-347.

Phipps, L.W. 1975. The Fragmentation of Oil Drops in Emulsions by a High-Pressure Homogenizer. *J. Phys. D: Appl. Phys.*, **8**, 448-462.

Pierucci, O. 1978. Dimensions of *Escherichia coli* at Various Growth Rates: Model for Envelope Growth. *J. Bacteriol.*, **135**, 559-574.

Pisabarro, A.G.; de Pedro, M.A.; Vazquez, D. 1985. Structural Modifications in the Peptidoglycan of *Escherichia coli* Associated with Changes in the State of Growth of the Culture. *J. Bacteriol.*, **161**, 238-242.

Quirk, A.V.; Woodrow, J.R. 1984. Investigation of the parameters affecting the separation of bacterial enzymes from cell debris by tangential flow filtration. *Enzyme Microb. Technol.*, **6**, 201-206.

Rietschel, E.T.; Brade, H.; Brade, L.; Kawahara, K.; Lüderitz, T.; Schade, U.; Tacken, A.; Zähringer, U. 1986. Lipid A, the endotoxic principle of bacterial lipopolysaccharides: chemical structure and biological activity. In *Biological Properties of Peptidoglycan*, Walter de Gruyter & Co., Berlin, 341-352.

Ryan, W.; Parulekar, S.J. 1991. Immobilization of *Escherichia coli* JM103[pUC8] in κ-Carrageenan Coupled with Recombinant Protein Release by in Situ Cell Membrane Permeabilization. *Biotechnol. Prog.*, **7**, 99-110.

Salusbury, T. 1989. Clarification and Extraction : Disruption. In *Protein purification methods: a practical approach.* E.L.V. Harris and S. Angal (-eds.), Chap. 2, IRL Press at Oxford University Press, Oxford, 87-97.

Sanchez-Ruiz, S.A. 1989. Studies on Cell Disruption and Cell Debris Removal in Downstream Bioprocessing. M.Sc. Thesis, Dept. of Applied Biological Sciences, M.I.T.

Sauer, T.; Robinson, C.W.; Glick, B.R. 1989. Disruption of Native and Recombinant *Escherichia coli* in a High-Pressure Homogenizer. *Biotechnol. Bioeng.*, **33**, 1330-1342.

Schein, C.H. 1989. Production of soluble recombinant proteins in bacteria. *Bio/Technology*, **7**, 1141-1149.

Schnaitman, C.A. 1971. Solubilization of the Cytoplasmic Membrane of *Escherichia coli* by Triton X-100. *J. Bacteriol.*, **108**, 545-552.

Schwarz, U.; Leutgeb, W. 1971. Morphogenetic Aspects of Murein Structure and Biosynthesis. *J. Bacteriol.*, **106**, 588-595.

Siddiqi, S.F.; Clarkson, A.I.; Keshavarz Moore, E.; Titchener-Hooker, N.J. 1991. Modelling of Process Interactions in Biochemical Processes. 1991 IChemE Research Event, 155-158.

Spratt, B.G. 1980. Biochemical and genetical approaches to the mechanism of action of penicillin. *Phil. Trans. R. Soc. Lond. B*, **289**, 273-283.

Taylor, G.; Hoare, M.; Gray, D.R.; Marston, F.A.O. 1986. Size and Density of Protein Inclusion Bodies. *Bio/Technology*, **4**, 553-557.

Thacker, J. 1973. An Approach to the Mechanism of Killing of Cells in Suspension by Ultrasound. *Biochimica et Biophysica Acta*, **304**, 240-248.

Thayer, A.M. 1991. Biopharmaceuticals Overcoming Market Hurdles. *Chem. Engng. News*, Feb. 25 1991, 27-48.

Treasure, C.R.G. 1964. Technical Paper No. 50. Whiting and Industrial Powders Research Council: Hatfield, Herts, U.K.

Trueba, F.J.; Woldringh, C.L. 1980. Changes in Cell Diameter During the Division Cycle of *Escherichia coli*. *J. Bacteriol.*, **142**, 869-878.

Tsuchido, T.; Katsui, N.; Takeuchi, A.; Takano, M.; Shibasaki, I. 1985. Destruction of the outer membrane permeability barrier of *Escherichia coli* by heat treatment. *Appl. Env. Microbiol.*, **50**, 298-303.

Tuomanen, E.; Cozens, R. 1987. Changes in Peptidoglycan Composition and Penicillin-Binding Proteins in Slowly Growing *Escherichia coli*. *J. Bacteriol.*, **169**, 5308-5310.

Tuomanen, E.; Markiewicz, Z.; Tomasz, A. 1988. Autolysis-Resistant Peptidoglycan of Anomalous Composition in Amino-Acid-Starved *Escherichia coli*. *J. Bacteriol.*, **170**, 1373-1376.

van Heijenoort, J.; Leduc, M.; van Heijenoort, Y.; Kasra, R. 1983. Autolysis of *Escherichia coli:* Induction and control. In *The Target of Penicillin*, Walter de Gruyter & Co., Berlin, 191-196.

Vervoorn, P.M.M.; Austin, L.G. 1990. The analysis of repeated breakage events as an equivalent rate process. *Powder Technol.*, **63**, 141-147.

Verwer, R.W.H.; Beachey, E.H.; Keck, W.; Stoub, A.M.; Poldermans, J.E. 1980. Orientated Fragmentation of *Escherichia coli* Sacculi by Sonication. *J. Bacteriol.*, **141**, 327-332.

Verwer, R.W.H.; Nanninga, N.; Keck, W.; Schwarz, U. 1978. Arrangement of Glycan Chains in the Sacculus of *Escherichia coli*. *J. Bacteriol.*, **136**, 723-729.

Vogels, G.; Kula, M.-R. 1992. Combination of Enzymatic and/or Thermal Pretreatment with Mechanical Cell Disintegration. *Chem. Eng. Sci.*, **47**, 123-131.

Walstra, P. 1969. Preliminary Note on the Mechanism of Homogenization. *Neth. Milk Dairy J.*, **23**, 290-292.

Wanner, U.; Egli, T. 1990. Dynamics of microbial growth and cell composition in batch culture. *FEMS Microbiol. Rev.*, **75**, 19-44.

Watson, J.S.; Cumming, R.H.; Street, G.; Tuffnell, J.M. 1987. Release of intracellular protein by thermolysis. In *Separations for Biotechnology*. M.S. Verrall and M.J. Hudson (-eds.), Chap. 7, Ellis Horwood, Chichester, 105-109.

White, M.D.; Marcus, D. 1988. Disintegration of Microorganisms. *Adv. Biotechnol. Process*, **8**, 51-96.

Williams, A.R. 1972. Shear-Induced Fragmentation of Human Erythrocytes. *Biorheology*, **10**, 303-311.

Wimpenny, J.W.T. 1967. Breakage of Micro-organisms. *Process Biochem.*, **2**, 41-44.

Yu, P.; San, K.-Y. 1992. Protein Release in Recombinant *Escherichia coli* Using Bacteriocin Release Protein. *Biotechnol. Prog.*, **8**, 25-29.

Zhang, Z.; Ferenczi, M.A.; Thomas, C.R. 1992. A micromanipulation technique with a theoretical cell model for determining mechanical properties of single mammalian cells. *Chem. Eng. Sci.*, **47**, 1347-1354.

Zorzopulos, J.; de Long, S.; Chapman, V.; Kozloff, L.M. 1989. Evidence for the net-like organization of lipopolysaccharide particles in the *Escherichia coli* outer membrane. *FEMS Microbiol. Lett.*, **61**, 23-26.